Distribution Agreement

In presenting this thesis or dissertation as a partial fulfillment of the requirements for an advanced degree from Emory University, I hereby grant to Emory University and its agents the non-exclusive license to archive, make accessible, and display my thesis or dissertation in whole or in part in all forms of media, now or hereafter known, including display on the world wide web. I understand that I may select some access restrictions as part of the online submission of this thesis or dissertation. I retain all ownership rights to the copyright of the thesis or dissertation. I also retain the right to use in future works (such as articles or books) all or part of this thesis or dissertation.

Signature:

_____ _____

K. Sabrina Lynn Date

CHARACTERIZATION OF TIGHT JUNCTION SPIKES AND THEIR ROLE IN REGULATING ALVEOLAR BARRIER FUNCTION

By
K. Sabrina Lynn
Doctor of Philosophy

Graduate Division of Biological and Biomedical Science
Biochemistry, Cell, and Developmental Biology

Michael Koval, Ph.D.
Advisor

Victor Faundez, M.D., Ph.D.
Committee Member

Andrew Kowalczyk, Ph.D.
Committee Member

Gregory Melikian, Ph.D.
Committee Member

Ruxana Sadikot, M.D.
Committee Member

Accepted:

Lisa A. Tedesco, Ph.D.
Dean of the James T. Laney School of Graduate Studies

Date

CHARACTERIZATION OF TIGHT JUNCTION SPIKES AND THEIR ROLE IN REGULATING ALVEOLAR BARRIER FUNCTION

By

K. Sabrina Lynn
B.S., Auburn University, 2013

Advisor: Michael Koval, Ph.D.

An abstract of
A dissertation submitted to the Faculty of the
James T. Laney School of Graduate Studies of Emory University
In partial fulfilment of the requirements for the degree of
Doctor of Philosophy
in Biochemistry, Cell, and Developmental Biology
2021

Abstract

CHARACTERIZATION OF TIGHT JUNCTION SPIKES AND THEIR ROLE IN REGULATING ALVEOLAR BARRIER FUNCTION

By K. Sabrina Lynn

Regulation of paracellular permeability within tissues is necessary for maintaining proper fluid balance and tissue function. This is especially important in the alveoli of the lungs, where careful tailoring of fluid helps to maintain open airspaces for gas exchange. Chronic alcohol abuse has been linked with leaky lung barrier function, priming it for acute respiratory distress syndrome (ARDS), a serious condition characterized by airspace flooding and widespread inflammation. Cells primarily modulate paracellular permeability through tight junction proteins, particularly transmembrane proteins called claudins. Here, we demonstrate in a rat model that chronic alcohol leads to an increase in claudin-5, which is necessary and sufficient for decreasing barrier function in alveolar epithelial cells (AECs). We further show that claudin-5 disrupts claudin-18 interactions with scaffolding protein ZO-1, suggesting a possible mechanism for alcohol-induced barrier dysfunction. Increased claudin-5 with alcohol was also associated with a rearrangement of tight junctions into spike-like structures perpendicular to cell junction interfaces. These “tight junction spikes” (TJ spikes) appear to be active areas of junction remodeling driven by increased endocytosis of tight junction proteins and form away from pools of β-catenin associated with actin filaments. This suggests a role for adherens junctions in determining the directionality of TJ spike formation. Treatment with the endocytosis inhibitor Dynasore, which targets the actin-binding protein dynamin, significantly reduces the number of TJ spikes and was associated with actin rearrangement into cortical actin. Dynamin-2 was found to colocalize with claudin-18 and ZO-1 at linear junctions but did not appear to localize with β-catenin and TJ spikes. We then used an *in situ* method of determining barrier function to show that TJ spikes were not sites of increased leak. To begin elucidating possible functions for TJ spikes, we investigated the local claudin-18 proteome using BioID, which showed association with multiple junction proteins including focal adhesion proteins. Of particular note, several proteins involved in signal transduction were biotin-labeled, setting the stage for future work defining potential roles for TJ spikes as signaling platforms.

CHARACTERIZATION OF TIGHT JUNCTION SPIKES AND THEIR ROLE IN REGULATING ALVEOLAR BARRIER FUNCTION

By

K. Sabrina Lynn
B.S. Auburn University, 2013

Advisor: Michael Koval, Ph.D.

A dissertation submitted to the Faculty of the
James T. Laney School of Graduate Studies of Emory University
In partial fulfilment of the requirements for the degree of
Doctor of Philosophy
in Biochemistry, Cell, and Developmental Biology
2021

Acknowledgements

I would first like to thank my advisor Mike Koval for his support and the opportunity to grow into a scientist. I've learned so much about developing and leading a research project by being in his lab. This is in part due to all of the wonderful people he's recruited to his lab, both past and present. These are some of the smartest, kindest, and funniest people I've met and I'm lucky to have worked alongside them! We have had a lot of fun moments together, from taking curling lessons, watching the eclipse, and of course any event with food. I also have made wonderful friends in this program, especially my classmates. I'm excited to see where everyone ends up in their careers so I can say I knew them when we were just trying to get through our foundations class.

There are so many people to thank here in Atlanta that have helped Atlanta feel more like home and helped me stay sane during grad school, especially (Dr.) Kelsey Maher, who was my roommate for most of grad school, and my friend Milanne, who's been there for me since middle school. I have wonderful friends that feel like family, and then friends who didn't get a choice because they are family. My wonderful extended family have provided endless support, along with my immediate family. My parents have been supportive from the beginning, and I know are eager to call me doctor, even though I'll have to remind them that I'm not that kind of doctor. My two incredibly smart brothers have been a wealth of encouragement during my grad school journey. I have wonderful loving in-laws, who have made me feel like family from day 1 and have given me my favorite person, my husband Taylor.

Taylor has kept me laughing through the lows, and smiling through the highs, and has always kept me fed. I can only take a little credit in that my grad school experience has helped him improve his cooking skills. He's been a wonderful partner and quarantine coworker, along with our dog Bantha, who provided a lot of affection and joy during the pandemic, even though she audibly snored during most of my zoom meetings (Mike can attest).

Special thanks to all of the people who offered a friendly ‘hello’ and smile while keeping the lab a clean and safe place, and to the cast of *Hamilton* for their soundtrack that helped me remember not to waste my shot. I know there are many people that I didn’t specifically acknowledge here, but who have added immensely to my time in grad school, so thank you and I wish you all success on your own journeys.

Table of Contents

CHAPTER 1: INTRODUCTION

Lung anatomy

Every cell in the body requires oxygen to perform cellular respiration, and the specialized structures within the lungs are vital in the acquisition of oxygen. Air flows through the trachea and bronchi, continuing down progressively smaller branches of bronchi in the respiratory tree. A network of branching conducting airways starting from the trachea, through bronchi to bronchioles directs air through the lungs, culminating in alveoli, which is where gas exchange occurs.

Each alveolus measures only 100-200 μm in diameter and together with pulmonary capillaries provides a thin boundary of 0.5 mm for oxygen to diffuse across to enter the bloodstream and carbon dioxide to exit the body.[1] Approximately 480 million alveoli are packed into the average lung with a volume at just over 3000 cm^3.[1,2] This amounts to a surface area within the lung of 70 m^2. With 12 to 18 breaths taken per a minute by the average adult, the division of the respiration zone into small air sacs known as alveoli helps to maximize diffusion capacity within the limited volume of the thoracic cavity.

Alveolar epithelium

Two major types of cells comprise the alveolar epithelium: type I and type II epithelial cells. Type I alveolar epithelial cells are thin at only 0.25 nm from apical to basolateral membrane, facilitating gas diffusion across them. Their sprawling squamous shape helps them account for 97 percent of the surface area of alveoli, though they only make up approximately 40% of all alveolar epithelial cells.[1,3] By contrast, type II cells, which are smaller and cuboidal, contain approximately half the volume of type I cells and have a footprint 27 times smaller than type I cells.[3] Alveolar epithelial cells fasten to an extracellular matrix, which provides both support to the alveoli during lung expansion, along with wound healing and tissue hydration.[4] Normal

alveolar cells interact with an extracellular matrix containing laminin and type IV collagen. Provisional matrix in injured alveoli contains fibronectin and type I collagen, promoting cell migration and wound healing. However, long-term culture on this provisional matrix leads to low resistance monolayers compared to cells on normal matrix.[5–8]

Type II cells secrete surfactant that is necessary in maintaining open alveoli by regulating surface tension.[9,10] In order to keep alveoli from collapsing from the pressure of surrounding tissue with every breath expiration, alveolar type II cells produce surfactant to provide structure to the alveoli. Pulmonary surfactant is a composition rich in proteins and lipids that reduce airspace surface tension. Surfactant is stored in lamellar bodies, distinct organelles within type II cells. Upon secretion, surfactant forms layered films, vesicles, and tubular myelin structures. Alveolar macrophages regulate surfactant turnover in concert with type II cells.[11] Surfactant secretion is controlled by stretch-activated calcium channels. Calcium is transferred from type I to type II cells via gap junctions, causing the fusion of lamellar bodies with plasma membrane to release surfactant.[12,13] Paracrine signaling through extracellular adenosine triphosphate (ATP) and purinergic receptors can also stimulate surfactant release. Interestingly, type I cells release more ATP than type II cells in response to stretch, suggesting they have a role as mechanosensors in the alveoli. In addition, type II cells facilitate the innate immune response through release of cytokines and can differentiate into type I cells to repair and maintain healthy alveoli.[14,15]

Fluid flux is a necessary component of healthy alveoli. Fluid efflux in the airspace is driven by electrochemical gradients created by ion flux through alveolar epithelial cells. These electrochemical gradients direct the passive flow of water between tissues. The primary ion flux in the alveoli occurs through sodium transport via apically-located epithelial sodium channels (ENaC) pumping sodium into cells and basolateral sodium-potassium adenosine triphosphatases (Na,K-ATPases) removing sodium from cells into the interstitium.[16]

Tight junctions

Tight junctions are protein complexes that form at contact sites between cells and provide a selective barrier, working in concert to prevent fluid leak into airspaces from the bloodstream, lymphatic system, and surrounding tissue. Thus they are critical in maintaining fluid balance in the lung[17,18], regulating small molecule and ion paracellular movement between adjacent cells, which in turn directs water flow through osmosis.[19] Tight junctions were first observed in the 1960s by transmission electron microscopy, when they were noted as the most apical contact structures. They were described as 'kissing points' where the outer plasma membrane leaflets of adjacent cells appeared to fuse, indicative of their barrier forming properties, while neighboring junctions like adherens junctions and desmosomes were observed 15-20 nm apart. [20–22]

The dual roles of tight junctions in cells have often been described as a "gate" function, which regulates paracellular permeability and creates paracellular ion channels and a "fence" function, defining the apical and basolateral sides of cells, which is necessary for directional transcellular transport. They consist of transmembrane proteins, cytosolic scaffolding proteins, and cytoskeletal proteins. The transmembrane proteins can be grouped by the number of transmembrane regions – single transmembrane region proteins (JAMs, Crb3, CAR), triple transmembrane region proteins (Bves), and four transmembrane region proteins (claudins, TJ-Associated MARVEL Proteins (TAMPs)).

The predominant tight junction proteins directly regulating barrier permeability are claudins. There are 27 claudins in mammals, most of which have a C-term PDZ binding motif that interacts with scaffolding proteins. All have intracellular N- and C-termini, four transmembrane regions, two extracellular loops, one intracellular loop and tend to anchor to the actin cytoskeleton through interactions with the scaffolding proteins Zonula Occludens (ZO)-1, -2 and -3. ZO proteins are necessary for tight junction formation.[23] Most claudins interacts with ZO-1 PDZ domain 1, occludin with ZO-1 hinge region and GuK domain, and tricellulin with a

ZO-1 binding site in the N-terminus. MarvelD3 interacts with occludin and tricellulin but not ZO-1.

Claudin classification

Mammalian claudins have been categorized based on sequence homology, forming historical groupings of "classic" and "non-classic" claudins. Classic claudins are structurally similar especially with regards to the second extracellular (EC) domain and have short C-terminal cytosolic domains. Non-classic claudins have longer C-terminal domains and have more heterogenous second EC domains within this grouping.[24] The lung expresses both classic and non-classic claudins, the most prevalent of which are classic claudins-1, -3, -4, -5, and -7, and non-classic claudin-18. Claudin-18 protein is highly expressed in the alveolar epithelium but not in the airways of the lung.[25,26] Alternatively, claudins can be categorized functionally based on their apparent ability to form paracellular pores, thereby increasing paracellular permeability, or their ability to "seal" or decrease paracellular permeability. Of the prevalently expressed claudins in the lung mentioned (claudins-1, -3, -4, -5, -7, and -18), all are considered sealing claudins, though context should be considered when defining sealing properties. The diversity of claudin expression in the lung hints at the necessity of maintaining a tight barrier in the lung epithelium to restrict fluid leak.[21,25]

Put in more specific terms, sealing or barrier forming properties are simply defined as the ability to "restrict free passage of water, ions, and larger solutes."[27] However, there are nuances to describing the ways claudins can increase paracellular permeability. The pore pathway has been described as "a high-capacity, size- and charge-selective paracellular route that appears to be defined by the subset of claudins expressed."[27] This is distinguished from the leak pathway described by as "a low-capacity, paracellular route that does not discriminate between solutes on the basis of charge and allows limited flux of large molecules." Classification of claudins as pore-

forming or sealing can be difficult, considering some claudins have different functional outcomes depending on the cellular system or the other claudins present.

When first defining the barrier functionality of particular claudins, the effect of knockdown or knockout of the particular claudin in animal models was observed. Claudins 1, 3, 5, 11, 14, and 19 were defined as clearly sealing in this way, due to the generation of severe tissue barrier defects after knockdown or knockout.[17] More direct measurements of paracellular permeability such as electrical resistance and small molecule flux have also been used to define barrier function particularly in *in vitro* models. For instance, overexpression of particular claudins in cells with low resistance can give insight into the functionality of the overexpressed claudin. Claudins-1 and -3 were found to significantly increase the barrier resistance of low-resistance MDCK cells already expressing claudin-2.[28,29] However, barrier function is further complicated given that electrical resistance is used as the basic measure of "tightness", but electrical resistance also includes electrochemical gradients created by ion channels, or transcellular ion transport. Measuring both ion and small molecule permeability is needed to fully define the sealing properties of claudins.

Pore-forming claudins can be defined as cation selective or anion selective. Claudins-2, 10b, and 15 are cation selective while claudins-10a and -17 are anion selective.[17] Through careful study, particularly with claudin-2, it was found that the extracellular domains, specifically extracellular loop 1 (ECL1), are important for charge selectivity of pores and pore-forming *trans* interactions. For example, the negatively charged D65 residue in the ECL1 of claudin-2 was found to be necessary for cation selectivity.[30,31] The ECL1 of claudin-2 is also sufficient to form homomeric *trans*-interactions, while the transmembrane (TM) region was necessary to form claudin-2 homodimers, giving insight into how claudin-2 forms pores.[32,33] Further evidence that ECL1 is responsible for pore-forming abilities of claudins comes from analysis of claudin-10 splice variants. Alternative splicing gives rise to claudin-10a and claudin-10b, which differ only

in their first TM and most of ECL1 but result in producing an anion-selective channel and cation-selective channel respectively.[34,35]

Not all claudins have shown consistent results favoring categorization as strictly sealing or strictly pore-forming. Claudins-4, -7, -8, and -16 show varying results when overexpressed or knocked-down.[17] For example, claudin-4 has been shown to be anion-selective or sealing depending on the cell type it is overexpressed in.[36,37] The varying results could be due to competition between different claudins present that can lead to displacement of certain claudins within the tight junction. This is seen with claudin-2 displacement when claudin-8 is overexpressed in MDCK II cells, leading to a decrease in paracellular cation flux, or inclusion in the tight junction, as is seen with the requirement of claudin-8 for claudin-4 tight junction recruitment in M-1 and mIMCD3 cells.[38–40] For claudins-6, -9, 12, -13, -18, and -20 through -27, even less is known about their sealing or pore forming capabilities. Some clues can be gathered based on whether claudins are expressed in tight epithelia such as the skin or blood-brain barrier or leaky epithelia such as the small intestines, but a strong categorization is difficult to draw from correlative observations. For example, claudin-12 is expressed in both tight epithelia (urinary bladder, blood-brain barrier) and leaky epithelia (jejunum and ileum of gastrointestinal tract).[17]

Protein interactions within tight junctions

Claudins interact with other claudin proteins to form strands that are the basis of the mesh-like networks encircling and connecting the apical portion of adjacent cells. Claudins can interact both in *cis* (within the same cell membrane) and *trans* (in opposing cell membranes). They can also interact in a homomeric (*cis* interactions) and homotypic (*trans* interactions) fashion when the polymeric interactions are formed between the same claudin, and heteromeric (*cis* interactions) and heterotypic (*trans* interactions) when polymeric interactions take place between different types of claudins.[17,18,41,42]

The first high resolution structure of a claudin (claudin-15) provided more insight into structural regions of claudins that promote *cis* and *trans* interactions.[43,44] The extracellular regions of claudin-15 were determined to be a β-sheet structure composed of β-strands within the extracellular loops. Variable regions between β-strands in both extracellular loops were suggested to play a role in *trans* interactions, while *cis* interactions are thought to be mediated by extracellular loop 1 (ECL1) and transmembrane domain 3 (TM3). Interestingly, TM3 is longer than the other three transmembrane domains, which are similar in height to the plasma membrane. Crosslinking experiments revealed that EC1 can bind to the exposed extracellular region of TM3, and complimentary electrostatic potentials exist on the claudin-15 molecule, which potentially facilitate *cis* interactions.[44] TM2 of claudin-2 was found to be important for homomeric *cis* interactions.[45]

The intracellular portions of claudins play an important role in interacting with cytoplasmic proteins found within the tight junction. Each claudin has an intracellular N-terminal tail (4-5 residues), intracellular loop (~20 residues), and C-terminal tail that can vary in length from 21 to 106 residues.[46] The C-terminal tail shows much sequence heterogeneity, though almost all contain YV residues that serves as a PDZ-binding motif.[47] The C-term tail can determine protein stability and correctly target claudins to the tight junction complex. Post-translational modifications of the C-term tail can affect claudin localization, regulating *cis* and *trans* interactions, and thereby affecting function. Common post-translational modifications include phosphorylation and palmitoylation.[48–53] Of significance are claudin interactions with PDZ domain-containing scaffolding proteins including the ZO-1, -2, and -3. ZO proteins act as a backbone for tight junction assembly, tethering claudins to the actin cytoskeleton. Most transmembrane proteins interact with at least one scaffolding/adapter protein.[19]

Cis and *trans* interactions between claudins is crucial to large-scale organization of tight junction stands that regulate bulk transport between cells. The predominant model for strand assembly is the joined anti-parallel double-row model based on insight from the claudin-15

crystal structure.[43,44,54,55] Two rows of anti-parallel claudins form a double row of *cis*-interacting claudins. Claudins are stabilized by hydrogen bonds between adjacent β-strands in neighboring anti-parallel claudins (face-to-face *cis* interactions) and *cis* interactions between the extracellular segments of claudins within each single parallel row. Two *cis* double rows on adjacent cell membranes interact in *trans*, forming pores lined by β-strands contributed by four rows of claudins.[56] Assembled strands are dynamic structures that can branch, break, and reanneal, which is believed to be of importance in the leak pathway and tissue remodeling.[55,57]

Tight junction recruitment and recycling

Claudin strands form the backbone of intercellular tight junction structures, but interactions with other tight junction components are necessary for their formation.[58] Adherens junctions precede the formation of tight junctions, and ZO proteins are the first tight junction proteins to be recruited to forming cell-cell contacts followed by JAM-A and occludin.[59–61] ZO-1 and ZO-2 are necessary for tight junction assembly, as their absence prevent formation of tight junctions.[23,62] Recent studies show ZO proteins form phase separated membrane bound compartments of concentrated ZO proteins, which can then recruit other tight junction components including claudins, occludin, and actin possibly via a tension-induced mechanisms that reveals binding sites on ZO proteins.[63] Actin polymerization was shown to be important in driving the distribution of phase separated ZO proteins along cell junctions.[64,65] Interestingly, claudins are added to the basolateral side of tight junctions instead of being directly added to junctions like occludin. It is possible that claudins are specifically targeted to certain areas of the tight junction strand network like strand breaks.[66] Cholesterol and ceramides have also been implicated tight junction formation since tight junctions have been associated with detergent-insoluble membrane microdomains.[67–70] It remains unclear whether there is a dominant mechanism of tight junction organization and recruitment or how these different components work together to assemble tight junctions.

Tight junction proteins can leave the plasma membrane by endocytosis via many different mechanisms including clathrin-dependent mechanisms and the clathrin-independent mechanisms macropinocytosis and caveolae-driven endocytosis.[71–73] Perhaps the most striking is the bulk internalization of *trans* interacting tight junction proteins from opposing membranes endocytosed into a single contributing cell.[74] Once endocytosed, tight junction proteins enter early endosomes, where they are either recycled back to the membrane or targeted for degradation. [75–78] Different tight junction components have varying levels of removal and recycling. Actin and ZO-1 have high turnover rates while claudins are relative stable.[27,79]

Claudins in the alveolar epithelium

Major claudins in the alveoli are claudin-3, -4, and -18 with 97% of claudin mRNA encoding one of these three claudins.[80] Claudin-3 is the predominant claudin expressed in type II alveolar cells, and is found at alveolar epithelial type I-type II junctions.[81,82] Interestingly, overexpressing claudin-3 increases permeability, suggesting that type I-type II junctions are leakier than type I-type I.[83] This is in contrast to the sealing properties that claudin-3 contributes in other cell contexts.[28] Claudin-3 forms many hetero interactions with other claudins, including heterotypic (*trans*) interactions with claudins-1, -2, and -5 and heteromeric (*cis*) interactions with claudin-4.[84–86] In lungs from alcohol-fed rats, claudin-3 expression is decreased, though claudin-3's specific role in regulating barrier function in this context is not clear.[87]

Claudin-4 is expressed throughout the lung epithelium and acts as a sealing claudin in the lungs.[83] Interestingly, in claudin-4 knockout mice only a mild lung phenotype is observed. These mice do experience mild impairment of alveolar fluid clearance and increased permeability to large molecules despite no change to ion flux.[88] Increasing claudin-4 expression in claudin-4 knockout mouse cells resulted in an increase in transepithelial resistance but did not affect small molecule flux or change the ratio of sodium/chloride permeability (P(Na)/P(Cl)).[83] Claudin-4 is thought to be protective against lung injury, as it is increased in patients with ventilator-induced

lung injury (VILI) and less claudin-4 correlates with increased ARDS severity.[89,90] No change in claudin-4 expression was reported with alcohol alone, but it does provide a possible therapeutic target for prevention or mitigation of lung injury.[87]

Of the three predominant claudins expressed, claudin-18 is specific to the alveoli while claudin-3 and -4 are found in other parts of the lung. Claudin-18 is found in two isoforms, claudin-18.1 specific to the lungs and claudin-18.2 found in the stomach. When claudin-18 was knocked out in mice, there was little impact on overall lung fluid balance. This was due to compensation for loss of claudin-18 by increased alveolar fluid clearance due to upregulation of ENaC and Na,K-ATPase activity and additional compensation by cystic fibrosis transmembrane conductance regulator (CFTR).[91] Claudin-18 deficiency was still associated with increased permeability, despite compensatory mechanisms. Tight junction morphology is greatly affected in the absence of claudin-18, leading to enlarged gaps between junctions and increased F-actin staining at cell junctions along with increased claudin-3 and -4 expression.[91,92] Claudin-18 has a longer C-term tail and more tightly associates with cytoskeleton-linked scaffolding proteins than claudin-3 and -4, suggesting that claudin-18 could play a role in cytoskeletal organization at the junction.[83,91,93] Alcohol and inflammation have both demonstrated changes in claudin-18 expression.[87,94,95] However, comparison of claudin-18 knockout mice at postnatal day 3 and week 4 reveals defects in alveolarization, suggesting claudin-18 could play an important role in lung development.[92] A role for claudin-18 in wound repair has been suggested, as claudin-18 deficient mice had increased alveolar epithelial type II cell proliferation through a Yes-associated protein (YAP)-dependent mechanism. However, claudin-18 deficiency also led to increased tumorigenesis with age, suggesting careful regulation is needed to make claudin-18 a viable therapeutic target for lung injury.[96]

Alcohol and acute respiratory distress syndrome

Acute respiratory distress syndrome (ARDS) is a severe type of acute lung injury (ALI) characterized by increased alveolar-capillary permeability (leak) and widespread accumulation of protein, neutrophiles, and red blood cells in in the alveoli.[97] This airspace flooding impairs lung compliance (the lung's ability to expand) and gas exchange including decreasing the body's ability to excrete carbon dioxide and absorb oxygen, both of which are predictors of mortality with ARDS. ARDS presents a significant public health concern, with roughly 200,000 new cases a year.[98] It can result from a multitude of insults including sepsis, pneumonia, trauma, and ventilator-induced injury, and is associated with several comorbidities such as alcohol abuse and smoking.[97] Though the pathophysiology of this condition is well characterized, the mortality rate remains high at 35 to 55 percent and there are no current pharmacological therapies.[97–99]

Surviving ARDS is dependent on the ability of the lung barrier to maintain fluid balance and prevent severe airspace flooding.[100] Histology samples from patients with ARDS indicate that diffuse alveolar damage is an early hallmark of this disease. To offset damage, alveolar epithelial cells must quickly repair alveoli and reestablish a tight barrier.[97] This is achieved through two complementary processes, barrier function that controls fluid diffusion into the airspace and sodium-driven fluid clearance. Tight junctions are of particular importance in alveoli, the small air-filled sacs responsible for gas-exchange, which sustain much of the damage that leads to airspace flooding in ARDS.[17,101,102]

Alcohol affects tight junction composition and decreases alveolar barrier function. This balance is perturbed in the alcoholic lung, where there is increased paracellular leakage of fluid into the airspace.[103–105] Compensatory fluid clearance is able to sustain fluid balance, but the alcoholic lung is primed for ARDS. The damaged lung barrier function seen with chronic alcohol abuse puts these patients at a higher risk for ARDS; additional injury from sepsis, trauma, or ventilator-induced injury can cause severe airspace flooding that can no longer be remediated by

fluid clearance.[105] Thus, improving lung barrier function will prevent the pathologic consequences of ARDS.

Though the effects of alcohol on the lung have been conjectured, a notable study in 1996 conclusively showed alcohol as a risk factor for the development of ARDS.[106] An increased susceptibility to acute lung injury and immune dysfunction associated with chronic alcohol abuse encompass a pre-disease state referred to as the "alcoholic lung." Though not outright edema, the alcoholic lung is more susceptible to second hits that lead to lung flooding, including sepsis, pneumonia, and trauma. The pathophysiology of the alcoholic lung is not fully known, but work conducted by several groups over the past 20 years have provided insight into how alcohol impairs the immune response, promotes oxidative stress, and facilitates lung flooding.

Oxidative Stress Due to Alcohol Exposure

Because lung airspaces are exposed to environmental oxygen, they are susceptible to oxidative stress. Transforming growth factor β (TGFβ) is one of the oxidative stress-producing signaling pathways that is induced with alcohol. TGFβ decreases the antioxidant glutathione while increasing production of reactive oxygen species.[107–110] In addition, a major by-product of alcohol metabolism is acetaldehyde, which leads to the generation of oxygen radicals and causes lipid peroxidation.[111,112] The body combats oxidative stress through the production of antioxidants such as glutathione. Glutathione is a thiol tripeptide molecule that can be found in high concentrations (400 μM) in the fluid lining the alveoli.[113,114] Animal and human studies have shown that chronic alcohol abuse is associated with decreased levels of glutathione, leaving the lung more vulnerable to oxidative damage. Additionally, decreases in glutathione levels in patients with a history of chronic alcohol abuse were associated with higher levels of proteinaceous fluid in the lungs, indicative of cellular damage.[115,116] Glutathione in alveolar type II cell mitochondria was diminished with alcohol ingestion, correlating with mitochondrial

dysfunction, decreased cell viability, increased alveolar barrier permeability and altered surfactant production.[117,118]

Without proper levels of glutathione, the lung's capacity to prevent oxidative damage is significantly reduced. Furthermore, oxidized glutathione is present at higher levels in lung lavage samples from alcoholic patients, indicative of oxidative stress in the lungs. These compounding circumstances leave the lung vulnerable and more susceptible to ARDS should a second oxidative stress occur like sepsis.[105] Glutathione is present in both the cytosol and mitochondria of type II alveolar epithelial cells, which are controlled by different pools of key metabolites. For instance, in a rat model of chronic alcohol consumption, N-acetylcysteine was only effective at preventing depletion of cytosolic pools of glutathione but did not prevent mitochondrial pool depletion, alcohol-induced surfactant dysfunction, or decreased cell viability (ref?).[117–119] By contrast, the glutathione precursor procysteine was effective at preventing both cytosolic and mitochondrial glutathione depletion and was more protective than N-acetylcysteine against alcohol-induced effects in alveolar epithelial cells.

Alcohol ingestion has been shown to increase reactive oxygen species in mitochondria in alveolar macrophages, affecting mitochondrial function and leading to impaired alveolar macrophage phagocytosis.[120–122] This oxidative stress in mitochondria damages mitochondrial DNA, leading to further dysfunction and triggering of an inflammatory response.[123–126] A recent study focused on the effect of alcohol on mitochondria function in alveolar macrophages and subsequent effects on barrier function in alveolar epithelial cells.[127] Alcohol treatment of mouse alveolar epithelial and mouse alveolar macrophage cell lines caused damage to mitochondrial DNA in both cell lines. Crosstalk between alveolar epithelial cells and alveolar macrophages perpetuated damage induced by alcohol, causing reduced phagocytic function and barrier function, exacerbating injury and inhibiting recovery mechanisms.

Transcription factors associated with lung injury

NF-κB is a transcription factor that controls inflammation and is regulated by IκB. When phosphorylated, IκB is degraded and can no longer sequester NF-κB, leaving NF-κB free to translocate to the nucleus and activate "pro-inflammatory" genes including those involved in cytokine production and responses to free radicals. When alveolar epithelial cells were treated with pro-inflammatory cytokines (IL-1β, TNFα, and IFNγ), paracellular permeability increased and reduced claudin-18 expression. Inhibition of the NF-kB pathway with an IκB kinase inhibitor protected against this effect.[94] Interestingly, in the absence of cytokine treatment, treatment with IκB kinase inhibitors in alveolar epithelial cells from alcohol-fed rats did not rescue barrier function, and in fact decreased barrier function.[128] In control cells, inhibition of the NF-κB pathway similarly decreased barrier function and caused significant changes in tight junction morphology. This suggests that though deleterious in inflammatory conditions, some amount of baseline NF-κB activity is necessary for alveolar barrier function.

Alveolar macrophages are important in eliminating invading pathogens and debris through phagocytosis in addition to releasing cytokines and chemokines to recruit further immune support. However, chronic alcohol abuse severely impairs alveolar macrophage function. For instance, alveolar macrophages from alcoholic subjects have reduced phagocytic capacity.[129] Receptors for granulocyte/monocyte colony-stimulating factor (GM-CSF), a signaling molecule that promotes macrophage maturation and function, were downregulated in alveolar epithelial cells and alveolar macrophages in response to alcohol ingestion. This was due to an alcohol-induced decrease in effects on PU.1, a transcription factor that acts as a master regulator of GM-CSF signaling. Treatment of alveolar epithelial cells and alveolar macrophages with recombinant GM-CSF restored macrophage function, PU.1 signaling and improved barrier function.[130,131]

Zinc provides necessary immune support to the host, in addition to playing a vital role in antioxidant synthesis and function.[132] Chronic alcohol ingestion decreases zinc bioavailability in alveolar macrophages and alveolar epithelial cells.[133] Studies found that treatment with zinc in a

rat model of chronic alcohol abuse not only improved macrophage function but appeared to reduce oxidative stress indicated by cysteine/cystine ratio (reduced/oxidized form respectively).[131] Furthermore, this appeared to be in part due to restored signaling, indicated by increased PU.1 (GM-CSF receptor expression) and Nrf2 (antioxidant response element activation) nuclear binding. Alveolar macrophages from alcoholic patients had significantly lower levels of intracellular zinc and phagocytic function when compared to controls but were remarkably improved with zinc acetate and glutathione treatment.[129,133] Unfortunately, this does provide more evidence of inhibited lung immune function even in otherwise healthy alcoholic patients, leaving them more susceptible to ARDS among other lung insults.

Barrier dysfunction

ARDS is characterized by widespread inflammation in the lungs, which can have its own adverse effects including promoting barrier dysfunction. Lung flooding and the increased proteinaceous fluid in lung lavage from alcoholic patients is in part due to a decrease in barrier function of the alveolar epithelium. A rat model of chronic alcohol abuse demonstrated increased lung epithelial permeability to a range of molecules.[116] This is in large part due to changes in tight junctions, protein complexes that form at contact sites between cells to regulate the paracellular flow of small molecules, water, and ions between adjacent cells.[19] They are critical in maintaining fluid balance in the lung, as they are the major functional units of the lung epithelial barrier, with particular importance in alveoli as they sustain much of the damage that leads to airspace flooding in ARDS.[17,100–102] Tight junctions are composed of distinct protein components that contribute to barrier function, including the claudin family transmembrane proteins and scaffolding proteins like Zonula Occludens (i.e. ZO-1, ZO-2) that link claudins to the actin cytoskeleton to promote barrier function.[17]

A look at whether chronic alcohol abuse affects tight junction proteins revealed decreases in key proteins including claudin-3, claudin-7, claudin-18, occludin, and ZO-1. Significantly,

claudin-5 was increased with alcohol, though not a major claudin in the alveoli.[87] Alcohol treatment correlated with more tight junction strand breaks and intracellular claudin staining, which has been noted along with decreased barrier function in other instances of increased claudin-5 expression.[26,81,82,87] Interestingly, when rat alveolar epithelial cells are removed and cultured, the defects in barrier function persisted, hinting at possible epigenetic regulation of this phenotype.

Though alcohol does not seem to cause edema alone, the lung is more prone to flooding. This could be due to altered lung fluid levels via increased net sodium flux by directly increasing Na,K-ATPase and ENaC. It is possible this is a mechanism meant to compensate for alcohol-induced leakiness.[134–136] This is mediated in part by cytokines such as TGFβ, which also was associated with changes in tight junction morphology and actin rearrangement.[137] Though originally it was thought that TGFβ could be mitigating damage in acute lung injury, it is now known that TGFβ could be further contributing to lung flooding.[138] TGFβ was found to be upregulated in the presence of alcohol in both alveolar epithelial cells and alveolar macrophages.[139,140] Furthermore, integrin αvβ6, which can act as a receptor for the inactive TGFβ complex, is upregulated in response to alcohol. TGFβ is usually bound in a latent complex and inactive until binding with a receptor either triggers active TGFβ release, which then binds other receptors to induce different cellular signaling pathways.[141] Inflammatory conditions like sepsis can cause an increase in the amount of active TGFβ released into the airspace, compounding the effects of alcohol-induced TGFβ upregulation. In addition to promoting inflammation in the lungs, TGFβ dampens the ability to recover from oxidative damage and injury by downregulating zinc importers, inhibiting glutathione synthesis, and decreasing GM-CSF signaling in alveolar macrophages.[142–146]

The ability of alveolar epithelial cells to repair wounds left by damaged and apoptotic alveolar cells is crucial in mitigating alveolar flooding. Increases in markers of apoptosis in alveolar epithelial cells are associated with ARDS.[147–149] Additionally, alcohol consumption

increases cell death in alveolar cells, and affects the wound repair response.[117,119] The extracellular matrix that alveolar epithelial cells interact with can trigger cell proliferation, migration, and wound healing. Though laminin and type IV collagen are the primary components in normal alveolar extracellular matrix, injured alveoli are often repaired with matrix enriched with fibronectin and type I collagen to facilitate rapid establishment of the epithelium.[150,151] However, increased inflammation and proliferation of fibroblasts can occur with continued exposure to fibronectin-rich matrix.[152,153] Chronic alcohol and alcohol-induced products like TGFβ can increase fibronectin expression and cause fibrosis, which can lead to worse outcomes in ARDS.[154–157] Preventing migration of invading neutrophils and fibroblasts into the airspace is necessary to control the immune response and avoid fibrosis development.

Cytoskeletal interactions and tight junction morphological changes

Changes in tight junction morphology have been observed accompanying changes in claudin expression. When primary rat lung alveolar type II epithelial cells were treated with TGFβ1, a decrease in claudin-18 and an increase in the rearrangement of claudin-18 and ZO-1 into spike-like protrusions at the membrane was observed.[137] This increase in spike-like structures and decrease in claudin-18 was associated with a decrease in barrier function. Conversely, treatment of rat alveolar epithelial cells with GM-CSF, which stimulates barrier recovery in the lungs, resulted in a decrease of claudin-18 spikes and increase in barrier function. These claudin-18 spikes colocalized with F-actin bundles perpendicular to the membrane with TGFβ1, while combined treatment with GM-CSF or GM-CSF alone showed a decrease in F-actin colocalization with claudin-18 spikes. Treating rat alveolar epithelial cells with an IκB kinase inhibitor decreased overall claudin-18 expression and resulted in claudin-18 spikes associated with F-actin bundles perpendicular to the membrane. This change in tight junction morphology was likewise accompanied by decreased barrier function and discontinuous ZO-1 and ZO-2 staining along with an increase in claudin-4 and claudin-5 expression.[128] This expands on observations

made by Li, et al in claudin-18 KO mice AEC monolayers, in which the loss of claudin-18 conferred a decrease in barrier function and increased F-actin near the plasma membrane. Although not quantified, ZO-1 staining of monolayers reveals spike-like structures at the membrane.[91] Treating rat alveolar epithelial cells with methanandamide increased the expression of claudin-3 and -5 significantly with claudin-5 being 12-fold higher than control cells. This increase in claudin expression was associated with a decrease in barrier function and the appearance of spike-like protrusions in ZO-1 and occludin staining similar to those observed with a decrease in claudin-18.[82] This suggests that changes in morphology could be conveying these changes in barrier function. Alternatively, the parallel changes give clues as to how claudins could be interacting with other tight junction proteins in the membrane and suggest these spike-like structures could be areas of unincorporated tight junction proteins.

Interestingly, many of the examples that relate altered tight junctions and decreased barrier function seem to have changes in the actin cytoskeleton in common. Assembly of tight junctions is regulated in part by the actin cytoskeleton.[158–161] Mechanical force is thought to play a role in association of tight junction proteins with ZO-1 by revealing binding sites on ZO-1.[63] A study conducted in MDCK II cells found that a weak link between actin and ZO-1 was necessary for higher barrier permeability, whereas a stronger affinity between ZO-1 and actin actually reduced barrier function.[162] An example of pulling forces exhibited by the actin cytoskeleton directly leading to morphological changes at the junction can be seen in the formation of focal adherens junctions (FAJs). These FAJ structures are marked by VE-cadherin, actin bundles, and vinculin and are formed from linear adherens junctions. Inhibition of Rho/Rock-actomyosin contractility inhibits FAJ formation. Interestingly, a mutated α-catenin incapable of binding vinculin resulted in FAJs that readily opened with force induction (thrombin).[163,164] This suggests that changes in the way force is distributed in cells can result in changes in barrier function and ultimately the structure. The cytoskeletal rearrangment accompanying these changes in tight junction morphology imply a role for claudins in regulating the cytoskeleton at the tight junction. This

hypothesis along with other observed tight junction morphologies is elaborated on in Chapter 2 of this dissertation.

Scope of dissertation

Though it is well established that changes in the expression and composition of tight junction proteins can drastically affect barrier function, the molecular mechanisms that control tight junction regulation and assembly require further characterization.[83] Our lab has extensively examined factors that affect tight junctions in alveolar epithelial cells (AECs) and therefore affect lung barrier function.[87,128,137] While investigating the effect of alcohol abuse on tight junctions in primary AECs, our lab observed a novel rearrangement of claudin-18 into structures perpendicular to the cell junction interface, which we refer to as TJ spikes. Furthermore, formation of TJ spikes correlated with impaired barrier function in primary AECs, providing evidence that tight junction rearrangement is likely to have pathophysiological consequences. Understanding how TJ spikes form requires reconsidering tight junction assembly.

In **Chapter 2**, I along with fellow graduate student and Koval lab member Raven Peterson, compiled and summarized the research done on tight junction morphologies, specifically ruffles and spikes, in epithelial cells and their effects on barrier function. Though several groups have observed differences in tight junction morphologies with protein expression and barrier function, a cumulative review of these studies has not been published. Not only could morphological changes serve as an indicator of barrier strength, these changes could also lend new insight into protein-protein interactions at tight junctions and how these interactions regulate barrier function. It also emphasizes evidence suggesting claudins can regulate scaffold protein and cytoskeleton interactions, thereby affecting tight junction morphology and barrier function.

In **Chapter 3**, I contributed to the work of former post-doc Barbara Schlingmann to understand the role of claudin-5 in barrier dysfunction with chronic alcohol consumption. Though barrier dysfunction has been associated with chronic alcohol abuse both clinically and with *in vivo* models, the role of claudins in conferring alcohol-induced barrier dysfunction has not been elucidated. Using an *in vitro* rat model of chronic alcohol abuse, claudin-5 was found to be expressed significantly higher in cells from alcohol-fed rats. The barrier function measurements transepithelial resistance and dye flux were used to correlate claudin-5 overexpression as necessary and sufficient to decrease barrier permeability. Additionally, alcohol and claudin-5 overexpression were associated with a change in tight junction morphology, specifically an increase in the number of cells with tight junction spikes. Through the use of super-resolution microscopy technique stochastic optical reconstruction microscopy (STORM) and proximity ligation assays, overexpression of claudin-5 correlated with an increase in claudin-5/claudin-18 co-localization and a decrease in claudin-18/ZO-1 co-localization. This suggests that claudin-5 *cis* interactions with claudin-18 disrupt interactions with scaffolding protein ZO-1, perhaps displacing claudin-18 from the tight junction complex integrated with the cytoskeleton. The prevailing model of tight junction assembly suggests that claudins assemble into tight junctions driven by interactions with scaffolding proteins and head-to-head interactions with tight junction proteins on adjacent cells.[23,47,165,166] Our lab challenged this model by demonstrating for the first time that *cis* claudin-claudin interactions can alter the ability to form a complex with the ZO-1 scaffold protein, disrupting assembly into barrier forming tight junctions. This evidence that tight junction assembly could be regulated by a change in claudin-18 interacting proteins suggests new routes to therapeutically improve barrier function by targeting factors that are responsible for rearrangement of claudin-18 into TJ spikes. Additionally, live-cell imaging revealed budding and fusion of vesicle-like particles at tight junction spikes. When treated with the endocytosis protein (dynamin) inhibitor Dynasore, the number of cells with tight junction spikes decreased, suggesting that tight junction spikes could

be areas of increased tight junction turnover and dynamin could be involved in tight junction spike function or formation. We found that the overexpression of claudin-5 in rat AECs contributed significantly to impaired barrier function and promoted the formation of spike-like protrusions at tight junctions, with ZO-1 and claudin-18 localized to spikes. Treating the cells with a peptide that antagonizes claudin-5 restored the barrier function and decreased the number of cells with the spike-like protrusions.

In **Chapter 4**, I used the observations we previously made in our rat model in Chapter 3 to further characterize tight junction spikes at a molecular level. By live-cell imaging, tight junction spikes appear to be relatively stable structures once formed. We auspiciously captured two tight junction spikes forming, which led to the observation that tight junction spikes undergo several morphological changes during formation. These different tight junction spike morphologies were captured in fixed samples imaged using the super-resolution Stimulated Emission Depletion (STED) microscopy technique. This technique allowed us to quantitatively determine increased enrichment of claudin-18 in tight junction spikes from control cells compared to spikes from alcohol cells. While the effects of dynamin inhibitors on rat lung alveolar epithelial cells have been measured, dynamin protein expression and localization were not fully characterized. We determined that dynamin-2 was the dominant dynamin isoform expressed by alveolar epithelial cells and show it was localizated to cell-cell junctions. We demonstrated an overall decrease in the number of tight junction spikes with Dynasore treatment. Interestingly, we noticed a change in actin morphology that accompanied the decrease in tight junction spikes with Dynasore treatment. We observed directional protrusion of tight junction spikes away from β-catenin rich junctions. Using a novel method for observing localized permeability, we observed an increase in permeability in cells overexpression claudin-5. Taken together, we demonstrated the heterogeneity of tight junction spikes and both a morphological and molecular level and suggest a possible role for dynamin-2 in tight junction spike formation through rearrangement of junctional actin.

In **Chapter 5**, I summarize my unpublished work on elucidating the local proteome of claudin-18 using BioID, a method of biotinylating proteins proximal to a BirA-conjugated protein (in this case, claudin-18). My results enabled identification of multiple candidate claudin-18 proximal proteins and revealed many untested interaction pathways that will be further investigated for their ability to regulate tight junction morphology and barrier function. Additionally, the experiments detailed in Chapter 5 provide a guide for conducting and troubleshooting future BioID experiments with BirA-claudin-18.

My dissertation research features a body of work focused on characterizing tight junction spikes and investigating their role in barrier function. I used a variety of established and novel techniques to examine and quantitatively assess tight junction spike composition and changes in tight junction spike populations in the context of chronic alcohol and claudin-5 overexpression. The findings from this body of work suggest a possible mechanism of tight junction spike-formation involving cytoskeletal changes facilitated by dynamin-2. The implications and future directions of this work are discussed in **Chapter 6**.

Literature cited

1 Betts JG, Young KA, Wise JA, Johnson E, Poe B, Kruse DH, *et al. Anatomy and Physiology*. Houston, Texas: OpenStax; 2013.

2 Ochs M, Nyengaard JR, Jung A, Knudsen L, Voigt M, Wahlers T, *et al.* The Number of Alveoli in the Human Lung. *Am J Resp Crit Care* 2012;**169**:120–4. https://doi.org/10.1164/rccm.200308-1107oc.

3 Crapo JD, Barry BE, Gehr P, Bachofen M, Weibel ER. Cell Number and Cell Characteristics of the Normal Human Lung. *American Review of Respiratory Disease* 1982;**126**:332–7. https://doi.org/10.1164/arrd.1982.125.6.740.

4 Pelosi P, Rocco PR. Effects of mechanical ventilation on the extracellular matrix. *Intens Care Med* 2008;**34**:631–9. https://doi.org/10.1007/s00134-007-0964-9.

5 Garat C, Kheradmand F, Albertine KH, Folkesson HG, Matthay MA. Soluble and insoluble fibronectin increases alveolar epithelial wound healing in vitro. *Am J Physiol-Lung C* 1996;**271**:L844–53. https://doi.org/10.1152/ajplung.1996.271.5.l844.

6 Chapman HA. Disorders of lung matrix remodeling. *J Clin Invest* 2004;**113**:148–57. https://doi.org/10.1172/jci20729.

7 Roman J. Extracellular matrix and lung inflammation. *Immunol Res* 1996;**15**:163–78. https://doi.org/10.1007/bf02918505.

8 Kim HJ, Henke CA, Savik SK, Ingbar DH. Integrin mediation of alveolar epithelial cell migration on fibronectin and type I collagen. *Am J Physiol-Lung C* 1997;**273**:L134–41. https://doi.org/10.1152/ajplung.1997.273.1.l134.

9 Chroneos Z, Sever-Chroneos Z, Shepherd V. Pulmonary Surfactant: An Immunological Perspective. *Cell Physiol Biochem* 2009;**25**:13–26. https://doi.org/10.1159/000272047.

10 Guillot L, Nathan N, Tabary O, Thouvenin G, Rouzic PL, Corvol H, *et al.* Alveolar epithelial cells: master regulators of lung homeostasis. *The International Journal of Biochemistry & Cell Biology* 2013;**45**:2568–73. https://doi.org/10.1016/j.biocel.2013.08.009.

11 Whitsett JA, Weaver TE. Hydrophobic Surfactant Proteins in Lung Function and Disease. *New Engl J Medicine* 2002;**347**:2141–8. https://doi.org/10.1056/nejmra022387.

12 Ashino Y, Ying X, Dobbs LG, Bhattacharya J. [Ca2+]i oscillations regulate type II cell exocytosis in the pulmonary alveolus. *Am J Physiol-Lung C* 2000;**279**:L5–13. https://doi.org/10.1152/ajplung.2000.279.1.l5.

13 Wang PM, Fujita E, Bhattacharya J. Vascular regulation of type II cell exocytosis. *Am J Physiol-Lung C* 2002;**282**:L912–6. https://doi.org/10.1152/ajplung.00303.2001.

14 Evans MJ, Cabral LJ, Stephens RJ, Freeman G. Transformation of alveolar Type 2 cells to Type 1 cells following exposure to NO2. *Exp Mol Pathol* 1975;**22**:142–50. https://doi.org/10.1016/0014-4800(75)90059-3.

15 Fehrenbach H. Alveolar epithelial type II cell: defender of the alveolus revisited. *Respir Res* 2001;**2**:33. https://doi.org/10.1186/rr36.

16 Eaton D, Helms M, Koval M. The contribution of epithelial sodium channels to alveolar function in health and disease. *Annu Rev Physiol* 2009. https://doi.org/10.1146/annurev.physiol.010908.163250.

17 Günzel D, Fromm M. Claudins and other tight junction proteins. *Comprehensive Physiology* 2012;**2**:1819–52. https://doi.org/10.1002/cphy.c110045.

18 Günzel D, Yu AS. Claudins and the modulation of tight junction permeability. *Physiological Reviews* 2013;**93**:525–69. https://doi.org/10.1152/physrev.00019.2012.

19 Itallie CM, Anderson JM. Architecture of tight junctions and principles of molecular composition. *Semin Cell Dev Biol* 2014;**36**:157–65. https://doi.org/10.1016/j.semcdb.2014.08.011.

20 Farquhar MG, Palade GE. Junctional complexes in various epithelia. *J Cell Biology* 1963;**17**:375–412. https://doi.org/10.1083/jcb.17.2.375.

21 Tsukita S, Furuse M, Itoh M. Multifunctional strands in tight junctions. *Nat Rev Mol Cell Bio* 2001;**2**:285–93. https://doi.org/10.1038/35067088.

22 Tsukita S, Furuse M, Tsukita S, Furuse M. Occludin and claudins in tight-junction strands: leading or supporting players? *Trends Cell Biol* 1999;**9**:268–73. https://doi.org/10.1016/s0962-8924(99)01578-0.

23 Umeda K, Ikenouchi J, Katahira-Tayama S, Furuse K, Sasaki H, Nakayama M, *et al.* ZO-1 and ZO-2 independently determine where claudins are polymerized in tight-junction strand formation. *Cell* 2006;**126**:741–54. https://doi.org/10.1016/j.cell.2006.06.043.

24 Krause G, Winkler L, Mueller SL, Haseloff RF, Piontek J, Blasig IE. Structure and function of claudins. *Biochimica et Biophysica Acta* 2008;**1778**:631–45. https://doi.org/10.1016/j.bbamem.2007.10.018.

25 Soini Y. Claudins in lung diseases. *Respir Res* 2011;**12**:70. https://doi.org/10.1186/1465-9921-12-70.

26 Coyne CB, Gambling TM, Boucher RC, Carson JL, Johnson LG. Role of claudin interactions in airway tight junctional permeability. *Am J Physiol-Lung C* 2003;**285**:L1166–78. https://doi.org/10.1152/ajplung.00182.2003.

27 Shen L, Weber CR, Raleigh DR, Yu D, Turner JR. Tight junction pore and leak pathways: a dynamic duo. *Annu Rev Physiol* 2011;**73**:283–309. https://doi.org/10.1146/annurev-physiol-012110-142150.

28 Milatz S, Krug SM, Rosenthal R, Günzel D, Müller D, Schulzke J-DD, *et al.* Claudin-3 acts as a sealing component of the tight junction for ions of either charge and uncharged solutes. *Biochimica et Biophysica Acta* 2010;**1798**:2048–57. https://doi.org/10.1016/j.bbamem.2010.07.014.

29 Inai T, Kobayashi J, Shibata Y. Claudin-1 contributes to the epithelial barrier function in MDCK cells. *Eur J Cell Biol* 1999;**78**:849–55. https://doi.org/10.1016/s0171-9335(99)80086-7.

30 Angelow S, Yu ASL. Structure-Function Studies of Claudin Extracellular Domains by Cysteine-scanning Mutagenesis. *J Biol Chem* 2009;**284**:29205–17. https://doi.org/10.1074/jbc.m109.043752.

31 Yu ASL, Cheng MH, Angelow S, Günzel D, Kanzawa SA, Schneeberger EE, *et al.* Molecular Basis for Cation Selectivity in Claudin-2–based Paracellular Pores: Identification of an Electrostatic Interaction Site. *J Gen Physiology* 2009;**133**:111–27. https://doi.org/10.1085/jgp.200810154.

32 Lim TS, Vedula SRK, Hui S, Kausalya PJ, Hunziker W, Lim CT. Probing effects of pH change on dynamic response of Claudin-2 mediated adhesion using single molecule force spectroscopy. *Exp Cell Res* 2008;**314**:2643–51. https://doi.org/10.1016/j.yexcr.2008.05.015.

33 Lim TS, Vedula SRK, Hunziker W, Lim CT. Kinetics of Adhesion Mediated by Extracellular Loops of Claudin-2 as Revealed by Single-Molecule Force Spectroscopy. *J Mol Biol* 2008;**381**:681–91. https://doi.org/10.1016/j.jmb.2008.06.009.

34 Günzel D, Stuiver M, Kausalya PJ, Haisch L, Krug SM, Rosenthal R, *et al.* Claudin-10 exists in six alternatively spliced isoforms that exhibit distinct localization and function. *J Cell Sci* 2009;**122**:1507–17. https://doi.org/10.1242/jcs.040113.

35 Itallie CMV, Rogan S, Yu A, Vidal LS, Holmes J, Anderson JM. Two splice variants of claudin-10 in the kidney create paracellular pores with different ion selectivities. *Am J Physiol-Renal* 2006;**291**:F1288–99. https://doi.org/10.1152/ajprenal.00138.2006.

36 Itallie CMV, Fanning AS, Anderson JM. Reversal of charge selectivity in cation or anion-selective epithelial lines by expression of different claudins. *American Journal of Physiology Renal Physiology* 2003;**285**:F1078-84. https://doi.org/10.1152/ajprenal.00116.2003.

37 Itallie CV, Rahner C, Anderson JM. Regulated expression of claudin-4 decreases paracellular conductance through a selective decrease in sodium permeability. *J Clin Invest* 2001;**107**:1319–27. https://doi.org/10.1172/jci12464.

38 Hou J, Renigunta A, Yang J, Waldegger S. Claudin-4 forms paracellular chloride channel in the kidney and requires claudin-8 for tight junction localization. *Proc National Acad Sci* 2010;**107**:18010–5. https://doi.org/10.1073/pnas.1009399107.

39 Angelow S, Schneeberger EE, Yu ASL. Claudin-8 Expression in Renal Epithelial Cells Augments the Paracellular Barrier by Replacing Endogenous Claudin-2. *J Membrane Biol* 2007;**215**:147–59. https://doi.org/10.1007/s00232-007-9014-3.

40 Angelow S, Kim K, Yu ASL. Claudin-8 modulates paracellular permeability to acidic and basic ions in MDCK II cells. *J Physiology* 2006;**571**:15–26. https://doi.org/10.1113/jphysiol.2005.099135.

41 Furuse M, Sasaki H, Fujimoto K, Tsukita S. A Single Gene Product, Claudin-1 or -2, Reconstitutes Tight Junction Strands and Recruits Occludin in Fibroblasts. *J Cell Biol* 1998;**143**:391–401. https://doi.org/10.1083/jcb.143.2.391.

42 Rossa J, Protze J, Kern C, Piontek A, Günzel D, Krause G, *et al.* Molecular and structural transmembrane determinants critical for embedding claudin-5 into tight junctions reveal a distinct four-helix bundle arrangement. *Biochem J* 2014;**464**:49–60. https://doi.org/10.1042/bj20140431.

43 Suzuki H, Nishizawa T, Tani K, Yamazaki Y. Crystal structure of a claudin provides insight into the architecture of tight junctions. *Null* 2014. https://doi.org/10.1126/science.1248571.

44 Suzuki H, Tani K, Tamura A, Tsukita S, Fujiyoshi Y. Model for the architecture of claudin-based paracellular ion channels through tight junctions. *J Mol Biol* 2014;**427**:291–7. https://doi.org/10.1016/j.jmb.2014.10.020.

45 Itallie CMV, Mitic LL, Anderson JM. Claudin-2 forms homodimers and is a component of a high molecular weight protein complex. *J Biol Chem* 2011;**286**:3442–50. https://doi.org/10.1074/jbc.m110.195578.

46 Lal-Nag M, Morin PJ. The claudins. *Genome Biol* 2009;**10**:235. https://doi.org/10.1186/gb-2009-10-8-235.

47 Itoh M, Furuse M, Morita K, Kubota K, Saitou M, Tsukita S. Direct binding of three tight junction-associated MAGUKs, ZO-1, ZO-2, and ZO-3, with the COOH termini of claudins. *J Cell Biol* 1999;**147**:1351–63.

48 Itallie CMV, Gambling TM, Carson JL, Anderson JM. Palmitoylation of claudins is required for efficient tight-junction localization. *J Cell Sci* 2005;**118**:1427–36. https://doi.org/10.1242/jcs.01735.

49 Itallie CMV, Tietgens AJ, LoGrande K, Aponte A, Gucek M, Anderson JM. Phosphorylation of claudin-2 on serine 208 promotes membrane retention and reduces trafficking to lysosomes. *J Cell Sci* 2012;**125**:4902–12. https://doi.org/10.1242/jcs.111237.

50 Itallie CMV, Anderson JM. Phosphorylation of tight junction transmembrane proteins: Many sites, much to do. *Tissue Barriers* 2017;**6**:e1382671. https://doi.org/10.1080/21688370.2017.1382671.

51 Banan A, Zhang LJ, Shaikh M, Fields JZ, Choudhary S, Forsyth CB, *et al.* θ Isoform of Protein Kinase C Alters Barrier Function in Intestinal Epithelium through Modulation of Distinct Claudin Isotypes: A Novel Mechanism for Regulation of Permeability. *J Pharmacol Exp Ther* 2005;**313**:962–82. https://doi.org/10.1124/jpet.105.083428.

52 Ikari A, Ito M, Okude C, Sawada H, Harada H, Degawa M, *et al.* Claudin-16 is directly phosphorylated by protein kinase a independently of a vasodilator-stimulated phosphoprotein-mediated pathway. *J Cell Physiol* 2008;**214**:221–9. https://doi.org/10.1002/jcp.21178.

53 Reiche J, Huber O. Post-translational modifications of tight junction transmembrane proteins and their direct effect on barrier function. *Biochimica Et Biophysica Acta Bba - Biomembr* 2020;**1862**:183330. https://doi.org/10.1016/j.bbamem.2020.183330.

54 Krystofiak ES, Heymann JB, Kachar B. Carbon replicas reveal double stranded structure of tight junctions in phase-contrast electron microscopy. *Commun Biology* 2019;**2**:98. https://doi.org/10.1038/s42003-019-0319-4.

55 Zhao J, Krystofiak ES, Ballesteros A, Cui R, Itallie CMV, Anderson JM, *et al.* Multiple claudin-claudin cis interfaces are required for tight junction strand formation and inherent flexibility. *Communications Biology* 2018;**1**:50. https://doi.org/10.1038/s42003-018-0051-5.

56 Piontek J, Krug SM, Protze J, Krause G, Fromm M. Molecular architecture and assembly of the tight junction backbone. *Biochim Biophys Acta Biomembr* 2020:183279. https://doi.org/10.1016/j.bbamem.2020.183279.

57 Varadarajan S, Stephenson RE, Miller AL. Multiscale dynamics of tight junction remodeling. *J Cell Sci* 2019;**132**:jcs229286. https://doi.org/10.1242/jcs.229286.

58 Otani T, Nguyen TP, Tokuda S, Sugihara K, Sugawara T, Furuse K, *et al.* Claudins and JAM-A coordinately regulate tight junction formation and epithelial polarityClaudins and JAM-A in tight junction formation. *J Cell Biology* 2019;**218**:3372–96. https://doi.org/10.1083/jcb.201812157.

59 Yonemura S, Itoh M, Nagafuchi A, Tsukita S. Cell-to-cell adherens junction formation and actin filament organization: similarities and differences between non-polarized fibroblasts and polarized epithelial cells. *J Cell Sci* 1995;**108 (Pt 1)**:127–42.

60 Ando-Akatsuka Y, Yonemura S, Itoh M, Furuse M, Tsukita S. Differential behavior of E-cadherin and occludin in their colocalization with ZO-1 during the establishment of epithelial cell polarity. *J Cell Physiol* 1999;**179**:115–25. https://doi.org/10.1002/(sici)1097-4652(199905)179:2<115::aid-jcp1>3.0.co;2-t.

61 Suzuki A, Ishiyama C, Hashiba K, Shimizu M, Ebnet K, Ohno S. aPKC kinase activity is required for the asymmetric differentiation of the premature junctional complex during epithelial cell polarization. *J Cell Sci* 2002;**115**:3565–73. https://doi.org/10.1242/jcs.00032.

62 Phua DCY, Xu J, Ali SM, Boey A, Gounko NV, Hunziker W. ZO-1 and ZO-2 Are Required for Extra-Embryonic Endoderm Integrity, Primitive Ectoderm Survival and Normal Cavitation in

Embryoid Bodies Derived from Mouse Embryonic Stem Cells. *Plos One* 2014;**9**:e99532. https://doi.org/10.1371/journal.pone.0099532.

63 Spadaro D, Le S, Laroche T, Mean I, Jond L, Yan J, *et al.* Tension-Dependent Stretching Activates ZO-1 to Control the Junctional Localization of Its Interactors. *Current Biology : CB* 2017. https://doi.org/10.1016/j.cub.2017.11.014.

64 Beutel O, Maraspini R, Pombo-García K, Martin-Lemaitre C, Honigmann A. Phase Separation of Zonula Occludens Proteins Drives Formation of Tight Junctions. *Cell* 2019;**179**:923-936.e11. https://doi.org/10.1016/j.cell.2019.10.011.

65 Schwayer C, Shamipour S, Pranjic-Ferscha K, Schauer A, Balda M, Tada M, *et al.* Mechanosensation of Tight Junctions Depends on ZO-1 Phase Separation and Flow. *Cell* 2019;**179**:937-952.e18. https://doi.org/10.1016/j.cell.2019.10.006.

66 Itallie CM, Lidman K, Tietgens A, Anderson J. Newly synthesized claudins but not occludin are added to the basal side of the tight junction. *Molecular Biology of the Cell* 2019;**30**:1406–24. https://doi.org/10.1091/mbc.e19-01-0008.

67 Shigetomi K, Ono Y, Inai T, Ikenouchi J. Adherens junctions influence tight junction formation via changes in membrane lipid composition. *J Cell Biol* 2018. https://doi.org/10.1083/jcb.201711042.

68 Lynch RD, Francis SA, McCarthy KM, Casas E, Thiele C, Schneeberger EE. Cholesterol depletion alters detergent-specific solubility profiles of selected tight junction proteins and the phosphorylation of occludin. *Exp Cell Res* 2007;**313**:2597–610. https://doi.org/10.1016/j.yexcr.2007.05.009.

69 Kady NM, Liu X, Lydic TA, Syed MH, Navitskaya S, Wang Q, *et al.* ELOVL4-Mediated Production of Very Long-Chain Ceramides Stabilizes Tight Junctions and Prevents Diabetes-Induced Retinal Vascular Permeability. *Diabetes* 2018;**67**:769–81. https://doi.org/10.2337/db17-1034.

70 Nusrat A, Parkos CA, Verkade P, Foley CS, Liang TW, Innis-Whitehouse W, *et al.* Tight junctions are membrane microdomains. *J Cell Sci* 2000;**113 (Pt 10)**:1771–81.

71 Ivanov AI, Nusrat A, Parkos CA. Endocytosis of epithelial apical junctional proteins by a clathrin-mediated pathway into a unique storage compartment. *Molecular Biology of the Cell* 2004;**15**:176–88. https://doi.org/10.1091/mbc.e03-05-0319.

72 Yu D, Turner JR. Stimulus-induced reorganization of tight junction structure: the role of membrane traffic. *Biochimica et Biophysica Acta* 2008;**1778**:709–16. https://doi.org/10.1016/j.bbamem.2007.07.027.

73 Bruewer M, Utech M, Ivanov AI, Hopkins AM, Parkos CA, Nusrat A. Interferon-γ induces internalization of epithelial tight junction proteins via a macropinocytosis-like process. *Faseb J* 2005;**19**:923–33. https://doi.org/10.1096/fj.04-3260com.

74 Matsuda M, Kubo A, Furuse M, Tsukita S. A peculiar internalization of claudins, tight junction-specific adhesion molecules, during the intercellular movement of epithelial cells. *J Cell Sci* 2004;**117**:1247–57. https://doi.org/10.1242/jcs.00972.

75 Capaldo CT, Farkas AE, Hilgarth RS, Krug SM, Wolf MF, Benedik JK, *et al.* Proinflammatory cytokine-induced tight junction remodeling through dynamic self-assembly of claudins. *Molecular Biology of the Cell* 2014;**25**:2710–9. https://doi.org/10.1091/mbc.e14-02-0773.

76 Dukes JD, Fish L, Richardson JD, Blaikley E, Burns S, Caunt CJ, *et al.* Functional ESCRT machinery is required for constitutive recycling of claudin-1 and maintenance of polarity in vertebrate epithelial cells. *Mol Biol Cell* 2011;**22**:3192–205. https://doi.org/10.1091/mbc.e11-04-0343.

77 Dukes JD, Whitley P, Chalmers AD. The PIKfyve Inhibitor YM201636 Blocks the Continuous Recycling of the Tight Junction Proteins Claudin-1 and Claudin-2 in MDCK cells. *PLoS One* 2012;**7**:e28659. https://doi.org/10.1371/journal.pone.0028659.

78 Morimoto S, Nishimura N, Terai T, Manabe S, Yamamoto Y, Shinahara W, *et al.* Rab13 Mediates the Continuous Endocytic Recycling of Occludin to the Cell Surface. *J Biol Chem* 2005;**280**:2220–8. https://doi.org/10.1074/jbc.m406906200.

79 Shen L, Weber CR, Turner JR. The tight junction protein complex undergoes rapid and continuous molecular remodeling at steady state. *J Cell Biology* 2008;**181**:683–95. https://doi.org/10.1083/jcb.200711165.

80 LaFemina MJ, Rokkam D, Chandrasena A, Pan J, Bajaj A, Johnson M, *et al.* Keratinocyte growth factor enhances barrier function without altering claudin expression in primary alveolar epithelial cells. *Am J Physiol-Lung C* 2010;**299**:L724–34. https://doi.org/10.1152/ajplung.00233.2010.

81 Overgaard CE, Mitchell LA, Koval M. Roles for claudins in alveolar epithelial barrier function. *Annals of the New York Academy of Sciences* 2012;**1257**:167–74. https://doi.org/10.1111/j.1749-6632.2012.06545.x.

82 Wang F, Daugherty B, Keise LL, Wei Z, Foley JP, Savani RC, *et al.* Heterogeneity of Claudin Expression by Alveolar Epithelial Cells. *Am J Resp Cell Mol* 2003;**29**:62–70. https://doi.org/10.1165/rcmb.2002-0180oc.

83 Mitchell LA, Overgaard CE, Ward C, Margulies SS, Koval M. Differential effects of claudin-3 and claudin-4 on alveolar epithelial barrier function. *Am J Physiol-Lung C* 2011;**301**:L40–9. https://doi.org/10.1152/ajplung.00299.2010.

84 Daugherty BL, Ward C, Smith T, Ritzenthaler JD, Koval M. Regulation of heterotypic claudin compatibility. *J Biol Chem* 2007;**282**:30005–13. https://doi.org/10.1074/jbc.m703547200.

85 Piontek J, Fritzsche S, Cording J, Richter S, Hartwig J, Walter M, *et al.* Elucidating the principles of the molecular organization of heteropolymeric tight junction strands. *Cell Mol Life Sci* 2011;**68**:3903–18. https://doi.org/10.1007/s00018-011-0680-z.

86 Furuse M, Sasaki H, Tsukita S. Manner of Interaction of Heterogeneous Claudin Species within and between Tight Junction Strands. *J Cell Biology* 1999;**147**:891–903. https://doi.org/10.1083/jcb.147.4.891.

87 Fernandez AL, Koval M, Fan X, Guidot DM. Chronic alcohol ingestion alters claudin expression in the alveolar epithelium of rats. *Alcohol (Fayetteville, NY)* 2007;**41**:371–9. https://doi.org/10.1016/j.alcohol.2007.04.010.

88 Kage H, Flodby P, Gao D, Kim YH, Marconett CN, DeMaio L, *et al.* Claudin 4 knockout mice: normal physiological phenotype with increased susceptibility to lung injury. *Am J Physiol Lung Cell Mol Physiol* 2014;**307**:L524-36. https://doi.org/10.1152/ajplung.00077.2014.

89 Rokkam D, LaFemina MJ, Lee JW, Matthay MA, Frank JA. Claudin-4 Levels Are Associated with Intact Alveolar Fluid Clearance in Human Lungs. *Am J Pathology* 2011;**179**:1081–7. https://doi.org/10.1016/j.ajpath.2011.05.017.

90 Wray C, Mao Y, Pan J, Chandrasena A, Piasta F, Frank JA. Claudin-4 augments alveolar epithelial barrier function and is induced in acute lung injury. *Am J Physiol Lung Cell Mol Physiol* 2009;**297**:L219-27. https://doi.org/10.1152/ajplung.00043.2009.

91 Li G, Flodby P, Luo J, Kage H, Sipos A, Gao D, *et al.* Knockout mice reveal key roles for claudin 18 in alveolar barrier properties and fluid homeostasis. *Am J Resp Cell Mol* 2014;**51**:210–22. https://doi.org/10.1165/rcmb.2013-0353oc.

92 LaFemina MJ, Sutherland KM, Bentley T, Gonzales LW, Allen L, Chapin CJ, *et al.* Claudin-18 deficiency results in alveolar barrier dysfunction and impaired alveologenesis in mice. *Am J Resp Cell Mol* 2014;**51**:550–8. https://doi.org/10.1165/rcmb.2013-0456OC.

93 Daugherty BL, Mateescu M, Patel AS, Wade K, Kimura S, Gonzales LW, *et al.* Developmental regulation of claudin localization by fetal alveolar epithelial cells. *Am J Physiol Lung Cell Mol Physiol* 2004;**287**:L1266-73. https://doi.org/10.1152/ajplung.00423.2003.

94 Fang X, Neyrinck AP, Matthay MA, Lee JW. Allogeneic Human Mesenchymal Stem Cells Restore Epithelial Protein Permeability in Cultured Human Alveolar Type II Cells by

Secretion of Angiopoietin-1. *Journal of Biological Chemistry* 2010;**285**:26211–22. https://doi.org/10.1074/jbc.m110.119917.

95 Schlingmann B, Overgaard CE, Molina SA, Lynn KS, Mitchell LA, White SD, *et al.* Regulation of claudin/zonula occludens-1 complexes by hetero-claudin interactions. *Nat Commun* 2016;**7**:12276. https://doi.org/10.1038/ncomms12276.

96 Zhou B, Flodby P, Luo J, Castillo DR, Liu Y, Yu F-XX, *et al.* Claudin-18-mediated YAP activity regulates lung stem and progenitor cell homeostasis and tumorigenesis. *The Journal of Clinical Investigation* 2018. https://doi.org/10.1172/jci90429.

97 Matthay MA, Zemans RL, Zimmerman GA, Arabi YM, Beitler JR, Mercat A, *et al.* Acute respiratory distress syndrome. *Nat Rev Dis Primers* 2019;**5**:18. https://doi.org/10.1038/s41572-019-0069-0.

98 Rubenfeld GD, Caldwell E, Peabody E, Weaver J, Martin DP, Neff M, *et al.* Incidence and outcomes of acute lung injury. *The New England Journal of Medicine* 2005;**353**:1685–93. https://doi.org/10.1056/NEJMoa050333.

99 Laffey JG, Bellani G, Pham T, Fan E, Madotto F, Bajwa EK, *et al.* Potentially modifiable factors contributing to outcome from acute respiratory distress syndrome: the LUNG SAFE study. *Intensive Care Medicine* 2016;**42**:1865–76. https://doi.org/10.1007/s00134-016-4571-5.

100 Ware LB, Matthay MA. Alveolar Fluid Clearance Is Impaired in the Majority of Patients with Acute Lung Injury and the Acute Respiratory Distress Syndrome. *Am J Resp Crit Care* 2001;**163**:1376–83. https://doi.org/10.1164/ajrccm.163.6.2004035.

101 Koval M. Claudin heterogeneity and control of lung tight junctions. *Annu Rev Physiol* 2013;**75**:551–67. https://doi.org/10.1146/annurev-physiol-030212-183809.

102 Overgaard CE, Daugherty BL, Mitchell LA, Koval M. Claudins: control of barrier function and regulation in response to oxidant stress. *Antioxidants & Redox Signaling* 2011;**15**:1179–93. https://doi.org/10.1089/ars.2011.3893.

103 Berkowitz DM, Danai PA, Eaton S, Moss M, Martin GS. Alcohol abuse enhances pulmonary edema in acute respiratory distress syndrome. *Alcoholism, Clinical and Experimental Research* 2009;**33**:1690–6. https://doi.org/10.1111/j.1530-0277.2009.01005.x.

104 Burnham EL, Halkar R, Burks M, Moss M. The effects of alcohol abuse on pulmonary alveolar-capillary barrier function in humans. *Alcohol and Alcoholism (Oxford, Oxfordshire)* 2009;**44**:8–12. https://doi.org/10.1093/alcalc/agn051.

105 Moss M, Parsons PE, Steinberg KP, Hudson LD, Guidot DM, Burnham EL, *et al.* Chronic alcohol abuse is associated with an increased incidence of acute respiratory distress syndrome and severity of multiple organ dysfunction in patients with septic shock. *Critical Care Medicine* 2003;**31**:869–77. https://doi.org/10.1097/01.ccm.0000055389.64497.11.

106 Moss M, Bucher B, Moore F, Moore E, Parsons P. The role of chronic alcohol abuse in the development of acute respiratory distress syndrome in adults. *JAMA* 1996;**275**:50–4. https://doi.org/10.1001/jama.1996.03530250054027.

107 Sturrock A, Cahill B, Norman K, Huecksteadt TP, Hill K, Sanders K, *et al.* Transforming growth factor-β1 induces Nox4 NAD(P)H oxidase and reactive oxygen species-dependent proliferation in human pulmonary artery smooth muscle cells. *Am J Physiol-Lung C* 2006;**290**:L661–73. https://doi.org/10.1152/ajplung.00269.2005.

108 Arsalane K, Dubois CM, Muanza T, Bégin R, Boudreau F, Asselin C, *et al.* Transforming Growth Factor- β1 Is a Potent Inhibitor of Glutathione Synthesis in the Lung Epithelial Cell Line A549: Transcriptional Effect on the GSH Rate-limiting Enzyme γ -Glutamylcysteine Synthetase. *Am J Resp Cell Mol* 1997;**17**:599–607. https://doi.org/10.1165/ajrcmb.17.5.2833.

109 Jardine H, MacNee W, Donaldson K, Rahman I. Molecular Mechanism of Transforming Growth Factor (TGF)-β1-induced Glutathione Depletion in Alveolar Epithelial Cells. *J Biol Chem* 2002;**277**:21158–66. https://doi.org/10.1074/jbc.m112145200.

110 Waghray M, Cui Z, Horowitz JC, Subramanian IM, Martinez FJ, Toews GB, *et al.* Hydrogen peroxide is a diffusible paracrine signal for the induction of epithelial cell death by activated myofibroblasts. *Faseb J* 2005;**19**:1–16. https://doi.org/10.1096/fj.04-2882fje.

111 Lieber C. Biochemical Factors in Alcoholic Liver Disease. *Semin Liver Dis* 1993;**13**:136–53. https://doi.org/10.1055/s-2007-1007345.

112 Brown LAS, Harris FL, Ping X-D, Gauthier TW. Chronic ethanol ingestion and the risk of acute lung injury: a role for glutathione availability? *Alcohol* 2004;**33**:191–7. https://doi.org/10.1016/j.alcohol.2004.08.002.

113 Morris PE, Bernard CR. Significance of Glutathione in Lung Disease and Implications for Therapy. *Am J Medical Sci* 1994;**307**:119–27. https://doi.org/10.1097/00000441-199402000-00010.

114 Moss M, Guidot DM, Wong-Lambertina M, Hoor TT, Perez RL, Brown LAS. The Effects of Chronic Alcohol Abuse on Pulmonary Glutathione Homeostasis. *Am J Resp Crit Care* 2000;**161**:414–9. https://doi.org/10.1164/ajrccm.161.2.9905002.

115 Burnham EL, Brown LAS, Halls L, Moss M. Effects of Chronic Alcohol Abuse on Alveolar Epithelial Barrier Function and Glutathione Homeostasis. *Alcohol Clin Exp Res* 2003;**27**:1167–72. https://doi.org/10.1097/01.alc.0000075821.34270.98.

116 Guidot DM, Modelska K, Lois M, Jain L, Moss IM, Pittet J-F, *et al.* Ethanol ingestion via glutathione depletion impairs alveolar epithelial barrier function in rats. *Am J Physiol Lung Cell Mol Physiol* 2000;**279**:L127–35. https://doi.org/10.1152/ajplung.2000.279.1.l127.

117 Brown LAS, Harris FL, Guidot DM. Chronic ethanol ingestion potentiates TNF-α-mediated oxidative stress and apoptosis in rat type II cells. *Am J Physiol-Lung C* 2001;**281**:L377–86. https://doi.org/10.1152/ajplung.2001.281.2.l377.

118 Guidot DM, Brown AS. Mitochondrial Glutathione Replacement Restores Surfactant Synthesis and Secretion in Alveolar Epithelial Cells of Ethanol-Fed Rats. *Alcohol Clin Exp Res* 2000;**24**:1070–6. https://doi.org/10.1111/j.1530-0277.2000.tb04652.x.

119 Brown LAS, Harris FL, Bechara R, Guidot DM. Effect of Chronic Ethanol Ingestion on Alveolar Type II Cell: Glutathione and Inflammatory Mediator-Induced Apoptosis. *Alcohol Clin Exp Res* 2001;**25**:1078–85. https://doi.org/10.1111/j.1530-0277.2001.tb02320.x.

120 Liang Y, Harris FL, Brown LAS. Alcohol induced mitochondrial oxidative stress and alveolar macrophage dysfunction. *Biomed Res Int* 2014;**2014**:1–13. https://doi.org/10.1155/2014/371593.

121 Liang Y, Harris FL, Jones DP, Brown LAS. Alcohol induces mitochondrial redox imbalance in alveolar macrophages. *Free Radical Bio Med* 2013;**65**:1427–34. https://doi.org/10.1016/j.freeradbiomed.2013.10.010.

122 Yeligar SM, Mehta AJ, Harris FL, Brown LAS, Hart CM. Peroxisome Proliferator–Activated Receptor γ Regulates Chronic Alcohol-Induced Alveolar Macrophage Dysfunction. *Am J Resp Cell Mol* 2015;**55**:35–46. https://doi.org/10.1165/rcmb.2015-0077oc.

123 Yeligar SM, Harris FL, Hart CM, Brown LAS. Ethanol Induces Oxidative Stress in Alveolar Macrophages via Upregulation of NADPH Oxidases. *J Immunol* 2012;**188**:3648–57. https://doi.org/10.4049/jimmunol.1101278.

124 Alli AA, Brewer EM, Montgomery DS, Ghant MS, Eaton DC, Brown LA, *et al.* Chronic ethanol exposure alters the lung proteome and leads to mitochondrial dysfunction in alveolar type 2 cells. *Am J Physiol-Lung C* 2014;**306**:L1026–35. https://doi.org/10.1152/ajplung.00287.2013.

125 Chakraborty K, Raundhal M, Chen BB, Morse C, Tyurina YY, Khare A, *et al.* The mito-DAMP cardiolipin blocks IL-10 production causing persistent inflammation during bacterial pneumonia. *Nat Commun* 2017;**8**:13944. https://doi.org/10.1038/ncomms13944.

126 Lee Y-L, Obiako B, Gorodnya OM, Ruchko MV, Kuck JL, Pastukh VM, *et al.* Mitochondrial DNA Damage Initiates Acute Lung Injury and Multi-Organ System Failure Evoked in Rats by Intra-Tracheal Pseudomonas Aeruginosa. *Shock* 2017;**48**:54–60. https://doi.org/10.1097/shk.0000000000000838.

127 Sadikot RT, Bedi B, Li J, Yeligar SM. Alcohol-induced mitochondrial DNA damage promotes injurious crosstalk between alveolar epithelial cells and alveolar macrophages. *Alcohol* 2018;**80**:65–72. https://doi.org/10.1016/j.alcohol.2018.08.006.

128 Ward C, Schlingmann B, Stecenko AA, Guidot DM, Koval M. NF-κB inhibitors impair lung epithelial tight junctions in the absence of inflammation. *Tissue Barriers* 2015;**3**:e982424. https://doi.org/10.4161/21688370.2014.982424.

129 Mehta AJ, Yeligar SM, Elon L, Brown LA, Guidot DM. Alcoholism causes alveolar macrophage zinc deficiency and immune dysfunction. *American Journal of Respiratory and Critical Care Medicine* 2013;**188**:716–23. https://doi.org/10.1164/rccm.201301-0061OC.

130 Joshi PC, Applewhite L, Mitchell PO, Fernainy K, Roman J, Eaton DC, *et al.* GM-CSF receptor expression and signaling is decreased in lungs of ethanol-fed rats. *Am J Physiol-Lung C* 2006;**291**:L1150–8. https://doi.org/10.1152/ajplung.00150.2006.

131 Mehta AJ, Joshi PC, Fan X, Brown LA, Ritzenthaler JD, Roman J, *et al.* Zinc supplementation restores PU.1 and Nrf2 nuclear binding in alveolar macrophages and improves redox balance and bacterial clearance in the lungs of alcohol-fed rats. *Alcoholism, Clinical and Experimental Research* 2011;**35**:1519–28. https://doi.org/10.1111/j.1530-0277.2011.01488.x.

132 Tudor R, Zalewski PD, Ratnaike RN. Zinc in health and chronic disease. *J Nutrition Heal Aging* 2005;**9**:45–51.

133 Joshi PC, Mehta A, Jabber WS, Fan X, Guidot DM. Zinc deficiency mediates alcohol-induced alveolar epithelial and macrophage dysfunction in rats. *Am J Resp Cell Mol* 2009;**41**:207–16. https://doi.org/10.1165/rcmb.2008-0209oc.

134 Otis JS, Mitchell PO, Kershaw CD, Joshi PC, Guidot DM. Na,K-ATPase expression is increased in the lungs of alcohol-fed rats. *Alcoholism, Clinical and Experimental Research* 2008;**32**:699–705. https://doi.org/10.1111/j.1530-0277.2008.00626.x.

135 Downs CA, Trac DQ, Kreiner LH, Eaton AF, Johnson NM, Brown LA, *et al.* Ethanol Alters Alveolar Fluid Balance via Nadph Oxidase (NOX) Signaling to Epithelial Sodium Channels (ENaC) in the Lung. *Plos One* 2013;**8**:e54750. https://doi.org/10.1371/journal.pone.0054750.

136 Peters DM, Vadász I, Wujak Ł, Wygrecka M, Olschewski A, Becker C, *et al.* TGF-β directs trafficking of the epithelial sodium channel ENaC which has implications for ion and fluid transport in acute lung injury. *Proc National Acad Sci* 2014;**111**:E374–83. https://doi.org/10.1073/pnas.1306798111.

137 Overgaard CE, Schlingmann B, White SD, Ward C, Fan X, Swarnakar S, *et al.* The relative balance of GM-CSF and TGF-β1 regulates lung epithelial barrier function. *Am J Physiol Lung Cell Mol Physiol* 2015;**308**:L1212-23. https://doi.org/10.1152/ajplung.00042.2014.

138 Pittet J-F, Griffiths MJD, Geiser T, Kaminski N, Dalton SL, Huang X, *et al.* TGF-β is a critical mediator of acute lung injury. *J Clin Invest* 2001;**107**:1537–44. https://doi.org/10.1172/jci11963.

139 Bechara RI, Brown LAS, Roman J, Joshi PC, Guidot DM. Transforming Growth Factor β1 Expression and Activation Is Increased in the Alcoholic Rat Lung. *Am J Resp Crit Care* 2004;**170**:188–94. https://doi.org/10.1164/rccm.200304-478oc.

140 Curry-McCoy TV, Venado A, Guidot DM, Joshi PC. Alcohol ingestion disrupts alveolar epithelial barrier function by activation of macrophage-derived transforming growth factor beta1. *Respiratory Research* 2013;**14**:39. https://doi.org/10.1186/1465-9921-14-39.

141 Taylor AW. Review of the activation of TGF-β in immunity. *J Leukocyte Biol* 2009;**85**:29–33. https://doi.org/10.1189/jlb.0708415.

142 Liu R-M, Pravia KAG. Oxidative stress and glutathione in TGF-β-mediated fibrogenesis. *Free Radical Bio Med* 2010;**48**:1–15. https://doi.org/10.1016/j.freeradbiomed.2009.09.026.

143 Feinberg MW, Cao Z, Wara AK, Lebedeva MA, SenBanerjee S, Jain MK. Kruppel-like Factor 4 Is a Mediator of Proinflammatory Signaling in Macrophages. *J Biol Chem* 2005;**280**:38247–58. https://doi.org/10.1074/jbc.m509378200.

144 Curry-McCoy TV, Guidot DM, Joshi PC. Chronic alcohol ingestion in rats decreases Krüppel-like factor 4 expression and intracellular zinc in the lung. *Alcoholism, Clinical and Experimental Research* 2013;**37**:361–71. https://doi.org/10.1111/j.1530-0277.2012.01946.x.

145 Bechara RI, Pelaez A, Palacio A, Joshi PC, Hart CM, Brown LAS, *et al.* Angiotensin II mediates glutathione depletion, transforming growth factor-β1 expression, and epithelial barrier dysfunction in the alcoholic rat lung. *Am J Physiol-Lung C* 2005;**289**:L363–70. https://doi.org/10.1152/ajplung.00141.2005.

146 Brown SD, Brown LAS. Ethanol (EtOH)-Induced TGF-β1 and Reactive Oxygen Species Production Are Necessary for EtOH-Induced Alveolar Macrophage Dysfunction and Induction of Alternative Activation. *Alcohol Clin Exp Res* 2012;**36**:1952–62. https://doi.org/10.1111/j.1530-0277.2012.01825.x.

147 Guinee D, Brambilla E, Fleming M, Hayashi T, Rahn M, Koss M, *et al.* The potential role of BAX and BCL-2 expression in diffuse alveolar damage. *Am J Pathology* 1997;**151**:999–1007.

148 Albertine KH, Soulier MF, Wang Z, Ishizaka A, Hashimoto S, Zimmerman GA, *et al.* Fas and Fas Ligand Are Up-Regulated in Pulmonary Edema Fluid and Lung Tissue of Patients with Acute Lung Injury and the Acute Respiratory Distress Syndrome. *Am J Pathology* 2002;**161**:1783–96. https://doi.org/10.1016/s0002-9440(10)64455-0.

149 Matute-Bello G, Winn RK, Jonas M, Chi EY, Martin TR, Liles WC. Fas (CD95) Induces Alveolar Epithelial Cell Apoptosis in Vivo Implications for Acute Pulmonary Inflammation. *Am J Pathology* 2001;**158**:153–61. https://doi.org/10.1016/s0002-9440(10)63953-3.

150 Sugahara K, Kiyota T, Clark RAF, Mason RJ. The effect of fibronectin on cytoskeleton structure and transepithelial resistance of alveolar type II cells in primary culture. *Virchows Archiv B* 1993;**64**:115–22. https://doi.org/10.1007/bf02915103.

151 Koval M, Ward C, Findley MK, Roser-Page S, Helms MN, Roman J. Extracellular Matrix Influences Alveolar Epithelial Claudin Expression and Barrier Function. *Am J Resp Cell Mol* 2010;**42**:172–80. https://doi.org/10.1165/rcmb.2008-0270oc.

152 Hernnäs J, Nettelbladt O, Bjermer L, Särnstrand B, Malmström A, Hällgren R. Alveolar accumulation of fibronectin and hyaluronan precedes bleomycin-induced pulmonary fibrosis in the rat. *European Respir J* 1992;**5**:404–10.

153 Roman J, Ritzenthaler JD, Bechara R, Brown LA, Guidot D. Ethanol stimulates the expression of fibronectin in lung fibroblasts via kinase-dependent signals that activate CREB. *Am J Physiol-Lung C* 2005;**288**:L975–87. https://doi.org/10.1152/ajplung.00003.2004.

154 Martin C, Papazian L, Payan M-J, Saux P, Gouin F. Pulmonary Fibrosis Correlates With Outcome in Adult Respiratory Distress Syndrome A Study in Mechanically Ventilated Patients. *Chest* 1995;**107**:196–200. https://doi.org/10.1378/chest.107.1.196.

155 Kelly M, Kolb M, Bonniaud P, Gauldie J. Re-evaluation of Fibrogenic Cytokines in Lung Fibrosis. *Curr Pharm Design* 2003;**9**:39–49. https://doi.org/10.2174/1381612033392341.

156 Burnham EL, Moss M, Ritzenthaler JD, Roman J. Increased Fibronectin Expression in Lung in the Setting of Chronic Alcohol Abuse. *Alcohol Clin Exp Res* 2007;**31**:675–83. https://doi.org/10.1111/j.1530-0277.2007.00352.x.

157 Brown LAS, Ritzenthaler JD, Guidot DM, Roman J. Alveolar type II cells from ethanol-fed rats produce a fibronectin-enriched extracellular matrix that promotes monocyte activation. *Alcohol* 2007;**41**:317–24. https://doi.org/10.1016/j.alcohol.2007.04.009.

158 Ito S, Okuda S, Abe M, Fujimoto M, Onuki T, Nishimura T, *et al.* Induced cortical tension restores functional junctions in adhesion-defective carcinoma cells. *Nat Commun* 2017;**8**:1834. https://doi.org/10.1038/s41467-017-01945-y.

159 Itoh M, Tsukita S, Yamazaki Y, Sugimoto H. Rho GTP exchange factor ARHGEF11 regulates the integrity of epithelial junctions by connecting ZO-1 and RhoA-Myosin II signaling. *Proc National Acad Sci* 2012;**109**:9905–10. https://doi.org/10.1073/pnas.1115063109.

160 Zenker J, White MD, Gasnier M, Alvarez YD, Lim HYG, Bissiere S, *et al.* Expanding Actin Rings Zipper the Mouse Embryo for Blastocyst Formation. *Cell* 2018;**173**:776-791.e17. https://doi.org/10.1016/j.cell.2018.02.035.

161 Shen L, Turner JR. Actin Depolymerization Disrupts Tight Junctions via Caveolae-mediated Endocytosis. *Mol Biol Cell* 2005;**16**:3919–36. https://doi.org/10.1091/mbc.e04-12-1089.

162 Belardi B, Hamkins-Indik T, Harris AR, Kim J, Xu K, Fletcher DA. A Weak Link with Actin Organizes Tight Junctions to Control Epithelial Permeability. *Dev Cell* 2020;**54**:792-804.e7. https://doi.org/10.1016/j.devcel.2020.07.022.

163 Dorland YL, Malinova TS, Stalborch A-MDM van, Grieve AG, Geemen D van, Jansen NS, *et al.* The F-BAR protein pacsin2 inhibits asymmetric VE-cadherin internalization from tensile adherens junctions. *Nat Commun* 2016;**7**:12210. https://doi.org/10.1038/ncomms12210.

164 Malinova TS, Huveneers S. Sensing of Cytoskeletal Forces by Asymmetric Adherens Junctions. *Trends in Cell Biology* 2018;**28**:328–41. https://doi.org/10.1016/j.tcb.2017.11.002.

165 Ivanov AI, Parkos CA, Nusrat A. Cytoskeletal Regulation of Epithelial Barrier Function During Inflammation. *Am J Pathol* 2010;**177**:512–24. https://doi.org/10.2353/ajpath.2010.100168.

166 Itallie CMV, Fanning AS, Bridges A, Anderson JM. ZO-1 Stabilizes the Tight Junction Solute Barrier through Coupling to the Perijunctional Cytoskeleton. *Mol Biol Cell* 2009;**20**:3930–40. https://doi.org/10.1091/mbc.e09-04-0320.

CHAPTER 2: RUFFLES AND SPIKES: CONTROL OF TIGHT JUNCTION MORPHOLOGY AND PERMEABILITY BY CLAUDINS

K. Sabrina Lynn*, Raven J. Peterson*, Michael Koval

This work is published in Biochemica et Biophysica Acta (BBA) – Biomembranes (2020) 1862: 183339. doi: 10.1016/j.bbamem.2020.183339.

*authors contributed equally, listed in order of seniority

Abstract

Epithelial barrier function is regulated by a family of transmembrane proteins known as claudins. Functional tight junctions are formed when claudins interact with other transmembrane proteins, cytosolic scaffold proteins and the actin cytoskeleton. The predominant scaffold protein, zonula occludens-1 (ZO-1), directly binds to most claudin C-terminal domains, crosslinking them to the actin cytoskeleton. When imaged by immunofluorescence microscopy, tight junctions most frequently are linear structures that form between tricellular junctions. However, tight junctions also adapt non-linear architectures exhibiting either a ruffled or spiked morphology, which both are responses to changes in claudin engagement of actin filaments. Other terms for ruffled tight junctions include wavy, tortuous, undulating, serpentine or zig-zag junctions. Ruffling is under the control of hypoxia induced factor (HIF) and integrin-mediated signaling, as well as direct mechanical stimulation. Tight junction ruffling is specifically enhanced by claudin-2, antagonized by claudin-1 and requires claudin binding to ZO-1. Tight junction spikes are sites of active vesicle budding and fusion that appear as perpendicular projections oriented towards the nucleus. Spikes share molecular

features with focal adherens junctions and tubulobulbar complexes found in Sertoli cells. Lung epithelial cells under stress form spikes due to an increase in claudin-5 expression that directly disrupts claudin-18 / ZO-1 interactions. Together this suggests that claudins are not passive cargoes controlled by scaffold proteins. We propose a model where claudins specifically influence tight junction scaffold proteins to control interactions with the cytoskeleton as a mechanism that regulates tight junction assembly and function.

Introduction

A major epithelial function is to provide a barrier that separates two distinct microenvironments, the apical and basolateral compartments of a wide range of organs. To support a physiologically functional barrier, epithelial cells must be selectively permeable to ions and solutes. Selective permeability requires cells to regulate two different pathways across the epithelial barrier: the transcellular and the paracellular routes that occur through and between cells, respectively.

Paracellular transport is regulated by specialized intercellular points of contact that form the apical junctional complex (AJC), which separates polarized cells into distinct apical and basolateral domains. The AJC encircles each cell, pairing with neighboring cells to create an adhesive network formed by several classes of intercellular junctions, including adherens junctions, tight junctions, gap junctions and desmosomes.[1, 2] The AJC also establishes the apical/basolateral polarity axis by organizing the Crumbs and Partitioning defective complexes.[3] The multifunctional nature of the AJC enables intercellular communication (gap junctions), provides mechanical integrity to epithelial monolayers (adherens junctions and desmosomes) and acts as a signaling hub that is sensitive to cell contact through differential interactions between transmembrane and cytosolic junction proteins.[4] In addition, the AJC also serves as a site for recruitment and organization of the actin cytoskeleton.[1, 5]

Tight junctions are the AJC component that regulates paracellular barrier permeability to water, small molecules, and ions (Figure 2.1). The main determinants of tight junction-regulated paracellular permeability are claudin-family transmembrane proteins. Claudins form paracellular ion channels of varying specificity and permeability (reviewed in citations 6-8). Tissue-specific claudin composition allows for organ-specific paracellular permeability. Claudin composition and assembly into tight junctions is also sensitive to environmental stressors, such as inflammation. Moreover, claudins do not act in isolation. In concert with other transmembrane proteins, including other claudins, MarvelD proteins (e.g. occludin, tricellulin) and Ig-superfamily proteins (e.g. JAM-A), claudins form complexes with cytoplasmic scaffold proteins that regulate interactions with the actin cytoskeleton. In addition to their role as paracellular channels, there is increasing evidence that claudins can also serve as part of a signaling hub through their specific interactions with different classes of scaffold proteins.[9, 10]

In addition to the regulation of ion and water permeability, tight junctions also regulate the paracellular flux of soluble molecules, including large macromolecules.[11] Soluble molecules do not move through stable, claudin-based pores. Instead, their diffusion across tight junctions is due to transient discontinuities that create a path of diffusion.[12, 13] Tricellular junctions also form a path for paracellular diffusion of soluble molecules that is regulated independently from bicellular tight junctions.[14, 15] Here, we consider changes to the morphology of bicellular tight junctions that correlate with increases in paracellular permeability.

One implication of the ability of claudins to differentially recruit tight junction scaffold proteins is that changes in claudin composition can impact scaffold/cytoskeletal interactions, thereby affecting the overall organization of tight junctions. This can be recognized by two characteristic non-linear tight junction morphologies that we refer to here as “tight junction ruffles” and “tight junction spikes”. Tight junction ruffles (Figure 2.2b) are largely parallel to the cell-cell contact but they differ from linear tight junctions (Figure 2.2a) in that they deviate from the most direct path interconnecting tricellular contact sites. By contrast, tight junction spikes

are structures that are perpendicular to tight junctions along sites of cell-cell contact (Figure 2.2c). As indicated in Figure 2.2 and described in detail below, linear tight junctions, ruffles and spikes are associated with characteristic differences in the organization of junction associated actin filaments.

In addition to tight junction ruffles and spikes, non-continuous distributions of claudins (e.g. strand breaks and puncta) at cell-cell contact sites also can influence paracellular permeability. Ruffles, spikes and strand breaks all correlate with impaired paracellular barrier function and thus provide a valuable indicator of altered assembly of tight junction proteins.

In this review, we describe signal transduction events that induce changes in claudin composition driving changes in tight junction morphology to regulate barrier function. We propose a model where interactions between claudins, scaffold proteins, and the actin cytoskeleton alter tight junction morphology and function by influencing the balance of tension at intercellular junctions.

Ruffled Junctions

When imaged by immunofluorescence microscopy, tight junctions typically appear as a relatively straight, continuous line that connects tricellular contact points (Figure 2.3), however, there are several conditions where tight junctions exhibit a ruffled morphology.[11, 16, 17] Ruffled tight junctions have been observed for several years (e.g. citations 18, 19) and more recently were first systematically quantified by Tokuda et al.[20] in a study correlating changes in claudin expression by MDCK cells with differences in the extent of tight junction ruffling.

Other terms used to describe ruffled tight junctions include: wavy [21-23], tortuous [20, 24-26], undulating [18, 27], serpentine [11, 26] or zig-zag [20, 28]. Referring to these structures as tight junction ruffles parallels the term plasma membrane ruffles, formed by the leading edge of migrating cells.[29] In addition to comparable morphology, the mechanisms that drive plasma membrane

ruffles at the leading edge and tight junction ruffles are likely to be comparable, (e.g. actin reorganization and branching by factors such as WASP).[30]

To date there have not been any examples of other junction proteins showing a ruffled morphology. Although there are no a priori reasons why other classes of junctions (e.g. adherens junctions) could not assume a ruffled conformation, junctional ruffles are likely unique to tight junctions. For instance, E-cadherin localization is not ruffled in intestinal epithelial cells that are forming tight junction ruffles.[31]

Ruffled junctions have a distinct appearance (Figure 2.3) and can be quantified by a measure sometimes referred to as the "zig zag index".[20] The zig zag index is the actual path length of a tight junction between two tricellular junctions (A) divided by the minimum path length (B). A junction is considered ruffled if A/B is significantly larger than 1, where 1 is a completely unruffled (or linear) tight junction.

Tight junction ruffling frequently correlates with increased paracellular permeability (or leak) [27, 32], although that is not always the case.[20] One intriguing hypothesis is that ruffling increases permeability by increasing tight junction circumference, thus enabling more functional claudin channels per cell.[24] In addition, ruffled and linear tight junctions are differentially associated with actin which is also likely to have an impact on their barrier function.[23]

Many stimuli have been shown to induce ruffling, including molecular manipulation of tight junction proteins, impaired oxygen signaling, integrin-mediated signaling and direct mechanical stimulation. Examples of each of these stimuli and the impact they have on claudin composition and tight junction morphology are described below and in Table 2.1.

Roles for claudin/ZO-1 interactions in tight junction ruffling

Claudins interact with each other both across tight junctions (trans-interactions) and within tight junctions (cis-interactions).[33-35] In addition the claudin C-terminal cytoplasmic domain

interacts with cytosolic scaffold proteins, which crosslink these proteins to the cytoskeleton and can also act as a signaling hub.[34, 36, 37] Foremost among these is the tight junction scaffold protein zonula occludens-1 (ZO-1), which has a PDZ1 domain that binds to the "YV" motif found at the extreme C-terminus of most, but not all claudins.[38] Other proteins that interact with the claudin YV motif include ZO-2 and ZO-3 [39], as well as other non-ZO related proteins such as the E3 ubiquitin ligase LINXp80 and COPII cargo sorting protein Sec24C, both of which have been shown to play a role in regulating incorporation of claudin-1 into tight junctions via vesicular trafficking.[40, 41]

ZO-1 helps crosslink claudins to the actin cytoskeleton[19] and is uniquely implicated in the control of junction ruffling. This was demonstrated in MDCK II cells where ZO-1 depletion or low levels of ZO-1 resulted in tight junctions that were highly linear, whereas high levels of ZO-1 expression were associated with significant tight junction ruffling.[20]

MDCK II cells engineered to be deficient in five claudins (MDCK quinKO) show non-ruffled, linear ZO-1 labeling under the control of JAM-A, underscoring a need for claudins in the formation of ruffled junctions.[42] Tight junction ruffling is unique to ZO-1/claudin interactions, since knocking out or overexpressing ZO-2 or ZO-3 has little effect on tight junction morphology.[20] Moreover, in order for ZO-1 to induce tight junction ruffles, it needs to have both the actin binding motif as well as the U6 region of the GUK domain.[43] Interestingly, the ZO-1 U6 domain plays a key role in conformational shifts in ZO-1 that limit occludin binding.[43, 44] This further supports a model where ZO-1 binding to claudins, but not occludin, form more ruffled junctions in contrast to the linear tight junctions produced with ZO-1 binding concurrently to claudins and occludin.

When MDCK II cells are transduced to overexpress ZO-1, the increase in tight junction ruffling is also associated with an increase in tight junction-associated claudin-2.[20] Consistent with a role for claudin-2 in regulating tight junction ruffling, MDCK I cells, which express low levels of claudin-2, tend to have less ruffled tight junctions than MDCK II cells that express high

levels of claudin-2.[20, 45] Claudin-2 is a pore forming claudin that increases tight junction ion and water permeability.[46, 47] Ruffled junctions have a higher capacity for claudin-2, which likely further enhances this effect.[24]

Claudin-2 competes with other claudins for the ability to integrate into tight junctions, including claudin-1, claudin-4 and claudin-7.[20, 48, 49] Although claudin-2 is less efficiently assembled into tight junction strands than claudin-1 and claudin-4 [50], claudin-2 has a longer half-life [51] and thus remains more effectively associated with tight junctions as compared with claudins having a shorter half-life. Control of claudin-2 turnover is a function of the C-terminal domain and does not require ZO-1 binding, suggesting that other, as yet unknown, factors uniquely regulate claudin-2 integration into tight junctions.[51]

Although high levels of claudin-2 correlated with tight junction ruffling, MDCK II cells deficient in claudin-2 expression did not have fully linear tight junctions.[49] Instead, increased expression of other claudins is also required to fully linearize tight junctions. For instance, claudin-2 deficient MDCK II cells transduced with exogenous claudin-4 have more linear tight junctions than claudin-2 deficient cells alone.[50] The ability of other claudins to influence formation of ruffled or linear tight junctions will require screening them for their effect on tight junction morphology and permeability.

How claudin-2 influences tight junction ruffling remains to be determined, although evidence is emerging that different claudins can influence downstream interactions between ZO-1 and other scaffold proteins. For instance, ZO-1 enhances assembly of claudin-1 into tight junction strands through interactions with the PDZ1 and PDZ3 motifs of ZO-1, whereas claudin-2 assembly requires the PDZ1 and PDZ2 motifs.[52] Potential roles for the ZO-1 PDZ2 motif in claudin-2 recruitment into tight junctions include the PDZ2 motif mediating ZO-1 dimerization [53] or binding to other scaffold proteins. As one possibility, claudin-2 may promote folding of ZO-1 into a conformation that promotes binding of the F-BAR protein TOCA-1 complexed to WASP, leading to termination of branched actin filaments at junctions (Figure 2.4). [54]

Claudin-dependent switching of ZO-1/scaffold protein complexes also provides a potential mechanism where the orientation of actin filaments interacting with tight junctions can switch between cortical (parallel to the plane of the plasma membrane) and filamentous (roughly perpendicular to the plasma membrane) (Figure 2.2). In this model, the tension exerted on ruffled tight junctions is higher than linear junctions, yet still symmetrical across the plane of the junction.

It is well established that myosin light chain kinase (MLCK) and rho family kinases regulate barrier function by altering the magnitude of tension on tight junctions.[1, 55, 56] Differential tension can also lead to changes in ZO-1 conformation that can affect its function and ability to interact with other proteins, including claudins.[57] In addition to tension, flow can also impact barrier function. For instance, blood flow through veins is much slower than through arteries, and veins are considerably more permeable than arteries.[58, 59] Consistent with this difference in permeability, venous endothelial cells have more ruffled junctions and are associated with actin stress fibers as opposed to arterial endothelial cells that form high resistance barriers and have linear junctions associated with cortical actin.[60]

Taken together, this suggests a model where claudin-directed reorientation of the actin cytoskeleton coordinated with changes in actomyosin-mediated tension regulates tight junction morphology and barrier function. Consistent with this model, tight junction ruffling was reversed by treatment with the myosin inhibitor blebbistatin, further underscoring a role for actin-associated tension in ruffle formation.[20]

Hypoxia-induced tight junction ruffles

Epithelial barrier function is highly sensitive to changes in oxygen tension, where each epithelial tissue has a particular oxygen set point ranging from hyperoxia (high oxygen tension) to hypoxia. The lung is an example of a hyperoxic tissue whereas the intestine and, counterintuitively, skin are hypoxic.[61-63]

Oxygen tension is sensed by the Hypoxia Inducible Factor (HIF)-1α and HIF-2α (Endothelial PAS Domain Protein 1; EPAS1) transcription factors that act in concert with HIF-1β.[64, 65] At normoxia, prolines on HIF transcription factors become hydroxylated targeting them to the proteasome to be degraded. However, in hypoxia, the non-hydroxylated forms of HIF-1α and HIF-2α translocate to the nucleus where they activate gene transcription.

Although HIF-1α and HIF-2α activate different subsets of the genome (e.g. citation 31) both influence epithelial tight junctions, since depletion of either of these proteins experimentally or due to chronic inflammation impairs barrier function.[66, 67] Specifically, it has been demonstrated in human intestinal epithelial cell lines that knockdown of either HIF-1α [27] or HIF-2α [31] induces a ruffled tight junction morphology as determined by immunofluorescence as well as decreased barrier function.

Despite the comparable effects of shRNA knockdown on tight junction morphology and permeability, HIF-1α and HIF-2α have different mechanisms of action. HIF-1α is directly linked to claudin-1 expression, since HIF-1α knockdown in intestinal and esophageal epithelial cells decreases claudin-1 and reporter assays demonstrate that HIF-1α interacts with the CLDN1 promoter.[27, 68] HIF-1β depleted cells show reduced claudin-1 expression (because of the impact on HIF-1α) and increased tight junction ruffling. Critically, transducing HIF-1β depleted cells to overexpress claudin-1 reverses the ruffled tight junctions into a linear morphology and restores barrier function, indicating a direct role of claudin-1 in regulating paracellular permeability that corresponds with tight junction assembly.[27]

In contrast to HIF-1α, HIF-2α does not directly regulate claudin-1 transcription [68], despite the observation that HIF-2α knockdown also induces tight junction ruffling. Instead, HIF-2α depletion decreases expression of several key enzymes involved in creatine metabolism, including creatine kinase M (CKM) and creatine kinase B (CKB), enzymes that otherwise co-localize with E-cadherin and ZO-1.[31] Critically, creatine supplementation rescues intestinal

epithelial barrier function of HIF-2α deficient cells in vitro and a dextran sodium sulfate inflammatory bowel disease model in vivo, underscoring a role for localized energy metabolism in regulating tight junction morphology and function. It remains to be determined whether CK and claudin-1 overlap or represent parallel pathways that regulate the extent of tight junction ruffling.

While increasing claudin-1 expression leading to increased barrier function is due in part to the barrier forming properties of claudin-1 [69], the precise mechanisms whereby claudin-1 changes tight junction morphology have not been fully elucidated. As described above, the influence of claudin-1 on ZO-1 function can affect the recruitment of other proteins that can then affect tight junction morphology. However, with the exception of ZO-1, specific claudin-1 interacting proteins that determine whether tight junctions are ruffled or linear have not yet been identified.

Integrin-stimulation by nanostructured surfaces

Contact of the basal surface of cells with the extracellular matrix has a considerable impact on cell phenotype and function, which is a key element in the ability to produce organoid cultures that faithfully mimics differentiated cell behavior in native tissues.[70] Specifically, receptors known as integrins bind to extracellular matrix components regulating the organization of the actin cytoskeleton that, in turn, have several downstream consequences impacting cell function.[71] In addition to the native biological substrates for integrins, recent work has determined that integrin contact with synthetic, nanostructured surfaces alters epithelial barrier function in a geometry-dependent manner.[16, 32] The effects of nanostructured surfaces on cells depend on several parameters, including feature aspect ratio, density, pattern and substrate chemistry.[32]

Several classes of nanostructured surfaces imprinted on inert polymers have been shown to increase paracellular permeability through direct contact with β1 integrin.[16, 17] This has utility for

design of devices for transdermal delivery of macromolecular therapeutics (e.g. Etanercept), since coating microneedles with a nanostructured surface significantly enhances macromolecule delivery as compared with bare stainless steel microneedles by increasing keratinocyte transepithelial permeability.[17] Agents delivered transdermally via nanostructure coated microneedles also are more effectively delivered to the cardiovascular and lymphatic systems by an as yet unknown mechanism.[17, 72, 73] One possibility that remains to be tested is that dermal cells stimulated by nanostructure contact secrete factors promoting downstream vessel permeability.

Epithelial cell contact with specific nanostructured surfaces increases paracellular leak and causes junctions to become ruffled.[11, 16, 17] This is accompanied by decreased expression of claudin-1 [17], consistent with the effect of HIF-1α knockdown described above. Claudin-4 expression is also reduced by nanostructure contact, which may be directly associated with an effect of nanostructures on integrins, since claudin-4 is closely associated with β1 and α2 integrin.[74]

In addition to the effects on claudin expression, nanostructure contact also stimulates focal adhesion kinase (FAK) and MLCK activity, both of which were required for the increase in paracellular permeability.[16, 17] Whether the changes in claudin expression and kinases have an additive or redundant effect on tight junction morphology is not yet known.

Ruffles formed by mechanical stimulation

Mechanical stimulation of cells can also lead to tight junction ruffling and changes in paracellular permeability. A particularly dramatic example of this is cyclic stretch of Caco-2 cells.[23] Cyclic stretch activates MLCK, suggesting a potential mechanism comparable to the effect of nanostructured surfaces on cells. Cyclic stretch also activates other kinases JNK and Src, which phosphorylate ZO-1 and occludin [23] and are likely to influence their ability to interact with each other (e.g. citations 75-77) and potentially other proteins. Consistent with the effects

of mechanical stress on tight junction assembly, precision cut lung slices subjected to stretch caused dissociation of claudins from ZO-1 in lung epithelial cells.[78] Moreover, cells transduced with constitutively activated MLCK show regions of localized ruffling that are deficient in claudin-1, further underscoring a role for claudin-1 in maintaining linear tight junctions.[18]

Tight junction spikes and discontinuities

In contrast to tight junction ruffles, tight junction spikes are an asymmetric deviation from linear tight junction morphology. Tight junction spikes appear as projections at cell-cell interfaces that orient in a perpendicular direction from junctions towards the nucleus (Figure 2.5). The asymmetry of tight junction spikes is shared by a comparable adherens junction structure, focal adherens junctions, that also can be asymmetric and have been studied in considerable detail (reviewed in citations.79, 80). Several other terms have been used to describe focal adherens junctions [81], including: perpendicular junctions [82, 83], spot junctions [84], discontinuous junctions [83, 85], punctate junctions [83], junction-associated intermittent lamellipodia [86] and buttons [87]. A comparable structure formed by desmosomes has been referred to as linear arrays [88] and another formed by gap junctions has been referred to as filadendrites [89].

Here we distinguish tight junction spikes from clearly discontinuous tight junctions, in that spikes typically project from intact regions of intercellular tight junctions. [83, 87, 90-92] While visually distinct, tight junction discontinuities and spikes also are quantifiable by image analysis of the relative amount of continuous, punctate and perpendicular junctions [83, 93], segmentation image analysis [94] or neural network analysis of patterns of junctional disruption based on differential labeling intensity [92].

Tight junction spikes differ from focal adherens junctions which are usually punctate. Also, tight junction spikes formed by alveolar epithelial cells are clearly distinct from adherens junctions, since they are deficient in the cadherin-binding protein β-catenin, which instead is

localized to areas that are adjacent to areas where tight spikes are formed.[95] The punctate nature of focal adherens junctions may reflect dissolution of lateral cadherin interactions that are weaker than trans cadherin interactions and thus more easily disrupted by increased tension.[96, 97] Another key difference is that tight junction spikes are more likely form from mature tight junctions as opposed to focal adherens junctions that tend to be precursors to fully mature adherens junctions.[79, 82]

Tight junction discontinuities generally correlate with gross disruption of the actin cytoskeleton [55, 98] leading to paracellular leak. By contrast, tight junction spikes align with actin filaments perpendicular to intercellular tight junctions.[95, 99, 100] Actin also has a comparable role in organizing spikes formed by desmosomes [88] and gap junctions [89].

Although tight junction ruffles and spikes are both organized by actin filaments that are perpendicular to the plane of the plasma membrane, they differ in that ruffles are organized by comparable, symmetric actin filaments on both sides of the AJC, however the arrangement of actin in spikes is asymmetric (Figure 2.2). Also, spikes are organized along the actin filaments (much as linear junctions are aligned along cortical actin) whereas ruffles are tethered to them. Otherwise, the molecular mechanisms that underlie tension generation and induces ruffle and spikes are comparable (e.g. MLCK, Rho kinase activation).[55, 56] Several other molecular features are conserved between ruffles and spikes, including recruitment of vinculin [17, 82] and F-BAR proteins [54, 81] as regulators of cytoskeletal tension and membrane curvature, respectively.

Tight junction spikes as organizers of vesicular traffic

It has long been appreciated that formation of adherens junctions precedes tight junction formation.[101] This has previously been associated with the relative strength of trans interactions between cadherins as opposed to claudins. A more subtle role for adherens junctions in stabilizing tight junctions was revealed by an examination of α-catenin-deficient EpH4 epithelial cells, which were subject to constitutive delivery and endocytosis of claudin-3 to the plasma

membrane.[102] The inability of α-catenin-deficient cells to form tight junctions was not due to a loss of mechanical junction stability, but instead was linked to an imbalance in plasma membrane cholesterol content. Replenishing cell cholesterol re-established the assembly of claudin-3 into tight junctions and stimulated the formation of claudin-3 containing spikes that also contained cholesterol.[102] These findings are consistent with previous studies demonstrating that tight junction proteins preferentially partition into cholesterol enriched microdomains [103] but extend this observation to include spikes as well as established tight junctions.

Although tight junctions appear to be relatively stable structures, in fact they are highly dynamic and are readily endocytosed.[104-107] In cells subjected to oxidative stress, tight junction spikes serve as active "hot spots" for vesicle budding and fusion.[108] Moreover, Eph4 epithelial cells plated at low density form tight junction spikes at cell-cell interfaces between two cells migrating in opposite directions that show double membrane structures by electron microscopy, indicating that one cell endocytoses both halves of a tight junction.[104] These data suggest that tight junction spikes are associated with responses to cell stress and/or tension. Whether spikes reflect unique vs. constitutive processes that regulate tight junction turnover is an open question at present.

Tight junction spikes are reminiscent of a structure found in seminiferous tubule junctions, the basal tubulobulbar complex.[109] Tubulobulbar complexes are enriched in claudin-11, which has a limited pattern of expression and may be uniquely required for their formation.[110] Tubulobulbar complexes are enriched for actin, actin-binding proteins, dynamin and are active sites of vesicle budding and fusion, all of which are associated with tight junction spikes in other epithelial cells.

Interestingly, tubulobulbar complexes are also associated with endoplasmic reticulum-plasma membrane (ER-PM) contact sites, which form a calcium signaling-complex that controls junction remodeling.[111] A comparable ER-PM contact site is also involved in epidermal growth factor receptor (EGFR) endocytosis and signaling.[112] It also has been shown that in MDCK II

cells, EGFR specifically induces claudin-2 endocytosis, but not claudin-1 endocytosis.[113] Whether claudin-2 turnover induced by EGFR occurs by a spike-mediated pathway is not known at present.

Claudin endocytosis is a regulated process. Moreover, different claudins are internalized by different endocytic pathways [105], which provide mechanisms to regulate barrier function by differential regulation of endocytosis. For instance, claudin-1, claudin-2 and claudin-4 are internalized by clathrin-mediated endocytosis, however claudin-5 is preferentially internalized by caveolar endocytosis.[105, 107, 113] Since claudins form complexes, it is likely that lateral claudin-claudin interactions can influence the endocytic pathways that mediate claudin turnover.[33, 35, 114]

Stimulation of acinar epithelial cell mAChR with carbachol induces claudin-4 phosphorylation, resulting in formation of a complex with β-arrestin2, subsequent internalization of claudin-4 and loss of barrier function.[107] Inhibiting clathrin-mediated endocytosis prevented the loss of claudin-4 and preserved barrier function. Involvement of tight junction spikes in this process was revealed by treatment with the proteasome inhibitor MG132, which stabilized spike-associated claudin-4 and also preserved barrier function.

Spikes formed in response to chronic alcohol exposure are due to impaired claudin/ZO-1 interactions

Chronic alcohol abuse is a risk factor for poor outcome in acute respiratory distress syndrome.[115, 116] This is due, in part, to the deleterious effect of alcohol exposure on lung epithelial barrier function.[117] Increased paracellular leak across alveolar epithelial cell monolayers is accompanied by an increase in tight junction spikes (Figure 2.5).[108] The effects of alcohol on alveolar epithelial tight junctions, including increased leak and stimulation of spike formation, can be recapitulated by TGFβ1 [99] and antagonizing GM-CSF [95], indicating that alcohol causes an imbalance in lung epithelial cytokine signaling.

Claudin-18 is prominently expressed by alveolar epithelial cells however, the healthy lung epithelium expresses low levels of claudin-5.[118] In response to alcohol exposure, alveolar epithelial cells increase claudin-5 expression, which correlates with an increase in tight junction spikes containing claudin-18.[108] Increased claudin-5 expression was both necessary and sufficient to induce spikes in alveolar epithelial cells. Using super-resolution microscopy and the proximity ligation assay to measure protein-protein interactions in situ, it was determined that increased claudin-5 binds to claudin-18 and inhibits it from interacting with ZO-1, resulting in increased tight junction spike formation (Figure 2.6).[108]

Although the precise mechanism by which claudin-5 affects claudin-18/ZO-1 interactions remains to be determined, it seems likely that there will be other examples of claudin-claudin interactions that affect organization of the tight junction scaffold. One possible model is that claudin-5 binding to claudin-18 causes a conformational shift in the C-terminus of claudin-18 displacing ZO-1 and enabling other, as yet unknown, factors to interact with claudin-18 (Figure 2.6). Whether this is the case will require identifying proteins that preferentially interact with spike associated claudin-18.

Roles for claudins in regulating tight junction ultrastructure

There is a considerable literature examining tight junctions at the ultrastructural level, using freeze fracture scanning electron microscopy, demonstrating a diversity of tight junction organization as meshworks that differ in strand number, shape and organization. By and large, tight junction permeability inversely correlates with meshwork depth and strand number (e.g. citations 119-121) although this is not always the case.[122] Tight junction ruffles do not necessarily correlate with changes in ultrastructure since there are examples where ruffled junctions do [43] and do not [18] have accompanying changes in tight junction ultrastructure that can be detected by freeze fracture electron microscopy.

Claudins are required to form tight junction strands at the ultrastructural level [42, 123] and the architecture of the tight junction meshwork is sensitive to claudin composition. For instance, overexpression of claudin-3 by MDCK cells causes a transition from an angular to a curved loop meshwork structure and decreased strand breaks [124]. The third transmembrane domain of claudin-3 has a unique bent conformation that has been directly linked to the control of tight junction strand morphology by altering claudin packing.[125] Increased claudin-4 expression by MDCK cells produces tight junctions that have a reticular network of parallel strands, whereas high levels of claudin-2 expression are associated with curved stands that are diffuse.[122]

Imaging using conventional confocal immunofluorescence microscopy has a limit of resolution of 200 nm. This is not sufficient resolution to detect strand breaks in the range of 20 nm - 200 nm, which are associated with increased paracellular leak due to changes in claudin expression.[124, 126] Super-resolution fluorescence microscopy has the capacity to image tight junction strands at high enough resolution to reveal differences in the ultrastructural meshwork formed by different claudins; this was demonstrated by analysis of claudin-null HEK293 cells transfected to express claudin-3 or claudin-5, which showed differences in tight junction ultrastructure that could be detected by freeze fracture electron microscopy and Spectral Position Determination Microscopy.[127] In native alveolar epithelial cells, tight junction spikes were detected by stochastic optical reconstruction microscopy (STORM).[108] However, alveolar epithelial cells are squamous and have a limited tight junction meshwork architecture [128, 129], so STORM did not detect any meshwork changes associated with tight junction spikes. Using super-resolution microscopy to assess ultrastructural changes formed by native claudins in cuboidal epithelia feasible using current technology, but likely challenging, since it will require super-resolution in the x-z axis in addition to the x-y plane.

Summary and future directions

Tight junction assembly and function are influenced by protein composition, post-translational modifications and the internal and external mechanical forces they are subjected to. Most models emphasize the impact of actin and the cytosolic scaffold on the assembly and behavior of claudins. However, evidence is emerging that this is a reciprocal relationship, where claudins themselves can be active determinants of scaffold protein conformation and function.

Claudins associated with ruffles are assembled into tight junctions. However, it is not known whether claudins associated with tight junction spikes are assembled into bona fide tight junctions. Cells forming tight junction spikes show evidence that intact tight junctions are maintained when they were engulfed by one cell from another.[104, 108] However, it is also possible that spikes contain a pool of non-junction associated claudins. One method to distinguish whether spike associated claudins are fully integrated into tight junctions is to use Fluorescence Recovery After Photobleaching (FRAP) analysis of YFP-tagged claudins which can differentiate junction associated claudins, based on rate and extent of recovery.[48] If spike associated claudins are not junctional, they could serve other roles. For instance, non-junctional pools of claudin-7 along the lateral plasma membrane regulate tumor cell growth and migration.[130, 131]

Since most approaches to measure epithelial permeability are based on overall measurements of an intact monolayer or tissue, the impact of tight junction morphological changes on paracellular permeability have not been well elucidated. Electrophysiologic methods that rely on scanning live cell monolayers to map local paracellular ion permeability have been developed, although these are difficult to use and correlate with tight junction morphology because they are low throughput.[132, 133]

Several imaging approaches have been established that enable local permeability to be measured. This includes a fluorescence barrier permeability assay based on plating cells on a biotinylated substrate that are subsequently probed with fluorescently tagged streptavidin and imaged by fluorescence microscopy (XPerT assay).[134] The XPerT assay has been successfully use

to identify sites of localized barrier dysfunction, primarily in endothelial cells monolayer.[78, 135-137] The ZnUMBA assay based on zinc permeability and a fluorescent reporter molecule represents another approach to visualize localized barrier permeability.[138] Coupling imaging methods with cells expressing fluorescently tagged tight junction proteins will enable sites of paracellular leak to be identified relative to areas where tight junctions are not linear.

Many advances have been made in defining the tight junction proteome, including the use of BioID to identify proteins that are in close proximity to ZO-1, claudin-4 and occludin.[74, 139] The utility of this approach is underscored by the finding that the N- and C- terminal domains of ZO-1 interact with different proteins.[139] Further expanding the use of BioID to identify proteins that interact with other claudins comparing conditions where tight junctions are linear, ruffled or forming spikes are anticipated to help define mechanisms where claudins control tight junction morphology and could help identify new proteins specific to ruffled or spike morphologies.

The ability of claudins to influence their own assembly and integration into tight junctions is beginning to be appreciated. Claudin-1, claudin-2 and claudin-5 have been associated with linear, ruffled and spiked tight junctions respectively. The ability of other claudins to influence tight junction morphology is less well established. In addition, the effect of claudins on tight junction morphology is likely to be context sensitive, especially due to interactions with other claudins present in tight junctions, and remains to be determined.

Undoubtedly, C-terminal domains of different claudins bind to different protein substrates, however, evidence is now emerging that claudins can influence the behavior of scaffold and other proteins. By analogy with connexins [140-142], the C-terminal domains of claudins are likely to be intrinsically disordered having significant structural plasticity. ZO-1 also has intrinsically disordered domains, is mechanosensitive and can exist in different phase states [143], underscoring the concept that tight junction assembly is highly context dependent with respect to both local protein composition and biophysical mechanical state. Taken together, we propose a model where complexes between different claudin C-terminal domains and scaffold proteins

influence each other to fold into unique conformations. One implication of this model is that determining the regulation epithelial paracellular barrier function will require taking into account how the reciprocal interplay between claudins, scaffold proteins and cytoskeletal tension affect tight junction assembly and function.

Acknowledgements

Supported by NIH grants R01-AA025854 and R01-HL137112 (MK), F31-HL139109 (KSL) and F31-GM130112 (RJP). We thank Jennifer Sucre for critical reading of the manuscript.

Author contributions

Raven J. Peterson researched and was lead author of sections on tight junction ruffles. K. Sabrina Lynn, researched and was lead author of sections on tight junction spikes. All co-authors contributed to interpretation, preparation and editing of the manuscript.

Abbreviations

AJC – apical junctional complex

BAR - Bin/Amphiphysin/Rvs

EGFR – epidermal growth factor receptor

FRAP - Fluorescence Recovery After Photobleaching

GUK - guanylate kinase

HEK – Human Embryonic Kidney

HIF - hypoxia induced factor

mAChR - muscarinic acetyl choline receptor

MDCK – Madin Darby Canine Kidney

MLCK – myosin light chain kinase

PDZ - postsynaptic density protein (PSD95), Drosophila disc large tumor suppressor (DlgA), and zonula occludens-1 protein (ZO-1)

TOCA - Transducer of Cdc42 dependent actin assembly

WASP - Wiskott–Aldrich syndrome protein

XPerT - express micromolecule permeability testing

ZnUMBA - Zinc-based Ultrasensitive Microscopic Barrier Assay

ZO – zonula occludens

Figure 2.1

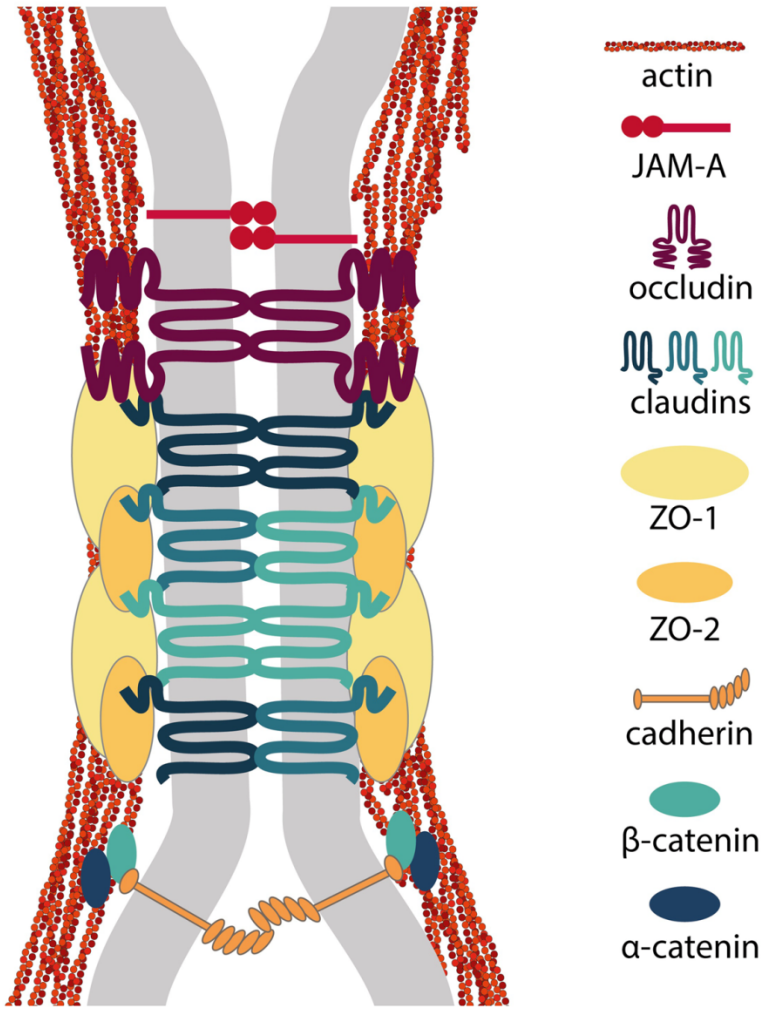

Figure 2.1 Protein composition of tight junctions and adherens junctions. Shown is a subset of transmembrane, cytosolic scaffold and cytoskeletal proteins associated with tight junctions (occludin, claudin, ZO-1, ZO-2) and adherens junctions (cadherin, α-catenin, β-catenin).

Figure 2.2

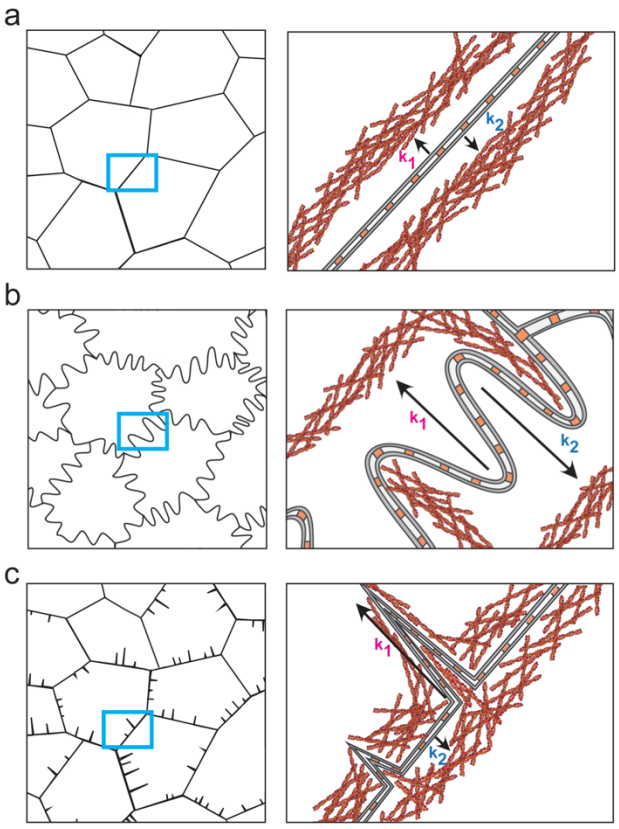

Figure 2.2 Roles for actin in control of tight junction morphology. A. Linear tight junctions showing cortical actin and symmetrical forces perpendicular to the plane of the membrane ($k_1 = k_2$). B. Tight junction ruffles, with tight junctions tethered to actin perpendicular to cortical actin and subjected to higher, symmetrical forces than linear junctions. C. Tight junction spikes subjected to asymmetrical tension ($k_1 > k_2$). and oriented along actin stress fibers.

Figure 2.3

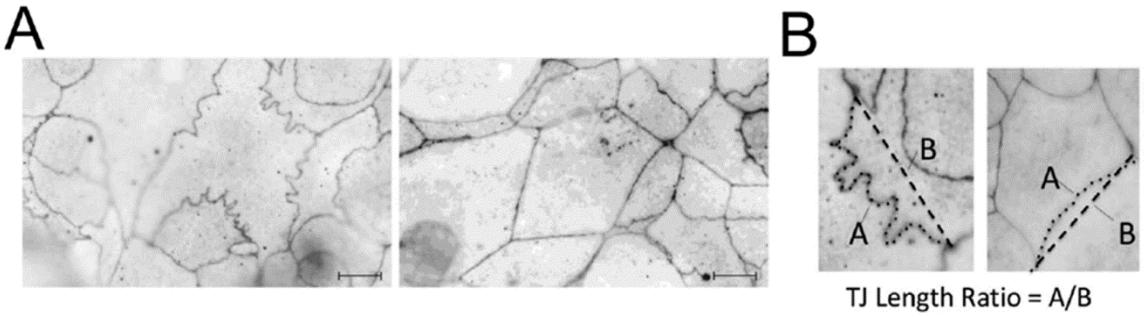

Figure 2.3 Quantitation of tight junction ruffles. A. ZO1 in HIF1β deficient Caco2 cells has a ruffled appearance. Transfection to overexpress claudin-1 cDNA normalizes ZO1 distribution to a linear morphology. B. Quantification of tight junction ruffling was performed by dividing the actual junction length (dotted line A) by the distance between tricellular junctions (dashed line B). Examples of ruffled (left) and linear (right) tight junction morphology are shown. Reproduced with permission. [27]

Figure 2.4

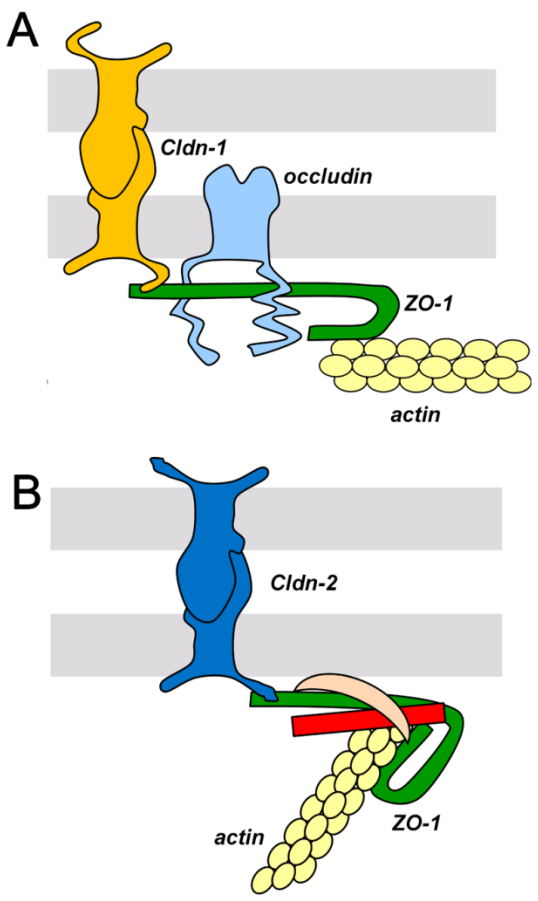

Figure 2.4 Model for claudin-directed changes in ZO-1 conformation. A. Claudin-1 binds to ZO-1 in a conformation enabling interactions with occludin that promote association with actin in a cortical orientation, parallel to the plane of the plasma membrane. B. ZO-1 associated with claudin-2 is proposed to have an alternative conformation. Shown here are induced interactions with TOCA-1 (crescent) and WASP (red bar), potentially re-orienting actin/ZO-1 interactions into a conformation that favors tight junction ruffling.

Figure 2.5

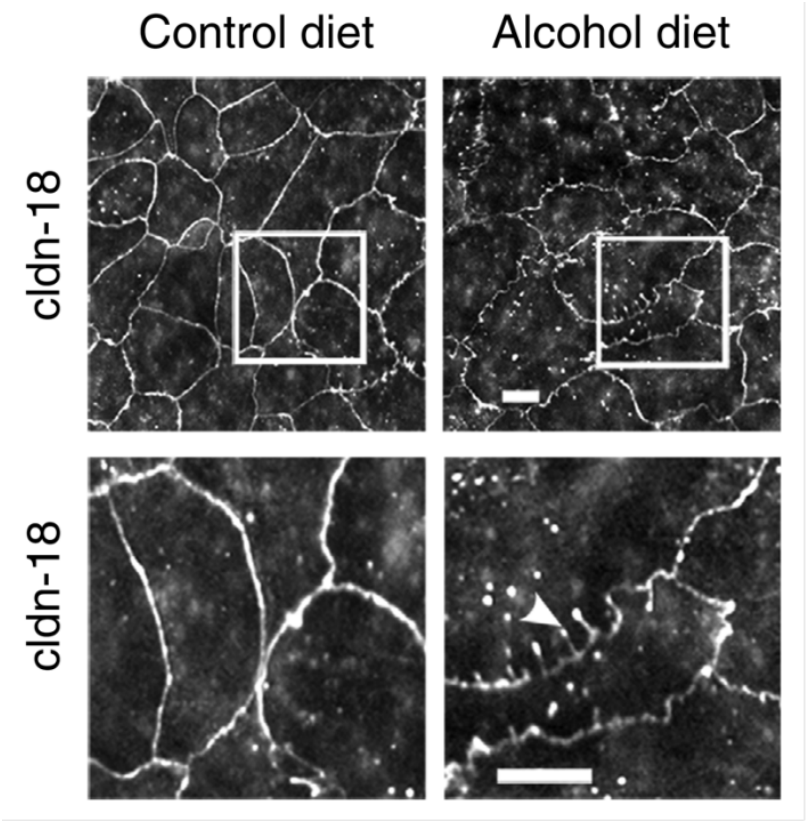

Figure 2.5 Tight junction spikes induced in lung epithelial cells. Alveolar epithelial cells isolated from alcohol or control-fed rats were cultured for 7 days on Transwell permeable supports and immunolabeled for claudin-18. Cells from alcohol fed rats showed enhancement of tight junction spikes, that are claudin-18 projections perpendicular to the cell-cell interface (arrowhead). Square regions in the top panels correspond to magnified images below. Note strand breaks, puncta and other discontinuities in claudin-18 present in cells from alcohol-fed rats (Bar, 10 μm). Reproduced with permission. [108]

Figure 2.6

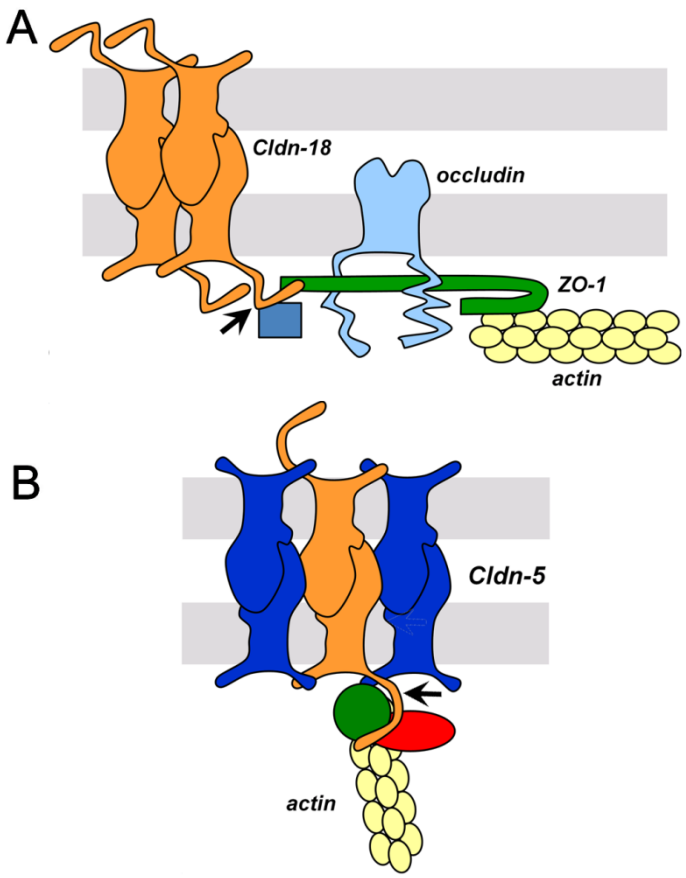

Figure 2.6 Model for claudin-claudin interactions affecting scaffold protein binding. A. Tight junctions enriched for claudin-18 show significant binding with ZO-1, as well as other associated proteins, indicated by the blue square, that orient actin in a cortical orientation (equivalent to Figure 2.3A). B. Increased claudin-5 interacts with claudin-18 to prevent an interaction with ZO-1. The red oval and grey circle denote putative C-terminal interacting proteins that bind to claudin-18 in the absence of ZO-1. In this model, claudin-5 is proposed to induce a conformational change in the C terminal domain of claudin-18 (arrows).

Table 2.1

Stimuli inducing ruffled tight junctions

Stimulus	Effect on Claudins	Effect on TER	Effect on paracellular flux	Reference
High expression of ZO-1	Cldn-2 high, Cldn-1, cldn-7 low	No significant change	Variable degrees of changes in permeability, but no real pattern	Tokuda, et al. [20]
ZO-1 truncation mutants	nd	nd	nd	Fanning et al. [19, 43]
TOCA-1 expression	No change in cldn-2	No significant change	Increase 3kDa Dextran	Van Itallie, et al. [54]
KD HIF1B knockdown	Decrease cldn 1	Decrease	Increase FITC dextran (3, 10, 40 kDa)	Saeedi, et al. [27]
KD HIF-2a knockdown	nd	Decrease	nd	Glover, et al. [31]
Reoxygenation after anoxia injury	Increase in cldn-4	Decrease	Increase FITC-dextran	Jin, et al. [21]
MLCK activation	Local decreases in cldn1	Decrease	Increase inulin, mannitol	Shen, et al. [18]
Cyclic stretch	nd	nd	Increase FITC inulin	Samak, et al. [23]
VAV3 inactivation	nd	Decrease	nd	Hilfenhaus, et al. [60]
Nanostructure contact	Decrease cldn 1, 4	Decrease	Increase FITC-BSA, FITC-IgG, Etanercept	Kam, et al. [16], Walsh, et al. [17], Stewart, et al. [11]

Literature cited

1. M. Quiros, A. Nusrat, RhoGTPases, actomyosin signaling and regulation of the epithelial Apical Junctional Complex, Seminars in cell & developmental biology, 36 (2014) 194-203.
2. S. Tsukita, M. Furuse, M. Itoh, Multifunctional strands in tight junctions, Nature reviews. Molecular cell biology, 2 (2001) 285-293.
3. Q. Wang, B. Margolis, Apical junctional complexes and cell polarity, Kidney Int, 72 (2007) 1448-1458.
4. L. Gonzalez-Mariscal, J. Miranda, H. Gallego-Gutierrez, M. Cano-Cortina, E. Amaya, Relationship between apical junction proteins, gene expression and cancer, Biochimica et biophysica acta. Biomembranes, (2020) 183278.
5. T. Yano, H. Kanoh, A. Tamura, S. Tsukita, Apical cytoskeletons and junctional complexes as a combined system in epithelial cell sheets, Annals of the New York Academy of Sciences, 1405 (2017) 32-43.
6. S.M. Krug, J.D. Schulzke, M. Fromm, Tight junction, selective permeability, and related diseases, Seminars in cell & developmental biology, 36 (2014) 166-176.
7. J.M. Anderson, C.M. Van Itallie, Physiology and function of the tight junction, Cold Spring Harbor perspectives in biology, 1 (2009) a002584.
8. D. Gunzel, Claudins: vital partners in transcellular and paracellular transport coupling, Pflugers Archiv : European journal of physiology, (2016).
9. A.A. Bhat, N. Syed, L. Therachiyil, S. Nisar, S. Hashem, M.A. Macha, S.K. Yadav, R. Krishnankutty, S. Muralitharan, H. Al-Naemi, P. Bagga, R. Reddy, P. Dhawan, A. Akobeng, S. Uddin, M.P. Frenneaux, W. El-Rifai, M. Haris, Claudin-1, A Double-Edged Sword in Cancer, International journal of molecular sciences, 21 (2020).
10. B. Zhou, P. Flodby, J. Luo, D.R. Castillo, Y. Liu, F.X. Yu, A. McConnell, B. Varghese, G. Li, N.O. Chimge, M. Sunohara, M.N. Koss, W. Elatre, P. Conti, J.M. Liebler, C. Yang, C.N. Marconett, I.A. Laird-Offringa, P. Minoo, K. Guan, B.R. Stripp, E.D. Crandall, Z. Borok,

Claudin-18-mediated YAP activity regulates lung stem and progenitor cell homeostasis and tumorigenesis, The Journal of clinical investigation, 128 (2018) 970-984.

11. T. Stewart, W.T. Koval, S.A. Molina, S.M. Bock, J.W. Lillard, Jr., R.F. Ross, T.A. Desai, M. Koval, Calibrated flux measurements reveal a nanostructure-stimulated transcytotic pathway, Experimental cell research, 355 (2017) 153-161.
12. E.E. Schneeberger, R.D. Lynch, The tight junction: a multifunctional complex, American journal of physiology. Cell physiology, 286 (2004) C1213-1228.
13. H. Sasaki, C. Matsui, K. Furuse, Y. Mimori-Kiyosue, M. Furuse, S. Tsukita, Dynamic behavior of paired claudin strands within apposing plasma membranes, Proceedings of the National Academy of Sciences of the United States of America, 100 (2003) 3971-3976.
14. S.M. Krug, S. Amasheh, J.F. Richter, S. Milatz, D. Gunzel, J.K. Westphal, O. Huber, J.D. Schulzke, M. Fromm, Tricellulin forms a barrier to macromolecules in tricellular tight junctions without affecting ion permeability, Molecular biology of the cell, 20 (2009) 3713-3724.
15. T. Higashi, S. Tokuda, S. Kitajiri, S. Masuda, H. Nakamura, Y. Oda, M. Furuse, Analysis of the 'angulin' proteins LSR, ILDR1 and ILDR2--tricellulin recruitment, epithelial barrier function and implication in deafness pathogenesis, Journal of cell science, 126 (2013) 966-977.
16. K.R. Kam, L.A. Walsh, S.M. Bock, M. Koval, K.E. Fischer, R.F. Ross, T.A. Desai, Nanostructure-mediated transport of biologics across epithelial tissue: enhancing permeability via nanotopography, Nano Lett, 13 (2013) 164-171.
17. L. Walsh, J. Ryu, S. Bock, M. Koval, T. Mauro, R. Ross, T. Desai, Nanotopography facilitates in vivo transdermal delivery of high molecular weight therapeutics through an integrin-dependent mechanism, Nano Lett, 15 (2015) 2434-2441.

18. L. Shen, E.D. Black, E.D. Witkowski, W.I. Lencer, V. Guerriero, E.E. Schneeberger, J.R. Turner, Myosin light chain phosphorylation regulates barrier function by remodeling tight junction structure, Journal of cell science, 119 (2006) 2095-2106.

19. A.S. Fanning, T.Y. Ma, J.M. Anderson, Isolation and functional characterization of the actin binding region in the tight junction protein ZO-1, FASEB journal : official publication of the Federation of American Societies for Experimental Biology, 16 (2002) 1835-1837.

20. S. Tokuda, T. Higashi, M. Furuse, ZO-1 knockout by TALEN-mediated gene targeting in MDCK cells: involvement of ZO-1 in the regulation of cytoskeleton and cell shape, PloS one, 9 (2014) e104994.

21. Y. Jin, A.T. Blikslager, Myosin light chain kinase mediates intestinal barrier dysfunction via occludin endocytosis during anoxia/reoxygenation injury, American journal of physiology. Cell physiology, 311 (2016) C996-C1004.

22. A.I. Ivanov, D. Hunt, M. Utech, A. Nusrat, C.A. Parkos, Differential roles for actin polymerization and a myosin II motor in assembly of the epithelial apical junctional complex, Molecular biology of the cell, 16 (2005) 2636-2650.

23. G. Samak, R. Gangwar, L.M. Crosby, L.P. Desai, K. Wilhelm, C.M. Waters, R. Rao, Cyclic stretch disrupts apical junctional complexes in Caco-2 cell monolayers by a JNK-2-, c-Src-, and MLCK-dependent mechanism, American journal of physiology. Gastrointestinal and liver physiology, 306 (2014) G947-958.

24. L. Gonzalez-Mariscal, A. Avila-Flores, A. Betanzos, The relationship between structure and function of tight junctions, in: J.M. Anderson, M. Cereijido (Eds.) Tight Junctions, Second Edition, CRC Press, Place Published, 2001, pp. 89-120.

25. C.M. Van Itallie, A.S. Fanning, A. Bridges, J.M. Anderson, ZO-1 stabilizes the tight junction solute barrier through coupling to the perijunctional cytoskeleton, Molecular biology of the cell, 20 (2009) 3930-3940.

26. S. Angelow, R. El-Husseini, S.A. Kanzawa, A.S. Yu, Renal localization and function of the tight junction protein, claudin-19, American journal of physiology. Renal physiology, 293 (2007) F166-177.

27. B.J. Saeedi, D.J. Kao, D.A. Kitzenberg, E. Dobrinskikh, K.D. Schwisow, J.C. Masterson, A.A. Kendrick, C.J. Kelly, A.J. Bayless, D.J. Kominsky, E.L. Campbell, K.A. Kuhn, G.T. Furuta, S.P. Colgan, L.E. Glover, HIF-dependent regulation of claudin-1 is central to intestinal epithelial tight junction integrity, Molecular biology of the cell, 26 (2015) 2252-2262.

28. S. Awadia, F. Huq, T.R. Arnold, S.M. Goicoechea, Y.J. Sun, T. Hou, G. Kreider-Letterman, P. Massimi, L. Banks, E.J. Fuentes, A.L. Miller, R. Garcia-Mata, SGEF forms a complex with Scribble and Dlg1 and regulates epithelial junctions and contractility, The Journal of cell biology, 218 (2019) 2699-2725.

29. M. Abercrombie, The crawling movement of metazoan cells, Proc. R . Soc. Lond. B Biol. Sci., 207 (1980) 129-147.

30. J.V. Small, T. Stradal, E. Vignal, K. Rottner, The lamellipodium: where motility begins, Trends in cell biology, 12 (2002) 112-120.

31. L.E. Glover, B.E. Bowers, B. Saeedi, S.F. Ehrentraut, E.L. Campbell, A.J. Bayless, E. Dobrinskikh, A.A. Kendrick, C.J. Kelly, A. Burgess, L. Miller, D.J. Kominsky, P. Jedlicka, S.P. Colgan, Control of creatine metabolism by HIF is an endogenous mechanism of barrier regulation in colitis, Proceedings of the National Academy of Sciences of the United States of America, 110 (2013) 19820-19825.

32. K.R. Kam, L.A. Walsh, S.M. Bock, J.D. Ollerenshaw, R.F. Ross, T.A. Desai, The effect of nanotopography on modulating protein adsorption and the fibrotic response, Tissue engineering. Part A, 20 (2014) 130-138.

33. G. Krause, J. Protze, J. Piontek, Assembly and function of claudins: Structure-function relationships based on homology models and crystal structures, Seminars in cell & developmental biology, 42 (2015) 3-12.

34. C.M. Van Itallie, J.M. Anderson, Claudin interactions in and out of the tight junction, Tissue Barriers, 1 (2013) e25247.

35. M. Koval, Differential pathways of claudin oligomerization and integration into tight junctions, Tissue Barriers, 1 (2013) e24518.

36. S. Gowrikumar, A.B. Singh, P. Dhawan, Role of Claudin Proteins in Regulating Cancer Stem Cells and Chemoresistance-Potential Implication in Disease Prognosis and Therapy, International journal of molecular sciences, 21 (2019).

37. D.N. Kotton, Claudin-18: unexpected regulator of lung alveolar epithelial cell proliferation, The Journal of clinical investigation, 128 (2018) 903-905.

38. M. Itoh, M. Furuse, K. Morita, K. Kubota, M. Saitou, S. Tsukita, Direct binding of three tight junction-associated MAGUKs, ZO-1, ZO-2, and ZO-3, with the COOH termini of claudins, The Journal of cell biology, 147 (1999) 1351-1363.

39. J.C. Herve, M. Derangeon, D. Sarrouilhe, N. Bourmeyster, Influence of the scaffolding protein Zonula Occludens (ZOs) on membrane channels, Biochimica et biophysica acta, 1838 (2014) 595-604.

40. S. Takahashi, N. Iwamoto, H. Sasaki, M. Ohashi, Y. Oda, S. Tsukita, M. Furuse, The E3 ubiquitin ligase LNX1p80 promotes the removal of claudins from tight junctions in MDCK cells, Journal of cell science, 122 (2009) 985-994.

41. P. Yin, Y. Li, L. Zhang, Sec24C-Dependent Transport of Claudin-1 Regulates Hepatitis C Virus Entry, Journal of virology, 91 (2017).

42. T. Otani, T.P. Nguyen, S. Tokuda, K. Sugihara, T. Sugawara, K. Furuse, T. Miura, K. Ebnet, M. Furuse, Claudins and JAM-A coordinately regulate tight junction formation and epithelial polarity, The Journal of cell biology, 218 (2019) 3372-3396.

43. A.S. Fanning, B.P. Little, C. Rahner, D. Utepbergenov, Z. Walther, J.M. Anderson, The unique-5 and -6 motifs of ZO-1 regulate tight junction strand localization and scaffolding properties, Molecular biology of the cell, 18 (2007) 721-731.

44. A.W. McGee, S.R. Dakoji, O. Olsen, D.S. Bredt, W.A. Lim, K.E. Prehoda, Structure of the SH3-guanylate kinase module from PSD-95 suggests a mechanism for regulated assembly of MAGUK scaffolding proteins, Molecular cell, 8 (2001) 1291-1301.

45. B.R. Stevenson, J.M. Anderson, D.A. Goodenough, M.S. Mooseker, Tight junction structure and ZO-1 content are identical in two strains of Madin-Darby canine kidney cells which differ in transepithelial resistance, The Journal of cell biology, 107 (1988) 2401-2408.

46. R. Rosenthal, S. Milatz, S.M. Krug, B. Oelrich, J.D. Schulzke, S. Amasheh, D. Gunzel, M. Fromm, Claudin-2, a component of the tight junction, forms a paracellular water channel, Journal of cell science, 123 (2010) 1913-1921.

47. C.M. Van Itallie, J. Holmes, A. Bridges, J.L. Gookin, M.R. Coccaro, W. Proctor, O.R. Colegio, J.M. Anderson, The density of small tight junction pores varies among cell types and is increased by expression of claudin-2, Journal of cell science, 121 (2008) 298-305.

48. C.T. Capaldo, A.E. Farkas, R.S. Hilgarth, S.M. Krug, M.F. Wolf, J.K. Benedik, M. Fromm, M. Koval, C. Parkos, A. Nusrat, Proinflammatory cytokine-induced tight junction remodeling through dynamic self-assembly of claudins, Molecular biology of the cell, 25 (2014) 2710-2719.

49. S. Tokuda, M. Furuse, Claudin-2 knockout by TALEN-mediated gene targeting in MDCK cells: claudin-2 independently determines the leaky property of tight junctions in MDCK cells, PloS one, 10 (2015) e0119869.

50. C.M. Van Itallie, K.F. Lidman, A.J. Tietgens, J.M. Anderson, Newly synthesized claudins but not occludin are added to the basal side of the tight junction, Molecular biology of the cell, 30 (2019) 1406-1424.

51. C.M. Van Itallie, O.R. Colegio, J.M. Anderson, The cytoplasmic tails of claudins can influence tight junction barrier properties through effects on protein stability, J Membr Biol, 199 (2004) 29-38.

52. L.S. Rodgers, M.T. Beam, J.M. Anderson, A.S. Fanning, Epithelial barrier assembly requires coordinated activity of multiple domains of the tight junction protein ZO-1, Journal of cell science, 126 (2013) 1565-1575.

53. A.S. Fanning, M.F. Lye, J.M. Anderson, A. Lavie, Domain swapping within PDZ2 is responsible for dimerization of ZO proteins, The Journal of biological chemistry, 282 (2007) 37710-37716.

54. C.M. Van Itallie, A.J. Tietgens, E. Krystofiak, B. Kachar, J.M. Anderson, A complex of ZO-1 and the BAR-domain protein TOCA-1 regulates actin assembly at the tight junction, Molecular biology of the cell, 26 (2015) 2769-2787.

55. A.I. Ivanov, C.A. Parkos, A. Nusrat, Cytoskeletal regulation of epithelial barrier function during inflammation, The American journal of pathology, 177 (2010) 512-524.

56. W.Q. He, J. Wang, J.Y. Sheng, J.M. Zha, W.V. Graham, J.R. Turner, Contributions of Myosin Light Chain Kinase to Regulation of Epithelial Paracellular Permeability and Mucosal Homeostasis, International journal of molecular sciences, 21 (2020).

57. D. Spadaro, S. Le, T. Laroche, I. Mean, L. Jond, J. Yan, S. Citi, Tension-Dependent Stretching Activates ZO-1 to Control the Junctional Localization of Its Interactors, Current biology : CB, 27 (2017) 3783-3795 e3788.

58. C. Crone, O. Christensen, Electrical resistance of a capillary endothelium, The Journal of general physiology, 77 (1981) 349-371.

59. W.N. Duran, F.A. Sanchez, J.W. Breslin, Microcirculatory Exchange Function in: R.F. Tuma, W.N. Duran, K. Ley (Eds.) Handbook of Physiology: Microcirculation Academic Press, Place Published, 2008, pp. 81-124.

60. G. Hilfenhaus, D.P. Nguyen, J. Freshman, D. Prajapati, F. Ma, D. Song, S. Ziyad, M. Cuadrado, M. Pellegrini, X.R. Bustelo, M.L. Iruela-Arispe, Vav3-induced cytoskeletal dynamics contribute to heterotypic properties of endothelial barriers, The Journal of cell biology, 217 (2018) 2813-2830.

61. A. Carreau, B. El Hafny-Rahbi, A. Matejuk, C. Grillon, C. Kieda, Why is the partial oxygen pressure of human tissues a crucial parameter? Small molecules and hypoxia, Journal of cellular and molecular medicine, 15 (2011) 1239-1253.

62. J. Karhausen, G.T. Furuta, J.E. Tomaszewski, R.S. Johnson, S.P. Colgan, V.H. Haase, Epithelial hypoxia-inducible factor-1 is protective in murine experimental colitis, The Journal of clinical investigation, 114 (2004) 1098-1106.

63. B. Bedogni, S.M. Welford, D.S. Cassarino, B.J. Nickoloff, A.J. Giaccia, M.B. Powell, The hypoxic microenvironment of the skin contributes to Akt-mediated melanocyte transformation, Cancer cell, 8 (2005) 443-454.

64. P.J. Ratcliffe, HIF-1 and HIF-2: working alone or together in hypoxia?, The Journal of clinical investigation, 117 (2007) 862-865.

65. G.L. Semenza, Oxygen homeostasis, Wiley interdisciplinary reviews. Systems biology and medicine, 2 (2010) 336-361.

66. L.E. Glover, S.P. Colgan, Epithelial Barrier Regulation by Hypoxia-Inducible Factor, Annals of the American Thoracic Society, 14 (2017) S233-S236.

67. K. Fluck, J. Fandrey, Oxygen sensing in intestinal mucosal inflammation, Pflugers Archiv : European journal of physiology, 468 (2016) 77-84.

68. J.C. Masterson, K.A. Biette, J.A. Hammer, N. Nguyen, K.E. Capocelli, B.J. Saeedi, R.F. Harris, S.D. Fernando, L.B. Hosford, C.J. Kelly, E.L. Campbell, S.F. Ehrentraut, F.N. Ahmed, H. Nakagawa, J.J. Lee, E.N. McNamee, L.E. Glover, S.P. Colgan, G.T. Furuta, Epithelial HIF-1alpha/claudin-1 axis regulates barrier dysfunction in eosinophilic esophagitis, The Journal of clinical investigation, 129 (2019) 3224-3235.

69. R. Rosenthal, D. Gunzel, D. Theune, C. Czichos, J.D. Schulzke, M. Fromm, Water channels and barriers formed by claudins, Annals of the New York Academy of Sciences, 1397 (2017) 100-109.

70. M. Simian, M.J. Bissell, Organoids: A historical perspective of thinking in three dimensions, The Journal of cell biology, 216 (2017) 31-40.

71. Y.A. Kadry, D.A. Calderwood, Chapter 22: Structural and signaling functions of integrins, Biochimica et biophysica acta. Biomembranes, (2020) 183206.

72. M.B. Aldrich, F.C. Velasquez, S. Kwon, A. Azhdarinia, K. Pinkston, B.R. Harvey, W. Chan, J.C. Rasmussen, R.F. Ross, C.E. Fife, E.M. Sevick-Muraca, Lymphatic delivery of etanercept via nanotopography improves response to collagen-induced arthritis, Arthritis research & therapy, 19 (2017) 116.

73. S. Kwon, F.C. Velasquez, J.C. Rasmussen, M.R. Greives, K.D. Turner, J.R. Morrow, W.J. Hwu, R.F. Ross, S. Zhang, E.M. Sevick-Muraca, Nanotopography-based lymphatic delivery for improved anti-tumor responses to checkpoint blockade immunotherapy, Theranostics, 9 (2019) 8332-8343.

74. K. Fredriksson, C.M. Van Itallie, A. Aponte, M. Gucek, A.J. Tietgens, J.M. Anderson, Proteomic analysis of proteins surrounding occludin and claudin-4 reveals their proximity to signaling and trafficking networks, PloS one, 10 (2015) e0117074.

75. G. Kale, A.P. Naren, P. Sheth, R.K. Rao, Tyrosine phosphorylation of occludin attenuates its interactions with ZO-1, ZO-2, and ZO-3, Biochemical and biophysical research communications, 302 (2003) 324-329.

76. R.K. Rao, S. Basuroy, V.U. Rao, K.J. Karnaky, Jr., A. Gupta, Tyrosine phosphorylation and dissociation of occludin-ZO-1 and E-cadherin-beta-catenin complexes from the cytoskeleton by oxidative stress, The Biochemical journal, 368 (2002) 471-481.

77. B.C. Elias, T. Suzuki, A. Seth, F. Giorgianni, G. Kale, L. Shen, J.R. Turner, A. Naren, D.M. Desiderio, R. Rao, Phosphorylation of Tyr-398 and Tyr-402 in occludin prevents its interaction with ZO-1 and destabilizes its assembly at the tight junctions, The Journal of biological chemistry, 284 (2009) 1559-1569.

78. M.J. Song, N. Davidovich, G.G. Lawrence, S.S. Margulies, Superoxide mediates tight junction complex dissociation in cyclically stretched lung slices, Journal of biomechanics, 49 (2016) 1330-1335.

79. M. Takeichi, Dynamic contacts: rearranging adherens junctions to drive epithelial remodelling, Nature reviews. Molecular cell biology, 15 (2014) 397-410.

80. T.S. Malinova, S. Huveneers, Sensing of Cytoskeletal Forces by Asymmetric Adherens Junctions, Trends in cell biology, 28 (2018) 328-341.

81. Y.L. Dorland, T.S. Malinova, A.M. van Stalborch, A.G. Grieve, D. van Geemen, N.S. Jansen, B.J. de Kreuk, K. Nawaz, J. Kole, D. Geerts, R.J. Musters, J. de Rooij, P.L. Hordijk, S. Huveneers, The F-BAR protein pacsin2 inhibits asymmetric VE-cadherin internalization from tensile adherens junctions, Nature communications, 7 (2016) 12210.

82. S. Huveneers, J. Oldenburg, E. Spanjaard, G. van der Krogt, I. Grigoriev, A. Akhmanova, H. Rehmann, J. de Rooij, Vinculin associates with endothelial VE-cadherin junctions to control force-dependent remodeling, The Journal of cell biology, 196 (2012) 641-652.

83. K.M. Gray, J.W. Jung, C.T. Inglut, H.C. Huang, K.M. Stroka, Quantitatively relating brain endothelial cell-cell junction phenotype to global and local barrier properties under varied culture conditions via the Junction Analyzer Program, Fluids and barriers of the CNS, 17 (2020) 16.

84. M.A. McGill, R.F. McKinley, T.J. Harris, Independent cadherin-catenin and Bazooka clusters interact to assemble adherens junctions, The Journal of cell biology, 185 (2009) 787-796.

85. Y. Kakei, M. Akashi, T. Shigeta, T. Hasegawa, T. Komori, Alteration of cell-cell junctions in cultured human lymphatic endothelial cells with inflammatory cytokine stimulation, Lymphatic research and biology, 12 (2014) 136-143.

86. H. Schnittler, M. Taha, M.O. Schnittler, A.A. Taha, N. Lindemann, J. Seebach, Actin filament dynamics and endothelial cell junctions: the Ying and Yang between stabilization and motion, Cell Tissue Res, 355 (2014) 529-543.

87. P. Baluk, J. Fuxe, H. Hashizume, T. Romano, E. Lashnits, S. Butz, D. Vestweber, M. Corada, C. Molendini, E. Dejana, D.M. McDonald, Functionally specialized junctions between endothelial cells of lymphatic vessels, The Journal of experimental medicine, 204 (2007) 2349-2362.

88. S.N. Stahley, M. Saito, V. Faundez, M. Koval, A.L. Mattheyses, A.P. Kowalczyk, Desmosome assembly and disassembly are membrane raft-dependent, PloS one, 9 (2014) e87809.

89. Y. Wang, Two-Color Fluorescent Analysis of Connexin 36 Turnover and Trafficking - Relationship to Functional Plasticity, Ophthalmology & Visual Science, University of Texas Health Science Center, Houston, UT GSBS Dissertations and Theses (Open Access) http://digitalcommons.library.tmc.edu/utgsbs_dissertations/589, 2015, pp. 132.

90. B.R. Stevenson, D.A. Begg, Concentration-dependent effects of cytochalasin D on tight junctions and actin filaments in MDCK epithelial cells, Journal of cell science, 107 (Pt 3) (1994) 367-375.

91. L. Shen, J.R. Turner, Actin depolymerization disrupts tight junctions via caveolae-mediated endocytosis, Molecular biology of the cell, 16 (2005) 3919-3936.

92. K.H. Ogawa, C.M. Troyer, R.G. Doss, F. Aminian, E.C. Balreira, J.M. King, Mathematical classification of tight junction protein images, Journal of microscopy, 252 (2013) 100-110.

93. K.M. Gray, D.B. Katz, E.G. Brown, K.M. Stroka, Quantitative Phenotyping of Cell-Cell Junctions to Evaluate ZO-1 Presentation in Brain Endothelial Cells, Ann Biomed Eng, 47 (2019) 1675-1687.

94. H. Brezovjakova, C. Tomlinson, N. Mohd Naim, P. Swiatlowska, J.C. Erasmus, S. Huveneers, J. Gorelik, S. Bruche, V.M. Braga, Junction Mapper is a novel computer vision tool to decipher cell-cell contact phenotypes, eLife, 8 (2019).

95. C. Ward, B. Schlingmann, A.A. Stecenko, D.M. Guidot, M. Koval, NF-kappaB inhibitors impair lung epithelial tight junctions in the absence of inflammation, Tissue Barriers, 3 (2015) e982424.

96. L.L. Pontani, I. Jorjadze, J. Brujic, Cis and Trans Cooperativity of E-Cadherin Mediates Adhesion in Biomimetic Lipid Droplets, Biophysical journal, 110 (2016) 391-399.

97. Y. Wu, X. Jin, O. Harrison, L. Shapiro, B.H. Honig, A. Ben-Shaul, Cooperativity between trans and cis interactions in cadherin-mediated junction formation, Proceedings of the National Academy of Sciences of the United States of America, 107 (2010) 17592-17597.

98. J.R. Turner, Molecular basis of epithelial barrier regulation: from basic mechanisms to clinical application, The American journal of pathology, 169 (2006) 1901-1909.

99. C.E. Overgaard, B. Schlingmann, S. Dorsainvil White, C. Ward, X. Fan, S. Swarnakar, L.A. Brown, D.M. Guidot, M. Koval, The relative balance of GM-CSF and TGF-beta1 regulates lung epithelial barrier function, American journal of physiology. Lung cellular and molecular physiology, 308 (2015) L1212-1223.

100. J. Zhao, E.S. Krystofiak, A. Ballesteros, R. Cui, C.M. Van Itallie, J.M. Anderson, C. Fenollar-Ferrer, B. Kachar, Multiple claudin-claudin cis interfaces are required for tight junction strand formation and inherent flexibility, Commun Biol, 1 (2018) 50.

101. A. Hartsock, W.J. Nelson, Adherens and tight junctions: structure, function and connections to the actin cytoskeleton, Biochimica et biophysica acta, 1778 (2008) 660-669.

102. K. Shigetomi, Y. Ono, T. Inai, J. Ikenouchi, Adherens junctions influence tight junction formation via changes in membrane lipid composition, The Journal of cell biology, 217 (2018) 2373-2381.

103. A. Nusrat, C.A. Parkos, P. Verkade, C.S. Foley, T.W. Liang, W. Innis-Whitehouse, K.K. Eastburn, J.L. Madara, Tight junctions are membrane microdomains, Journal of cell science, 113 (Pt 10) (2000) 1771-1781.

104. M. Matsuda, A. Kubo, M. Furuse, S. Tsukita, A peculiar internalization of claudins, tight junction-specific adhesion molecules, during the intercellular movement of epithelial cells, Journal of cell science, 117 (2004) 1247-1257.

105. D. Zwanziger, C. Staat, A.V. Andjelkovic, I.E. Blasig, Claudin-derived peptides are internalized via specific endocytosis pathways, Annals of the New York Academy of Sciences, 1257 (2012) 29-37.

106. B.L. Daugherty, M. Mateescu, A.S. Patel, K. Wade, S. Kimura, L.W. Gonzales, S. Guttentag, P.L. Ballard, M. Koval, Developmental regulation of claudin localization by fetal alveolar epithelial cells, American journal of physiology. Lung cellular and molecular physiology, 287 (2004) L1266-1273.

107. X. Cong, Y. Zhang, J. Li, M. Mei, C. Ding, R.L. Xiang, L.W. Zhang, Y. Wang, L.L. Wu, G.Y. Yu, Claudin-4 is required for modulation of paracellular permeability by muscarinic acetylcholine receptor in epithelial cells, Journal of cell science, 128 (2015) 2271-2286.

108. B. Schlingmann, C.E. Overgaard, S.A. Molina, K.S. Lynn, L.A. Mitchell, S. Dorsainvil White, A.L. Mattheyses, D.M. Guidot, C.T. Capaldo, M. Koval, Regulation of claudin/zonula occludens-1 complexes by hetero-claudin interactions, Nature communications, 7 (2016) 12276.

109. A.W. Vogl, M. Du, X.Y. Wang, J.S. Young, Novel clathrin/actin-based endocytic machinery associated with junction turnover in the seminiferous epithelium, Seminars in cell & developmental biology, 30 (2014) 55-64.

110. M. Du, J. Young, M. De Asis, J. Cipollone, C. Roskelley, Y. Takai, P.K. Nicholls, P.G. Stanton, W. Deng, B.B. Finlay, A.W. Vogl, A novel subcellular machine contributes to basal junction remodeling in the seminiferous epithelium, Biology of reproduction, 88 (2013) 60.

111. K. Lyon, A. Adams, M. Piva, P. Asghari, E.D. Moore, A.W. Vogl, Ca2+ signaling machinery is present at intercellular junctions and structures associated with junction turnover in rat Sertoli cells, Biology of reproduction, 96 (2017) 1288-1302.

112. G. Caldieri, E. Barbieri, G. Nappo, A. Raimondi, M. Bonora, A. Conte, L. Verhoef, S. Confalonieri, M.G. Malabarba, F. Bianchi, A. Cuomo, T. Bonaldi, E. Martini, D. Mazza, P. Pinton, C. Tacchetti, S. Polo, P.P. Di Fiore, S. Sigismund, Reticulon 3-dependent ER-PM contact sites control EGFR nonclathrin endocytosis, Science, 356 (2017) 617-624.

113. A. Ikari, A. Takiguchi, K. Atomi, J. Sugatani, Epidermal growth factor increases clathrin-dependent endocytosis and degradation of claudin-2 protein in MDCK II cells, Journal of cellular physiology, 226 (2011) 2448-2456.

114. N. Rajagopal, F.J. Irudayanathan, S. Nangia, Computational Nanoscopy of Tight Junctions at the Blood-Brain Barrier Interface, International journal of molecular sciences, 20 (2019).

115. M. Moss, P.E. Parsons, K.P. Steinberg, L.D. Hudson, D.M. Guidot, E.L. Burnham, S. Eaton, G.A. Cotsonis, Chronic alcohol abuse is associated with an increased incidence of acute respiratory distress syndrome and severity of multiple organ dysfunction in patients with septic shock, Critical care medicine, 31 (2003) 869-877.

116. A.J. Mehta, D.M. Guidot, Alcohol and the Lung, Alcohol research : current reviews, 38 (2017) 243-254.

117. P. Smith, L.A. Jeffers, M. Koval, Effects of different routes of endotoxin injury on barrier function in alcoholic lung syndrome, Alcohol, 80 (2019) 81-89.

118. B. Schlingmann, S.A. Molina, M. Koval, Claudins: Gatekeepers of lung epithelial function, Seminars in cell & developmental biology, 42 (2015) 47-57.

119. H. Schmitz, C. Barmeyer, M. Fromm, N. Runkel, H.D. Foss, C.J. Bentzel, E.O. Riecken, J.D. Schulzke, Altered tight junction structure contributes to the impaired epithelial barrier function in ulcerative colitis, Gastroenterology, 116 (1999) 301-309.

120. P. Claude, D.A. Goodenough, Fracture faces of zonulae occludentes from "tight" and "leaky" epithelia, The Journal of cell biology, 58 (1973) 390-400.

121. D. Hayashi, A. Tamura, H. Tanaka, Y. Yamazaki, S. Watanabe, K. Suzuki, K. Suzuki, K. Sentani, W. Yasui, H. Rakugi, Y. Isaka, S. Tsukita, Deficiency of claudin-18 causes

paracellular H+ leakage, up-regulation of interleukin-1beta, and atrophic gastritis in mice, Gastroenterology, 142 (2012) 292-304.

122. O.R. Colegio, C. Van Itallie, C. Rahner, J.M. Anderson, Claudin extracellular domains determine paracellular charge selectivity and resistance but not tight junction fibril architecture, American journal of physiology. Cell physiology, 284 (2003) C1346-1354.

123. M. Furuse, H. Sasaki, K. Fujimoto, S. Tsukita, A single gene product, claudin-1 or -2, reconstitutes tight junction strands and recruits occludin in fibroblasts, The Journal of cell biology, 143 (1998) 391-401.

124. S. Milatz, S.M. Krug, R. Rosenthal, D. Gunzel, D. Muller, J.D. Schulzke, S. Amasheh, M. Fromm, Claudin-3 acts as a sealing component of the tight junction for ions of either charge and uncharged solutes, Biochimica et biophysica acta, 1798 (2010) 2048-2057.

125. S. Nakamura, K. Irie, H. Tanaka, K. Nishikawa, H. Suzuki, Y. Saitoh, A. Tamura, S. Tsukita, Y. Fujiyoshi, Morphologic determinant of tight junctions revealed by claudin-3 structures, Nature communications, 10 (2019) 816.

126. S. Zeissig, N. Burgel, D. Gunzel, J. Richter, J. Mankertz, U. Wahnschaffe, A.J. Kroesen, M. Zeitz, M. Fromm, J.D. Schulzke, Changes in expression and distribution of claudin 2, 5 and 8 lead to discontinuous tight junctions and barrier dysfunction in active Crohn's disease, Gut, 56 (2007) 61-72.

127. R. Kaufmann, J. Piontek, F. Grull, M. Kirchgessner, J. Rossa, H. Wolburg, I.E. Blasig, C. Cremer, Visualization and quantitative analysis of reconstituted tight junctions using localization microscopy, PloS one, 7 (2012) e31128.

128. E.E. Schneeberger, M.J. Karnovsky, Substructure of intercellular junctions in freeze-fractured alveolar-capillary membranes of mouse lung, Circulation research, 38 (1976) 404-411.

129. H. Bartels, H.J. Oestern, G. Voss-Wermbter, Communicating-occluding junction complexes in the alveolar epithelium. A freeze-fracture study, The American review of respiratory disease, 121 (1980) 1017-1024.

130. Z. Lu, D.H. Kim, J. Fan, Q. Lu, K. Verbanac, L. Ding, R. Renegar, Y.H. Chen, A non-tight junction function of claudin-7-Interaction with integrin signaling in suppressing lung cancer cell proliferation and detachment, Molecular cancer, 14 (2015) 120.

131. S. Kuhn, M. Koch, T. Nubel, M. Ladwein, D. Antolovic, P. Klingbeil, D. Hildebrand, G. Moldenhauer, L. Langbein, W.W. Franke, J. Weitz, M. Zoller, A complex of EpCAM, claudin-7, CD44 variant isoforms, and tetraspanins promotes colorectal cancer progression, Molecular cancer research : MCR, 5 (2007) 553-567.

132. L. Zhou, Y. Gong, A. Sunq, J. Hou, L.A. Baker, Capturing Rare Conductance in Epithelia with Potentiometric-Scanning Ion Conductance Microscopy, Analytical chemistry, 88 (2016) 9630-9637.

133. C.R. Weber, G.H. Liang, Y. Wang, S. Das, L. Shen, A.S. Yu, D.J. Nelson, J.R. Turner, Claudin-2-dependent paracellular channels are dynamically gated, eLife, 4 (2015) e09906.

134. O. Dubrovskyi, A.A. Birukova, K.G. Birukov, Measurement of local permeability at subcellular level in cell models of agonist- and ventilator-induced lung injury, Laboratory investigation; a journal of technical methods and pathology, 93 (2013) 254-263.

135. N. Klusmeier, H.J. Schnittler, J. Seebach, A Novel Microscopic Assay Reveals Heterogeneous Regulation of Local Endothelial Barrier Function, Biophysical journal, 116 (2019) 1547-1559.

136. M. Ghim, P. Alpresa, S.W. Yang, S.T. Braakman, S.G. Gray, S.J. Sherwin, M. van Reeuwijk, P.D. Weinberg, Visualization of three pathways for macromolecule transport across cultured endothelium and their modification by flow, Am J Physiol Heart Circ Physiol, 313 (2017) H959-H973.

137. P. Belvitch, M.E. Brown, B.N. Brinley, E. Letsiou, A.N. Rizzo, J.G.N. Garcia, S.M. Dudek, The ARP 2/3 complex mediates endothelial barrier function and recovery, Pulm Circ, 7 (2017) 200-210.

138. R.E. Stephenson, T. Higashi, I.S. Erofeev, T.R. Arnold, M. Leda, A.B. Goryachev, A.L. Miller, Rho Flares Repair Local Tight Junction Leaks, Dev Cell, 48 (2019) 445-459 e445.

139. C.M. Van Itallie, A. Aponte, A.J. Tietgens, M. Gucek, K. Fredriksson, J.M. Anderson, The N and C termini of ZO-1 are surrounded by distinct proteins and functional protein networks, The Journal of biological chemistry, 288 (2013) 13775-13788.

140. G. Spagnol, M. Al-Mugotir, J.L. Kopanic, S. Zach, H. Li, A.J. Trease, K.L. Stauch, R. Grosely, M. Cervantes, P.L. Sorgen, Secondary structural analysis of the carboxyl-terminal domain from different connexin isoforms, Biopolymers, 105 (2016) 143-162.

141. B.J. Hirst-Jensen, P. Sahoo, F. Kieken, M. Delmar, P.L. Sorgen, Characterization of the pH-dependent interaction between the gap junction protein connexin43 carboxyl terminus and cytoplasmic loop domains, The Journal of biological chemistry, 282 (2007) 5801-5813.

142. D. Bouvier, F. Kieken, A. Kellezi, P.L. Sorgen, Structural changes in the carboxyl terminus of the gap junction protein connexin 40 caused by the interaction with c-Src and zonula occludens-1, Cell communication & adhesion, 15 (2008) 107-118.

143. C. Schwayer, S. Shamipour, K. Pranjic-Ferscha, A. Schauer, M. Balda, M. Tada, K. Matter, C.P. Heisenberg, Mechanosensation of Tight Junctions Depends on ZO-1 Phase Separation and Flow, Cell, 179 (2019) 937-952 e918.

CHAPTER 3: REGULATION OF CLAUDIN/ZONULA OCCLUDENS-1 COMPLEXES BY HETERO-CLAUDIN INTERACTIONS

Barbara Schlingmann, Christian E. Overgaard, Samuel A. Molina, K. Sabrina Lynn, Leslie A. Mitchell, StevenClaude Dorsainvil White, Alexa L. Mattheyses, David M. Guidot, Christopher T. Capaldo, Michael Koval

This work is published in Nature Communications (2016) 7:12276. doi: 10.1038/ncomms12276.

Supplemental figures and tables can be found in the online publication.

Abstract

Claudins are tetraspan transmembrane tight junction proteins that regulate epithelial barriers. In the distal airspaces of the lung, alveolar epithelial tight junctions are crucial to regulate airspace fluid. Chronic alcohol abuse weakens alveolar tight junctions, priming the lung for acute respiratory distress syndrome (ARDS), a frequently lethal condition caused by airspace flooding. Here we demonstrate that in response to alcohol, increased claudin-5 paradoxically accompanies an increase in paracellular leak and rearrangement of alveolar tight junctions. Claudin-5 is necessary and sufficient to diminish alveolar epithelial barrier function by impairing the ability of claudin-18 to interact with a scaffold protein, Zonula Occludens 1 (ZO-1), demonstrating that one claudin affects the ability of another claudin to interact with the tight junction scaffold. Critically, a claudin-5 peptide mimetic reverses the deleterious effects of alcohol on alveolar barrier function. Thus, claudin controlled claudin-scaffold protein interactions are a novel target to regulate tight junction permeability.

Introduction

There are ample clinical data demonstrating that alcoholics are at increased risk of ARDS compared to non-alcoholic patients due to a failure in lung fluid clearance leading to airspace flooding which critically impairs gas exchange across the alveolar epithelium. [1, 2] Dietary alcohol significantly impairs alveolar epithelial cell tight junctions that are required to provide a barrier between fluid filled tissues and the airspace.[3] However, the molecular basis for the effects of alcohol on alveolar epithelial tight junctions is not well understood. Here we have used isolated primary rat alveolar epithelial cells (AECs) that differentiate into a model type I monolayer that enables barrier function to be studied at a molecular level. Rats fed dietary alcohol for 8 weeks provide an animal model system that faithfully recapitulates the pathologic consequences of chronic alcohol ingestion on lung barrier function.[4, 5] Moreover, primary cells derived from alcohol-fed rats ("alcohol-exposed AECs") have impaired barrier function that persists in vitro, as compared with AECs isolated from animals fed an isocaloric control diet.

Thus, we studied cultured polarized AECs derived from control and alcohol fed animals as a model system that reflects the behavior of these cells in vivo in forming the alveolar barrier. AECs from alcohol-fed animals have significant changes in tight junction protein expression that are associated with a decrease in epithelial barrier function. Among these changes is an increase in claudin-5 expression. By molecular manipulation of AECs we find that claudin-5 is both necessary and sufficient to disrupt AEC tight junctions. Increased claudin-5 expression induces the formation of claudin-containing structures perpendicular to the axis of the cell-cell interface (tight junction spikes) that are active sites of vesicle budding and fusion. The appearance of tight junction spikes correlates with increased paracellular leak between AECs. Using several complementary approaches, including super-resolution microscopy and the proximity ligation assay, we find that claudin-5 interacted with claudin-18 and that this decreases the ability of claudin-18 to productively interact with ZO-1. This provides the first example of one claudin affecting the ability of another claudin to interact with the tight junction scaffold. This

mechanism is targetable using a claudin-5 mimetic peptide, suggesting a potential therapeutic approach to promote alveolar barrier function.

Results

Chronic alcohol alters lung tight-junction permeability.

The difference between AECs isolated from control- and alcohol-fed animals (alcohol-exposed AECs) is demonstrated in Figure 3.1a-c, using two different measures of barrier function: transepithelial resistance (TER) and paracellular flux to soluble tracer molecules. Consistent with an increase in paracellular leak, alcohol-exposed AECs had significantly decreased TER and showed increased flux of both calcein (0.62 kDa) and Texas Red Dextran (10 kDa). Thus, alcohol exposure has a deleterious effect on AEC tight junctions, consistent with previous reports.[4, 6]

As claudins are central to the regulation of tight junction permeability [7-9], claudin protein composition of control- and alcohol-exposed AECs cultured on Transwell permeable supports was examined by immunoblot. The decrease in AEC barrier function induced by alcohol correlated with decreased claudin-4 protein (Figure 3.1d,e). Claudin-1, claudin-3 and claudin-7 were unaffected. However, AEC-associated claudins did not simply decrease in response to alcohol. Instead, claudin-5 was significantly increased in alcohol-exposed AECs as compared with control AECs (Figure 3.1d,e), consistent with previous analysis of freshly isolated type II cells and AECs cultured on tissue culture plastic.[10] There also was a trend towards increased claudin-18 in alcohol-exposed AECs as compared with control AECs ($p=0.15$, $n=3$, unpaired two-tailed t-test). Since there was increased paracellular leak accompanying increased claudin-5 expression, we examined the effects of claudin remodeling in response to alcohol to determine whether this had a destabilizing effect on tight junctions.

Increased claudin-5 causes increased paracellular leak.

In particular, increased claudin-5 expression by lung epithelial cells has previously been associated with an increase in paracellular leak by alveolar epithelial cells.[11] To confirm whether increased claudin-5 was sufficient to increase paracellular leak, we examined the dose response of increased YFP-claudin-5 expression using an adenovector to transduce primary AECs. A four-fold increase in claudin-5 expression [(YFP-claudin-5+claudin-5)/claudin-5] significantly decreased TER (Figure 3.1f-h) and increased paracellular flux (Supplementary Fig. 1a,b). Critically, this level of YFP-claudin-5 expression is in the physiologic range, comparable to the increase in endogenous AEC claudin-5 expression induced by alcohol (Figure 3.1e). In the converse experiment, lentiviral shRNA constructs were used to decrease claudin-5 expression (Supplementary Table 1). As shown in Figure 3.1i-k, using shRNA to decrease claudin-5 expression by AECs from alcohol-fed rats caused a significant increase in TER and also decreased paracellular flux (Supplementary Fig. 1c,d).

Since claudin-4 decreased in response to dietary alcohol, it could also have a negative impact on AEC barrier function in combination with increased claudin-5. Thus, we examined whether increased claudin-4 could rescue the effects of alcohol on AECs. As shown in Supplementary Fig. 2a, alcohol-exposed AECs transduced with CFP-claudin-4 had only a partial increase in TER compared to control AECs. Moreover, the effects of increased claudin-4 were antagonized by a concurrent transduction with YFP-claudin-5. That claudin-5 countered the ability of claudin-4 to promote paracellular barrier function suggests that these claudins are directly interacting. Formation of complexes containing native claudin-4 and native claudin-5 was confirmed by co-immunopurification analysis of AECs (Supplementary Fig. 2b). We also observed using co-immunopurification that native claudin-5 directly interacts with native claudin-18 and ZO-1 (Supplementary Fig. 2g). These data further support the hypothesis that increased claudin-5 has a deleterious and dominant effect on other claudins and thereby impairs AEC barrier function.

Tight junction spikes are associated with barrier disruption.

As revealed by immunofluorescence microscopy of claudin-18 (Figure 3.2a), AECs from alcohol-fed rats have changes in tight junction morphology, most notably increased formation of tight junction spikes (Figure 3.2d), which are actin-associated structures perpendicular to the axis of the cell-cell interface that correlate with an increase in paracellular leak. [4,5] Normal AECs transduced to express increased claudin-5 also showed an increase in claudin-18 containing spikes, comparable to the effect of alcohol on tight junction morphology (Figure 3.2b,e). Morphologic disruption of tight junctions was not restricted to claudin-18, as claudin-5 (Figure 3.2b) and ZO-1 (Supplementary Fig. 3j-l) were also impaired in YFP-claudin-5 transduced AECs. To determine whether ZO-1 disruption was specifically linked to increased claudin-5, we examined the effect of increased YFP-claudin-3 on ZO-1 localization by AECs and found there was little effect on tight junction morphology based on localization of claudin-18 (Supplementary Fig. 3g-i) or ZO-1 (Supplementary Fig. 3m-o).[12] In a complementary experiment, we determined whether the ability of alcohol to induce formation of tight junction spikes was antagonized by depleting claudin-5 using shRNA. As shown in Figure 3.2c,f, this was the case for two different specific claudin-5 shRNAs. Thus, claudin-5 was necessary and sufficient to enhance formation of tight junction spikes.

To rule out an effect of YFP-claudin-5 expression on levels of other key AEC tight junction proteins, we examined expression of claudin-1, claudin-3, claudin-4, endogenous claudin-5, claudin-7, claudin-18 and ZO-1 by AECs transduced with YFP-claudin-5. As shown in Supplementary Fig. 4, YFP-claudin-5 expression had little effect on total levels of these tight junction proteins in AECs. We also wanted to ensure that the effects of YFP-claudin-5 on AECs were not due to the N-terminal YFP tag. AECs transduced with untagged claudin-5 faithfully recapitulated the effects of alcohol on these cells, namely increased formation of tight junction spikes and impaired barrier function (Supplementary Fig. 5).

Although tight junction spikes correlated with diminished paracellular barrier function, how spikes were mechanistically linked to paracellular leak was not known. We hypothesized that spikes represented areas of enhanced tight junction protein reorganization, which is known to increase paracellular leak. To address this, we used AECs expressing YFP-claudin-18 that were adjacent to untransfected AECs (Figure 3.2g,h). Note that YFP-claudin-18 acts to label tight junction spikes in live cells and did not induce formation of spikes in a manner comparable to claudin-5. Spike associated YFP-claudin-18 was found to be internalized by neighboring, non-transduced cells, suggesting that the adjacent cells internalized claudin-18 from neighboring cells. Moreover, co-localization of ZO-1 to YFP-claudin-18 was variable, since there were readily visualized YFP-claudin-18 structures that lacked co-localization with ZO-1(Figure 3.2h; arrowheads) although claudin-18 and ZO-1 did co-localize in other spike-associated structures (Figure 3.2h; arrows).

To further characterize the behavior of claudins associated with tight junction spikes, we used live cell imaging microscopy of alcohol exposed AECs transduced to express either YFP-claudin-5 (Figure 3.3a,b; Supplementary Video 1) or YFP-claudin-18 (Figure 3.3c,d; Supplementary Video 2), which revealed the dynamic nature of tight junction spikes. Specifically claudin-labeled vesicles were found to both fuse with (Figure 3.3a,c) and bud from (Figure 3.3b,d) tight junction spikes. To further confirm that spikes were sites of active claudin vesicle formation and fusion [13], we examined the effects of the dynamin inhibitor Dynasore [14] on spike formation by alcohol-exposed AECs. Consistent with this, treatment with Dynasore at 160 μM for 4 h caused a significant decrease in the number of cells with tight junction spikes (Figure 3.3e,f) comparable to the number of cells containing spikes observed for untreated control AECs (Figure 3.3e,g). Dynasore treated cells also showed an increase in punctate YFP-claudin-18 labeling, which likely represents secretory and endocytic vesicles that are inhibited from fusing with target intracellular membranes by Dynasore. Since an increase in tight junction spikes correlated with decreased barrier function, these data suggest that increased vesicle-mediated

trafficking of claudins both into and out of tight junctions contributes to paracellular leak in response to alcohol.

Claudin-5 alters interactions between claudin-18 and ZO-1.

Since tight junctions are multi-protein complexes, paracellular barrier function requires coordinating heterologous interactions between tight junction proteins. In intact cell junctions, protein-protein interactions are reflected by co-localization of two or more proteins in the same intracellular location when resolved at sufficient resolution. To understand how alcohol-induced changes affect tight junctions at a molecular level, we examined AECs isolated from control- and alcohol-fed rats by a form of super-resolution immunofluorescence microscopy, STochastic Optical Reconstruction Microscopy (STORM), which has an X-Y resolution down to 20 nm (Figure 3.4, Supplementary Fig. 6). [15, 16] By the nature of the technique, STORM provides images that are composed of point densities, resulting in a particulate image at high magnification. We noticed that STORM images obtained using the same labeling and imaging conditions appeared to have differences in the size of particulate clusters when comparing control vs alcohol-exposed AECs. Thus, we quantified the distribution of particulate clusters (Supplementary Fig. 7). STORM imaging of normal AECs showed that claudin-18, claudin-5 and ZO-1 clusters had median areas of 1240, 1410 and 1590 nm^2 respectively (Supplementary Fig. 7g-i). By contrast, alcohol-exposed AECs had claudin-18, claudin-5 and ZO-1 clusters with median areas of 1410, 1000 and 1120 nm^2, respectively. The alcohol-induced decrease in median cluster size for claudin-5 and ZO-1 was significant, as determined by Mann Whitney U test, however, Claudin-18 cluster size was statistically unchanged. Since these images were obtained using the same labeling and imaging conditions, the change in claudin-5 and ZO-1 cluster size induced by alcohol is likely to reflect tight junction re-organization in response to alcohol, despite the inability to assign a specific physiologic correlate to particulate clusters. As shown in Figure 3.4 and Supplementary Fig. 6, STORM images of AEC tight junctions showed a

predominant linear intercellular complex with some projections and limited meshwork architecture. Some images also showed tight junction spikes. This contrasts with the super resolution images obtained by Kauffmann, et al.[17] using a comparable technology (Spectral Position Determination Microscopy) to analyze claudin-transfected HEK293 cells expressing claudin-3 or claudin-5 at levels optimized to form a native-equivalent junctional meshwork on the apical surface. Nonetheless, it was not surprising that STORM analysis of AECs did not show an extensive meshwork since tight junctions between adjacent type I AECs *in situ* were shown to have a fairly limited architecture. [18, 19] Moreover, STORM images are obtained using the Total Internal Reflection Fluorescence mode of illumination and so any junctional elements perpendicular to the narrow plane of focus would not be revealed using our approach. Here we optimized the STORM imaging conditions for co-localization analysis between tight junction proteins as opposed to maximizing imaging resolution.

STORM enabled quantitative differences in co-localization to be measured, as we performed these measurements where crosstalk between the two different channels was minimized (Supplementary Fig. 8). In alcohol-exposed AECs, there was a significant decrease in co-localization between claudin-18 and ZO-1 as compared with control AECs (Figure 3.4d). Conversely, there was an increase in co-localization between claudin-18 and claudin-5 in AECs isolated from alcohol-fed rats as compared with controls (Figure 4e). This reciprocal relationship supports the hypothesis that in response to interacting with claudin-5, claudin-18 dissociates from ZO-1.

To further investigate the alcohol induced changes in ZO-1:claudin-18 co-localization, we examined AECs using the proximity ligation assay (PLA) which has a resolving power of 30-40 nm. [20, 21] As shown in Figure 3.5 and Supplementary Fig. 9, PLA analysis of claudin-18 and ZO-1 in control AECs gave a robust signal. Negative controls are shown in Supplementary Fig. 10. By contrast, alcohol-exposed AECs had a significantly diminished PLA signal (Figure 3.5c). Conversely, claudin-18 and claudin-5 had a PLA signal that was increased in alcohol-exposed

AECs as compared with control AECs (Figure 5n). ZO-1:claudin-5 co-localization was comparable for control and alcohol-exposed AECs although the PLA signals have a slightly different appearance because the cluster size for both ZO-1 and claudin-5 is sensitive to alcohol (Supplementary Fig. 7). These results parallel our analysis of the effects of alcohol on claudin-18, claudin-5 and ZO-1 co-localization by STORM (Figure 3.4d-f). Thus, two independent approaches demonstrate that ZO-1:claudin-18 proximity was diminished by alcohol and correlated with an increase in claudin-18:claudin-5 proximity.

To determine whether increased claudin-5 was sufficient to decrease association of claudin-18 and ZO-1, we examined AECs transduced with YFP-claudin-5 by STORM (Figure 3.6a and Supplementary Fig. 6s-x). As opposed to untransduced AECs, where the co-localization index between claudin-18 and ZO-1 was 30.5 $\pm$ 3.6% (mean $\pm$ SEM; n=3; Figure 3.4d), AECs expressing YFP-claudin-5 had significantly decreased co-localization between claudin-18 and ZO-1 (16.4 $\pm$ 3.0%, n=3, p=0.029, unpaired two-tailed t-test) that was comparable to alcohol-exposed AECs (15.2 $\pm$ 0.7, n=3, unpaired two-tailed t-test; Figure 3.4d). The significant drop in co-localization between ZO-1 and claudin-18 is consistent with a decrease in interaction between these two proteins which we hypothesize would alter the assembly state of claudin-18.

In AECs, both claudin-18 and ZO-1 are highly resistant to Triton X-100 [12] (Figure 3.6b,c), suggesting that ZO-1:claudin-18 complexes are tightly associated with the cytoskeleton.[22] Thus, we examined the effects of increased claudin-5 on the extractability of claudin-18, claudin-5 and ZO-1 by Triton X-100. Consistent with previous measurements, less than ~35% of claudin-18 can be solubilized by Triton X-100 under conditions where the insoluble fraction primarily reflects proteins incorporated into tight junctions [12] (Figure 3.6c). By contrast, the majority of cell-associated claudin-5 is extractable by Triton X-100.

When AECs were transduced with YFP-claudin-5, the Triton X-100 soluble pool of claudin-18 significantly increased from 35.2 $\pm$ 1.8 to 42.1 $\pm$ 0.6 (n=3; p=0.003, unpaired two-tailed t-test), representing a 20% increase in claudin-18 solubility (Figure 3.6c). However, ZO-1

solubility was unchanged by increased claudin-5 (43.1 ± 6.4 vs. 40.4 ± 5.5 (n=3)). Instead, the increase in claudin-18 solubility induced by YFP-claudin-5 expression (Figure 3.6) correlated with the decrease in co-localization between claudin-18 and ZO-1 from ~31% to ~16% as measured by STORM (see above). This decrease in co-localization suggests that decreased ZO-1:claudin-18 interactions induced by increased claudin-5 are sufficient to destabilize the tight junctional pool of claudin-18.

A claudin-5 peptide improves alveolar barrier function.

Claudin peptide mimetics corresponding to the extracellular domain [23-28] and *Clostridium perfringens* enterotoxin variants [29,30] have been successfully used to alter tight junction permeability and probe for claudin-claudin interactions. This suggested that targeting claudin-5 using an extracellular domain peptide might be an effective approach to improve the barrier function of AECs by inhibiting integration into tight junctions. Analogous to an approach used by Baumgartner, et al. [27] to target claudin-3 and claudin-4, we used an acetylated D-amino acid peptide corresponding to the region of the second extracellular (E2) domain directly adjacent to the third transmembrane (TM3) domain of claudin-5 (Ac-EFYDP-NH_2). The E2/TM3 region is implicated in mediating cis-claudin interactions, based on the crystal structure of claudin-15 [31], as well as functional studies of claudin-3:claudin-5 [32] and homomeric claudin-5 interactions [33]. Also, the corresponding region of claudin-18 (NFWMS) is not conserved and this region is sufficiently divergent from the corresponding DFYNP sequence found in other major claudins found in the lung, including claudin-3, -4, and -7. Claudin-1 does have an EFYDP motif, however, it is present at low levels in AECs, suggesting that the Ac-EFYDP-NH_2 peptide could effectively target claudin-5 and reverse the effects of alcohol on tight junctions.

As shown in Figure 3.7b,d,f, overnight incubation of alcohol-exposed AECs with the Ac-EFYDP-NH_2 peptide increased barrier function, as measured by an increase in TER and decrease in paracellular flux of calcein and Texas Red Dextran. By contrast, control AECs were

unaffected by the Ac-EFYDP-NH_2 peptide (Figure 3.7a,c,e). A control peptide, Ac-LYQY-NH_2, had no effect on AEC barrier function in either control or alcohol-exposed cells. The ability of Ac-EFYDP-NH_2 to improve the barrier function of alcohol-exposed AECs correlated with a decrease in tight junction spike formation (Figure 3.7g,h) and a specific decrease in total claudin-5 content (Figure 3.7j,l). Claudin-18 and ZO-1 were unaffected (Figure 3.7i-l) as was claudin-1 (Supplementary Fig. 11e,f). These data provide an additional demonstration that an increase in endogenous claudin-5 diminishes AEC barrier function in response to alcohol and underscore the potential to directly target claudin-5 as a therapeutic approach to prevent alcoholic lung syndrome.

Discussion

This study provides the first demonstration that an inter-claudin interaction has the capacity to affect claudin-scaffold protein interactions. Specifically, increased claudin-18:claudin-5 interactions decreased ZO-1:claudin-18 co-localization, which correlated with weakened assembly into tight junctions as evidenced by an increase in Triton X-100 solubility (Figure 3.6). The net effect of decreased interactions between claudin-18 and ZO-1 is to destabilize tight junctions that, in turn, increases paracellular leak. [34] It is likely that claudin-claudin interactions beyond claudin-18:claudin-5 interactions will be found to play significant roles in the context of regulating assembly of claudins into tight junctions as well as in the organization of junctional scaffold complexes as signaling platforms that, in turn, affect paracellular permeability. Future work will determine whether or not this is the case.

Whether claudin-18:claudin-5 complexes are preformed or claudin-5 molecules newly delivered to the membrane destabilize claudin-18, is not known at present. Two examples of claudin-claudin interactions that occur prior to delivery to the plasma membrane are claudin-4:claudin-8 [35] and claudin-16:claudin-19.[36] In each of those cases, depletion or misfolding of one claudin resulted in intracellular accumulation of the other, evidence that these pairs of

claudins serve as co-chaperones. Interestingly, in kidney epithelia, claudin-18 trafficking was independent of claudin-16 and claudin-19, [36] indicating specificity of cis claudin interactions. In AECs, the intracellular pools of claudin-5 and claudin-18 are limited, largely vesicular and do not show complete co-localization. Since the effects of claudin-5 on claudin-18 largely affect tight junction morphology in AECs and that these effects are antagonized by a claudin-5 extracellular mimetic peptide, it seems more likely that claudin-5 and claudin-18 interact within tight junctions or other regions of the plasma membrane rather than prior to delivery. Considering that tight junction associated claudins are highly dynamic [37, 38], there is certainly the capacity for claudin remodeling to occur within pre-formed tight junctions at cell-cell interfaces as well as in claudins newly delivered to the plasma membrane. [39]

Critically, this provides a novel mechanism for alcoholic lung syndrome whereby cis-interactions between claudin-5 and claudin-18 can diminish barrier function by affecting the ability of claudin-18 to form complexes with ZO-1. Cis-interactions between claudin-5 and claudin-3 have previously been characterized at a molecular level,[32, 40] but this is the first demonstration that claudin-5 can regulate the ability of another claudin, in this case claudin-18, to interact with the cytoplasmic scaffold. Cytoplasmic scaffold proteins, including ZO-1 and ZO-2, have classically been thought of as being the primary regulators of claudin assembly into tight junction strands by crosslinking claudins to the actin cytoskeleton.[38,41,42] In this model, claudins are essentially considered to be passive components that are directed by scaffold proteins such as ZO-1 to interact with actin and to sites were intercellular contacts can form.[34]

The ability of claudin-claudin interactions to regulate association of scaffold proteins with transmembrane components of tight junctions complements the classical model for scaffold protein-claudin interactions in which ZO-1 binds to the extreme C-terminal domain of nearly all claudins and promotes interactions with the actin cytoskeleton. The hypothesis that claudin-claudin interactions can affect how the C-terminal tail interacts with the scaffold suggests that adjacent or co-heteroligomerized claudins have the capacity to attain conformations that either

permit or restrict interactions with scaffold proteins. Although current high resolution structural models of claudins have provided some insights into how claudins pack and form paracellular ion channels,[31,43] the C-terminus is relatively unstructured and therefore how claudin-claudin interactions can affect its conformation are not known. From the gap junction literature, there are several examples where C-termini of connexins in heteromeric channels regulates their conformation and channel function.[44,45] Although it remains to be determined, since ZO-1 interacts with the extreme terminal PDZ binding motif of most claudins, interactions with ZO-1 are unlikely to occur unless the C-terminus is fully extended and not sterically hindered.

Claudin-5 increased formation of tight junction spikes that, in turn, correlated with increased paracellular leak. Association of tight junction spikes with increased paracellular permeability is consistent with previous studies demonstrating that spikes and barrier dysfunction are also induced by Transforming Growth Factor β [4] and NF-kB inhibitors.[5] In fact, normal AECs treated with the NF-kB inhibitor BMS-345541 showed both increased claudin-5 expression and increased formation of tight junction spikes as a result of interfering with GM-CSF signaling that mimics the effects of alcohol on AECs.[5] Here, live cell imaging was used to confirm that these were sites where claudin-containing vesicles were observed to bud and fuse from the ends of spikes. Linking tight junction spikes and enhanced endocytosis with a decrease in barrier function is also consistent with our previous demonstration that treatment of fetal AECs with endocytosis inhibitors almost doubled TER,[46] as well as studies by other researchers demonstrating that increased junction protein endocytosis is associated with epithelial barrier dysfunction.[47-50]

Structures comparable to the tight junction spikes observed here are also associated with keratinocyte desmosomal endocytosis induced by *Pemphigus vulgaris* antisera[51], suggesting that spikes may be a general feature of squamous epithelial cells representing sites of active vesicle traffic involving deposition and internalization of junction proteins. It is also possible

that spikes are sites where vesicle traffic is more readily visualized and that vesicle budding and fusion occur at other locations in tight junctions, although the correlation between spike number and barrier dysfunction would argue against this possibility. In addition, whether spikes are formed by cuboidal epithelia remains to be determined and likely will require high resolution three dimensional imaging.

Given that tight junction spikes are associated with alcohol and claudin-5 expression, and that these are sites of active vesicle trafficking of claudin-containing vesicles, our data demonstrate that increased claudin-5 is both necessary and sufficient to account for the deleterious effects of dietary alcohol on AEC barrier function. Although the effects of increased claudin-5 appear to contradict the role of claudin-5 in promoting endothelial barrier function[4], our data demonstrate that claudin-5 function is cell type dependent and influenced by the context of expression. For example, claudin-5 has the capacity to increase barrier function of MDCK II cells which are otherwise exceptionally leaky, with baseline TER in the range of 100 Ohm x cm^2.[52] In AECs, which are much tighter, claudin-5 had the opposite effect. It is also possible that the ability of claudin-5 to impair tight junctions is specifically dependent on an interaction with claudin-18, which is not present in MDCK cells. A specific interaction between claudin-5 and claudin-18 has particular relevance to alveolar barrier function. Although increased claudin-5 was associated with alcoholic lung disease, the mechanism by which alcohol induces claudin-5 expression is under investigation at present and could either be transcriptional or post-translational.

As claudin-5 has a dramatic effect on AEC barrier function, it represents an appealing potential pharmacologic target to improve alveolar barrier function in vulnerable individuals. Using a claudin-5 mimetic peptide (Ac-EFYDP-NH_2) designed according to Baumgartner, et al. [27] we confirmed the feasibility of this approach, since this peptide specifically increased barrier function of alcohol-exposed AECs (Figure 3.7a-f). We used an Ac-EFYDP-NH_2 composed of D-amino acids, since the Baumgartner group demonstrated that the D-amino acid version of an

Ac-DFYNP-NH_2 mimetic is 10-100 fold more effective than the corresponding L-amino acid version. [27] Unlike the DFYNP sequence which is shared by several claudins important for lung barrier function, including claudin-3 and claudin-4, the EFYDP corresponding to claudin-5 is unlikely to cross react with other non-homologous claudins and claudin-1 expression in the lung is low and unaffected by the peptide (Supplementary Fig. 11e,f). Whether this level of specificity is sufficient to promote alveolar barrier function *in vivo* remains to be determined.

EFYDP is in the E2 region of the protein directly adjacent to the TM3 domain, a region of claudin-5 that mediates cis-claudin interactions [32, 33, 53], consistent with our model that claudin-5 interactions with claudin-18 have a deleterious effect on the ability of claudin-18 to interact with ZO-1. The ability of a cis claudin interaction to affect interactions of another claudin with the tight junction scaffold represents a novel mode of tight junction regulation with the potential to be pharmacologically manipulable. Specific and direct targeting of claudin-5 using these approaches offers the potential of preventing ARDS, particularly in those individuals at greatest risk due to underlying alcohol abuse, by improving alveolar barrier function and fluid clearance.

Methods

Cell culture

Animal protocols were reviewed and approved by the Institutional Animal Care and Use Committee of Emory University. Adult male Sprague-Dawley rats were pair-fed ethanol (36% of total calories) or control isocaloric maltin-dextrin using the liquid Lieber DeCarli Diet (Research Diets, New Brunswick, NJ) ad libitum for 6 to 8 weeks.[4] Animal use was limited to their use as a source for primary cells and so sample size and randomization are not relevant variables.

Type II alveolar epithelial cells were isolated from rats fed either alcohol or a control diet according to Dobbs [54] with modifications. To remove red blood cells, lungs were perfused *in situ* with solution II (5.5 mM Dextrose, 10 mM HEPES, 2 mM $CaCl_2$,12.3 mM $MgSO_4$, 5 mM KCl, 140 mM NaCl, pH 7.4) at 37°C. Lungs were then removed, lavaged with cold PBS then lavaged with

cold solution I (5.5 mM Dextrose, 10 mM HEPES, 0.197 mM EGTA,12.3 mM $MgSO_4$, 5 mM KCl, 140 mM NaCl, pH 7.4). Elastase (103 units/40 ml solution II) was instilled into the lungs which were incubated for 30 min at 37°C. The lungs were then manually diced and resuspended in 5 ml FBS + 5 ml DNase solution (1 mg/ml in solution II). The cells suspension was incubated for 10 min at 37°C under gentle rotation, sequentially filtered through a 100 μm and then a 40 μm cell strainer (BD Biosciences), then centrifuged at 150 x g for 8 minutes at 4°C. The cell pellet was resuspended in 10 ml Dulbecco's modified Eagle media (DMEM; Sigma) containing 0.25 μg/ml amphotericin B (ThermoFisher), 100 U/ml penicillin:10 mg/ml streptomycin (Sigma), then biopanned to remove macrophages in polystyrene bacteriological 100 mm Petri dishes pretreated with 1.5 mg rat IgG/dish for 1h at 37°C. Using this approach, preparations routinely contained >90–95% type II alveolar epithelial cells.

To produce model type I alveolar epithelial cells (AECs), 7.5 x 10^5 cells in DMEM + 10% Fetal Bovine Serum were plated in 1.12 cm^2 Transwell permeable supports (Corning 3460) pre-coated with 250μl of 20 μg/ml rat tail type I collagen in PBS (Roche Diagnostics, Mannheim, Germany), conditions that support differentiation to a type I-like phenotype.[55, 56] Culture media on both the apical and basolateral wells were changed every other day and cells were used for experiments on day 6 or 7 after seeding.

Virus production and infection

Adenovectors encoding for NH_2-terminal enhanced yellow fluorescent protein (YFP)-claudin-3 and control EGFP were prepared as previously described [12]. YFP-claudin-5 cDNA was produced as previously described [57], removed using KpnI and XbaI, and then ligated into pAdLox using standard molecular biological techniques. YFP-claudin-18 and untagged claudin-5 were cloned into pAdeasy-1. Note that for all claudin constructs the YFP was located on the N-terminus of the claudin. Adenovirus particles were packaged and amplified by ViraQuest Inc (North Liberty, IA). YFP-Claudin-5/AdLox was packaged by the National Heart, Lung, and

Blood Institute Viral Vector Core at the University of Pittsburgh. Alternatively, pAdLox plasmids were packaged and amplified by infecting HEK AD293 cells cultured in DMEM containing 5% heat inactivated FBS, 0.25 μg/ml amphotericin B and 100 U/ml penicillin,10 mg/ml streptomycin. Virus particles were purified by cesium chloride centrifugation followed by dialysis against PBS.[58]

Control and claudin-5 specific lentivector shRNAs (Supplementary Table 1) were cloned into a modified expression vector pFH1þU6-UG-W using NheI and PacI as described.[59] Lentiviral particles were produced by the Emory Neuroscience NINDS Viral Core Facility.

AECs cultured on Transwell permeable supports were transduced 4 days after isolation with either adenovector or lentivectors by adding virus particles to both the apical and basal media. For adenovectors and lentivectors, transduction was done at a multiplicity of infection (MOI) of 5, and analyzed 48 h after transduction, unless otherwise stated. Analysis was done 48 h post transduction. For lentivectors, cell media were changed 24 h after transduction.

Barrier function measurements

Transepithelial resistance (TER) measurements of AECs cultured on Transwell permeable supports in Ringer's saline buffer (150 mM NaCl, 2 mM $CaCl_2$, 1 mM $MgCl_2$, 10 mM glucose, 10 mM HEPES, pH 7.4) was measured using an Ohmmeter (World Precision Instruments, Sarasota, FL). Paracellular dye permeability was assessed by simultaneous measurement two different-sized fluorescent dyes across the cell monolayer for 2 h at 37°C [5, 12]. Flux assays were performed in Ringer's saline containing 50 μg/ml Texas Red Dextran (10kDa) (ThermoFisher) and 2 μg/ml Calcein (0.62 kDa) (ThermoFisher) in the apical chamber. The amount of fluorophore that diffused into the basal chamber was measured using a microplate reader (Biotek Winooski, VT).

Biochemical analysis

After 6 days in culture, AECs on Transwell permeable supports were washed 2x with DPBS and incubated for 20 min in 50 µl RIPA buffer (Cell Signaling). Cell were scraped off and debris were pelleted by centrifugation for 10 minutes at 13.200 x g at 4°C. Protein concentration of the supernatant was determined by BCA assay (ThermoFisher Pierce #23225). Reducing SDS sample buffer (10% glycerol, 1.25% SDS, 50 mM Tris pH 6.7, 8.3 mg/ml DTT) was added to the supernatant. Protein samples were heated for 10min at 70°C then resolved by SDS-PAGE using 4-15% Mini-PROTEAN TGX stain-free gradient SDS polyacrylamide gels, transferred to PVDF or nitrocellulose membranes (BioRad, Hercules, CA) and immunostained using primary antibodies and secondary antibodies indicated in Supplementary Table 2. For band detection, either Clarity Western ECL Substrate (BioRad) was used and imaged with the ChemiDocTMXRS system (BioRad, Hercules CA, USA) or fluorescence imaging was used with the Odyssey Classic imager (LI-COR). Image analysis and quantification was done using Image Lab software (BioRad) or using Image studio (LI-COR). Relative protein quantification was relative to actin. LI-COR images of immunoblots were pseudocolored to greyscale images in the Figures. Uncropped versions of immunoblots shown in the main body of the text are in Supplementary Fig.12.

Co-Immunoprecipitation

AECs were isolated and 2.5 x10^6 cells/well were plated on 6 well Transwell permeable supports (Corning 3450) coated with 20µg/ml rat tail collagen (Roche) and cultured for 6 days as described above. Cells were washed 2x with ice cold DPBS containing Ca^{2+} and Mg^{2+} (DPBS++). Cells were scraped in DPBS++ containing protease inhibitor cocktail without EDTA (Roche) and centrifuged at 4°C, 500g for 8 min. Then cells were resuspended in DPBS++ with protease inhibitor cocktail without EDTA (Roche) containing 0.1% (v/v) Triton X-100, sonicated 3x for 1 sec and incubated for 30 min on ice. Cell lysates were centrifuged at 500g for 8 min at 4°C to remove large aggregates.

Prior to use, protein A magnetic beads (Sure Beads; BioRad) for co-immunoprecipitation were washed 3x in DPBS++ (100 µl beads/1ml) and then blocked with DPBS++ containing protease inhibitor cocktail, 0.25%BSA, 0.2% Gelatin for 1h at 4°C. The cell supernatant was then incubated with 100µl blocked, unlabeled beads for 3 h at 4°C to remove non-specific interacting proteins. Precleared supernatant then was mixed with bead/antibody complexes (100 µl beads labeled with 1µg antibody for 15 min at 4°C) and incubated over night at 4°C. The next day, beads were washed 3x with DPBS++ containing protease inhibitor cocktail. Beads were resuspended in 1x SDS-PAGE sample buffer, then incubated for 10 min at 70°C to elute proteins bound to beads. Protein samples were analyzed by SDS-PAGE and immunoblot as described above.

Triton-X solubility assay

Tight junction proteins were assessed for changes to Triton X-100 extractability as described earlier[12] with modifications. After 6 days in culture on Transwell permeable supports AECs were washed 2 x with ice cold DPBS. After washing, 4 wells were combined and cells were scraped 2 x into ice cold DPBS containing Protease inhibitor cocktail with EDTA (Roche). Cells were centrifuged for 8 minutes at 500 x g at 4°C, resuspended in DPBS with protease inhibitor cocktail (Roche, Nutley, NJ) containing 0.1% (v/v) Triton X-100 and incubated for 30 min at 4°C. Then, cells were centrifuged at 100,000 x g for 30 min at 4°C to separate the lysate into Triton-soluble (supernatant) and -insoluble (pellet) fractions. The samples were equivalently diluted in SDS-PAGE sample buffer, heated for 10min at 70°C, then analyzed by SDS-PAGE and immunoblot as described above.

Fluorescence microscopy

AECs were cultured for 6 days on Transwell permeable supports, were washed 3x with DPBS containing Ca^{2+} and Mg^{2+} (DPBS++), fixed with 1:1 methanol/acetone for 2 min at RT and then

washed again 3x with DPBS++. For permeabilization cells were washed once with DPBS++ containing 0.5% Triton X-100, 3x with DPBS++ containing 0.5%Triton X-100 and 5% normal goat serum for 5 min. Then cells were labeled for 1 h in DPBS++ containing 5% normal goat serum for 1 h at RT containing primary antibodies (Supplementary Table 2) . Before secondary antibody incubation cells were washed 3x with DPBS containing 5% goat serum for 5 min, respectively. Cells were then incubated for 1 h with Cy-2 and/or or Cy3-conjugated antibodies (Supplementary Table 2) in DPBS with 5% normal goat serum. Cells were washed 3x with DPBS++ with 5% normal goat serum, and another 3x with DPBS++ before mounted in Mowiol (Kuraray, Houston, TX) under a glass coverslip. Fluorescence images were taken using an Olympus IX70 microscope with a U-MWIBA filter pack (BP460–490, DM505, BA515–550) or U-MNG filter pack (BP530–550, DM570, BA590–800). Minimum and maximum intensities were adjusted for images in parallel, so that the intensity scale remained linear to maximize dynamic range.

For Dynasore experiments, 5.0 x 10^5 AECs isolated from control or alcohol fed rats were plated on collagen coated Transwells and cultured for 6 days. On day six the cells were washed once with serum free media. Serum free media containing 0.25% DMSO (vehicle control), 40μM, 80μM or 160μM (in 0.25%DMSO) was put into each well. Cells were incubated for 4 h. Afterwards cells were washed twice with DPBS++ and fixed with 1 ml Methanol/Acetone solution for 2 min before being immunostained for claudin-18.

Tight junction spike quantitation was done using cells immunolabeled for claudin-18. Samples used for morphometric analysis were blinded. Cells containing 3 or more projections that were perpendicular to the orientation of the intercellular junction were considered to be cells containing tight junction spikes that were scored and expressed as a percentage of the total number of cells in the field. In Figure 2, for control vs. alcohol-exposed cells: 11 fields from two independent experiments each; number of cells scored: 383 control AECs and 563 alcohol-exposed AECs. For EGFP vs. YFP-claudin-5 transduced cells: 11 fields from two independent

experiments each; number of cells scored: 615 EGFP-transduced AECs and 392 YFP-cldn-5-transduced AECs. For alcohol exposed AECs transduced with claudin-5 shRNA: 5 fields each; number of cells scored: 294 control cells, 206 shRNA1-treated cells and 244 shRNA2-treated cells. In Figure 3, for Dynasore treated alcohol-exposed cells: 8 fields from two independent experiments each; number of cells scored: 826 control cells, 728 cells treated with 40 μM Dynasore, 752 cells treated with 80 μM Dynasore and 863 cells treated with 160 μM Dynasore. For Dynasore treated control cells: 9 fields from two independent experiments each; number of cells scored: 341 control cells, 227 cells treated with 40 μM Dynasore, 228 cells treated with 80 μM Dynasore and 273 cells treated with 160 μM Dynasore. In Figure 7, for peptide treated cells: 9-10 fields from two independent experiments each; number of cells scored: 165 untreated control cells, 186 untreated alcohol-exposed cells, 207 control treated alcohol-exposed cells, 253 peptide-treated alcohol-exposed cells.

For live cell imaging, 7.5×10^5 alcohol exposed AECs were plated on onto glass bottom culture dishes (MatTek Corp, Ashland, MA P50G-1.5-14-F) coated with rat tail type I collagen (20 μg/ml) (Roche Diagnostics, Mannheim, Germany). On day 4 cells were transduced with adenovirus encoding for YFP-claudin-5 or YFP-claudin-18 with an MOI of 5, respectively. Media was changed 24 h after transduction. After 48 h expression, live cell imaging using a Nikon A1R confocal laser scanning microscope with temperature control/CO_2 chamber stage (40× oil lens, numerical aperture 1.3) and autofocus control was performed. Imaging was performed in phenol red free Optimem containing 10% FBS, 0.25 μg/ml amphotericin B (Life technologies) 100 U/ml penicillin and 10 mg/ml streptomycin (sigma) at 37°C and 5%CO_2. Data were collected with NIS-Elements AR 4.0 software (Nikon, Melville, NY). Imaging was performed over a time period of 20 min with 30 sec intervals. Pictures were taken in 1024x1024 pixels resolution (excitation 488 nm, emission 525 nm) with low excitation laser power of 1.2% to minimize photo bleaching. Images and movies were processed with Image J. Minimum and maximum intensities were

adjusted for images in parallel, so that the intensity scale remained linear to maximize dynamic range.

STochastic Optical Reconstruction Microscopy (STORM)

To analyze the co-localization and particle size of claudin-18, ZO-1 and claudin-5 within the cell membrane STochastic Optical Reconstruction Microscopy (STORM) was performed.[15, 16] Double labeled secondary antibodies were prepared using donkey anti-rabbit (Jackson Immuno Research 711-005-152) and donkey anti-mouse IgG (Jackson Immuno Research 715-005-151). Stock labeling reagents were Alexa 647 carboxylic acid succinimidyl ester (2μg/μl; ThermoFisher A30000), Cy2 bisreactive dye (2 μg/μl; GE Healthcare PA22000) and Cy3 monoreactive dye (2 μg/μl; GE Healthcare PA23001) in anhydrous DMSO. For donkey anti-rabbit IgG, 1.5 μl Cy2, 0.6 μl Alexa 647 and 6 μl 1 M $NaHCO_3$ were added to 62.5 μg /50 μl IgG and incubated at RT for 30 min. The sample was diluted to 200 μl with PBS, then filtered using a NAP-5 Sephadex G-25 DNA Grade column (GE Healthcare 17-0853-02), washed with 550 μl PBS and eluted with 300 μl PBS. Donkey anti-mouse IgG was labeled in a similar manner, using 1.5 μl Cy3 instead of Cy2. Antibodies were stored at 4°C and used within 2 months of preparation.

For immunolabeling, AECs were prepared as described above and plated onto glass bottom culture dishes (MatTek Corp, Ashland, MA P50G-1.5-14-F) coated with rat tail type I collagen (20 μg/ml; Roche Diagnostics, Mannheim, Germany). After 6 days in culture, the cells immunostaining of claudin-18, ZO-1 and claudin-5 was performed as described above with the following changes. After permeabilization cells were treated with 0.1% NaBH4 for 10 min at RT. Secondary incubation were washed with 3 x 1 ml DPBS++ then fixed/permeabilized with 1 ml 1:2 methanol/acetone for 2 min at RT. The cells were washed 3x with DPBS++, treated with 0.1% $NaBH_4$ for 10 min at RT, washed 3x with DPBS++, washed once with DPBS++ with 0.5% Triton X-100, then twice with DPBS++ containing 0.5% TX-100, 2% normal goat serum. The

cells were then incubated with rabbit anti-claudin-18 + mouse anti-claudin-5 or rabbit anti-claudin-18 + mouse anti-ZO-1 in DPBS++ containing 2% normal goat serum for 1 h at RT on a rotator platform. After primary antibody incubation, cells were washed 3x with DPBS++ containing 2% normal goat serum and then incubated with a 1:100 dilution of double labeled secondary antibody mixed in DPBS++ for 30 min at RT on a rotator platform. The cells were then washed 2x 1 h with DPBS++ containing 2% normal goat serum then 3x DPBS++. Samples were post fixed with 3% paraformaldehyde + 0.1% glutaraldehyde for 10 min at RT, washed 3x with DPBS++. For imaging, antibody labeled cells were incubated in 1.4 ml mercaptoethylamine (MEA) imaging buffer (0.7 mg/ml glucose oxidase, 42.5 ug /ml catalase, 100 mM cystamine, 8.9 mM NaCl, 8.9% glucose in 44.3 mM Tris-HCl, pH 8.0).

The samples were imaged with a Nikon N-STORM system based on an Eclipse Ti inverted microscope with the Perfect Focus System, a 100x 1.49 oil immersion objective, and an Andor iXon DU897 EMCCD camera. Data were collected and analyzed with NIS-Elements Software. Samples were excited with 457 nm, 561 nm, and 647 nm laser lines. Data collection involved alternating cycles of lower intensity 457 nm and 561 nm activation pulses and high intensity 647 nm imaging for localization and deactivation. High resolution STORM images were collected over 20-30 min. Data was corrected for stage drift and localization fitted to Gaussian distributions using NIS-Elements set at minimum height of 250 nm and CCD baseline of 220 nm. Single labeled and unlabeled samples were collected using the same parameters to ensure that there was a lack of non-specific signal detection and minimal crosstalk between fluorescent channels (Supplementary Fig. 7).

To analyze the size distribution of clusters containing claudin-18, claudin-5 or ZO-1 in the membrane, STORM images were analyzed using ImagePro 3.0. Objects that consisted of 10 contiguous pixels with a threshold intensity of greater than 50/255 were considered as the minimum cluster size. 10 pixels corresponded to an area of 585 nm^2. Co-localization between of double labeled STORM images was analyzed by using ImageJ software. Given that total claudin-

5 changes dramatically when comparing cells from control and alcohol-fed animals, we calculated the co-localization index as the amount of claudin-18 or ZO-1 co-localizing with claudin-5 as opposed to the opposite calculation, which would be much more sensitive to changes in total claudin-5. Co-localized area between the red and the green channel was identified using a co-localization plugin for ImageJ (http://rsb.info.nih.gov/ij/plugins/co-localization.html). Two pixels were considered co-localized when the respective threshold of each channel was higher than 50 (out of a range of 0-255) and the intensity ratio of the red and the green channel was higher than 50%. Co-localized area as well as the area in the red and the green channel was quantified by using the particle analyzer.

Proximity Ligation Assay

For the Proximity Ligation Assay (PLA) AECs were cultured on Transwell permeable supports for 6 days. On day 6, cells were washed 3x with DPBS with Ca^{2+}/Mg^{2+} and fixed with freshly made Methanol/Acetone (1:2) for 2 minutes. After fixation, the cells were washed 3x with DPBS++, permeabilized with DPBS++ containing 0.5% (v/v) Triton X-100 for 5 min, then blocked with DPBS++ containing 0.5% (v/v) Triton X-100 and 5% goat serum (Sigma-Aldrich) 2x for 5 min under gentle agitation. Cells were incubated overnight in 250 µl DPBS++ containing 5% goat serum with primary antibody pairs (mouse anti-claudin-5 + rabbit anti-claudin-18, rabbit anti-claudin-5+ mouse anti-ZO-1 or rabbit anti-claudin-18 + mouse anti-ZO-1; Supplementary Table 2). The next day filters were washed with DPBS++ containing 5% goat serum (v/v) 3x for 5 min under gentle agitation. After washing, the Transwell filters were cut out and put upside down on Parafilm and a 50 µl solution containing the secondary antibodies (anti-rabbit Plus (DUO92002) and anti-mouse Minus (DUO92004) diluted in DPBS++ containing 5% goat serum (v/v)) was pipetted under the filter. Filters were incubated for 1h in a humidified incubator at 37°C, 5% CO_2. For the detection of protein-protein interactions, the detection Kit Red (DUO92008) was used according to the manufacturer's instructions. Filters

were mounted on slides using Duolink In Situ Mounting Medium with DAPI (DUO82040), covered with glass cover slips and sealed with nail polish and stored at -20°C until imaging. Fluorescence images were taken using an Olympus IX70 microscope with a U-MWIBA filter pack (BP460–490, DM505, BA515–550) or U-MNG filter pack (BP530–550, DM570, BA590–800). Minimum and maximum intensities were adjusted for images in parallel, so that the intensity scale remained linear to maximize dynamic range. Image analysis was performed using the Fiji particle analyzer tool. PLA signal intensity was analyzed by measuring the number of individual clusters above a threshold intensity value of 70.

Claudin-5 mimetic peptide treatment

To antagonize the deleterious effects of claudin-5 on barrier function in alcohol exposed AECs a short D-peptide targeting claudin-5 was designed (Ac-EFYDP-NH_2; Ac=Acetylation, NH_2= amide) analogous to the claudin-3/4 peptide that was previously described [27] and synthesized by LifeTein (Sumerset, NJ). A Ac-LYQY-NH_2 peptide was also synthesized and used as peptide control [27]. Peptides were dissolved in 30% DMSO in water at a concentration of 30 mM (30,000x stock). AECs from either control- or alcohol-fed rats were cultured for 5 days on Transwell permeable supports and then the apical medium was replaced with 500 µl DMEM media containing 10µM peptide (final DMSO conc. 0.01%). DMSO alone was used for untreated controls. AECs were incubated for 16h and then assessed for barrier function, immunofluorescence or immunoblot as described above.

Statistics

All statistics were calculated using GraphPad Prism 6.0. Statistical significance for parametric data was determined using unpaired two-tailed t-test to compare one dependent variable against one independent variable, one way ANOVA with Tukey multiple comparisons test to compare one dependent variable against multiple independent variables, and two way

ANOVA with Bonferroni multiple comparisons test to compare multiple dependent variables against multiple independent variables and non-parametric data using the Mann Whitney U test. Sample size was determined so that we could detect a minimum 20% difference in values with standard error of ± 10%. Variance between compared groups was comparable throughout the study. Data in most graphs represent average ± standard error, box and whisker plots in Supplementary Fig. 7g-i show the median value, 25th and 75 percentiles as the limits of the box and 5th and 95th percentiles as the limits of the whiskers.

Data availability

The source data that support the findings of this study are available from the corresponding author (MK) upon request.

Acknowledgements

We thank Christina Ward for technical assistance. This work was supported by Emory Alcohol and Lung Biology Center/National Institutes of Health (NIH) grant P50-AA013757 (MK, DMG), R01-HL116958 (MK), T32-AA013528 (CEO, SAM, LAM), the German Academic Exchange Service (DAAD) (BS), T32-GM008367 (KSL), R25-GM099644 (SDW), the Veterans Administration through a Merit Review (DMG), the Emory University Research Committee (MK), Emory+Children's Center of Excellence for Cystic Fibrosis Research (MK), Emory University Integrated Cellular Imaging Microscopy Core of the Winship Cancer Institute Comprehensive Cancer Center Grant P30CA138292, and a Crohn's and Colitis Foundation of America Career Development award to CTC. Lentiviral shRNA vectors were packaged and amplified by the Emory Neuroscience NINDS Viral Vector Core funded by NIH P30-NS055077.

Author contributions

B.S., C.E.O., S.A.M., K.S.L, L.A.M., S.D.W, C.T.C and M.K. performed experiments and interpreted results. B.S. and L.A.M. designed, produced and packaged molecular constructs used for the study, B.S., A.L.M. and M.K. performed, quantified and interpreted super-resolution microscopy studies, B.S. and C.T.C performed live cell imaging microscopy studies. B.S., C.E.O., D.M.G. and M.K. designed and interpreted experiments related to the effects of alcohol on barrier function. B.S. and M.K wrote the first draft of the manuscript. B.S., C.E.O., S.A.M., K.S.L, L.A.M., S.D.W, A.L.M., D.M.G., C.T.C and M.K. edited and approved the final version of the manuscript.

Figure 3.1

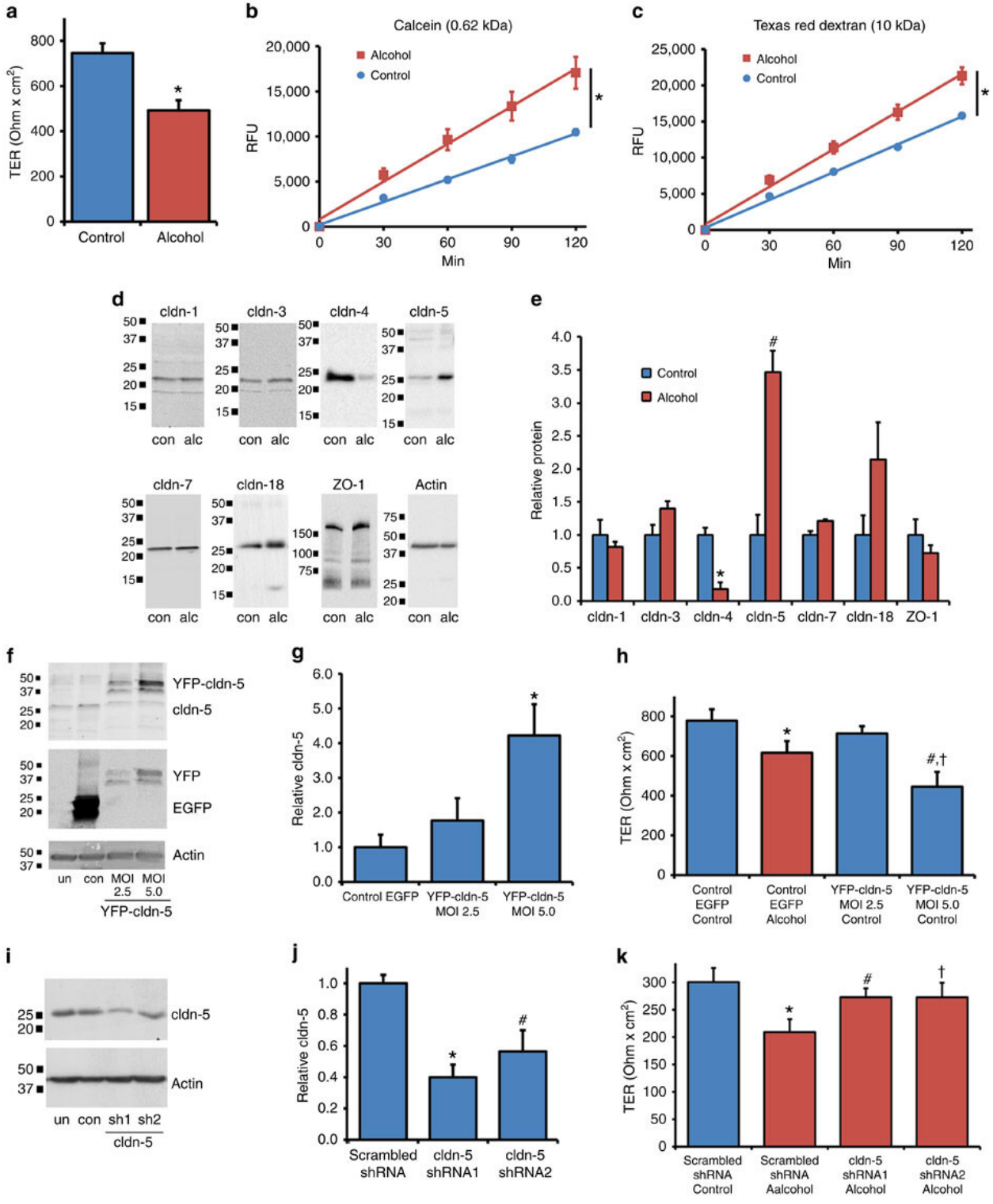
a
TER (Ohm x cm²)
800
600
400
200
0
Control
Alcohol
*
b
Calcein (0.62 kDa)
Alcohol
Control
RFU
20,000
15,000
10,000
5,000
0
0
30
60
90
120
Min
*
c
Texas red dextran (10 kDa)
Alcohol
Control
RFU
25,000
20,000
15,000
10,000
5,000
0
0
30
60
90
120
Min
*
d
cldn-1
cldn-3
cldn-4
cldn-5
cldn-7
cldn-18
ZO-1
Actin
50
37
25
20
15
75
150
100
con alc
e
Relative protein
4.0
3.5
3.0
2.5
2.0
1.5
1.0
0.5
0.0
Control
Alcohol
#
*
cldn-1
cldn-3
cldn-4
cldn-5
cldn-7
cldn-18
ZO-1
f
YFP-cldn-5
cldn-5
YFP
EGFP
Actin
un
con
MOI 2.5
MOI 5.0
YFP-cldn-5
g
Relative cldn-5
6.0
5.0
4.0
3.0
2.0
1.0
0.0
*
Control EGFP
YFP-cldn-5 MOI 2.5
YFP-cldn-5 MOI 5.0
h
TER (Ohm x cm²)
800
600
400
200
0
*
#,†
Control EGFP Control
Control EGFP Alcohol
YFP-cldn-5 MOI 2.5 Control
YFP-cldn-5 MOI 5.0 Control
i
cldn-5
Actin
un
con
sh1
sh2
cldn-5
j
Relative cldn-5
1.0
0.8
0.6
0.4
0.2
0.0
*
#
Scrambled shRNA
cldn-5 shRNA1
cldn-5 shRNA2
k
TER (Ohm x cm²)
300
250
200
150
100
50
0
*
#
†
Scrambled shRNA Control
Scrambled shRNA Aalcohol
cldn-5 shRNA1 Alcohol
cldn-5 shRNA2 Alcohol

Figure 3.1: Alcohol dependent upregulation of claudin-5 is necessary and sufficient to impair alveolar barrier function. AECs from alcohol fed rats and controls were cultured on Transwell permeable supports and then transepithelial resistance (TER) **(a)** and dye flux with calcein **(b)** and Texas Red Dextran **(c)** were measured. Alcohol-exposed AECs showed a significantly lower TER (n=6, * - p <0.001, unpaired two-tailed t-test) as well as significantly higher calcein (n=3, * - p<0.001, two way ANOVA with Bonferroni multiple comparisons test) and Texas Red Dextran permeability (n=3, * - p<0.001, two way ANOVA) *vs.* cells from control fed rats. **(d,e)** By immunoblot, alcohol exposure significantly decreased claudin-4 expression (n=3, * - p=0.002, t-test) and significantly increased claudin-5 expression by AECs (n=3, # - p=0.005, t-test). **(f-h)** Control AECs were transduced with adenovector YFP-claudin-5 at MOI of 2.5 or 5 for or EGFP adenovector at MOI of 5 as a control. The EGFP/EYFP doublet has been seen by others [60, 61] and has no bearing on our results since untagged claudin-5 has a comparable effect on AECs (Supplementary Fig. 5). **(f,g)** YFP-claudin-5 at MOI of 5 significantly increased claudin-5 expression (n=3, * - p=0.022, one way ANOVA with Tukey multiple comparisons test) and **(h)** decreased TER (n=3, # - p=0.0005 vs. EGFP transduced control AECs; † - p =0.028 vs. EGFP transduced alcohol exposed cells, one way ANOVA). In **(h),** TER of alcohol exposed cells was significantly lower than comparable control cells (n=3, * - p=0.036, one way ANOVA). **(i-k)** Claudin-5 protein expression in alcohol-exposed AECs was depleted using a lentiviral system delivering shRNA targeting claudin-5 or control scrambled shRNAs. **(i,j)** Claudin-5 was significantly depleted by specific shRNAs *vs.* scrambled shRNA treated cells (n=4, * - p=0.006, # - p=0.036, one way ANOVA). **(k)** decreased claudin-5 expression in alcohol-exposed cells significantly increased TER as compared with cells transduced with scrambled shRNAs (n=4, # - p< 0.001, † - p< 0.001, one way ANOVA). TER of cells from alcohol exposed cells treated with shRNA was significantly lower than comparable control cells (n=4, * - p<0.001, one way ANOVA). All quantitative data represents average $\pm$ SEM.

Figure 3.2

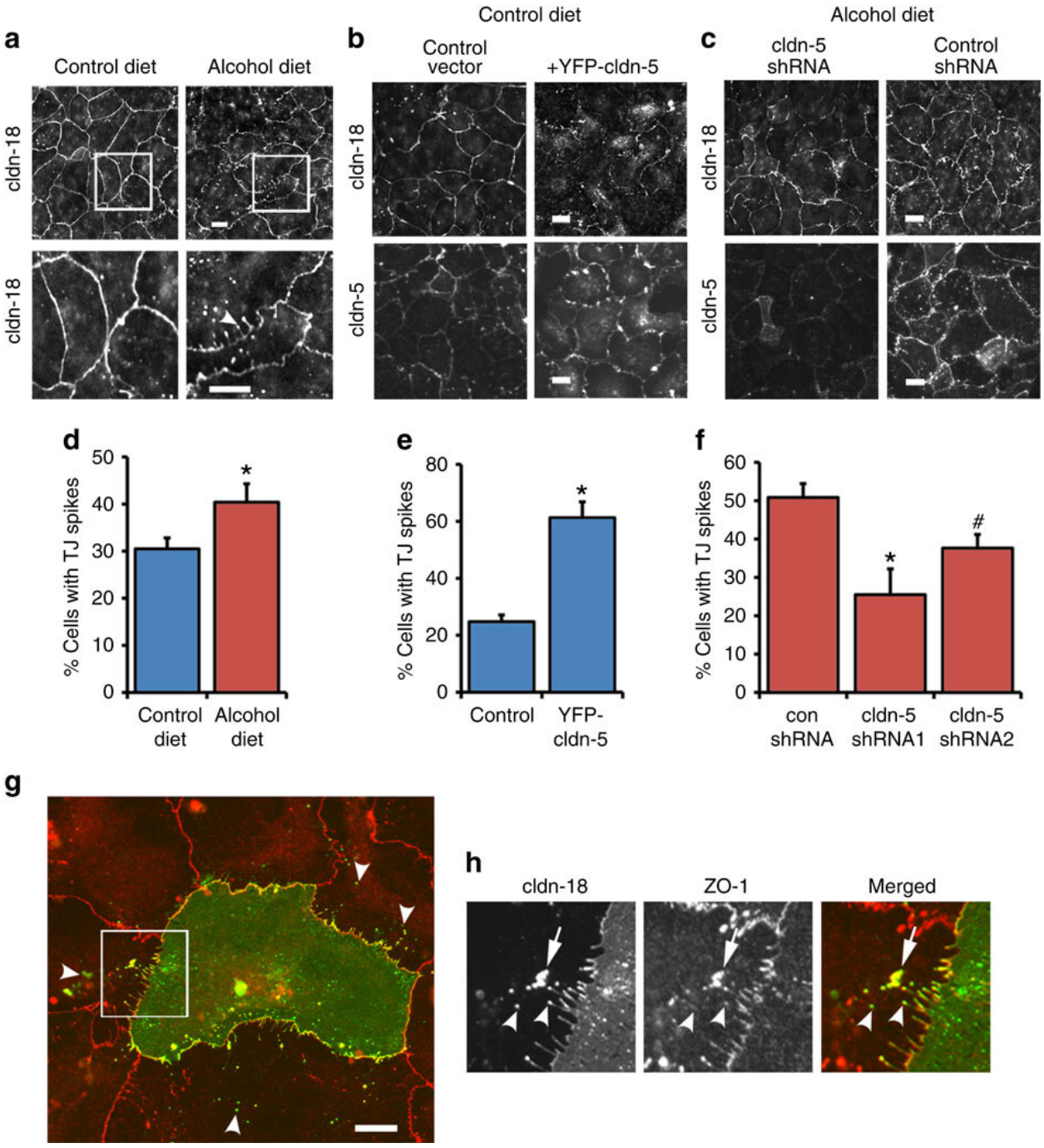

Figure 3.2: Increased claudin-5 expression enhances the formation of tight junction spikes. AECs isolated from alcohol or control fed rats were cultured for 5-7 days on transwell permeable supports and immunolabeled for claudin-18. **(a)** Cells from alcohol fed

rats showed enhancement of tight junction spikes, that are claudin-18 projections perpendicular to the cell-cell interface (d; arrowhead). Square regions in the top panels correspond to magnified images in below (Bar – 10 μm). **(b)** Control AECs transduced with YFP-claudin-5 increased the appearance of tight junction spikes as determined by labeling for cldn-18 or cldn-5 (Bar – 10 μm). **(c)** Alcohol-exposed AECs transduced with claudin-5 shRNA had a decrease in tight junction spikes (Bar – 10 μm). **(d-f)** Quantification of the % of cells containing 3 or more tight junction spikes oriented towards the nucleus demonstrated that alcohol exposed and YFP-claudin-5 transduced AECs had significantly more spikes than comparable controls **(d)** control vs. alcohol: n=11 fields, * - p=0.035, unpaired two-tailed t-test. **(e)** EGFP vs. YFP-claudin-5: n=11 fields, * - p<0.001, unpaired two-tailed t-test. **(f)** Alcohol exposed AECs transduced with claudin-5 shRNA1 had significantly fewer spikes than cells treated with control shRNA (n=5 fields, * - p=0.011, one way ANOVA with Tukey multiple comparisons test). Cells treated with shRNA2 showed a trend towards decreased spikes (n=5, # - 0.18, one way ANOVA with Tukey multiple comparisons test) **(g)**. Control AECs were partially transfected with YFP-claudin-18 then fixed and immunolabeled for ZO-1. YFP-claudin-18 expressing cells adjacent to untransfected cells showed uptake of YFP-claudin-18 in intracellular vesicles (arrows, Bar – 10 μm). **(h)** Magnified images corresponding to the square region in **(g)** showing spike associated claudin-18 internalized into adjacent cells. Arrowheads show areas where claudin-18 does not co-localize with ZO-1. The arrow indicates a structure where YFP-claudin-18 and ZO-1 co-localize. All quantitative data represents average $\pm$ SEM.

Figure 3.3

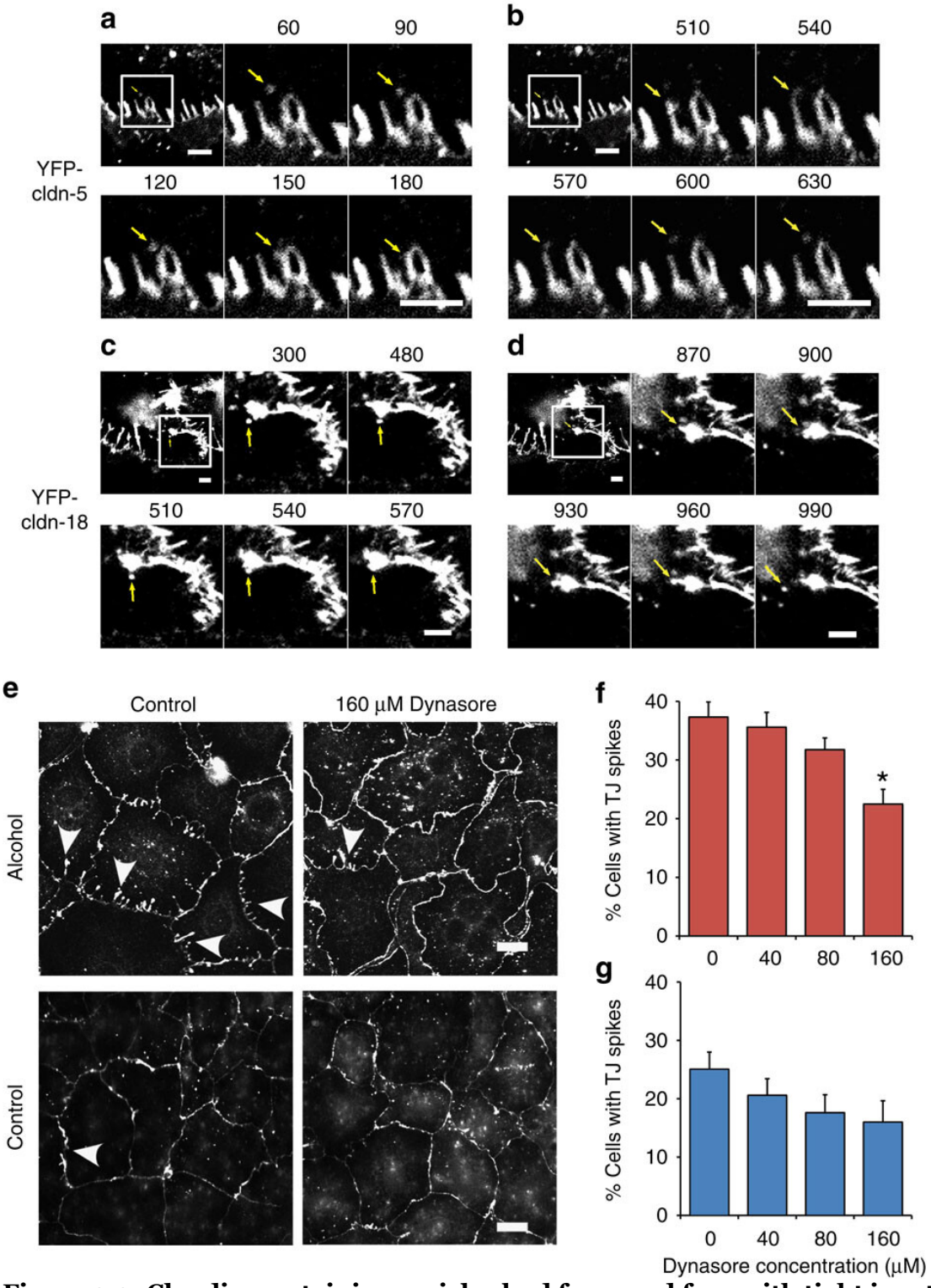

Figure 3.3: Claudin-containing vesicles bud from and fuse with tight junction spikes. (a-d) Live cell imaging was performed with alcohol exposed AECs transduced with

Adenovirus encoding either YFP-claudin-5 **(a,b)** or YFP-claudin-18 **(c,d)**. Shown are still images from videos acquired over a 20 minute time period with a frame capture of 30 second intervals. Labeled vesicles containing YFP-claudin-5 or YFP-claudin-18 were found to both fuse to **(a,c)** and bud from **(b,d)** tight junction spikes, demonstrating that these are dynamic structures. The top left panel in each series is a lower magnification image, the square region represents the time series, which is time stamped in seconds. Bar – 5 μm. **(e)** Cells from alcohol fed or control fed rats were cultured for 7 days and then treated with either DMSO vehicle control or the dynamin inhibitor Dynasore at varying concentrations for 4 h at 37 ^{o}C in serum free media. The cells were then fixed and immunolabeled for claudin-18. Representative images show vehicle-treated and 160 μM Dynasore treated cells. Arrowheads show tight junction spikes. Bar - 10 μm. **(f,g)** Quantification of the % cells containing 3 or more tight junction spikes oriented towards the nucleus demonstrated that 160 μM Dynasore significantly decreased the number of cells from alcohol fed rats containing spikes (n=8-9 fields, * - p =0.002, one way ANOVA with Tukey multiple comparisons test). All quantitative data represents average $\pm$ SEM.

Figure 3.4

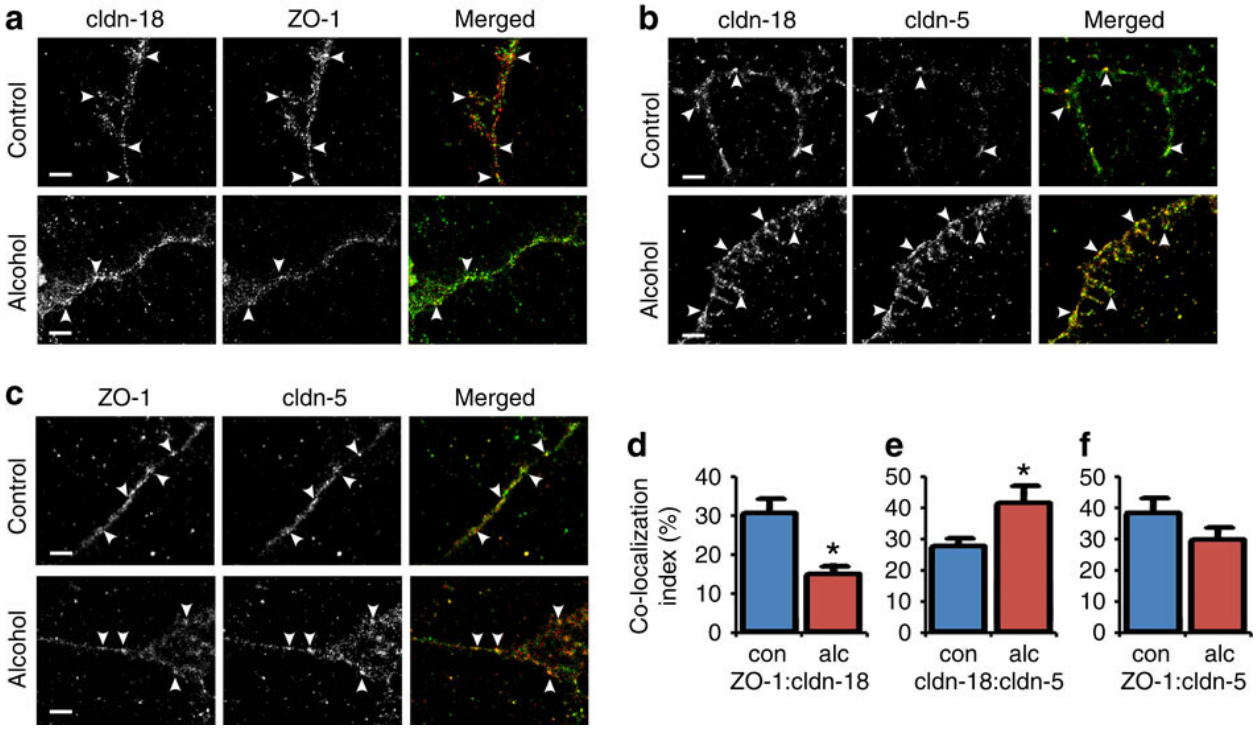

Figure 3.4: Claudin-5 induced by alcohol decreases ZO-1:claudin-18 co-localization as determined by super-resolution microscopy. (a-c) AECs isolated from alcohol (alc) or control (con) fed rats were cultured, immunolabeled and imaged by STORM. Cells were double-labeled for claudin-18 and ZO-1 **(a)**, claudin-5 and claudin-18 **(b)** or claudin-5 and ZO-1 **(c)**. Images were analyzed for protein co-localization **(d-f)**. Alcohol exposed AECs showed a reduction in the co-localization between claudin-18 and ZO-1 and an increase in co-localization between claudin-18 and claudin-5. Co-localization between claudin-5 and ZO-1 was comparable for both control and alcohol exposed cells. Arrowheads denote areas of co-localization. Bar, 1 μm. **(d-f)** Quantification of co-localization using STORM images demonstrated a significant change. In alcohol-exposed AECs there was a significant decrease in ZO-1:claudin-18 (n=4 fields (control), n=3 fields (alcohol exposed AECs),* - p=0.014, unpaired two-tailed t-test) **(d)** which correlated with a significant increase in claudin-18:claudin-5 co-localization (n=3 fields, * -

p=0.039, unpaired two-tailed t-test) **(e)**. ZO-1:claudin-5 co-localization was unchanged (n=4 fields, unpaired two-tailed t-test) **(f)**. Data in **(d-f)** represent average ± SEM.

Figure 3.5

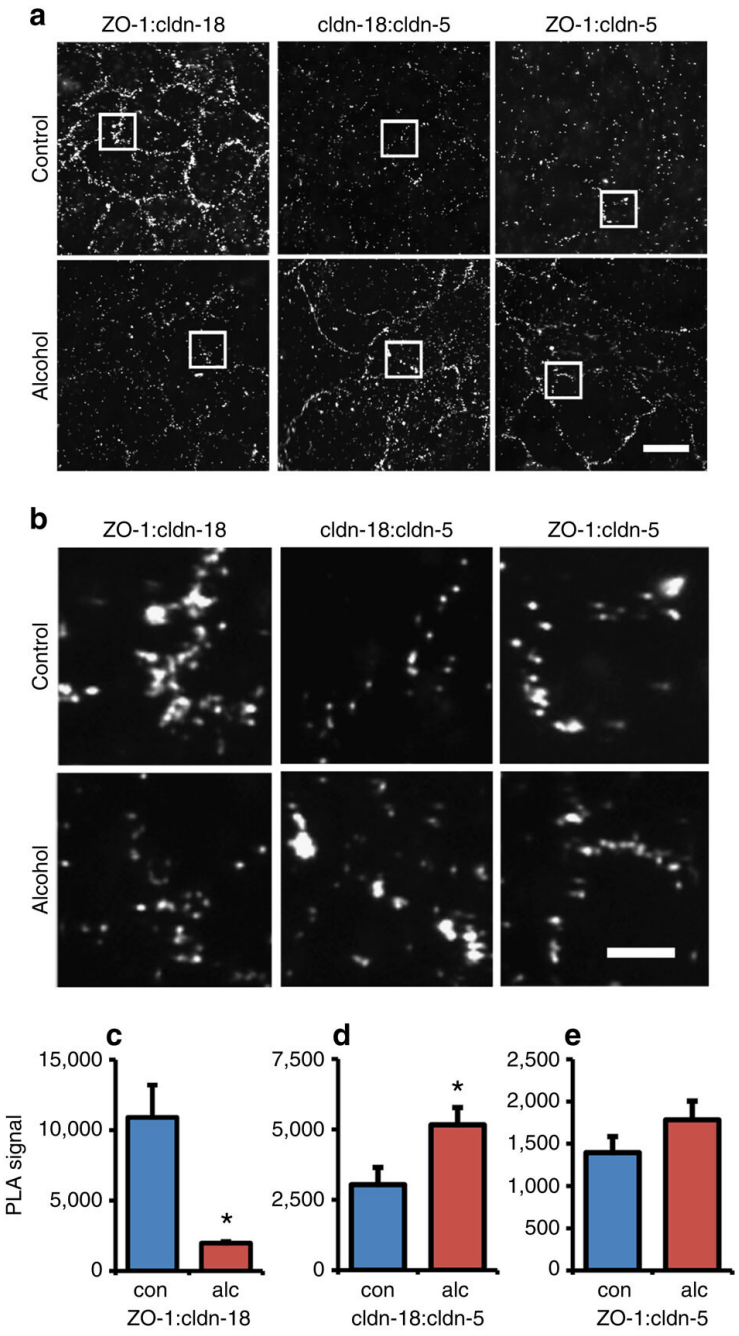

Figure 3.5: Claudin-5 induced by alcohol decreases ZO-1:claudin-18 co-localization as determined by proximity ligation assay. (a,b) AECs isolated from alcohol (alc) or control (con) fed rats were cultured, immunolabeled and analyzed using the proximity ligation

assay (PLA). Cells were PLA-labeled for claudin-18 and ZO-1, claudin-5 and claudin-18 or claudin-5 and ZO-1. Images in **(b)** are magnifications of regions in **(a)** as denoted by the squares. Bar, 20 μm. Negative controls are shown in Supplementary Fig. 10. Alcohol exposed AECs showed a reduction in the co-localization between claudin-18 and ZO-1 and an increase in co-localization between claudin-18 and claudin-5. Co-localization between claudin-5 and ZO-1 was comparable for both control and alcohol exposed cells. **(c-e)** Quantification of co-localization using PLA demonstrated a significant change. In alcohol-exposed AECs there was a significant decrease in ZO-1:claudin-18 (n=6 fields,* - p=0.018, unpaired two-tailed t-test) **(c)** which correlated with a significant increase in claudin-18:claudin-5 co-localization (n=10 fields, * - p=0.026, unpaired two-tailed t-test) **(d)**. ZO-1:claudin-5 co-localization was unchanged (n=6 fields, unpaired two-tailed t-test) **(e)**. Data in **(c-e)** represent average $\pm$ SEM.

Figure 3.6

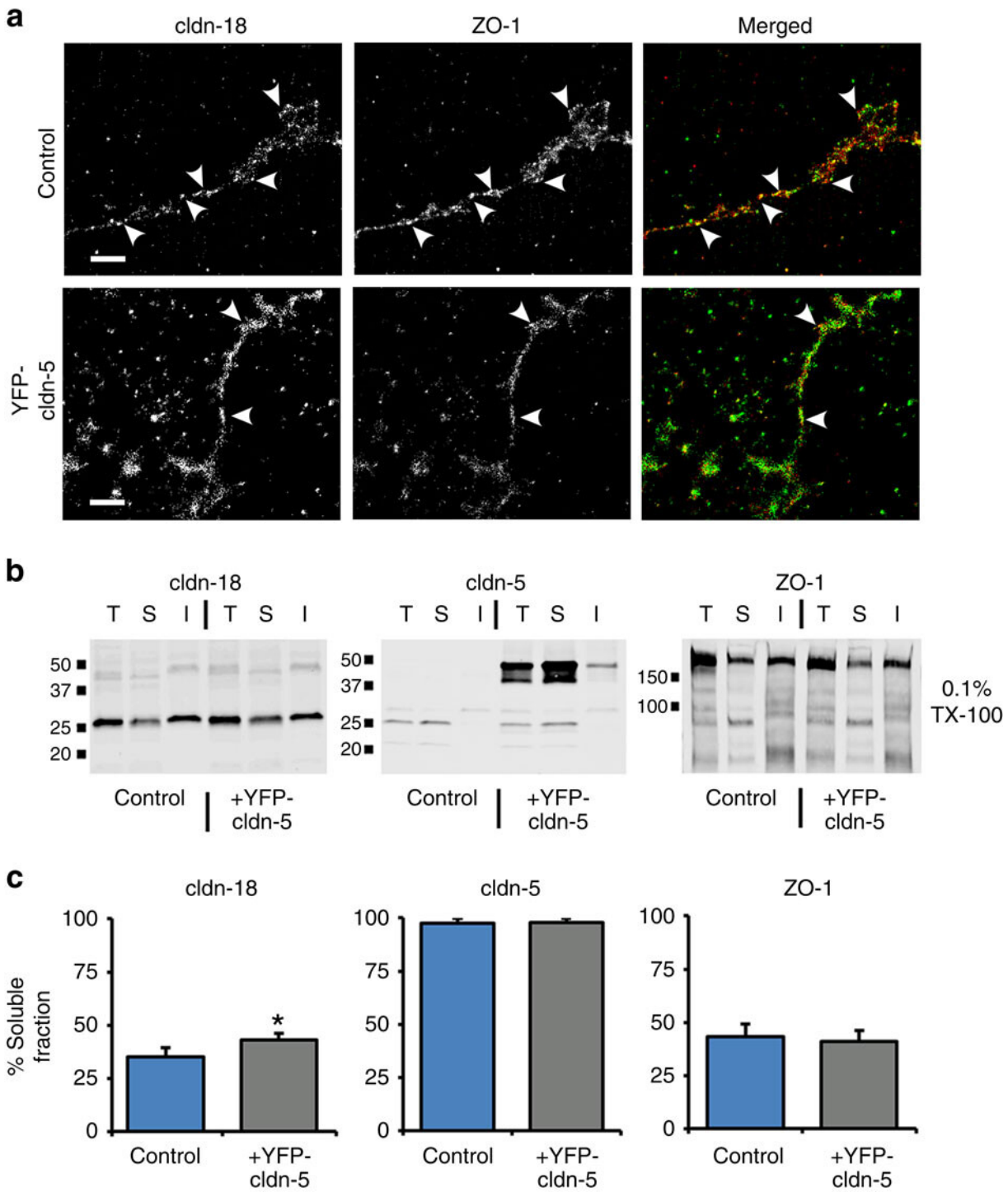

Figure 3.6: Claudin-5 expression is sufficient to decrease ZO-1:claudin-18 co-localization and increase claudin-18 solubilization. (a) Control or YFP-claudin-5

transduced AECs were cultured for 6 days, immunolabeled and then imaged by STORM for claudin-18 and ZO-1. Increased claudin-5 expression decreased the extent of ZO-1:claudin-18 co-localization (see text). Arrowheads show sites of co-localization. Bar -1μm. **(b,c)** Biochemical analysis of protein insolubility was assessed by a Triton X-100 solubilization assay comparing control AECs to YFP-claudin-5 transduced cells. At 6 days in culture, AECs were harvested and extracted using 0.1% Triton X-100, an aliquot of total protein (T) was set aside and the remainder was centrifuged to separate Triton X-100 soluble (S) and insoluble (I) fractions that were measured by immunoblot for claudin-18, claudin-5 and ZO-1. Quantification of the soluble fraction revealed that YFP-claudin-5 expression significantly increased claudin-18 solubility from 35.2 $\pm$ 1.8 to 42.1 $\pm$ 0.6 (n=3, * - p=0.003, unpaired two-tailed t-test) while claudin-5 and ZO-1 solubility did not significantly change. All quantitative data represents average $\pm$ SEM.

Figure 3.7

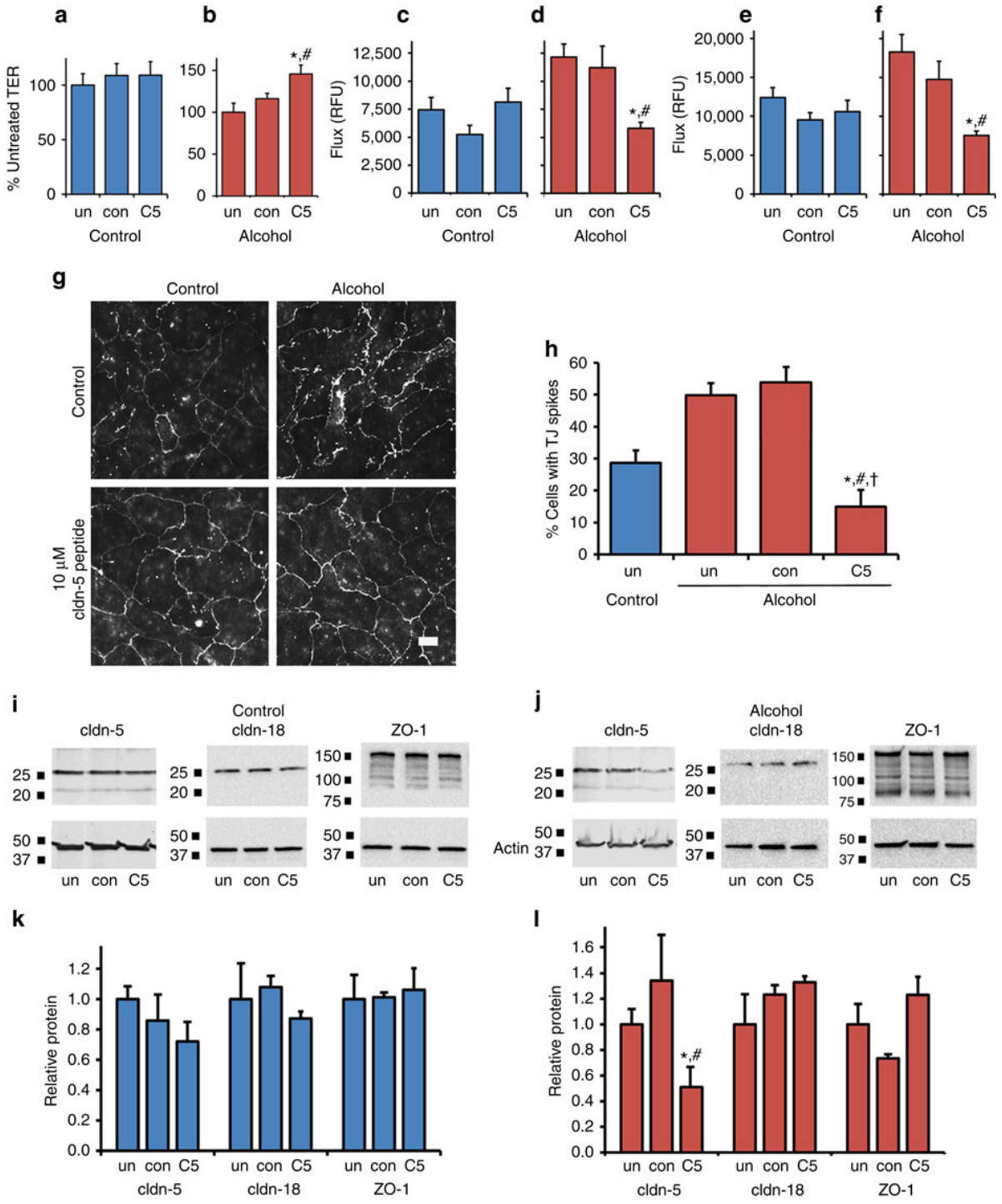

Figure 3.7: A claudin-5 extracellular domain mimetic increases barrier function of alcohol-exposed AECs. (a-f) AECs isolated from control **(a,c,e)** or alcohol fed rats **(b, d, f)**

were cultured on Transwell permeable supports for 5 days and then either untreated (un), or incubated with 10 μM control peptide (con; Ac-LYQY-NH_2) or a claudin-5 extracellular domain mimetic peptide (C5; Ac-EFYDP-NH_2) for 16 h. The cells were examined for barrier function by transepithelial resistance (TER) **(a,b)** and paracellular flux of calcein **(c,d)** and 10 kDa Texas Red dextran **(e,f)**. The C5 peptide had little effect on barrier function of control AECs (a,c,e) however, it significantly increased TER (*, p=0.014 vs untreated; # p=0.042 vs control; n=6, one way ANOVA with Tukey multiple comparisons test) **(b)**, and decreased paracellular flux of calcein (*,p=0.007 vs untreated; #, p – 0.054 vs control; n=3, one way ANOVA with Tukey multiple comparisons test) **(d)**, and Texas Red Dextran (*,p=0.009 vs untreated; #, p – 0.040 vs control; n=3, one way ANOVA with Tukey multiple comparisons test) **(f)**. **(g)** AECs as treated above were processed and examined by immunofluorescence for claudin-18 localization. Bar – 20 μm. Cells from alcohol fed rats showed a decrease in tight junction spikes, that was significantly less than that of untreated controls and alcoholic AECs that were either untreated or treated with a control peptide (*, p <0.001 vs untreated; #, p<0.001 vs control peptide; †, p – 0.041 vs untreated control AECs, n=9-11 fields from two independent experiments, one way ANOVA with Tukey multiple comparisons test) **(h)**. Claudin-5 immunofluorescence is shown in Supplementary Fig. 11. **(i-l)** AECs as treated above were processed and examined by immunoblot for claudin-5, claudin-18 and ZO-1. Cells from alcohol-fed rats that were treated with the C5 peptide showed a significant and specific decrease in claudin-5 (*, p=0.042 vs untreated; #, p=0.016 vs control; n=9, one way ANOVA with Tukey multiple comparisons test) **(l)**. All quantitative data represents average $\pm$ SEM.

Literature cited

1. Guidot, D.M. & Hart, C.M. Alcohol abuse and acute lung injury: epidemiology and pathophysiology of a recently recognized association. J Investig Med 53, 235-245 (2005).
2. Moss, M., Bucher, B., Moore, F.A., Moore, E.E. & Parsons, P.E. The role of chronic alcohol abuse in the development of acute respiratory distress syndrome in adults. JAMA 275, 50-54 (1996).
3. Koval, M. Claudin heterogeneity and control of lung tight junctions. Annu Rev Physiol 75, 551-567 (2013).
4. Overgaard, C.E. et al. The relative balance of GM-CSF and TGFbeta1 regulates lung epithelial barrier function. Am J Physiol Lung Cell Mol Physiol 308, L1212-L1223 (2015).
5. Ward, C., Schlingmann, B., Stecenko, A.A., Guidot, D.M. & Koval, M. NF-kB inhibitors impair lung epithelial tight junctions in the absence of inflammation. Tissue Barriers 3, e982424 (2015).
6. Simet, S.M. et al. Alcohol increases the permeability of airway epithelial tight junctions in Beas-2B and NHBE cells. Alcohol Clin Exp Res 36, 432-442 (2012).
7. Furuse, M. & Tsukita, S. Claudins in occluding junctions of humans and flies. Trends Cell Biol 16, 181-188 (2006).
8. Van Itallie, C.M. & Anderson, J.M. Architecture of tight junctions and principles of molecular composition. Semin Cell Dev Biol 36C, 157-165 (2014).
9. Gunzel, D. & Fromm, M. Claudins and other tight junction proteins. Compr Physiol 2, 1819-1852 (2012).
10. Fernandez, A.L., Koval, M., Fan, X. & Guidot, D.M. Chronic alcohol ingestion alters claudin expression in the alveolar epithelium of rats. Alcohol 41, 371-379 (2007).
11. Wang, F. et al. Heterogeneity of claudin expression by alveolar epithelial cells. Am J Respir Cell Mol Biol 29, 62-70 (2003).

12. Mitchell, L.A., Overgaard, C.E., Ward, C., Margulies, S.S. & Koval, M. Differential effects of claudin-3 and claudin-4 on alveolar epithelial barrier function. Am J Physiol Lung Cell Mol Physiol 301, L40-49 (2011).

13. Matsuda, M., Kubo, A., Furuse, M. & Tsukita, S. A peculiar internalization of claudins, tight junction-specific adhesion molecules, during the intercellular movement of epithelial cells. J Cell Sci 117, 1247-1257 (2004).

14. Macia, E. et al. Dynasore, a cell-permeable inhibitor of dynamin. Dev Cell 10, 839-850 (2006).

15. Rust, M.J., Bates, M. & Zhuang, X. Sub-diffraction-limit imaging by stochastic optical reconstruction microscopy (STORM). Nat Methods 3, 793-795 (2006).

16. Burnette, D.T., Sengupta, P., Dai, Y., Lippincott-Schwartz, J. & Kachar, B. Bleaching/blinking assisted localization microscopy for superresolution imaging using standard fluorescent molecules. Proc Natl Acad Sci U S A 108, 21081-21086 (2011).

17. Kaufmann, R. et al. Visualization and quantitative analysis of reconstituted tight junctions using localization microscopy. PLoS One 7, e31128 (2012).

18. Bartels, H., Oestern, H.J. & Voss-Wermbter, G. Communicating-occluding junction complexes in the alveolar epithelium. A freeze-fracture study. Am Rev Respir Dis 121, 1017-1024 (1980).

19. Schneeberger, E.E. & Karnovsky, M.J. Substructure of intercellular junctions in freeze-fractured alveolar-capillary membranes of mouse lung. Circ Res 38, 404-411 (1976).

20. Soderberg, O. et al. Direct observation of individual endogenous protein complexes in situ by proximity ligation. Nat Methods 3, 995-1000 (2006).

21. Rhett, J.M., Jourdan, J. & Gourdie, R.G. Connexin 43 connexon to gap junction transition is regulated by zonula occludens-1. Mol Biol Cell 22, 1516-1528 (2011).

22. Van Itallie, C.M., Fanning, A.S., Bridges, A. & Anderson, J.M. ZO-1 stabilizes the tight junction solute barrier through coupling to the perijunctional cytoskeleton. Mol Biol Cell 20, 3930-3940 (2009).

23. Mrsny, R.J. et al. A key claudin extracellular loop domain is critical for epithelial barrier integrity. Am J Pathol 172, 905-915 (2008).

24. Sauer, R.S. et al. Safety, efficacy, and molecular mechanism of claudin-1-specific peptides to enhance blood-nerve-barrier permeability. J Control Release 185, 88-98 (2014).

25. Staat, C. et al. Mode of action of claudin peptidomimetics in the transient opening of cellular tight junction barriers. Biomaterials 54, 9-20 (2015).

26. Dabrowski, S. et al. Redox-sensitive structure and function of the first extracellular loop of the cell-cell contact protein claudin-1: lessons from molecular structure to animals. Antioxid Redox Signal 22, 1-14 (2015).

27. Baumgartner, H.K., Beeman, N., Hodges, R.S. & Neville, M.C. A D-peptide analog of the second extracellular loop of claudin-3 and -4 leads to mislocalized claudin and cellular apoptosis in mammary epithelial cells. Chem Biol Drug Des 77, 124-136 (2011).

28. Zwanziger, D. et al. A peptidomimetic tight junction modulator to improve regional analgesia. Mol Pharm 9, 1785-1794 (2012).

29. Veshnyakova, A. et al. Mechanism of Clostridium perfringens Enterotoxin Interaction with Claudin-3/-4 Protein Suggests Structural Modifications of the Toxin to Target Specific Claudins. J Biol Chem 287, 1698-1708 (2012).

30. Winkler, L. et al. Molecular determinants of the interaction between clostridium perfringens enterotoxin fragments and claudin-3. J Biol Chem 284, 18863-18872 (2009).

31. Suzuki, H. et al. Crystal structure of a claudin provides insight into the architecture of tight junctions. Science 344, 304-307 (2014).

32. Rossa, J. et al. Claudin-3 and claudin-5 protein folding and assembly into the tight junction are controlled by non-conserved residues in the transmembrane 3 (TM3) and extracellular loop 2 (ECL2) segments. J Biol Chem 289, 7641-7653 (2014).

33. Irudayanathan, F.J., Trasatti, J.P., Karande, P. & Nangia, S. Molecular Architecture of the Blood Brain Barrier Tight Junction Proteins-A Synergistic Computational and In Vitro Approach. J Phys Chem B 120, 77-88 (2016).

34. Ivanov, A.I., Parkos, C.A. & Nusrat, A. Cytoskeletal regulation of epithelial barrier function during inflammation. Am J Pathol 177, 512-524 (2010).

35. Hou, J., Renigunta, A., Yang, J. & Waldegger, S. Claudin-4 forms paracellular chloride channel in the kidney and requires claudin-8 for tight junction localization. Proc Natl Acad Sci U S A 107, 18010-18015 (2010).

36. Hou, J. et al. Claudin-16 and claudin-19 interaction is required for their assembly into tight junctions and for renal reabsorption of magnesium. Proc Natl Acad Sci U S A 106, 15350-15355 (2009).

37. Capaldo, C.T. et al. Proinflammatory cytokine-induced tight junction remodeling through dynamic self-assembly of claudins. Mol Biol Cell 25, 2710-2719 (2014).

38. Shen, L., Weber, C.R. & Turner, J.R. The tight junction protein complex undergoes rapid and continuous molecular remodeling at steady state. J Cell Biol 181, 683-695 (2008).

39. Koval, M. Differential pathways of claudin oligomerization and integration into tight junctions. Tissue Barriers 1, e24518 (2013).

40. Piontek, J. et al. Elucidating the principles of the molecular organization of heteropolymeric tight junction strands. Cell Mol Life Sci 68, 3903-3918 (2011).

41. Fanning, A.S., Van Itallie, C.M. & Anderson, J.M. Zonula occludens-1 and -2 regulate apical cell structure and the zonula adherens cytoskeleton in polarized epithelia. Mol Biol Cell 23, 577-590 (2012).

42. Umeda, K. et al. ZO-1 and ZO-2 independently determine where claudins are polymerized in tight-junction strand formation. Cell 126, 741-754 (2006).

43. Saitoh, Y. et al. Tight junctions. Structural insight into tight junction disassembly by Clostridium perfringens enterotoxin. Science 347, 775-778 (2015).

44. Bouvier, D. et al. Characterization of the structure and intermolecular interactions between the connexin40 and connexin43 carboxyl-terminal and cytoplasmic loop domains. J Biol Chem 284, 34257-34271 (2009).

45. Kopanic, J.L. et al. Characterization of the connexin45 carboxyl-terminal domain structure and interactions with molecular partners. Biophys J 106, 2184-2195 (2014).

46. Daugherty, B.L. et al. Developmental regulation of claudin localization by fetal alveolar epithelial cells. Am J Physiol Lung Cell Mol Physiol 287, L1266-1273 (2004).

47. Utech, M. et al. Mechanism of IFN-gamma-induced endocytosis of tight junction proteins: myosin II-dependent vacuolarization of the apical plasma membrane. Mol Biol Cell 16, 5040-5052 (2005).

48. Ivanov, A.I., Nusrat, A. & Parkos, C.A. Endocytosis of epithelial apical junctional proteins by a clathrin-mediated pathway into a unique storage compartment. Mol Biol Cell 15, 176-188 (2004).

49. Marchiando, A.M. et al. Caveolin-1-dependent occludin endocytosis is required for TNF-induced tight junction regulation in vivo. J Cell Biol 189, 111-126 (2010).

50. Stamatovic, S.M., Keep, R.F. & Andjelkovic, A.V. Tracing the endocytosis of claudin-5 in brain endothelial cells. Methods Mol Biol 762, 303-320 (2011).

51. Stahley, S.N. et al. Desmosome assembly and disassembly are membrane raft-dependent. PLoS One 9, e87809 (2014).

52. Piehl, C., Piontek, J., Cording, J., Wolburg, H. & Blasig, I.E. Participation of the second extracellular loop of claudin-5 in paracellular tightening against ions, small and large molecules. Cell Mol Life Sci 67, 2131-2140 (2010).

53. Piontek, J. et al. Formation of tight junction: determinants of homophilic interaction between classic claudins. Faseb J 22, 146-158 (2008).

54. Dobbs, L.G., Gonzalez, R. & Williams, M.C. An improved method for isolating type II cells in high yield and purity. Am Rev Respir Dis 134, 141-145 (1986).

55. Borok, Z. et al. Modulation of t1alpha expression with alveolar epithelial cell phenotype in vitro. Am J Physiol 275, L155-164. (1998).

56. Koval, M. et al. Extracellular Matrix Influences Alveolar Epithelial Claudin Expression and Barrier Function. Am J Respir Cell Mol Biol 42, 172-180 (2010).

57. Daugherty, B.L., Ward, C., Smith, T., Ritzenthaler, J.D. & Koval, M. Regulation of heterotypic claudin compatibility. J Biol Chem 282, 30005-30013 (2007).

58. Jager, L. et al. A rapid protocol for construction and production of high-capacity adenoviral vectors. Nat Protoc 4, 547-564 (2009).

59. Mitchell, L.A. et al. Junctional adhesion molecule a promotes epithelial tight junction assembly to augment lung barrier function. Am J Pathol 185, 372-386 (2015).

60. Salewsky, B., Schmiester, M., Schindler, D., Digweed, M. & Demuth, I. The nuclease hSNM1B/Apollo is linked to the Fanconi anemia pathway via its interaction with FANCP/SLX4. Hum Mol Genet 21, 4948-4956 (2012).

61. Jain, R.K., Joyce, P.B., Molinete, M., Halban, P.A. & Gorr, S.U. Oligomerization of green fluorescent protein in the secretory pathway of endocrine cells. Biochem J 360, 645-649 (2001).

CHAPTER 4: ASYMMETRIC DISTRIBUTION OF DYNAMIN-2 AND β-CATENIN RELATIVE TO TIGHT JUNCTION SPIKES IN ALVEOLAR EPITHELIAL CELLS

K. Sabrina Lynn, Kristen F. Easley, Francisco J. Martinez, Barbara Schlingmann, and Michael Koval

This work has been submitted to *Tissues Barriers*.

Abstract

Tight junctions between lung alveolar epithelial cells maintain an air-liquid barrier necessary for healthy lung function. Previously, we found that rearrangement of tight junctions from a linear, cortical orientation into perpendicular protrusions (tight junction spikes) is associated with a decrease in alveolar barrier function, especially in alcoholic lung syndrome. Using quantitative super-resolution microscopy, we found that spikes in control cells were enriched for claudin-18 as compared with alcohol exposed cells. Moreover, using an in situ method to measure barrier function, tight junction spikes were not associated with localized increases in permeability. This suggests that tight junction spikes have a regulatory role as opposed to causing a physical weakening of the epithelial barrier. We found that tight junction spikes form at cell-cell junctions oriented away from pools of β-catenin associated with actin filaments, suggesting that adherens junctions determine the directionality of tight junction spikes. Dynamin-2 was associated with junctional claudin-18 and ZO-1, but showed little localization with β-catenin and tight junction spikes. Dynasore, a dynamin inhibitor, increased paracellular leak of calcein (0.62 kDa), yet decreased permeability to 10 kDa Texas Red dextran. Dynasore also decreased the number of tight junction spikes/cell and stimulated actin to redistribute to cortical tight junctions. These data suggest a novel role for dynamin-2 in tight

junction spike formation by reorienting junction associated actin. Moreover, the greater spatial separation of adherens and tight junctions in squamous alveolar epithelial cells as compared with columnar epithelial cells facilitates analysis of molecular regulation of the apical junctional complex.

Introduction

Lung epithelia provide a selective and specific barrier that maintains separation between external airspaces and internal fluid filled tissues to enable gas exchange to occur[1]. It also serves as the first line of defense from threats as varied as invading pathogens and direct injury. Disruption of alveolar lung fluid balance can lead to acute respiratory distress syndrome (ARDS), which is characterized by widespread flooding of the alveoli. Chronic alcohol consumption can perturb normal lung fluid balance, increasing the risk of developing ARDS[2,3].

Epithelial barrier function is critically regulated by tight junctions, multiprotein complexes integrated into the plasma membrane of cells that act as selectively permeable barriers between neighboring cells[4–6]. We have previously observed that alveolar epithelial cells under stress, such as chronic exposure to alcohol, reorganize tight junctions into unidirectional protrusions oriented towards the nucleus, referred to as tight junction spikes[7]. There is a correlation between tight junction spikes and deficits in alveolar epithelial barrier function, where monolayer permeability (leak) increases with an increasing number of cells containing spikes[8]. However, the molecular composition of tight junction spikes and mechanisms by which spikes are regulated have not been fully characterized.

Here primary rat alveolar epithelial cells were used to further investigate the characteristics of tight junction spikes. Surprisingly, the molecular composition of tight junction spikes was sensitive to chronic alcohol exposure, in that alveolar epithelial cells from alcohol fed rats were deficient in claudin-18 as compared with unexposed cells. Alveolar epithelial cells also provided a unique platform to define the relative orientation of adherens junctions to tight junctions and

tight junction spikes, since their squamous morphology provided spatial separation between these different elements of the apical junctional complex that is not readily observed in columnar cells. We also identified a novel role for dynamin-2 in regulating tight junction spike formation. Although, dynamin inhibitors have previously been shown to inhibit endocytosis in alveolar epithelial cells[9,10], our findings are consistent with accumulating evidence demonstrating that dynamins can act as an actin bundling protein[11–15].

Materials and Methods

Primary Alveolar Epithelial Cell Isolation

All animal protocols were reviewed and approved by the Institutional Animal Care and Use Committee of Emory University and performed with the approval of the Division of Animal Resources. Adult male Sprague-Dawley rats (150-200g, Charles River Laboratory) were used as a source of primary alveolar epithelial cells. In most cases, rats were given standard chow and water ad libitum. For experiments using the chronic alcohol rat model, Sprague-Dawley rats (50-100g, Charles River Laboratory) were pair-fed an ethanol or control isocaloric maltose-dextrin Lieber-DeCarli liquid diet (Research Diets) ad libitum for 6-8 weeks prior to cell isolation[8].

Type II AECs were isolated from rats according to Dobbs with modifications[16]. Lungs were perfused with PBS with calcium and magnesium, then removed and lavaged with solution II (5.5 mM Dextrose, 10 mM HEPES, 2 mM $CaCl_2$, 1.3 mM $MgSO_4$, 140 mM NaCl, 5 mM KCl, pH 7.4). Elastase (1.6 units/ml, Worthington, Cat# LS002292) was instilled and continually circulated in lavaged lungs while incubating in a 37^{o}C water bath for 30-45 minutes. The lungs were then manually dissected into 1 mm^3 pieces, taking care to remove the trachea and bronchial tissue. Diced lungs were resuspended in 5 mL fetal bovine serum (FBS) and 5 mL DNase solution (≥ 400 Kunitz units/mL in solution II, Sigma Cat# DN25). Lung suspensions were incubated for

10-20 minutes with gentle rotation in a 37°C water bath. Lung suspensions were then filtered through a 100 μm cell strainer (Greiner Bio-one, Cat# 542-000) followed by 40 μm cell strainer (Greiner Bio-one, Cat# 542-040). Filtered cell suspensions were centrifuged at 250 *g* for 8 minutes. Remaining red blood cells were removed from cell pellets by resuspending in 5 mL of 0.87% ammonium chloride in 10 mM Tris (pH 7.6) for 5 minutes. 10 mL of Dulbecco's Modified Eagle Media (Corning Cat# 10-013-CV) containing 10% FBS (Atlanta Biologicals Cat# S11550), 100 U/mL penicillin (Sigma Cat# P4333), 10 mg/mL streptomycin (Sigma Cat# P4333), 0.25 μg/mL amphotericin B (VWR, Cat# 0414-1G), and 50 μg/mL gentamycin (Sigma Cat# G1397) (DMEM) were added to the cell suspension, which was then centrifuged at 250 *g* for 8 minutes. The cells were resuspended in 30 mL of DMEM and biopanned to remove macrophages on rat IgG (0.5 mg IgG/mL 10 mM Tris buffer, pH 9.5, Sigma Cat# I8015)-coated cell culture grade petri dishes (Genesee Scientific Cat# 25-202) for 1 hour at 37°C. Cell isolations using this method routinely obtained 90-95% type II AECs cell suspensions.

To produce model Type I AEC monolayers, isolated Type II AECs were plated on rat tail type-I collagen (20 μg/mL, Roche Cat# 111791790) coated 12 mm Transwell-permeable supports (500,000 cells) or 12 mm #1.5H coverslips (250,000 cells, Electron Microscopy Sciences Cat# 72290-01) unless otherwise stated. Cells were plated and refed every other day using DMEM. Cells differentiated into a confluent model type I AEC monolayer after 4-5 days, and cells were used for experiments on day 5 or 6.

Virus Transduction

AECs were transduced with adenovector encoding a NH2-terminal enhanced YFP-claudin-18 or untagged claudin-5 on day 4 or 5 after isolation. Adenovector was bilaterally added to media at the stated multiplicity before dispensing on cells. Cells were analyzed 48 hours after virus addition unless otherwise stated.

Localized Permeability Assay

The XPerT assay was performed according to Dubrovskyi et al with modifications[17]. Bovine skin Type B gelatin (Sigma) was dissolved in 0.1 M bicarbonate buffer (pH 8.3) to a final concentration of 10 mg/mL gelatin. Gelatin was stirred while heated in a water bath at 70°C until completely dissolved. EZ-link NHS-LC-LC-biotin (Thermo) dissolved in DMSO to a concentration of 5.7 mg/mL was added to gelatin to a final concentration of 0.57 mg/mL biotin. Biotin/gelatin solution was aliquoted and frozen until needed. Biotin/gelatin-coated coverslips were prepared by diluting 0.57 mg/mL biotin with 0.1 M bicarbonate buffer (pH 8.3) to a final concentration of 0.25 mg/mL biotin and sterilized using a 0.22 um Steriflip filter. Diluted biotin/gelatin was then added to coverslips and placed on a rocker at 4°C overnight. Excess biotin/gelatin was removed by washing coverslips twice with warmed PBS with calcium and magnesium before plating cells.

AECs were plated on biotin/gelatin-coated coverslips and allowed to differentiate for five days. AECs were incubated with 25 μg/mL FITC-avidin (Invitrogen Cat# 434411) in serum-free DMEM media with 100 U/mL penicillin (Sigma Cat# P4333), 10 mg/mL streptomycin (Sigma Cat# P4333), 0.25 μg/mL amphotericin B (VWR, Cat# 0414-1G), and 50 μg/mL gentamycin (Sigma Cat# G1397) for five minutes unless otherwise stated. AECs were then washed and fixed for ZO-1 immunofluorescence as described below.

Paracellular permeability

Transepithelial resistance (TER) and paracellular permeability were measured on model Type I AECs plated on Transwell-permeable supports. Cells were incubated in Ringer's saline buffer (150 mM NaCl, 2 mM $CaCl_2$, 1 mM $MgCl_2$, 10 mM glucose, and 10 mM HEPES pH 7.4) 15 minutes prior to TER measurement and dye addition. TER was measured using an Ohmmeter (World Precision Instruments, Sarasota, FL). Paracellular dye permeability was assessed by simultaneous measurement of two different-sized fluorescent dyes, 2 μg/ml Calcein (0.62 kDa)

(ThermoFisher) and 50 μg/mL Texas Red Dextran (10 kDa, ThermoFisher), in Ringer's saline buffer added to the apical chamber. The amount of dye that diffused to the basolateral chamber over a two-hour incubation was measured using a microplate reader (Biotek Winooski, VT).

Dynamin Inhibitor Treatment

AECs were plated on collagen-coated coverslips and differentiated to a model type I AEC monolayer as described above. On day 4 after cell plating, AEC media was changed to serum-free DMEM. On day 5, cells were treated for four hours with 160 μM Dynasore in serum-free DMEM. Cells were then prepared for immunofluorescence as described. All inhibitors were dissolved in DMSO (Sigma Cat# D2438), with 0.25% DMSO used as a vehicle control in serum-free DMEM.

Immunoblot

Model Type I AECs were washed twice with PBS with calcium and magnesium and incubated for 30 minutes on ice with RIPA buffer (Cell Signaling) containing Complete Protease Inhibitor Cocktail (Roche Cat# 4693132001). Cells were scraped and collected, then briefly sonicated on ice. Protein pellets were centrifuged for 10 minutes at 13200 *g* at 4°C. Protein concentration was determined by BCA assay (Thermo Fisher Scientific Cat# 23225). Reducing SDS sample buffer (10% glycerol, 1.25% SDS, 50 mM Tris pH 6.7 and 8.3 mg/mL dithiothreitol) was added to supernatant. SDS sample buffer-protein samples were heated at 70°C for 10 minutes. Proteins were resolved by SDS-PAGE using 4-20% Mini-PROTEAN TGX stain-free gradient SDS-polyacrylamide gels, then transferred to nitrocellulose membranes (Bio-Rad Cat# 1704270). The primary antibodies used for protein detection were rabbit anti-dynamin-1 (1:1,500, Abcam 3465), rabbit anti-dynamin-2 (1:1,500, Abcam 65556), rabbit anti-dynamin-3 (1:1,500, Abcam 183904), and mouse anti- β-actin (1:10,000, Sigma A5441). The secondary antibodies used were goat anti-rabbit IgG IRDye 800CW (1:20,000, LI-COR) and goat anti-mouse IgG IRDye 680RD

(1:20,000, LI-COR). Membranes were imaged using a Bio-Rad ChemiDoc MP Imaging System. Relative protein quantification was relative to actin. LI-COR fluorescent images of immunoblots were pseudocolored to greyscale images in the figures.

Immunofluorescence

Cell monolayers were washed twice with PBS with calcium and magnesium, then fixed for ten minutes with 4% paraformaldehyde in PBS. Cells were then washed once with PBS and incubated with 1 M glycine for five minutes. Cells were washed twice with PBS before being permeabilized with 0.5% Triton X-100 (Fisher Scientific Cat# BP151-500) in PBS for five minutes. Cells were blocked twice for five minutes with 0.5% Triton-X100 + 3% bovine serum albumin (BSA, Fisher BP1600-100) in PBS. Primary antibodies were prepared in 3% BSA in PBS and incubated overnight at 4°C. Cells were washed three times with 3% BSA in PBS and then incubated with secondary antibodies prepared in 3% BSA in PBS for one hour at room temperature. Cells were washed three times with 3% BSA in PBS followed by three washes with PBS before mounting slides to coverslips. ProLong Diamond mounting solution (Invitrogen Cat# P36961) was used to mount slides. Slides were allowed to dry at room temperature overnight, then were sealed with clear sealant.

The following primary antibodies were used for immunofluorescence: rabbit anti-dynamin-1 (1:200, Abcam 3465), rabbit anti-dynamin-2 (1:200, Abcam ab65556), rabbit anti-dynamin-3 (1:200, Abcam 183904), rabbit anti-claudin-18 (1:200, Thermo Fisher 700178), rabbit anti-claudin-18 (1:125, Thermo Fisher 388100), rabbit anti- β-catenin (1:400, Abcam ab32572), mouse anti-α-catenin (1:250, Invitrogen 13-9700), mouse anti-ZO-1 (1:500, Invitrogen 339100), and rabbit anti-ZO-1 (1:500, Invitrogen 40-2300).

The following secondary stains were used for immunofluorescence: goat anti-rabbit IgG Texas Red (1:500, Jackson 111-075-144), goat anti-mouse IgG Cy2 (1:1,000, Jackson 115-225-166), goat anti-rabbit IgG Cy2 (1:1,000, Jackson 115-165-166), goat anti-mouse IgG Cy3 (1:1,000,

Jackson 111-225-144), goat anti-rabbit IgG AlexaFluor 488 (1:500, Abcam ab150073), goat anti-mouse IgG AlexaFluor 594 (1:500, Abcam ab150116), goat anti-rabbit IgG AlexaFluor 594 (1:500, Invitrogen R37117), phalloidin-AlexaFluor-405 (1:40, Thermo A30104).
Slides were blinded before imaging. Widefield images were collected on using an Olympus IX70 microscope with a U-MWIBA filter pack (BP460-490, DM505, BA515-550) or U-MNG filter pack (BP530-550, DM570, BA590-800). Minimum and maximum intensities for images were adjusted in parallel so that the intensity scale remained linear to maximize dynamic range.

Stimulated Emission Depletion Microscopy

AECs from control-fed and alcohol-fed Sprague-Dawley rats were plated on coverslips coated with rat tail type-I collagen (20 μg/mL, Roche Cat# 111791790). Immunolabeling was performed as described above with modifications. Prior to 4% PFA fixation, cells were washed twice with PBS with calcium and magnesium then 1:1 methanol/acetone fixation was performed for three minutes. Cells were then washed once with PBS and fixed with 4% PFA as previously described. Cells were permeabilized for five minutes with 0.5% Triton-X100 (Fisher Scientific Cat# BP151-500) in PBS, then blocked twice for five minutes with 5% goat serum (Sigma Cat# G6767) with 0.5% Triton-X100 in PBS. Primary antibodies were made in 5% goat serum in PBS and incubated on cells overnight at 4°C. Cells were washed three times for five minutes with 5% goat serum in PBS, then incubated with secondary antibodies in 5% goat serum in PBS for one hour at room temperature. Cells were washed three times for five minutes with 5% goat serum in PBS, three times for five minutes with PBS. Coverslips were then mounted on slides using Abberior TDE mounting media (Abberior). Primary antibodies used were rabbit anti-claudin-18 (1:125, Invitrogen 388000) and mouse anti-ZO-1 (1:200, Invitrogen 339100). Secondary antibodies used were goat anti-rabbit IgG STAR580 (1:100, Abberior) and goat anti-mouse IgG STARRED (1:100, Abberior). Samples were imaged using an Abberior easy3D STED Expert Line system with Olympus IX83 inverted body microscope, Olympus Objective UPlanSApo

100x/1.40 oil, and Excelitas APD detectors. Data were collected and analyzed using Abberior ImSpector software. Samples were excited with 561 nm and 640 nm pulsed laser lines and depleted with a 775 nm pulsed STED laser line.

Live-cell imaging

AECs were plated onto glass-bottom chamber slides (Lab-Tek II Cat# 155382) coated with rat tail type I-collagen (20 μg/mL, Roche Cat# 111791790). On day 4, cells were transduced with adenovirus encoding YFP-claudin-18 with a multiplicity of infection of 20. Media was changed 24 hours after transduction and one hour before live-cell imaging to phenol red-free DMEM media (Sigma Ca#D1145) containing 10% FBS (Atlanta Biologicals Cat# S11550), 100 U/mL penicillin (Sigma Cat# P4333), 10 mg/mL streptomycin (Sigma Cat# P4333), 0.25 μg/mL amphotericin B (VWR, Cat# 0414-1G), and 50 μg/mL gentamycin (Sigma Cat# G1397) before being moved to a Tokai Hit STXG stagetop incubator heated at 37°C with 5% CO_2. In some samples, cells were treated with 80 □M Dynasore for 10 minutes prior to imaging. Under those conditions, 2 out of 35 spikes increased in length and none of them became shorter. All images were collected with a Nikon A1R HD25 confocal unit on a Nikon Ti2-E equipped with a Plan Apo λ 20x/0.75NA lens and the Perfect Focus System for maintenance of focus over time. EYFP fluorescence excitation was with the 20 mW 488 DPSS laser in a LU-NV unit (selected with an AOTF) and collected with a 525/50 filter. Confocal images were collected with a GaAsP PMT using an 8 kHz resonant scanner with 16x averaging. Data were collected using NIS-Elements AR 5.20.01 software (Nikon). Imaging was performed over a time period of 35.5 minute at several multipoint locations with z-stacks (3 z-series/time-point/multipoint position, step-size of 0.85 microns) collected at 30 s intervals using an 8 kHz resonant scanner. Images were taken in 1024x1024 with a pixel size of 155nm pixels resolution with excitation laser power of 1.3% to minimize photobleaching (excitation 488 nm with 525/50 emission filter cube). All z-stacks are displayed as a maximum z-projection image. Images and movies were processed with ImageJ[18].

Minimum and maximum intensities for images were adjusted in parallel so that the intensity scale remained linear to maximize dynamic range.

ImageJ

Spike length measurements were collected using freehand line drawing tool in ImageJ to trace tight junction spikes. Intensity along tight junction spikes was used on traced tight junction spikes in merged two-channel images using the BAR plug-in multi-channel plot tool.

Statistics

All statistics were calculated using GraphPad Prism 8.0. Statistical significance for parametric data was determined using unpaired two-tailed *t*-test to compare one dependent variable against on independent variable. One-way analysis of variance with Tukey's multiple comparisons test was used to compare one dependent variable against multiple independent variables. Two-way analysis of variance with Tukey multiple comparisons test was used to compare multiple dependent variables against multiple independent variables. Non-parametric data used the Mann-Whitney *U*-test. Data in graphs represent average +/- SD.

Results

Morphological classification of tight junction spikes

Stimulated emission depletion (STED) super-resolution immunofluorescence microscopy revealed a broad range of tight junction spike morphologies in alveolar epithelial cells (AECs; Figure 4.1 a,b). These could be categorized as short triangular protrusions, thinner spikes with triangular bases, and elongated spikes with and without bulbous ends. The range of spike morphologies and lengths observed using STED microscopy suggested that shorter triangular protrusions might lengthen to form spikes. While STED microscopy allowed better resolution to

distinguish the range of spike morphologies (Supplemental Figure 4.1), differences in spikes could also be resolved by standard confocal immunofluorescence microscopy, which enabled us to examine spikes in AECs expressing EYFP-claudin-18 by live cell microscopy. Previously, we used this approach to demonstrate that tight junction spikes are sites of active vesicle budding and fusion[8]. However, vesicle budding and fusion mainly occurred on elongated spikes, which, over a 30-40 minute time course, did not show obvious changes in length[8]. To further investigate changes in spike length, we screened fields from two independent preparations and identified 55 tight junction spikes, of which only two showed an increase in length of at least 2 microns over a ~30 minute period of observation (Figure 4.1c; online publication, Supplemental Movie 1). This suggests that spikes are relatively stable structures and that their formation is a rare event.

We then used STED microscopy to detect claudin-18 and ZO-1 localization in tight junction spikes. Super-resolution microscopy revealed that these tight junction proteins were not uniformly distributed along the length of spikes, since there were regions that were enriched for claudin-18, ZO-1 or showed equivalent amounts of both proteins (Figure 4.2 a,b). Given these differences, we quantified the distribution of claudin-18 and ZO-1 in line scans of tight junction spikes in AECs isolated from either control-fed rats or from rats fed an alcohol diet, conditions that increase the formation of tight junction spikes and also induce paracellular leak across tight junctions[8]. Tight junction spikes from control AECs showed an increase in claudin-18 and a decrease in ZO-1 along the length of spikes (Figure 4.2 c,d). By contrast, spikes in alcohol-exposed AECs showed a decrease in claudin-18 along spike length, which paralleled the decrease in ZO-1. The difference between spikes in control vs alcohol-exposed AECs was more readily apparent when the claudin-18/ZO-1 ratio was calculated (Figure 4.2 e,f), where spikes from control AECs had an overall enrichment in claudin-18 relative to ZO-1 along spike length as compared with spikes from alcohol-exposed AECs. The claudin-18/ZO-1 ratio at the end of spikes (7 μm) was significantly higher in control AECs compared with alcohol AECs (Figure

4.2g). This supports a model where claudin-18 differentially associates with tight junction scaffold proteins and is impacted by chronic exposure to alcohol, consistent with previous observations.[8]

Tight junction spikes are not sites of increased paracellular leak

There are several lines of evidence correlating an increase in tight junction spikes with increased barrier permeability.[8,19,20] We thus hypothesized that tight junction spikes might correspond to areas which are prone to increased paracellular permeability. To define where AEC monolayers were preferentially permeable, we employed the XPerT assay, which is based on the ability of FITC-avidin (~67 kDa) to have access to biotinylated residues on the extracellular matrix[17]. For this assay, freshly isolated AECs were plated on biotin/gelatin-coated coverslips and allowed to differentiate for 6 days into a type I cell monolayer. The monolayers were then incubated with FITC-avidin for 5 minutes, followed by fixation and immunofluorescence staining for ZO-1 as a marker for tight junctions (Figure 4.3). Control AECs showed little FITC-avidin labeling, consistent with their forming a tight monolayer; however, there were some foci that did show increased permeability (Figure 4.3 b,e).

We then performed the XPerT assay on AECs that were transduced with claudin-5, which causes increased paracellular leak and mimics the effects of chronic alcohol exposure on barrier function.[8] As shown in Figure 4.3 f-h, AECs expressing increased claudin-5 showed increased paracellular leak as compared with control AECs. There were multiple sites labeled with FITC-avidin in claudin-5 expressing AECs, however, these sites corresponded to areas with significant discontinuities in ZO-1 localization, as opposed to sites containing tight junction spikes. These data suggest that spikes in and of themselves are not prone to paracellular leak, and instead more likely to have a different role in regulating AEC barrier function.

Adherens junctions are asymmetrically opposed to tight junction spikes

Adherens junctions associate closely with tight junctions as part of the apical junctional complex and regulate tight junction formation.[21–23] Since tight junction spikes orient asymmetrically from cell-cell junctions, we examined the localization of the adherens junction protein β-catenin to determine where it was localized relative to claudin-18 and ZO-1 containing tight junction spikes. Immunostaining of AECs demonstrated that β-catenin was asymmetrically localized, relative to tight junctions, and only partially overlapped with ZO-1 and claudin-18 (Figure 4.4 a,c), consistent with our previous qualitative analysis.[19]

We then quantified the orientation of β-catenin in areas where it was adjacent to tight junction spikes from four independent preparations (Figure 4.4b). Of 751 identified sites with a high concentration of β-catenin, 582 were localized at areas adjacent to sites where tight junction spikes containing ZO-1 were present. Interestingly, β-catenin areas were overwhelmingly oriented away from tight junction spikes, with an average of 71 percent of them protruding away from β-catenin. β-catenin showed a similar pattern of localization adjacent to tight junction spikes labeled for claudin-18 (Figure 4.4c) as well as α-catenin (Supplemental Figure 4.2).

This analysis benefitted from the squamous morphology of AECs, which showed good separation between adherens junctions and tight junctions. Whether these morphological hallmarks also occur in columnar epithelial cells remains an open question, primarily since adherens junction and tight junction proteins imaged in the x-y plane of focus normally appear as a continuous overlapping band demarking the circumference of each cell[24,25] and the x-z plane is more difficult to resolve.

Adherens junctions and tight junctions both interact with the actin cytoskeleton, specifically through scaffold proteins such as catenins and ZO-1, respectively[26–29]. To visualize co-localization of these proteins with the actin cytoskeleton, we double labeled AECs with Alexa 405-phalloidin, labeling actin, along with either anti-β-catenin or anti-ZO-1 (Figure 4.5). AECs

had prominent actin filaments that radiated from a central point in the interior of the cell, that co-localized with β-catenin at the terminal ends (Figure 4.5a). Tight junction spikes also co-localized with radiating actin filaments, with spikes projecting along actin filaments towards the cell interior (Figure 4.5b). In addition to actin filaments, we observed faintly visible cortical actin that co-localized with ZO-1 at AEC tight junctions as previously described.[19]

Dynamin-2 regulates tight junction morphology and function

The alcoholic lung phenotype is associated with increased paracellular permeability both *in vitro* and *in vivo* and correlates with an increase in tight junction spikes[19,20,30]. Dynamin has previously been shown to induce membrane bending (including vesicle fission) and also interacts with actin[14,31–33], suggesting that dynamins are candidate regulators of both processes. Consistent with this, we previously found that a dynamin inhibitor, Dynasore, decreased the number of AECs containing tight junction spikes[8]. Thus, we measured the effects of Dynasore (four hours,160 μM) on AEC barrier function of cells from either control-fed or alcohol-fed rats (Figure 4.6). Consistent with our previous analysis, we found that AECs from alcohol-fed rats were leakier than control AECs, based on measurements of transepithelial resistance (TER), and paracellular flux of calcein and Texas Red Dextran (10 kDa) (Figure 4.6a).

Surprisingly, AEC monolayers showed a decrease in TER in response to Dynasore, suggesting an increase in paracellular leak, regardless of whether the AECs were from control or alcohol-fed rats. We also measured the effect of Dynasore on paracellular flux of calcein through control and alcohol-fed AEC monolayers, which also increased (Figure 4.6 b,c). However, although Dynasore increased calcein permeability, Texas Red Dextran (10 kDa) permeability decreased in both control and alcohol-exposed AECs (Figure 4.6 d,e). These data support a model where Dynasore specifically alters paracellular flux by simultaneously increasing small molecule leakage and decreasing large molecule permeability. This differential pattern of changes in tight junction permeability is not without precedent, since claudin-5 deficient mice

show a similar preferential increase in small molecule permeability to the blood brain barrier[34,35].

Given the effect of Dynasore on AEC permeability, we measured expression of the three isoforms of dynamin in AECs by immunoblot. Consistent with other epithelial cells, dynamin-2 was the dominant isoform present[36,37], however there were low levels of dynamin-1 (Figure 4.7 a,b). Dynamin-3 was undetectable. Localization of dynamin-2 was determined by immunofluorescence microscopy, where AECs were double-labeled with anti-dynamin-2 and anti-β-catenin, claudin-18, or ZO-1 (Figure 4.7 c-e). Dynamin-2 strongly localized to linear cell-cell junctions including areas with tight junction spikes, co-localizing with the tight junction proteins claudin-18 and ZO-1. Slight dynamin-2 staining was visible co-localizing with some tight junction spikes, though dynamin-2 was predominantly localized at linear intercellular tight junctions. In areas with asymmetrical β-catenin, line scans show that dynamin-2 is predominantly localized at one edge of β-catenin near the linear cell-cell junction with fainter dynamin-2 staining visible throughout areas containing β-catenin.

To determine whether Dynasore-induced changes in barrier function correlated with morphological changes to tight junctions and adherens junctions, we investigated localization of ZO-1, β-catenin, and actin with and without Dynasore treatment (four hours,160 μM). Consistent with our previous work [8], Dynasore caused a significant decrease in the number of tight junction spikes (Figure 4.8). From 327 AEC tight junction spikes analyzed, the median spike length was 2.1 microns. Based on this, we used a cutoff of two microns to distinguish shorter spikes from longer spikes. Dynasore treatment affected tight junction spikes of all lengths, with no observed preferentiality to groups of spikes below or above 2 microns in length (Figure 4.8c).

Dynasore treatment also decreased actin stress fibers, and concurrently increased the appearance of cortical actin. Cortical actin co-localized with ZO-1 staining at linear junctions, suggesting that when dynamin-inhibition decreases tight junction spikes, ZO-1 and actin were

reabsorbed back into intercellular linear tight junctions. Conversely, para-junctional regions enriched for β-catenin remained present in Dynasore-treated cells. This suggests a model where dynamin-2 acts as an intermediary between adherens junctions and linear tight junctions to drive the formation of tight junction spikes (Figure 4.9).

Discussion

In this study, we defined the molecular composition of tight junction spikes and investigated their role in barrier function in AECs. There was a distinct, asymmetrical separation of tight junction spikes and adherens junctions. Despite the striking separation of adherens junctions and tight junction spikes, we found that these regions were not prone to increased paracellular permeability using a local permeability immunofluorescence assay. For the first time, we found that dynamin-2 localized to AEC tight junctions. Consistent with this observation, the dynamin inhibitor Dynasore decreased tight junction spikes, rescued barrier function, and induced formation of cortical actin. These findings suggest a model where cytoskeletal rearrangement induces tight junction spike formation and a disruption in barrier capabilities at tight junctions.

We observed a unique orientation of lateral junctions at cell-cell interfaces. Unlike cuboidal polarized epithelia, which form closely opposed tight junctions and adherens junctions[38] AECs are squamous and have overlapping areas of cell-cell contact[39]. Though often portrayed in models as forming junctions at non-overlapping cell-cell interfaces, the asymmetrical staining pattern we observed of β-catenin relative to ZO-1 suggests that tight junctions form at the edge of overlapping cells and adherens junctions form along the majority of the overlapping cell-cell interface. Given that AECs are squamous and very thin (0.1-0.2 microns), overlap of these cells in culture conditions is highly likely and has been noted in EM sections of intact alveoli.[24,39]

Squamous AECs afforded the unique viewpoint of the lateral junction interface that facilitated visualization of crosstalk between the actin cytoskeleton, tight junctions, and adherens junctions. Specifically, we can better observe associations between tight junction spike

formation and changing actin morphology at junctions. This unique view separating tight junctions and adherens junctions along the x-y plane confirms our hypothesis that spike formation occurs specifically at tight junctions.

This orientation of the cell-cell interface provides an optimal view of lateral junction interactions especially with the actin cytoskeleton. The asymmetrical localization of β-catenin relative to tight junctions, particularly at areas with tight junction spikes, and the association with actin stress fibers suggests that cytoskeletal orientation of tension could be partly responsible for the asymmetrical localization of β-catenin and tight junction spikes. Moreover, changes in tension between cells can be sensed and regulated by adherens junctions[59,60]. The asymmetrical distribution of β-catenin at junction interfaces suggests an asymmetry in cytoskeletal forces at the junction. The opposing orientations of tight junction spikes and asymmetrical β-catenin staining suggest opposing cytoskeletal-mediated tension pulling separately at the tight junction and adherens junction, such as contractile forces exerted by actomyosin. Consistent with this, myosin II regulatory light chain phosphorylation, a marker of actomyosin contraction, has been correlated with an increase in tight junction permeability[40,41].

Alternatively, actin filaments could be propelling tight junction spike formation through actin polymerization similar to the construction of other cell appendages like filopodia and lamellipodia, with asymmetrical adherens junctions perhaps representing the starting point of the apical junctional complex prior to tight junction spike formation. This scenario hints at a lack of opposing forces countering tight junction formation. One notable example in MDCK cells demonstrated aberrant apical membrane expansion enriched in F-actin and dysregulated microvilli structures occurring with ZO-1 knockdown, in addition to an increase in cortical actin staining[42]. Interestingly, Dynasore treatment of ZO-1-depleted cells rescued these phenotypes, suggesting that in addition to its role as a cytoskeletal organizer, ZO-1 could play a role in regulating membrane traffic[15,27]. It is possible that disassociation of ZO-1 from the actin cytoskeleton could be leading to dysregulation of membrane trafficking and an increase in tight

junction spikes. This supports a model of tight junction spike formation through unchallenged and unequal cytoskeletal force distribution, but further work is needed to better define whether this is the case.

Previous work demonstrated that ZO-1- and claudin-18-labelled vesicles budded from and fused with tight junction spikes, suggesting that spikes could be areas of increased tight junction turnover and trafficking.[8, 43, 44] We demonstrated a decrease in tight junction spikes with inhibition of the endocytosis protein dynamin using the inhibitor Dynasore. Dynamin is a large GTPase that primarily plays a role in clathrin-mediated endocytosis. Dynamin facilitates endocytic vesicle formation by dimerizing and wrapping around the neck of a budding vesicle. The hydrolysis of GTP causes dynamin to cinch the neck of the budding vesicle, effectively merging the plasma membrane to release the vesicle[45]. It is possible that incomplete scission by dynamin or friction-induced elongation of vesicles during endocytosis plays a role in tight junction spike formation[46].

Alternatively, dynamin has more recently been shown to interact with the actin cytoskeleton to create actin filament bundles. Dynamin's association with actin has been well documented. One particularly relevant example in a drosophila cell line revealed that dynamin was able to facilitate invadasome structures through assembly with actin filaments[32]. Similarly, in a rat glioma-derived cell line, inhibition of dynamin-1 resulted in decreased actin bundling and stunted filopodia and lamellipodia formation[31]. Considering that dynamin colocalized with ZO-1 at cell-cell junctions, partially overlapped with β-catenin, and that Dynasore treatment induced cytoskeletal rearrangement, it is likely that dynamin is facilitating tight junction spike formation through association with actin filaments. However, these results should be interpreted with caution, since Dynasore has been shown to have off-target effects such as cholesterol perturbation[36,47].

We found that tight junction spikes themselves were not the sites of increased leak, suggesting an indirect role for them in controlling paracellular barrier function. For instance, it

is possible that tight junctions respond to changes in tension that result in increased leakiness[48–50]. The rearrangement of cortical actin structures with Dynasore treatment correlated with a decrease in tight junction spikes and a recovery of large molecule permeability, suggesting that the formation of spikes is coupled with tensile-actin forces, which can induce leak at stress points in cell monolayers, such as with focal adherens junction formation[51]. Interestingly, when rat type I AECs were stretched to 25 percent change in surface area (equivalent to 100 percent total lung capacity), rearrangement of actin into more cortical structures was observed without changes to tight junction morphology[52]. Whether tight junction spikes are formed by changes in tension remains to be determined.

The association of tight junction spikes with leaky alveolar monolayer phenotypes (i.e. chronic alcohol models, increased claudin-5 expression) suggested that tight junction spikes could be areas of increased paracellular leak. However, we directly tested this hypothesis and found that this was not the case. Instead, the presence of vesicles at tight junction spikes suggests that these spikes are areas of increased tight junction turnover, which also could be associated with increased leak. Similar spike structures have been visualized at desmosomes in keratinocytes treated with *Pemphigus vulgaris* antisera and associate with endocytosis of junctional proteins[53]. It is also possible that these spikes are pools of tight junction proteins that are separate from strand-incorporated tight junctions. Previous data surveying tight junction proteins in cells from alcohol-fed rats saw a significant increase in claudin-5, but not a significant increase in other claudins or ZO-1. This suggests that the lengthening of tight junctions through the formation of tight junction spikes is not being compensated with an increase in tight junction proteins, and therefore the stoichiometry of tight junction proteins in the apical junctional complex could be affected.

There is considerable heterogeneity in the intracellular distribution of junction proteins and only a subset of cells within a monolayer have tight junction spikes. Our data demonstrate that the impact of chronic alcohol use on barrier function is also heterogenous across the alveolar

monolayer. Further work defining how interactions between adherens junctions and tight junction are affected by alcohol and other stresses at a molecular level will help determine their impact on alveolar barrier function and susceptibility to acute lung injury.

Acknowledgements

We thank members of the Koval laboratory for critical reading of the manuscript and for William Giang for his microscopy assistance. Supported by NIH grants R01-AA025854 (MK), F31-HL139109 (KSL) and the Emory University Integrated Cellular Imaging Microscopy Core (NIH S10-OD028673).

Figure 4.1

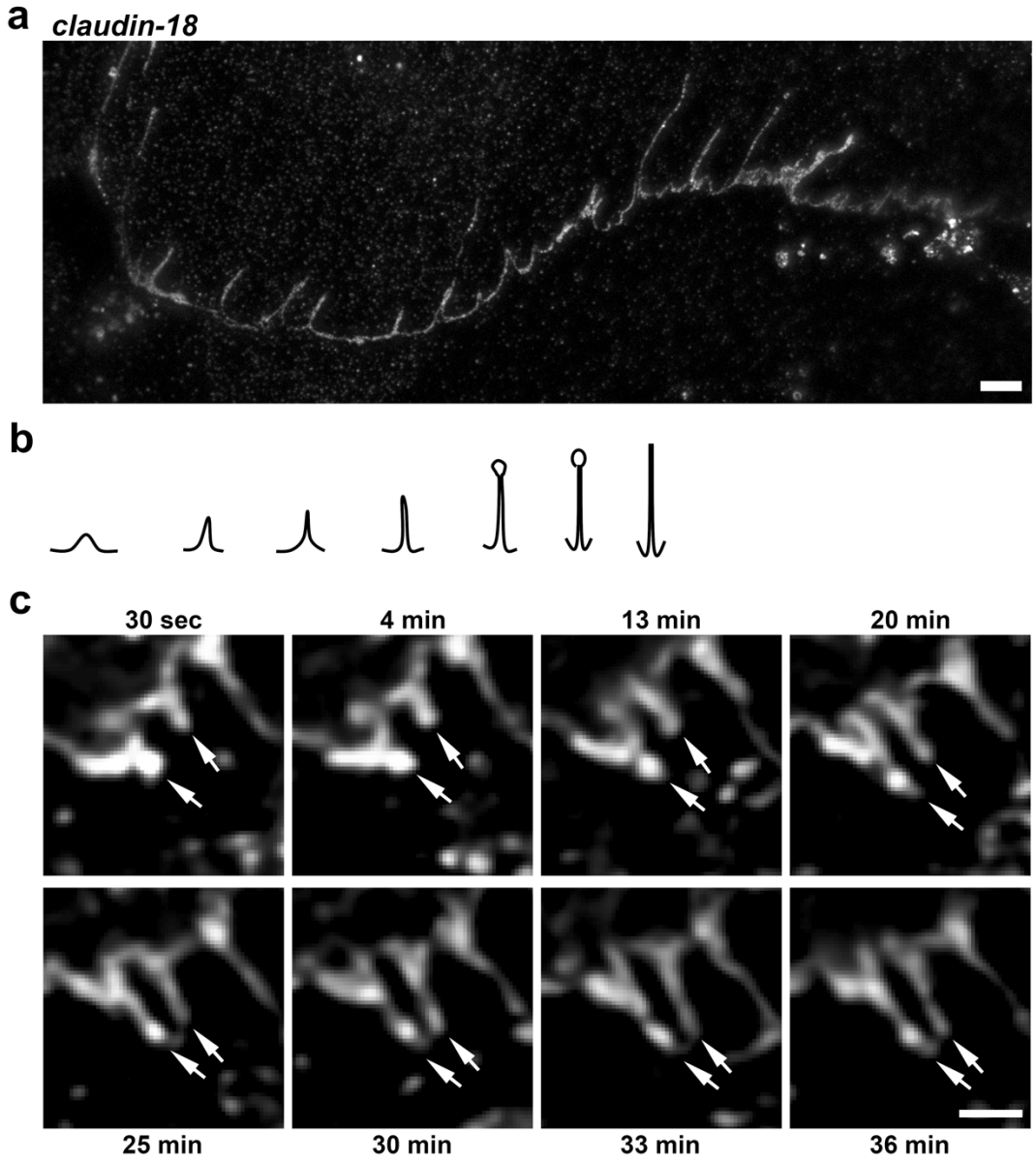

Figure 4.1: Morphological diversity of tight junction spikes. (a) AECs isolated from Sprague-Dawley rats were cultured on collagen-coated coverslips for 6 days. The cells were then fixed, permeabilized, immunolabeled for claudin-18 and analyzed by stimulated emission depletion (STED) super-resolution microscopy, Bar: 2.5 microns. Images are representative of n = 14 fields collected from 3 coverslips from N = 2 biological replicates. (B) Diagram showing different morphological profiles of tight junction spikes observed by immunofluorescence. (c)

Live-cell imaging of AECs expressing EYFP-cldn-18 showing two examples of tight junction spikes increasing in length over a 30 minute period of observation (arrows). Bar: 2.5 microns.

Figure 4.2

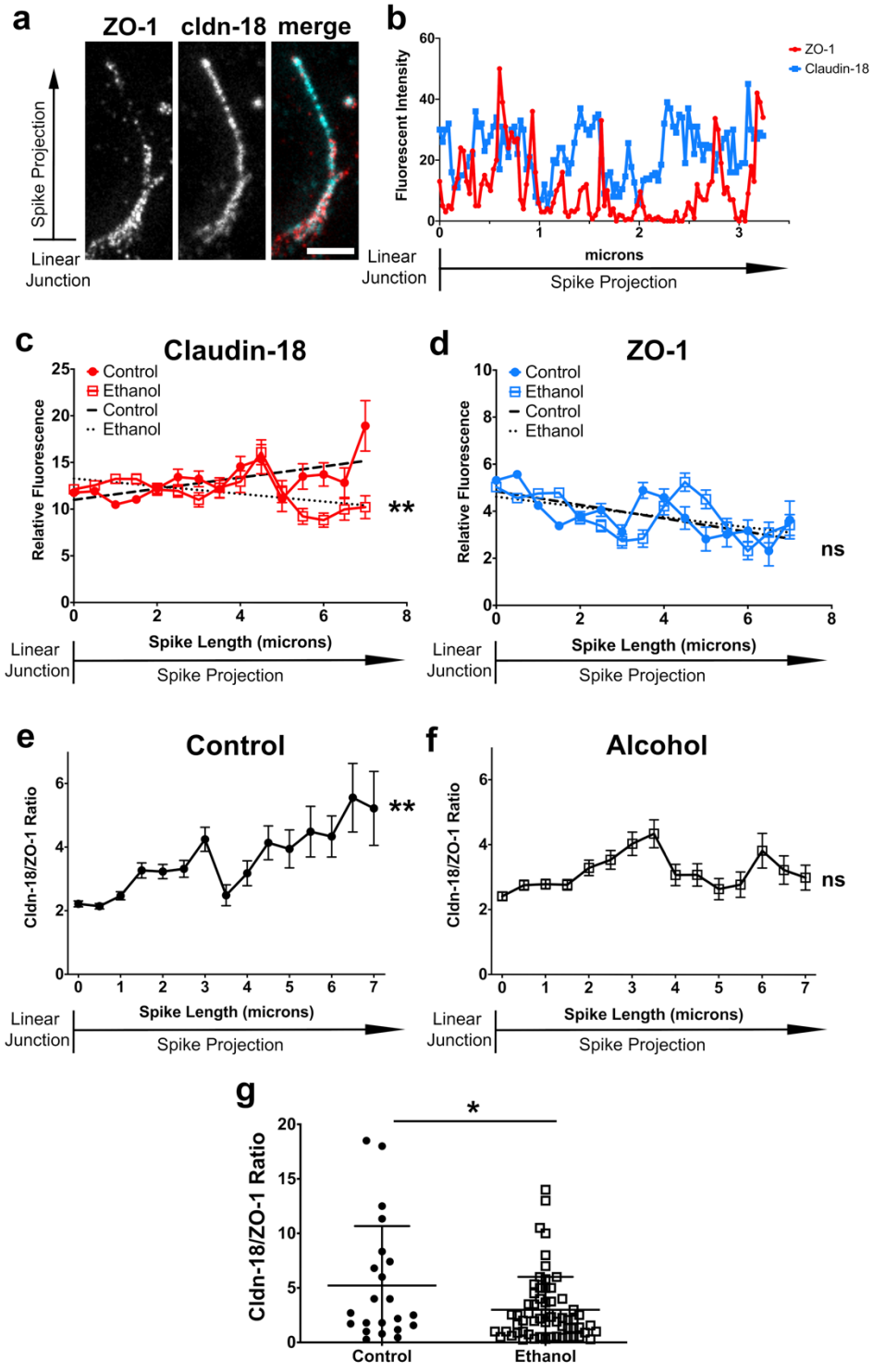

Figure 4.2: Distribution of claudin-18 and ZO-1 differs along length of tight junction spikes. (a) AECs isolated from control and alcohol-fed Sprague-Dawley rats were

cultured on collagen-coated coverslips for 6 days. The cells were then fixed, permeabilized, immunolabeled for ZO-1 (red) and claudin-18 (cyan) and analyzed by stimulated emission depletion (STED) super-resolution microscopy. Shown is an example of an individual tight junction spike. Bar: 1 micron. (b) Line scans of the image in (a) show differential distribution of ZO-1 and claudin-18. (c,d) Aggregate intensity data of claudin-18 (c) and ZO-1 (d) calculated as mean $\pm$ SD from control AECs (2 biological replicates, 84 spikes) and alcohol-exposed AECs (2 biological replicates, 92 spikes). Trend lines show claudin-18 intensity increased with spike projection length for control AECs and decreased for alcohol-exposed AECs (**p=0.0014, simple linear regression with slope comparison), however ZO-1 intensity decreased for both classes of AECs (ns – not significant, simple linear regression with slope comparison). (e,f) The claudin-18/ZO-1 ratio increased for spikes in control AEC (** p=0.0016, one-way ANOVA with Tukey's test of multiple comparisons) but not for alcohol-exposed AECs (ns – not significant). (g) The claudin-18/ZO-1 ratio at 7 microns was higher for spikes from control AECs (n=22) vs alcohol exposed AECs (n=43) (* p=0.021, unpaired two-tailed t-test). Images are representative of n = 178 spikes imaged across 14 fields from 3 coverslips from N = 2 biological replicates.

Figure 4.3

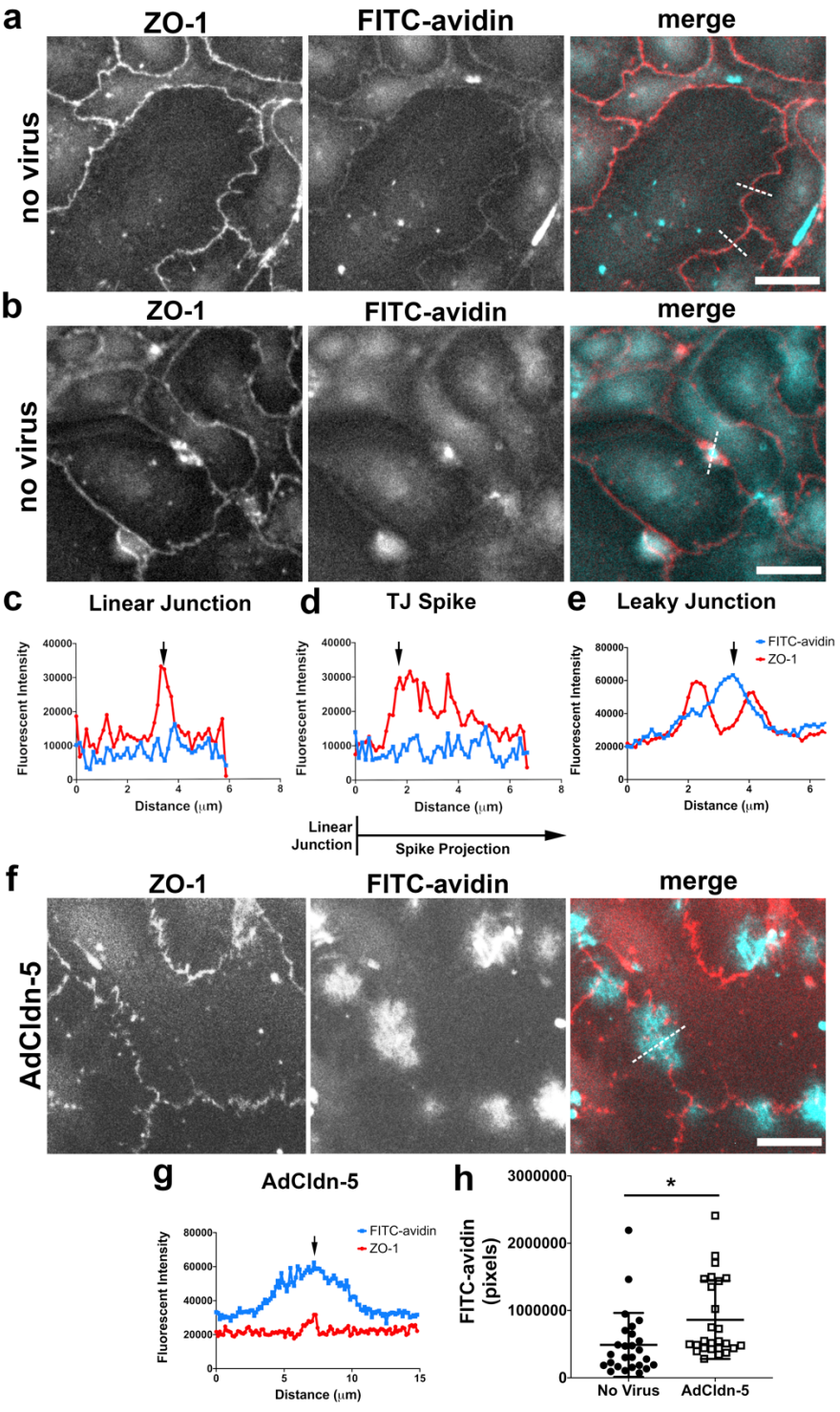

Figure 4.3: Claudin-5 induced paracellular leak is localized. (a-e) AECs isolated from Sprague-Dawley rats were cultured on biotinylated gelatin-coated coverslips for 6 days. The live

cells were then incubated with FITC-avidin (cyan) for 5 minutes, then fixed and immunolabeled for ZO-1 (red). Examples of fields are shown in (a,b). Line scans of representative areas containing a linear tight junction (c), a tight junction spike (d) or a localized area with increased permeability (e) are shown where the blue line represents FITC-avidin and the red line represents ZO-1. Dashed lines in merged images denote where line scans were taken. (f) AECs were cultured on biotinylated gelatin-coated coverslips and transduced at day 2 with claudin-5 (AdCldn-5) at MOI=25 . AECs were further cultured for a total of 6 days before labeling with FITC-avidin and ZO-1, which revealed several areas of enhanced FITC-avidin permeability. A line scan of an area with enhanced permeability is shown in (g). (h) AdCldn-5 transduced cells were significantly more permeable to FITC-avidin as compared with untreated AECs (* p=0.015, unpaired two-tailed t-test). Images are representative of n = 26 control fields and 26 AdCldn-5 fields collected from N = 4 individual coverslips. Bars: 10 microns.

Figure 4.4

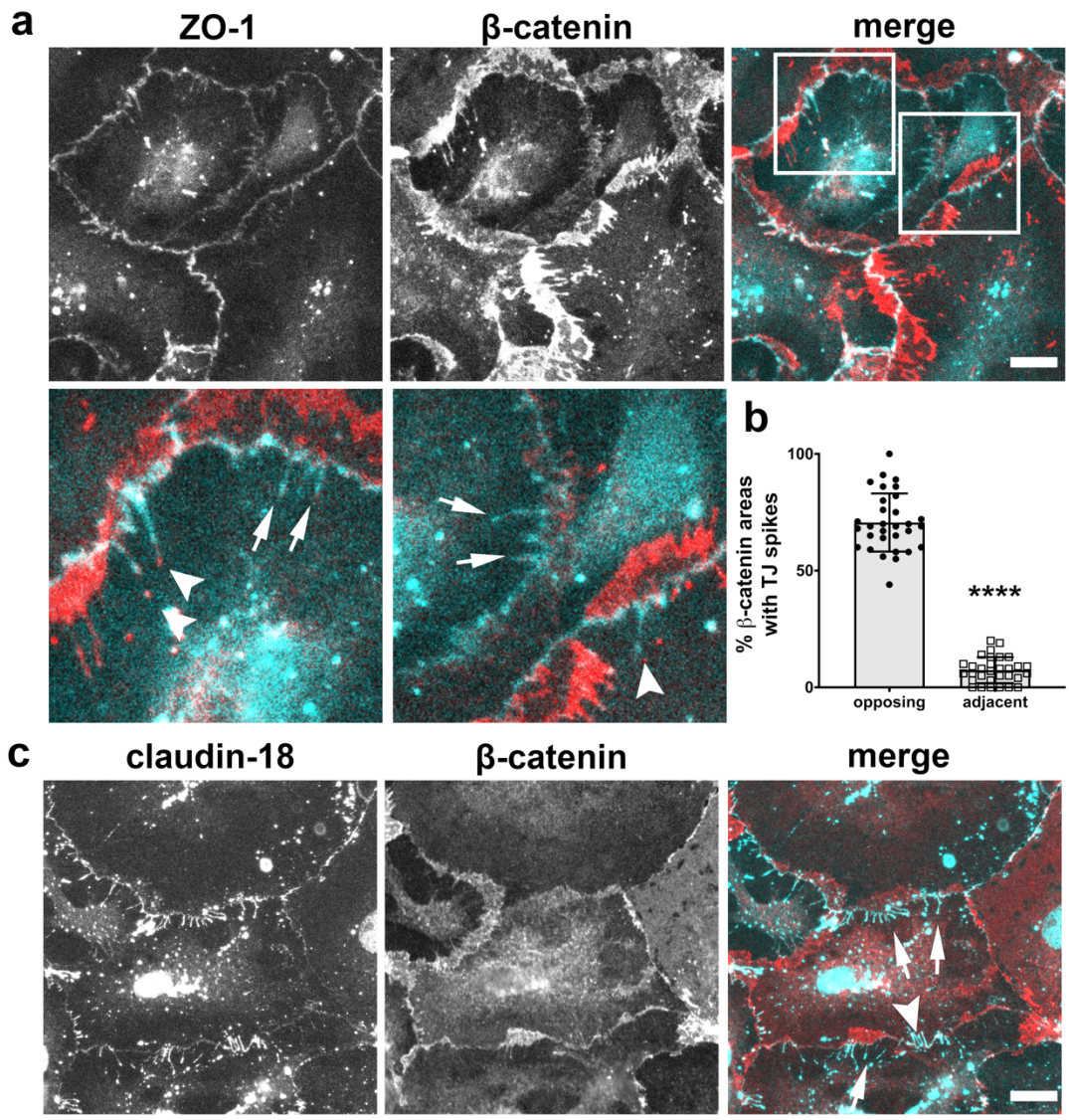

Figure 4.4: Asymmetric localization of β-catenin relative to tight junction spikes. (a) AECs isolated from control Sprague-Dawley rats were cultured on collagen-coated coverslips for 6 days. The cells were then fixed, permeabilized, immunolabeled for β-catenin (red) and ZO-1 (cyan) and imaged by immunofluorescence microscopy. The majority of β-catenin preferentially localized to areas opposed to sites containing tight junction spikes. Squares indicate magnified areas. Most β-catenin localized at the opposing side of tight junction spikes at bicellular junctions (arrows), but some β-catenin localized adjacent to tight junction spikes

(arrowheads). There was occasional β-catenin localized at or near the ends of tight junction spikes, but most spikes did not contain β-catenin. (b) The number of regions containing β-catenin opposed to tight junction spikes was significantly higher than the number of β-catenin regions coincident with tight junction spikes (**** $p < 0.0001$; 5 biological replicates, n=751 regions of interest; unpaired two-tailed t-test, average $\pm$ SD). (c) β-catenin (red) predominantly localized opposite to spike-associated Claudin-18 (cyan) (arrows) and occasionally adjacent to Claudin-18 (arrowheads). Images are representative of four independent experiments. Bars: 10 microns.

Figure 4.5

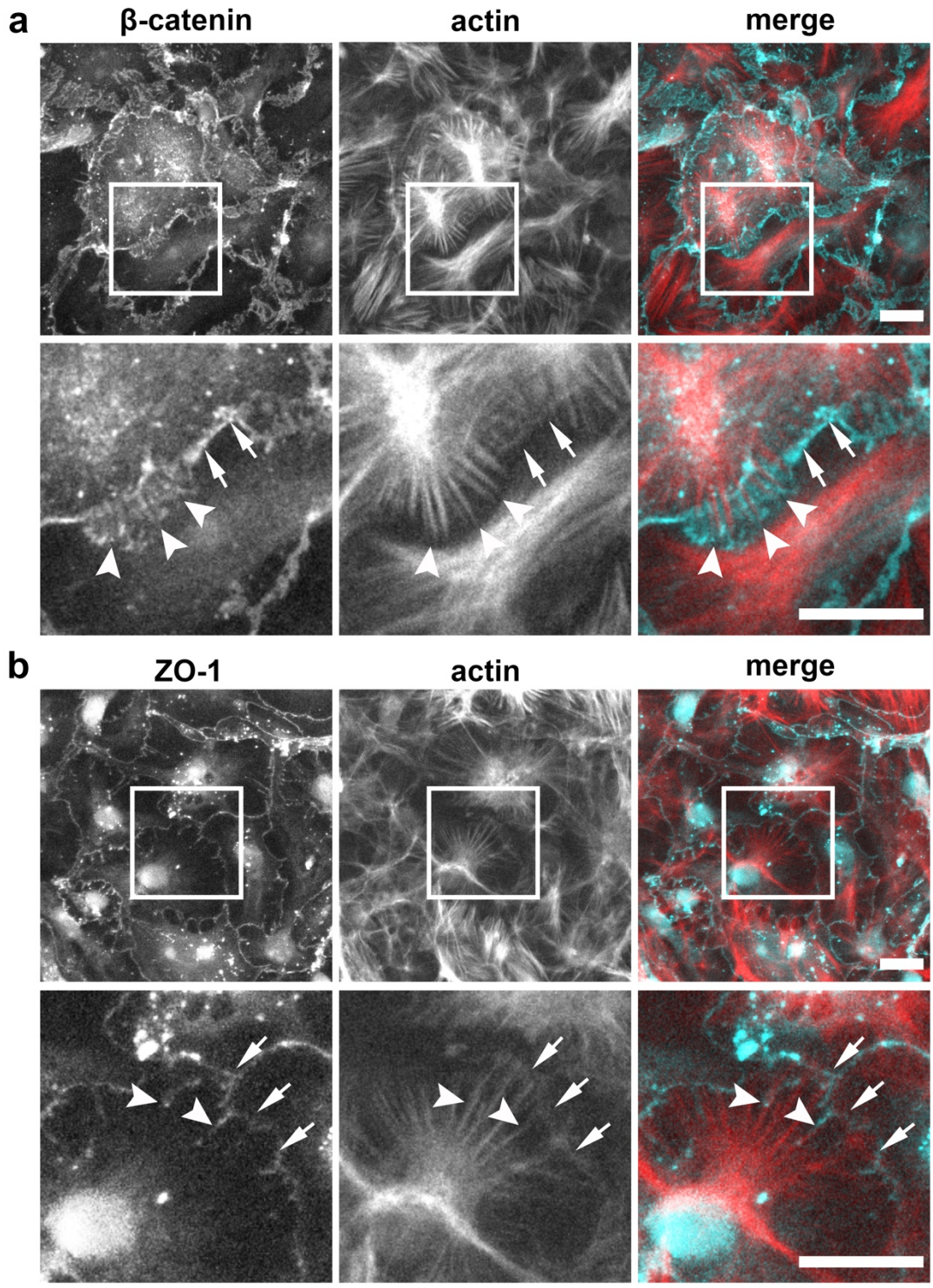

Figure 4.5: Localization of β-catenin and ZO-1 relative to actin stress fibers. (a) AECs isolated from Sprague-Dawley rats were cultured on collagen-coated coverslips for 6 days.

The cells were then fixed, permeabilized, and immunolabeled for β-catenin (cyan) and actin (red). Squares show position of magnified regions below. Arrows indicate β-catenin at intercellular linear junctions. Actin filaments appear to terminate in regions containing high levels of β-catenin (arrowheads). (b) AECs double labeled with ZO-1 (cyan) and actin (red) show tight junction spikes aligning along actin filaments (arrowheads) distinct from ZO-1 at linear intercellular junctions (arrows). Images are representative from three independent experiments. Bars: 10 microns.

Figure 4.6

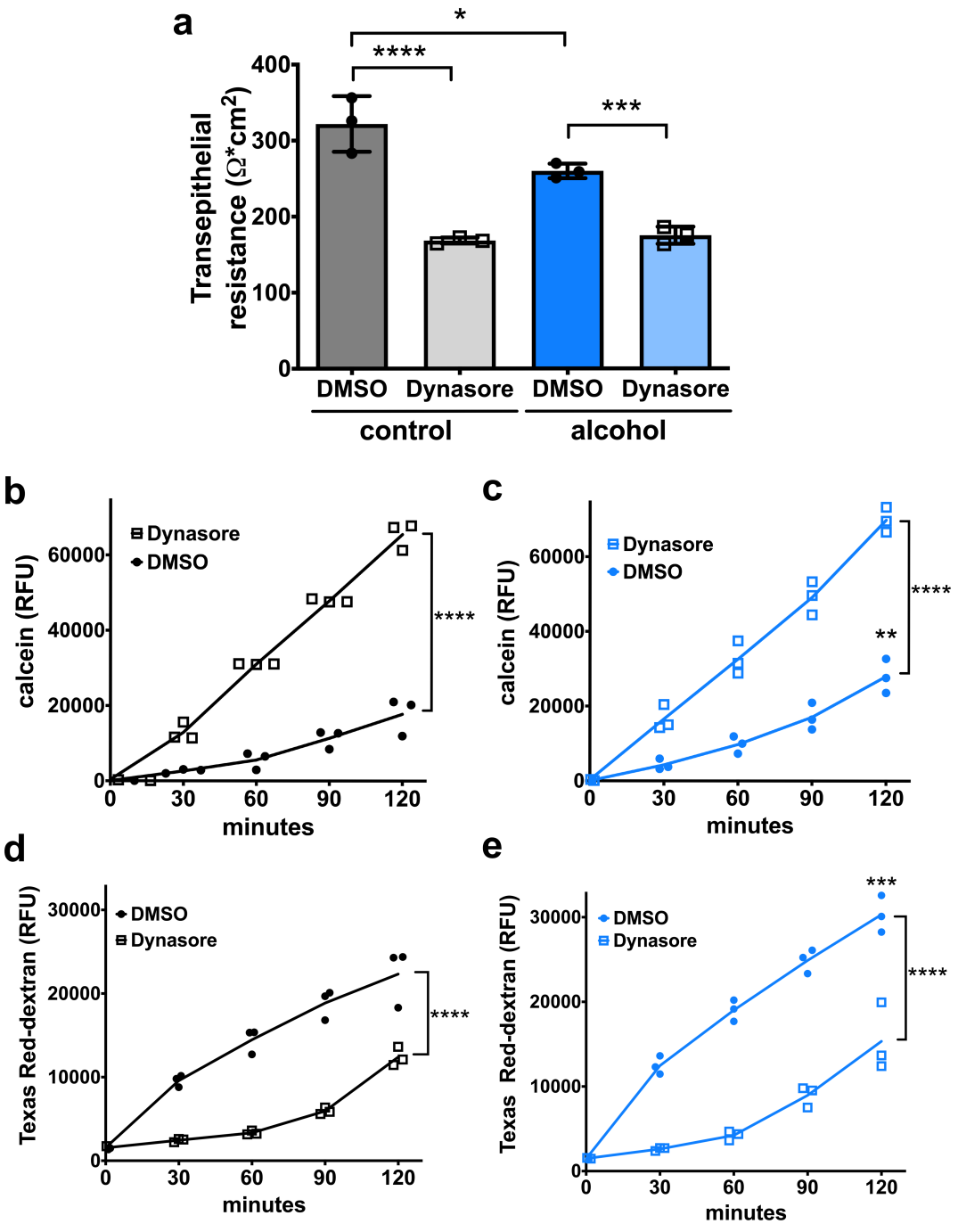

Figure 4.6: **Dynasore alters alveolar epithelial barrier permeability.** AECs isolated from control and alcohol-fed Sprague-Dawley rats were cultured on collagen-coated Transwell permeable supports for 6 days, then treated with dynasore (160 uM) for 4 hours. Barrier

permeability was measured by transepithelial resistance (TER; a) and paracellular flux of calcein (b,c) and 10 kDa Texas Red dextran (d,e). Alcohol-exposed AECs were leakier than control AECs as measured by TER (* p=0.020, n=3), calcein flux (** p=0.0027, n=3) and Texas Red dextran flux (*** p=0.0005, n=3). For both control and alcohol-exposed AECs, Dynasore treatment decreased TER (**** p< 0.0001; *** p=0.0006) and increased calcein flux (**** p < 0.0001). However, paracellular flux of Texas Red dextran was inhibited by Dynasore (**** p<0.0001), suggesting a specific block of macromolecular flux but not small molecule flux.

Figure 4.7

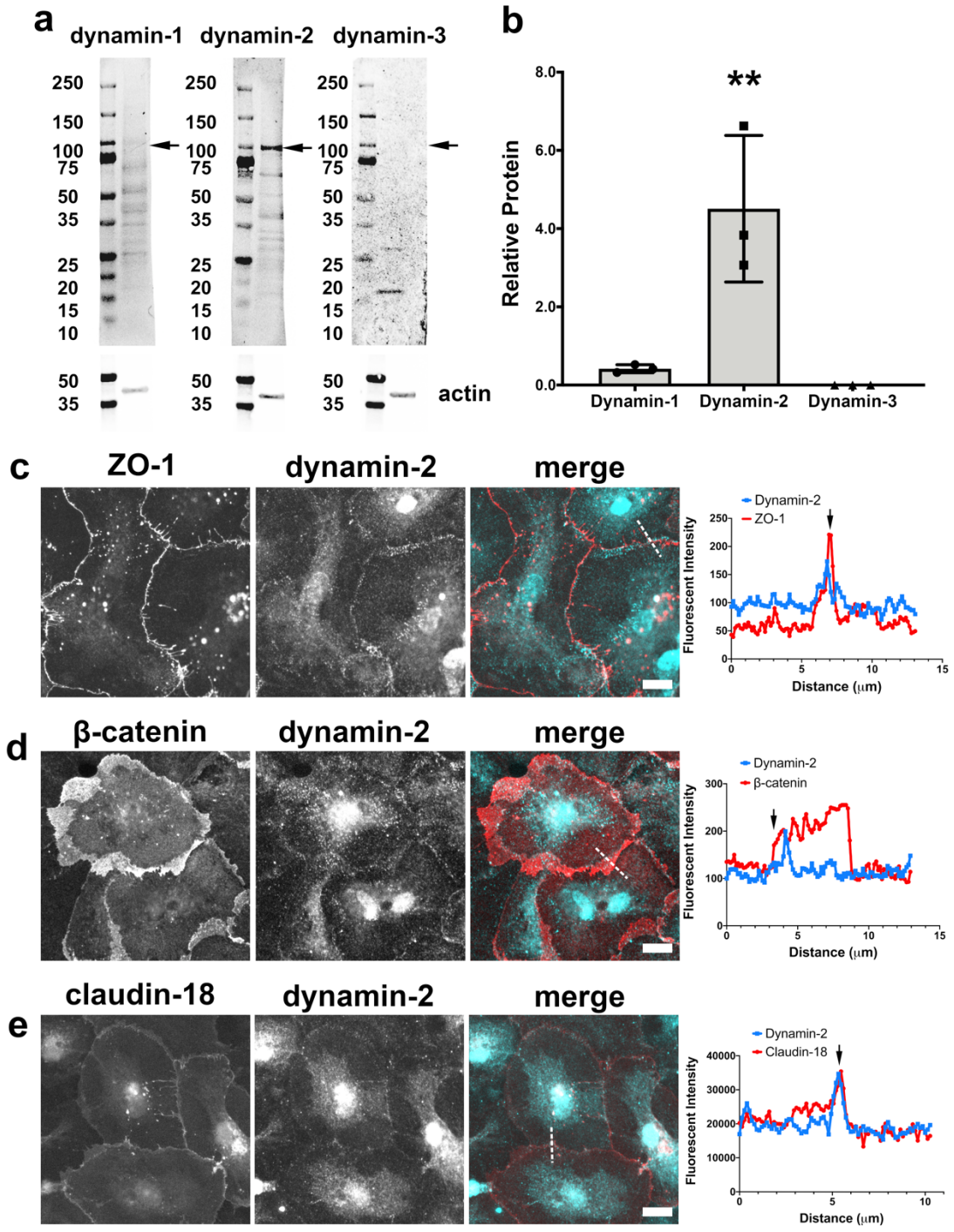

Figure 4.7: Dynamin-2 localizes to tight junctions. (a,b) AECs isolated from Sprague-Dawley rats were cultured on collagen-coated Transwell permeable supports for 6 days and then collected as protein lysates for immunoblot analysis (n = 3 biological replicates). ** p=0.004,

one-way ANOVA with Tukey's test of multiple comparisons, average ± SD. (c,d) AECs on collagen-coated coverslips were fixed and immunolabeled for (c) ZO-1 (red) and dynamin-2 (cyan) or (d) β-catenin (red) and dynamin-2 (cyan). (e) AECs transduced with EYFP-claudin-18 (red) at MOI 25 on day 2 were fixed and immunolabeled for dynamin-2 (cyan). Dashed lines in (c-e) merged images denote where line scans were taken. Dynamin-2 showed sharp localization with tight junctions, (arrows), but only partially localized with β-catenin (d). Images are representative from three independent experiments.

Figure 4.8

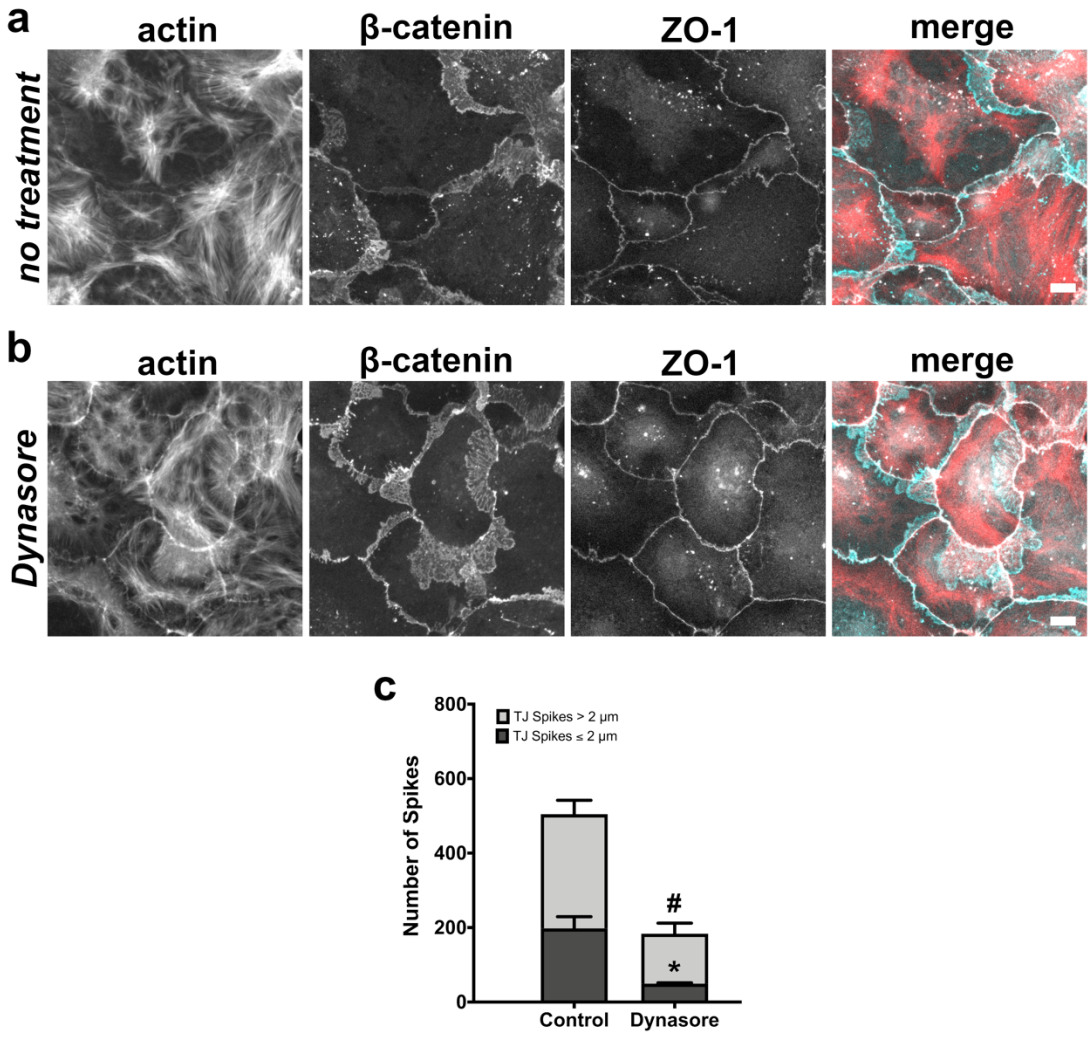

Figure 4.8: Dynasore treatment decreases spike formation and increased cortical actin. AECs isolated from Sprague-Dawley rats were cultured on collagen-coated coverslips for 6 days. The cells were then treated with vehicle control (a) or Dynasore (160 uM) for 4 hours (b), then fixed and triple labeled with AlexaFluor405-phalloidin (actin, red), β-catenin (cyan), and ZO-1 (white). Compared with control AECs (a), Dynasore treated AECs (b) showed enhanced cortical actin as well as increased actin associated with β-catenin. Bar: 10 microns. (c) Dynasore treatment also significantly decreased the number of tight junction spikes as determined by ZO-1 immunofluorescence, comparing control AECs (2 biological replicates, 396 spikes $\leq$ 2 um, 613

spikes > 2 um) and Dynasore treated AECs (2 biological replicates, 99 spikes ≤ 2 um, 268 spikes > 2 um). * $p = 0.021$, # $p = 0.012$, two-way ANOVA with Tukey's test of multiple comparisons, average ± SD. Images are representative of n = 6 fields from two independent experiments.

Figure 4.9

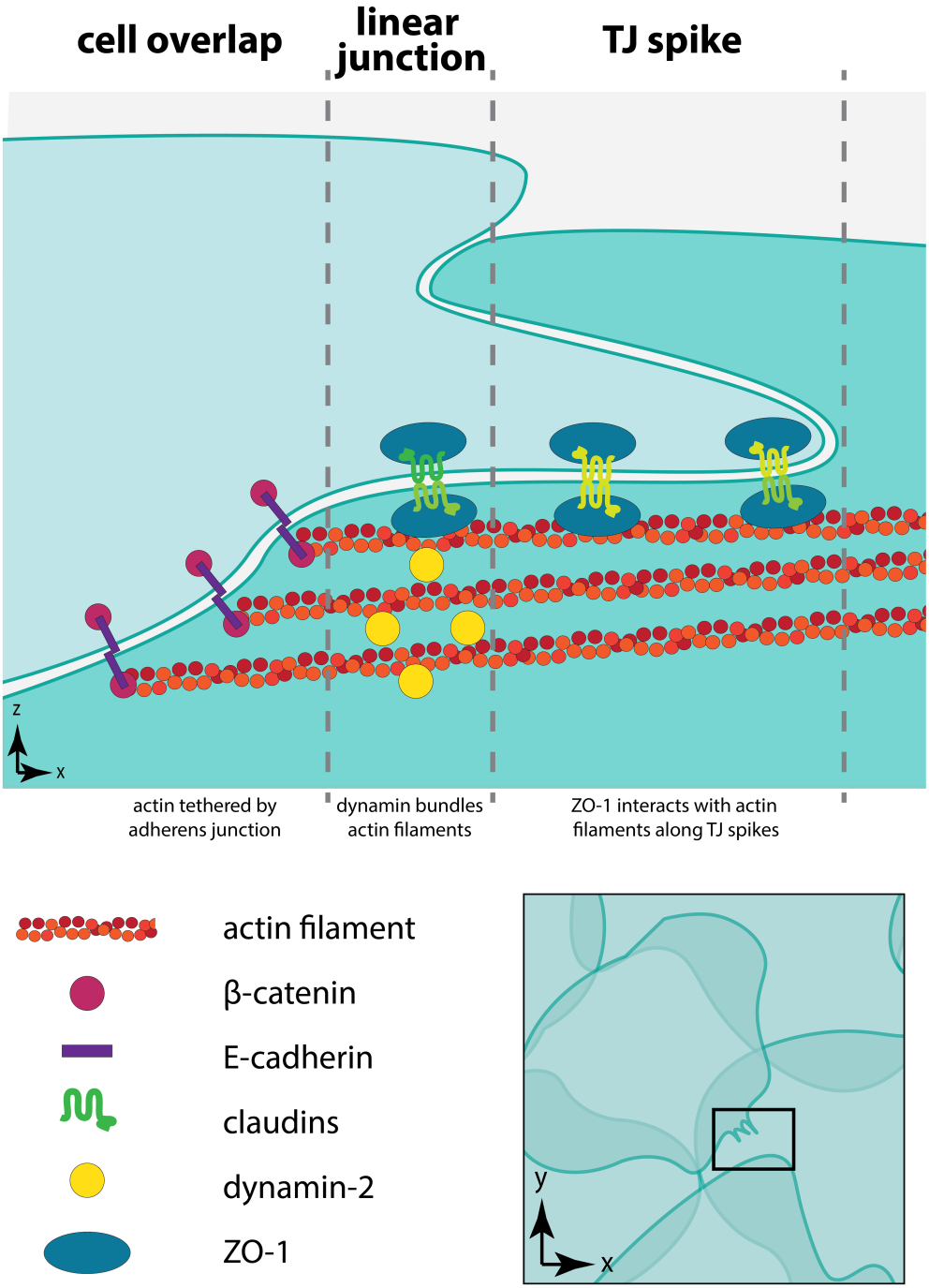

Figure 4.9: Organization of dynamin, actin, and junctions at tight junction spikes. This model represents three regions in squamous rat alveolar epithelial cells present near tight junction spikes. The region of overlap between neighboring cells is depicted with adherens

junctions tethering actin filaments at cell-cell junctions. Dynamin localized to linear tight junctions bundles actin filaments, facilitating interactions with ZO-1 to enable formation of tight junction spikes.

Supplemental Figure 4.1

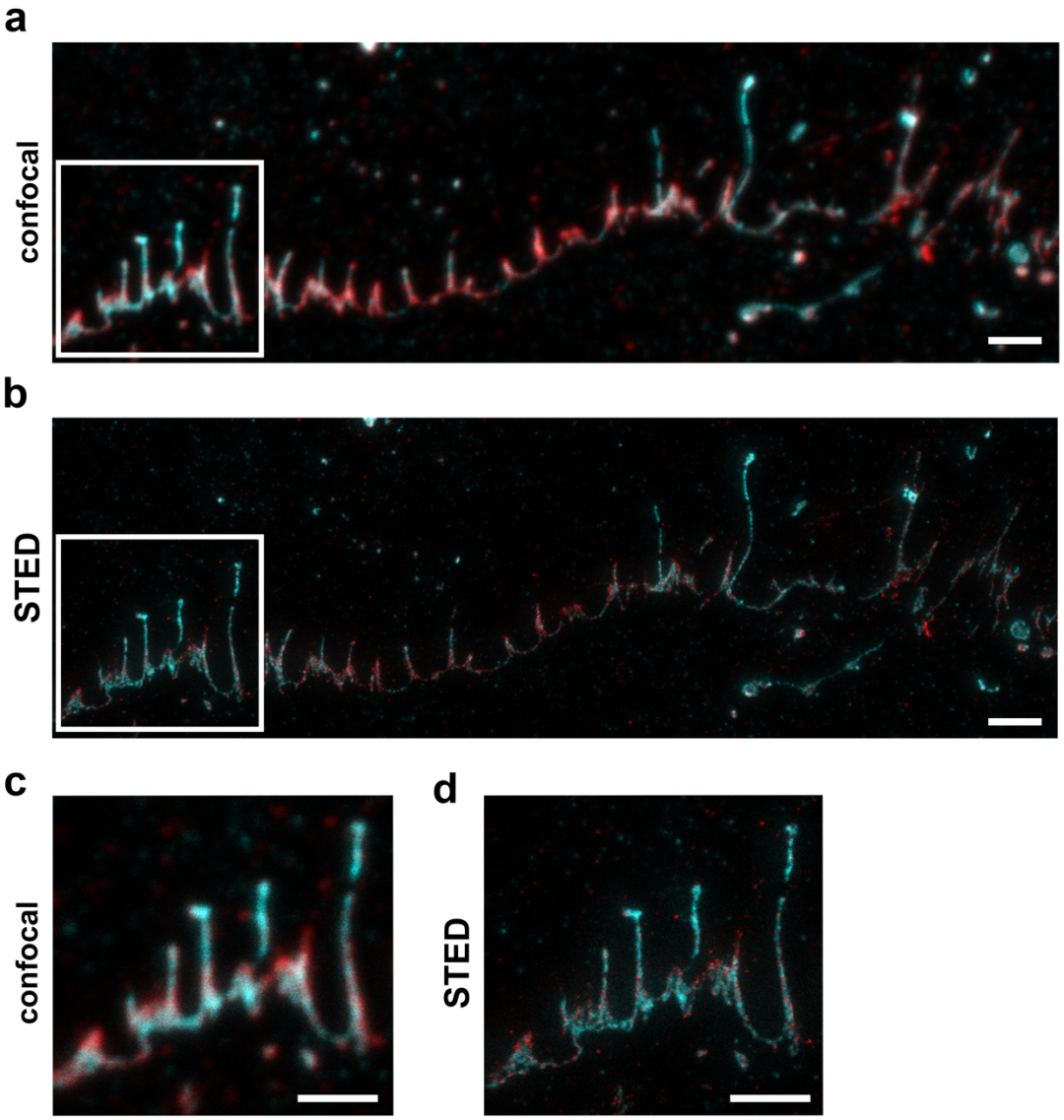

Supplemental Figure 4.1. STED microscopy enhances resolution of tight junction spikes. AECs isolated from Sprague-Dawley rats were cultured on collagen-coated coverslips for 6 days. The AECs were fixed, immunolabeled for claudin-18 (cyan) and ZO-1 (red), then imaged using conventional confocal fluorescence microscopy (a,c) and stimulated emission depletion (STED) super resolution microscopy (b,d). Inset boxes in (a) and (b) correspond to (c) and (d), respectively. Images are representative of n = 6 (control-fed) and 8 (alcohol-fed) fields. Bars: 10 microns.

Supplemental Figure 4.2

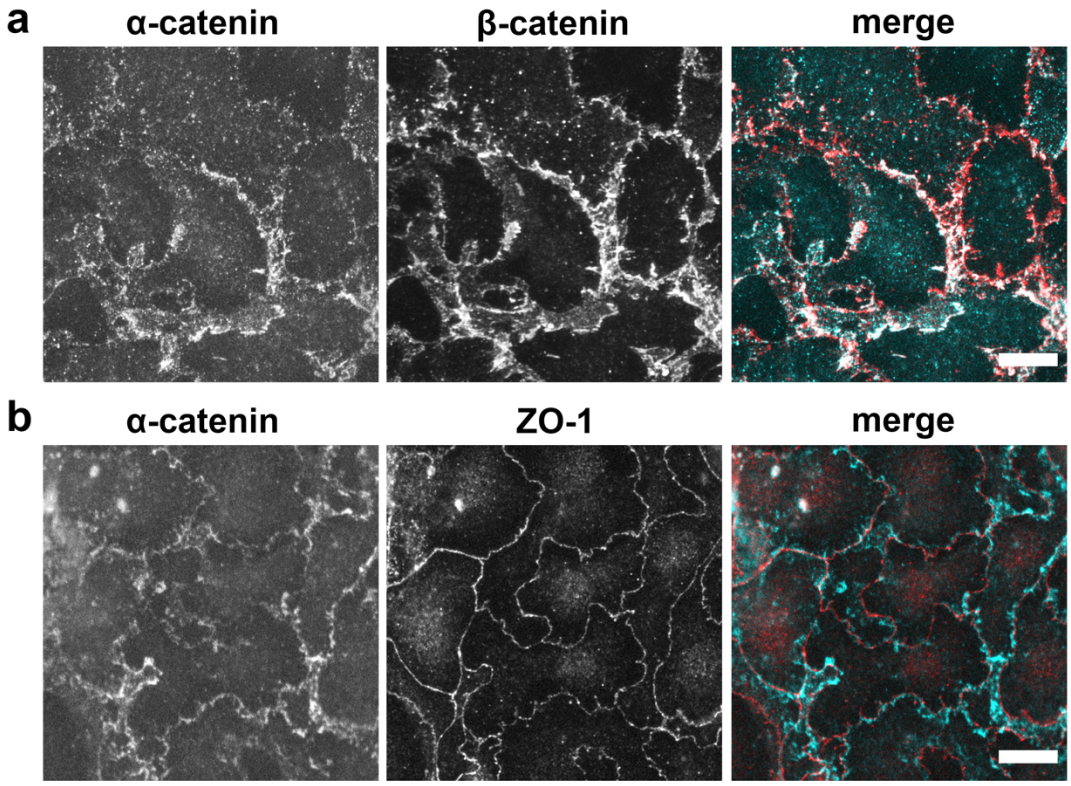

Supplemental Figure 4.2: Colocalization of α-catenin and β-catenin. AECs isolated from Sprague-Dawley rats were cultured on collagen-coated coverslips for 6 days. The cells were then fixed, immunolabeled for α-catenin (cyan) and β-catenin (red) (a) or α-catenin (cyan) and ZO-1 (red). α-catenin and β-catenin showed comparable distribution and co-localization, consistent with their association with adherens junctions. Images are representative from three independent experiments. Images are representative from three independent experiments. Bar: 10 microns.

Literature Cited

1 Matthay MA, Robriquet L, Fang X. Alveolar epithelium: role in lung fluid balance and acute lung injury. Proc Am Thorac Soc 2005;2:206–13. https://doi.org/10.1513/pats.200501-009ac.

2 Guidot DM, Hart C. Alcohol abuse and acute lung injury: epidemiology and pathophysiology of a recently recognized association. J Investig Med 2005;53:235–45. https://doi.org/10.2310/6650.2005.53506.

3 Moss M, Bucher B, Moore F, Moore E, Parsons P. The role of chronic alcohol abuse in the development of acute respiratory distress syndrome in adults. JAMA 1996;275:50–4. https://doi.org/10.1001/jama.1996.03530250054027.

4 Koval M. Claudin heterogeneity and control of lung tight junctions. Annu Rev Physiol 2013;75:551–67. https://doi.org/10.1146/annurev-physiol-030212-183809.

5 Li G, Flodby P, Luo J, Kage H, Sipos A, Gao D, et al. Knockout mice reveal key roles for claudin 18 in alveolar barrier properties and fluid homeostasis. Am J Resp Cell Mol 2014;51:210–22. https://doi.org/10.1165/rcmb.2013-0353oc.

6 Schlingmann B, Molina SA, Koval M. Claudins: Gatekeepers of lung epithelial function. Semin Cell Dev Biol 2015;42:47–57. https://doi.org/10.1016/j.semcdb.2015.04.009.

7 Lynn KS, Peterson RJ, Koval M. Ruffles and spikes: Control of tight junction morphology and permeability by claudins. Biochim Biophys Acta Biomembr 2020;1862:183339. https://doi.org/10.1016/j.bbamem.2020.183339.

8 Schlingmann B, Overgaard CE, Molina SA, Lynn KS, Mitchell LA, White SD, et al. Regulation of claudin/zonula occludens-1 complexes by hetero-claudin interactions. Nat Commun 2016;7:12276. https://doi.org/10.1038/ncomms12276.

9 Ikehata M, Yumoto R, Kato Y, Nagai J, Takano M. Mechanism of insulin uptake in rat alveolar type II and type I-like epithelial cells. Biol Pharm Bull 2009;32:1765–9. https://doi.org/10.1248/bpb.32.1765.

10 Fazlollahi F, Sipos A, Kim YH, Hamm-Alvarez SF, Borok Z, Kim K-JJ, et al. Translocation of PEGylated quantum dots across rat alveolar epithelial cell monolayers. Int J Nanomedicine 2011;6:2849–57. https://doi.org/10.2147/IJN.S26051.

11 Mears JA, Ray P, Hinshaw JE. A Corkscrew Model for Dynamin Constriction. Structure 2007;15:1190–202. https://doi.org/10.1016/j.str.2007.08.012.

12 Hinshaw JE. Dynamin and its role in membrane fission1. Cell Dev Biology 2000;16:483–519. https://doi.org/10.1146/annurev.cellbio.16.1.483.

13 Sauvonnet N, Dujeancourt A, Dautry-Varsat A. Cortactin and dynamin are required for the clathrin-independent endocytosis of γc cytokine receptor. J Cell Biol 2005;168:155–63. https://doi.org/10.1083/jcb.200406174.

14 Mooren OL, Kotova TI, Moore AJ, Schafer DA. Dynamin2 GTPase and Cortactin Remodel Actin Filaments. J Biol Chem 2009;284:23995–4005. https://doi.org/10.1074/jbc.m109.024398.

15 Chua J, Rikhy R, Lippincott-Schwartz J. Dynamin 2 orchestrates the global actomyosin cytoskeleton for epithelial maintenance and apical constriction. Proc National Acad Sci 2009;106:20770–5. https://doi.org/10.1073/pnas.0909812106.

16 Dobbs LG, Gonzalez R, Williams MC. An Improved Method for Isolating Type II Cells in High Yield and Purity1–3. Am Rev Respir Dis 2015;134:141–5. https://doi.org/10.1164/arrd.1986.134.1.141.

17 Dubrovskyi O, Birukova AA, Birukov KG. Measurement of local permeability at subcellular level in cell models of agonist- and ventilator-induced lung injury. Lab Invest 2013;93:254–63. https://doi.org/10.1038/labinvest.2012.159.

18 Schindelin J, Arganda-Carreras I, Frise E, Kaynig V, Longair M, Pietzsch T, et al. Fiji: an open-source platform for biological-image analysis. Nat Methods 2012;9:676–82. https://doi.org/10.1038/nmeth.2019.

19 Ward C, Schlingmann B, Stecenko AA, Guidot DM, Koval M. NF-κB inhibitors impair lung epithelial tight junctions in the absence of inflammation. Tissue Barriers 2015;3:e982424. https://doi.org/10.4161/21688370.2014.982424.

20 Overgaard CE, Schlingmann B, White SD, Ward C, Fan X, Swarnakar S, et al. The relative balance of GM-CSF and TGF-β1 regulates lung epithelial barrier function. Am J Physiol Lung Cell Mol Physiol 2015;308:L1212-23. https://doi.org/10.1152/ajplung.00042.2014.

21 Capaldo CT, Macara IG. Depletion of E-Cadherin Disrupts Establishment but Not Maintenance of Cell Junctions in Madin-Darby Canine Kidney Epithelial Cells. Mol Biol Cell 2007;18:189–200. https://doi.org/10.1091/mbc.e06-05-0471.

22 Rajasekaran AK, Hojo M, Huima T, Rodriguez-Boulan E. Catenins and zonula occludens-1 form a complex during early stages in the assembly of tight junctions. J Cell Biol 1996;132:451–63. https://doi.org/10.1083/jcb.132.3.451.

23 Liu Y, Nusrat A, Schnell FJ, Reaves TA, Walsh S, Pochet M, et al. Human junction adhesion molecule regulates tight junction resealing in epithelia. J Cell Sci 2000;113 (Pt 13):2363–74.

24 Schneeberger EE, Lynch RD. The tight junction: a multifunctional complex. Am J Physiol Cell Physiol 2004;286:C1213-28. https://doi.org/10.1152/ajpcell.00558.2003.

25 Quiros M, Nusrat A. RhoGTPases, actomyosin signaling and regulation of the epithelial Apical Junctional Complex. Semin Cell Dev Biol 2014;36:194–203. https://doi.org/10.1016/j.semcdb.2014.09.003.

26 Hartsock A, Nelson WJ. Adherens and tight junctions: Structure, function and connections to the actin cytoskeleton. Biochim Biophys Acta Biomembr 2008;1778:660–9. https://doi.org/10.1016/j.bbamem.2007.07.012.

27 Fanning AS, Jameson BJ, Jesaitis LA, Anderson JM. The Tight Junction Protein ZO-1 Establishes a Link between the Transmembrane Protein Occludin and the Actin Cytoskeleton. J Biol Chem 1998;273:29745–53. https://doi.org/10.1074/jbc.273.45.29745.

28 Buckley CD, Tan J, Anderson KL, Hanein D, Volkmann N, Weis WI, et al. The minimal cadherin-catenin complex binds to actin filaments under force. Science 2014;346:1254211–1254211. https://doi.org/10.1126/science.1254211.

29 Desai R, Sarpal R, Ishiyama N, Pellikka M, Ikura M, Tepass U. Monomeric α-catenin links cadherin to the actin cytoskeleton. Nat Cell Biol 2013;15:261–73. https://doi.org/10.1038/ncb2685.

30 Guidot DM, Modelska K, Lois M, Jain L, Moss IM, Pittet J-F, et al. Ethanol ingestion via glutathione depletion impairs alveolar epithelial barrier function in rats. Am J Physiol Lung Cell Mol Physiol 2000;279:L127–35. https://doi.org/10.1152/ajplung.2000.279.1.l127.

31 Abe T, La TM, Miyagaki Y, Oya E, Wei F-Y, Sumida K, et al. Phosphorylation of cortactin by cyclin-dependent kinase 5 modulates actin bundling by the dynamin 1-cortactin ring-like complex and formation of filopodia and lamellipodia in NG108-15 glioma-derived cells. Int J Oncol 2018;54:550–8. https://doi.org/10.3892/ijo.2018.4663.

32 Zhang R, Lee DM, Jimah JR, Gerassimov N, Yang C, Kim S, et al. Dynamin regulates the dynamics and mechanical strength of the actin cytoskeleton as a multifilament actin-bundling protein. Nat Cell Biol 2020;22:674–88. https://doi.org/10.1038/s41556-020-0519-7.

33 Kusumi N, Watanabe M, Yamada H, Li S-A, Kashiwakura Y, Matsukawa T, et al. Implication of Amphiphysin 1 and Dynamin 2 in Tubulobulbar Complex Formation and Spermatid Release. Cell Struct Funct 2007;32:101–13. https://doi.org/10.1247/csf.07024.

34 Nitta T, Hata M, Gotoh S, Seo Y, Sasaki H, Hashimoto N, et al. Size-selective loosening of the blood-brain barrier in claudin-5-deficient mice. J Cell Biol 2003;161:653–60. https://doi.org/10.1083/jcb.200302070.

35 Sonoda N, Furuse M, Sasaki H, Yonemura S, Katahira J, Horiguchi Y, et al. Clostridium perfringens Enterotoxin Fragment Removes Specific Claudins from Tight Junction Strands:

Evidence for Direct Involvement of Claudins in Tight Junction Barrier. J Cell Biol 1999;147:195–204. https://doi.org/10.1083/jcb.147.1.195.

36 Park RJ, Shen H, Liu L, Liu X, Ferguson SM, Camilli PD. Dynamin triple knockout cells reveal off target effects of commonly used dynamin inhibitors. J Cell Sci 2013;126:5305–12. https://doi.org/10.1242/jcs.138578.

37 Cao H, Garcia F, McNiven MA. Differential Distribution of Dynamin Isoforms in Mammalian Cells. Mol Biol Cell 1998;9:2595–609. https://doi.org/10.1091/mbc.9.9.2595.

38 Farquhar MG, Palade GE. Junctional complexes in various epithelia. J Cell Biol 1963;17:375–412. https://doi.org/10.1083/jcb.17.2.375.

39 LaFemina MJ, Sutherland KM, Bentley T, Gonzales LW, Allen L, Chapin CJ, et al. Claudin-18 deficiency results in alveolar barrier dysfunction and impaired alveologenesis in mice. Am J Resp Cell Mol 2014;51:550–8. https://doi.org/10.1165/rcmb.2013-0456OC.

40 Turner JR, Rill BK, Carlson SL, Carnes D, Kerner R, Mrsny RJ, et al. Physiological regulation of epithelial tight junctions is associated with myosin light-chain phosphorylation. Am J Physiol Cell Physiol 1997;273:C1378–85. https://doi.org/10.1152/ajpcell.1997.273.4.c1378.

41 Yuhan R, Koutsouris A, Savkovic S, Hecht G. Enteropathogenic Escherichia coli-induced myosin light chain phosphorylation alters intestinal epithelial permeability. Gastroenterology 1997;113:1873–82. https://doi.org/10.1016/s0016-5085(97)70006-4.

42 Odenwald MA, Choi W, Kuo W-TT, Singh G, Sailer A, Wang Y, et al. The scaffolding protein ZO-1 coordinates actomyosin and epithelial apical specializations in vitro and in vivo. J Biol Chem 2018;293:17317–35. https://doi.org/10.1074/jbc.RA118.003908.

43 Gehne N, Lamik A, Lehmann M, Haseloff RF, Andjelkovic AV, Blasig IE. Cross-over endocytosis of claudins is mediated by interactions via their extracellular loops. PLoS One 2017;12:e0182106. https://doi.org/10.1371/journal.pone.0182106.

44 Fletcher SJ, Poulter NS, Haining EJ, Rappoport JZ. Clathrin-mediated endocytosis regulates occludin, and not focal adhesion, distribution during epithelial wound healing. Biol Cell 2012;104:238–56. https://doi.org/10.1111/boc.201100004.

45 Antonny B, Burd C, Camilli PD, Chen E, Daumke O, Faelber K, et al. Membrane fission by dynamin: what we know and what we need to know. EMBO J 2016;35:2270–84. https://doi.org/10.15252/embj.201694613.

46 Simunovic M, Manneville J-B, Renard H-F, Evergren E, Raghunathan K, Bhatia D, et al. Friction Mediates Scission of Tubular Membranes Scaffolded by BAR Proteins. Cell 2017;170:172-184.e11. https://doi.org/10.1016/j.cell.2017.05.047.

47 Preta G, Cronin JG, Sheldon IM. Dynasore - not just a dynamin inhibitor. Cell Commun Signal 2015;13:24. https://doi.org/10.1186/s12964-015-0102-1.

48 Turner JR. 'Putting the squeeze' on the tight junction: understanding cytoskeletal regulation. Semin Cell Dev Biol 2000;11:301–8. https://doi.org/10.1006/scdb.2000.0180.

49 Madara JL, Moore R, Carlson S. Alteration of intestinal tight junction structure and permeability by cytoskeletal contraction. Am J Physiol Cell Physiol 1987;253:C854–61. https://doi.org/10.1152/ajpcell.1987.253.6.c854.

50 Ma TY, Hollander D, Tran LT, Nguyen D, Hoa N, Bhalla D. Cytoskeletal regulation of Caco-2 intestinal monolayer paracellular permeability. J Cell Physiol 1995;164:533–45. https://doi.org/10.1002/jcp.1041640311.

51 Dorland YL, Malinova TS, Stalborch A-MDM van, Grieve AG, Geemen D van, Jansen NS, et al. The F-BAR protein pacsin2 inhibits asymmetric VE-cadherin internalization from tensile adherens junctions. Nat Commun 2016;7:12210. https://doi.org/10.1038/ncomms12210.

52 Cavanaugh KJ, Oswari J, Margulies SS. Role of Stretch on Tight Junction Structure in Alveolar Epithelial Cells. Am J Resp Cell Mol 2001;25:584–91. https://doi.org/10.1165/ajrcmb.25.5.4486.

53 Stahley SN, Saito M, Faundez V, Koval M, Mattheyses AL, Kowalczyk AP. Desmosome assembly and disassembly are membrane raft-dependent. PLoS One 2014;9:e87809. https://doi.org/10.1371/journal.pone.0087809.

54 Sucre JMS, Deutsch GH, Jetter CS, Ambalavanan N, Benjamin JT, Gleaves LA, et al. A Shared Pattern of β-Catenin Activation in Bronchopulmonary Dysplasia and Idiopathic Pulmonary Fibrosis. Am J Pathol 2018;188:853–62. https://doi.org/10.1016/j.ajpath.2017.12.004.

55 Sucre JMS, Vickers KC, Benjamin JT, Plosa EJ, Jetter CS, Cutrone A, et al. Hyperoxia Injury in the Developing Lung is Mediated by Mesenchymal Expression of Wnt5A. Am J Respir Crit Care Med 2019;0:1249–62. https://doi.org/10.1164/rccm.201908-1513oc.

56 Sucre JMS, Vijayaraj P, Aros CJ, Wilkinson D, Paul M, Dunn B, et al. Posttranslational modification of β-catenin is associated with pathogenic fibroblastic changes in bronchopulmonary dysplasia. Am J Physiol Lung Cell Mol Physiol 2017;312:L186–95. https://doi.org/10.1152/ajplung.00477.2016.

57 Aberle H, Bauer A, Stappert J, Kispert A, Kemler R. β-catenin is a target for the ubiquitin–proteasome pathway. EMBO J 1997;16:3797–804. https://doi.org/10.1093/emboj/16.13.3797.

58 Ladoux B, Nelson WJ, Yan J, Mège RM. The mechanotransduction machinery at work at adherens junctions. Integr Biol (Camb) 2015;7:1109–19. https://doi.org/10.1039/c5ib00070j.

59 Huveneers S, Rooij J de. Mechanosensitive systems at the cadherin-F-actin interface. J Cell Sci 2013;126:403–13. https://doi.org/10.1242/jcs.109447.

60 Nishida K, Brune KA, Putcha N, Mandke P, O'Neal WK, Shade D, et al. Cigarette smoke disrupts monolayer integrity by altering epithelial cell-cell adhesion and cortical tension. Am J Physiol Lung Cell Mol Physiol 2017;313:L581–91. https://doi.org/10.1152/ajplung.00074.2017.

CHAPTER 5: IDENTIFICATION OF THE CLAUDIN-18 PROXIMAL PROTEOME USING AN N-TERMINAL BIOTIN LIGASE

K. Sabrina Lynn, Barbara Schlingmann, Michael Koval

This work is in the preliminary phase of data analysis has not been published.

Introduction

Tight junctions are protein complexes that form at contact sites between cells to regulate the paracellular flow of small molecules, water, and ions between adjacent cells.[1] They are composed of distinct protein components that contribute to barrier function, including claudin family transmembrane proteins and scaffolding proteins like Zonula Occludens (i.e. ZO-1, ZO-2) that link claudins to the actin cytoskeleton to promote barrier function.[2] Though it is well established that changes in the expression and composition of tight junction proteins can drastically affect barrier function, the molecular mechanisms that control tight junction regulation and assembly require further characterization.

A unique spike-like morphology has been observed in tight junction spikes of primary rat alveolar epithelial and associated with increased barrier permeability. We have previously demonstrated that increased tight junction spike (TJ spike) formation correlated with changes in interacting partners of claudin-18.[3] Specifically, this was demonstrated by an increase in claudin-18/claudin-5 colocalization and decrease in claudin-18/ZO-1 colocalization at 20 nm resolution. The decrease in claudin-18/ZO-1 colocalization associated with a change in barrier function suggests that changes in claudin-18 interacting proteins promote TJ spike formation. However, isolating membrane-associated tight junction proteins biochemically is difficult different tight junction proteins are differentially sensitive to detergent solubilization. Also, biochemical isolation techniques disrupt the native microenvironment of tight junctions. Thus,

methods to identify novel spike-associated claudin-18 protein interactors are necessary to elucidate the molecular mechanisms behind TJ spike formation.

The tight junction proteome is known to contain cytoskeleton, polarity, and signaling proteins but the breadth of interacting partners has not been fully elucidated. Recent employment of the BioID method has proven successful in identifying interacting partners of several tight junction proteins, including ZO-1, occludin, and claudin-4 as well as the adherens junction protein E-cadherin.[4–6] BioID utilizes a promiscuous biotinylating enzyme BirA identified in Escherichia coli that has the capacity to biotinylate proximal and interacting proteins within a 20 to 30 nm radius.[7] BioID analysis of claudin-4 and occludin revealed interactions with other expected tight junction proteins, but also identified proteins associated with signaling and endocytic trafficking, with claudin-4 and occludin interacting with distinct proteins within these categories.

Remarkably, BioID of the proteome of comparing BirA linked to either the N- and C-terminus of ZO-1 revealed distinct differences in protein interactions, with the N-terminus favoring interactions with tight junction proteins and the C-terminus favoring interactions with the cytoskeleton.[4] In each case, BioID revealed hundreds of biotinylated proteins including both known and previously unknown protein interactions. This indicates that the tight junction proteome is vast and BioID could provide insight into the molecular machinery at tight junctions responsible in TJ spike formation. Here, we used a BirA-claudin-18 chimera to investigate the proximal claudin-18 proteome in primary rat alveolar epithelial cells (AECs).

Materials and Methods

Adenovirus production and infection

Adenovirus particles were packaged and amplified by ViraQuest Inc. and Vector Builder. AECs were transduced with adenovector encoding a NH2-terminal enhanced YFP-claudin-18 or NH2-terminal BirA-claudin-18 on day 4 or 5 after isolation. Adenovector was added to media at

the stated multiplicity of infection (MOI) before dispensing on cells. Cells were analyzed 48 h after virus addition unless otherwise stated.

Primary Alveolar Epithelial Cell Isolation

All animal protocols were reviewed and approved by the Institutional Animal Care and Use Committee of Emory University and performed with the approval of the Division of Animal Resources. Adult male Sprague-Dawley rats (150-200g, Charles River Laboratory) were used as a source of primary alveolar epithelial cells. In most cases, rats were given standard chow and water ad libitum. For experiments using the chronic alcohol rat model, Sprague-Dawley rats (50-100g, Charles River Laboratory) were pair-fed an ethanol or control isocaloric maltose-dextrin Lieber-DeCarli liquid diet (Research Diets) ad libitum for 6-8 weeks prior to cell isolation.[3]

Type II AECs were isolated from rats according to Dobbs with modifications.[8] Lungs were perfused with PBS with calcium and magnesium, then removed and lavaged with solution II (5.5 mM Dextrose, 10 mM HEPES, 2 mM CaCl2, 1.3 mM MgSO4, 140 mM NaCl, 5 mM KCl, pH 7.4). Elastase (1.6 units/ml, Worthington, Cat# LS002292) was instilled and continually circulated in lavaged lungs while incubating in a 37°C water bath for 30-45 min. The lungs were then manually dissected into 1 mm3 pieces, taking care to remove the trachea and bronchial tissue. Diced lungs were resuspended in 5 mL fetal bovine serum (FBS) and 5 mL DNase solution (☐ 400 Kunitz units/mL in solution II, Sigma Cat# DN25).

Lung suspensions were incubated for 10-20 min with gentle rotation in a 37°C water bath then filtered through a 100 μm cell strainer (Greiner Bio-one, Cat# 542-000) followed by 40 μm cell strainer (Greiner Bio-one, Cat# 542-040). Filtered cell suspensions were centrifuged at 250 g for 8 min. Remaining red blood cells were removed from cell pellets by resuspending in 5 mL of 0.87% ammonium chloride in 10 mM Tris (pH 7.6) for 5 min. 10 mL of Dulbecco's Modified Eagle Media (Corning Cat# 10-013-CV) containing 10% FBS (Atlanta Biologicals Cat# S11550),

100 U/mL penicillin (Sigma Cat# P4333), 10 mg/mL streptomycin (Sigma Cat# P4333), 0.25 μg/mL amphotericin B (VWR, Cat# 0414-1G), and 50 μg/mL gentamycin (Sigma Cat# G1397) (DMEM/10) were added to the cell suspension, which was then centrifuged at 250 g for 8 min. The cells were resuspended in 30 mL of DMEM/10 and biopanned to remove macrophages on rat IgG (0.5 mg IgG/mL 10 mM Tris buffer, pH 9.5, Sigma Cat# I8015)-coated cell culture grade tissue culture dishes (Genesee Scientific Cat# 25-202) for 1 h at 37°C. Cell isolations using this method routinely obtained 90-95% type II AECs cells.

To produce model Type I AEC monolayers, isolated Type II AECs were plated on rat tail type-I collagen (20 μg/mL, Roche Cat# 111791790) coated 12 mm Transwell-permeable supports (500,000 cells) unless otherwise stated. Cells were plated and refed every other day using DMEM/10. Cells differentiated into a confluent model type I AEC monolayer after 4-5 days, and cells were used for experiments on day 5 or 6.

Analysis of BioID by Immunofluorescence

Rat type II AECs were plated on collagen-coated Transwells. The cells were cultured for three days, then transduced with either YFP-claudin-18 or BirA-claudin-18 at MOI 10 or 50. 48 h after transduction, the medium was replaced with Opti-MEM containing 100 uM biotin and further incubated for 12 h at 37°C prior to processing for immunofluorescence.

Cell monolayers cultured on Transwells were washed twice with PBS containing calcium and magnesium, then fixed for 15 min with 4% paraformaldehyde in PBS. Cells were washed twice with PBS before being permeabilized with 0.5% Triton X-100 (Fisher Scientific Cat# BP151-500) in PBS for 5 min. The samples were blocked twice for 5 min with 0.5% Triton-X100 + 3% bovine serum albumin (BSA, Fisher BP1600-100) in PBS.

Rabbit anti-claudin-18 (1:125, Thermo Fisher 388100) was prepared in 3% BSA in PBS then added to samples which were incubated overnight at 4°C. The samples were washed three times with 3% BSA in PBS, incubated with goat anti-rabbit IgG Cy2 (1:1,000, Jackson 115-165-166),

and streptavidin-Cy3 (Jackson 016-160-084) prepared in 3% BSA in PBS for 1 h at room temperature. Cells were washed three times with 3% BSA in PBS followed by three washes with PBS before mounting slides to coverslips. ProLong Diamond mounting solution (Invitrogen Cat# P36961) was used to mount slides. Slides were allowed to dry at room temperature overnight prior to application of clear sealant.

Widefield images were collected on using an Olympus IX70 microscope with a U-MWIBA filter pack (BP460-490, DM505, BA515-550) or U-MNG filter pack (BP530-550, DM570, BA590-800). Minimum and maximum intensities for images were adjusted in parallel so that the intensity scale remained linear to maximize dynamic range.

Analysis of BioID by Immunoblot

Type II AECs isolated from two control or alcohol fed rats were plated in two collagen-coated 60 mm tissue culture dishes (24.5 million control cells each, 15.5 million alcohol exposed cells each). The cells were cultured for three days, then transduced with either YFP-claudin-18 or BirA-claudin-18 at MOI 25. 48 h after transduction, the medium was replaced with Opti-MEM containing 100 uM biotin and further incubated for 12 h at 37^{o}C.

Following biotinylation, the cells were washed twice with PBS with calcium and magnesium, trypsinized in 100 ul for 5 min at 37^{o}C, transferred to 1.5 ml Eppendorf tubes and 100 ul of PBS containing NaF (1:500), and PMSF (1:200) was added. The cells were centrifuged at 5900 x g, the supernatant removed and 100 ul lysis buffer (Buffer A, 0.5% Triton X-100, and 50X Protease complete) was added to the cells. The cells were sonicated with five 1-sec pulses, kept on ice for 30 min to promote solubilization and then centrifuged at 13200 g for 15 min at 4^{o}C. The supernatant was transferred to a new tube. Both pellet and supernatant were stored at -20^{o}C.

Dynabeads MyOne Streptavidin C1 (Streptavidin Dynabeads; Thermo Fisher) were resuspended and washed prior to use according to the manufacturer's instructions. The beads were vortexed for 10 sec followed by incubation on an Argos Rotoflex Plus a rotating platform

for 5 min at RT. To wash the beads, 30 uL beads were added to 1 mL of IP Buffer (Buffer A, 0.1% Triton X-100) in a 1.5 ml Eppendorf tube, vortexed for 2 sec, mixed for 5 min at RT using the Argos Rotoflex Plus, centrifuged for 10 sec at 13800 g then concentrated using a BioRad magnetic isolator for 2 min. The supernatant was removed with a small-bore pipette and the washing was repeated with 1 mL IP buffer for a total of five washes.

The protein content of each supernatant sample was measured using the BCA assay, diluted to a total protein concentration of 1 mg/ml (for immunoblot; ~1:10 dilution) using IP buffer, and 30 uL of Streptavidin Dynabeads was added per mL of supernatant. Samples were mixed overnight at 4°C using the Argos Rotoflex Plus.

To separate bound from unbound protein, the samples were centrifuged for 10 sec at 13800 x g, then concentrated using a BioRad magnetic isolator for 2 min. The supernatant was removed and stored at -20°C for further analysis. The beads were washed five times in 1 ml IP buffer for 5 min at 4°C as described above, followed by five washes in sterile PBS without calcium and magnesium for 5 min at 4°C to remove detergent. It should be noted that during the final washes, protein-bound beads were not pelleting, instead producing smears on the Eppendorf tube walls. Protein bound Streptavidin Dynabead pellets were resuspended in 100 uL PBS without calcium and magnesium and stored at -20°C until they were used for further analysis.

Elution Method 1: 10 uL of protein bound beads were transferred into a new Eppendorf tube, centrifuged for 1 min at 13800 g and the supernatant removed., then resuspended in 50 uL 1X reducing SDS sample buffer (10% glycerol, 1.25% SDS, 50 mM Tris pH 6.7) with 1 mg/ml (4 mM) biotin and 100 mg/mL dithiothreitol. Samples were heat shocked at 65°C for 10 min, then cooled on ice prior to further analysis by immunoblot. Elution Method 2: to test whether an additional heat shock would improve elution, samples processed as in Elution Method 1 above were subjected to a -20°C freeze/thaw cycle, either heat shocked for a second time at 90°C for 10 min or not, then sonicated with five 1 sec pulses prior to immunoblot analysis. As a third

approach, protein bound beads stored at -20°C were thawed and 20 uL of beads were added to 5 uL of 6x sample buffer (BioRad) with or without 25 mM biotin (1.2 mg/ml final concentration), then heat shocked at either 65°C or 95°C for 5 min. Samples were cooled on ice and 25 uL RIPA buffer was added prior to immunoblot analysis.

Proteins were resolved by SDS-PAGE using 4-20% Mini-PROTEAN TGX stain-free gradient SDS-polyacrylamide gels, then transferred to nitrocellulose membranes (Bio-Rad Cat# 1704270). The primary antibodies used for protein detection were rabbit anti-claudin-18 (1:1,500, Invitrogen 388000), mouse anti-ZO-1 (1:1,500, Invitrogen 339100), rabbit anti-claudin-5 (1:1,500, Invitrogen 341600), and mouse anti- β-actin (1:10,000, Sigma A5441). Detection was done using goat anti-rabbit IgG IRDye 800CW (1:20,000, LI-COR), goat anti-mouse IgG IRDye 680RD (1:20,000, LI-COR) or streptavidin IRDye 800CW (LI-COR). Membranes were imaged using a Bio-Rad ChemiDoc MP Imaging System. Protein quantification was relative to actin. LI-COR fluorescent images of immunoblots were pseudocolored to greyscale images in the figures.

BioID Mass Spectrometry Analysis

Rat type II AECs were plated onto twenty 60 mm tissue culture dishes (14-15 million cells each), were cultured for three days, then transduced with either YFP-claudin-18 or BirA-claudin-18 at MOI 25.24 h after transduction, the medium was replaced with Opti-MEM containing 100 uM biotin and the cells further incubated for 15 h at 37°C. The cells were then washed twice with PBS with calcium and magnesium, PMSF (1:200), and pepstatin (1:1000), scraped into 0.5 ml/dish, collected in 15 mL conical tubes, centrifuged at 450 g for 5 min and the supernatant was removed. Cells were resuspended in 0.5 ml lysis buffer and transferred to 1.5 mL Eppendorf tubes. The cells were sonicated with five 1-sec pulses, kept on ice for 30 min to promote solubilization and then centrifuged at 500 x g for 8 min at 4°C. The supernatant was transferred to a new tube. Both pellet and supernatant were stored at -20°C.

Streptavidin Dynabeads were resuspended and washed as described above, then blocked with 0.5 mL blocking buffer (PBS with calcium and magnesium, 0.25% BSA, 0.2% gelatin, 0.05% Triton X-100, 0.1% SDS) overnight at 4°C with mixing, followed by 4 washes with 1 mL IP buffer/sample tube.

The protein content of each supernatant sample was measured using the BCA assay, diluted to a total protein concentration of 2 mg/ml (for mass spectrometry; ~1:5 dilution) using IP buffer, and 30 uL of Streptavidin Dynabeads was added per mL of supernatant. Samples were mixed overnight at 4°C using the Argos Rotoflex Plus.

To separate bound from unbound protein, the samples were centrifuged for 10 sec at 13800 x g, then concentrated using a BioRad magnetic isolator for 2 min. The supernatant was removed and stored at -20°C for further analysis. The beads were washed five times in 0.4 ml IP buffer for 5 min at 4°C as described above, followed by three washes in 0.5 ml sterile PBS without calcium and magnesium for 5 min at 4°C to remove detergent. Protein bound Streptavidin Dynabeads pellets were resuspended in 50 uL PBS without calcium and magnesium and stored at -20°C until they were used for mass spectrometry. Note that calcium and magnesium can interfere with enzyme digestion of proteins for mass spectrometry.

Peptides identified by mass spectrometry were considered to be BirA-claudin-18 positive hits if they had identified peptide spectra matches (PSMs) > 5 and showed a PSM ratio (BirA/YFP) > 1.2. Protein function and localization was determined using the Uniprot website (https://www.uniprot.org/) accessed on 1/31/2021, using the Accession Number. In cases where the Accession Number was obsolete (e.g. F1M4W3), the protein was identified using a BLAST search of the amino acid sequence. Functional groupings of mass spectrometry proteins in KEGG pathway and WikiPathways was determined using g:Profiler (https://biit.cs.ut.ee/gprofiler/gost).[9] In instances where proteins were not represented in the KEGG or WikiPathways databases, they were manually assigned to functional groups.[10,11]

Results

BirA-claudin-18 localizes to cell junctions

In order to determine correct trafficking and localization of BirA-claudin-18 to tight junctions, alveolar epithelial cells were transduced with adenovirus to express BirA-claudin-18 for 48 h and then incubated with 100 μM biotin for 12 h. Two different multiplicities of infection (MOI) were used to determine how low and high MOIs of BirA-claudin-18 affect the amount of biotinylation. Cells were stained with claudin-18 to detect BirA-claudin-18 and streptavidin-Cy3 to determine localization of BirA-claudin-18 and colocalization of BirA-claudin-18 with biotinylated proteins (Figure 5.1).

In cells transduced with BirA-claudin-18, claudin-18 staining appeared faint however, BirA-claudin-18 localized to tight junctions as expected. This is in contrast to non-infected controls, suggesting that the BirA fusion product partially interfered with the ability of anti-claudin-18 antibodies to recognize BirA-claudin-18. More claudin-18 staining was apparent in cells transduced with a higher MOI of BirA-claudin-18.

Cells not expressing BirA-claudin-18 did not appear to have any significant biotinylation, as determined by a lack of streptavidin-Cy3 binding. By contrast, cells with BirA-claudin-18 showed a dose response where transduced at MOI 10 had less biotinylation than cells transduced at MOI 50. Of note, biotinylation was evident at cell junctions in BirA-claudin-18 expressing cells, colocalizing with claudin-18. However, biotinylation was not restricted to cell junctions. For instance, transduced cells showed perinuclear biotin labeling. Given the 12 hour binotinylation protocol used to label these cells, this is not surprising and suggests BirA-claudin-18 labeling in the biosynthetic pathway. Consistent with this, as described below, we identified several ER-localized, biotinylated proteins by mass spectrometry.

Evaluation of streptavidin bead elution methods

We initially attempted to use a candidate-based approach to identify targets biotinylated by BirA-claudin-18, examining protein lysates prepared from AECs isolated from either control-fed or alcohol-fed rats, adapting methods used by Zlatic et al.[12] and Schlingmann et al.[3] for co-immunoprecipitation. AECs were transduced with either YFP-claudin-18 as a negative control or BirA-claudin-18 and then biotinylated and processed as described in Methods using Streptavidin Dynabeads as a reagent to enrich for biotinylated targets.

Five elution methods were tested (Figures 5.2-5.4), using immunoblot for claudin-18, claudin-5, ZO-1, and β-actin as a method to detect biotinylated substrates that were isolated using Streptavidin Dynabeads. In each of the protocols used, of the four proteins we probed for, only β-actin was detectable. One elution method, 95°C heat shock in samples that were not supplemented with biotin, there was a band detected with anti-claudin-5 however it migrated lower than the expected 22 kDa molecular weight (Figure 5.4). Beads only negative controls confirmed β-actin was only present in samples prepared from cell lysates, however, there was detectable β-actin in samples derived from YFP-claudin-18 transduced cells (Figure 5.2), suggesting that at least some bead associated β-actin was due to non-specific labeling.

Given the lack of robust signal for claudin-18, claudin-5 and ZO-1, we instead employed a discovery-based approach, using IRDye streptavidin-800 CW to stain for biotinylated proteins in protein-bound bead samples (Figure 5.5). This proved more fruitful and revealed several biotinylated bands associated with the Streptavidin Dynabeads. Of note was a prominent band at ~70 kDa in all of the biotinylated samples, as well as another band at ~30 kDa and several fainter bands. This suggested that we were getting targets biotinylated by BirA-claudin-18 and so we moved ahead with mass spectrometry BioID analysis.

Proteins biotinylated by BirA-claudin-18

Mass spectrometry and protein identification revealed 3771 identified protein matches within the BirA-claudin-18 sample and 3178 identified protein matches within the YFP-claudin-18 sample. Good coverage of proteins within peptide samples is indicated by approximately 50 percent of the identified proteins having peptide spectrum matches (PSMs) of five or more. BirA-claudin-18 and YFP-claudin-18 samples had 1482 and 1321 protein matches, respectively, meeting this criterium, about 40 percent of total identified proteins. Mass spectrometry results were then sorted by PSM ratio (number of PSMs detected in BirA-claudin-18 sample to PSMs detected in YFP-claudin-18 sample) and all results with BirA-claudin-18 PSMs below 5 were removed.

Note that claudin-18 and claudin-5 were present in samples analyzed by mass spectrometry but had a low PSM of 1 below the threshold of 5 for confident detection. This is consistent with our inability to detect claudin-18 and claudin-5 by immunoblot analysis (Figures 5.2-5.4). This also reflects the isolation protocol we used, which is optimized to recover proteins near claudin-18 that are cytosolic or transiently associated with membranes through protein-protein interactions, as opposed to transmembrane proteins.

It is less clear why ZO-1 (Tjp1) was not detected by immunoblot (Figure 5.2-5.4), since it was prominent in our dataset (BirA PSMs = 21; PSM ratio = 1.5). One possibility is that ZO-1 was not effectively released from streptavidin Dynabeads or biotinylation may interfere with detection by immunoblot. There are candidate bands in the streptavidin IRDye 800CW blot in the range of 220 kDa, which may represent ZO-1 (Figure 5.5). With respect to the prominent ~70 kDa and ~30 kDa bands recognized by streptavidin IRDye 800CW (Figure 5.5), these could correspond to several candidate molecules that were identified by mass spectrometry including, but not limited to, Ttll12 (73.9 kDa), ATIC (64.2 kDa), Pdia4 (72.7 kDa), and Prohibitin (29.8 kDa).

There were 83 proteins that had a PSM ratio of 3.0 or higher, meaning proteins that were at least three times enriched in BirA-claudin-18 samples compared to YFP-claudin-18 samples

(Table 1). Of these, 22 candidates had no YFP-claudin-18 PSMs, so they had a PSM ratio that was undefined and greater than 15. 24 of the 83 most highly enriched proteins have already been identified to regulate of intercellular junctions. Based on their documented localization in the Uniprot database, most of these proteins are associated with the plasma membrane and either the cytoskeleton or cytosol. Localization to the plasma membrane and cytoskeleton, suggest candidates serving a role as crosslinking scaffold proteins. These include Acf7/Macf1, Llgl2, Pacsin2, Palld, Parva, Pdcd6ip, Rai14, Tjp2 (ZO-2), and Vcl (vinculin), several of which have been validated as to crosslink the cytoskeleton to intercellular junctions.

Two of these candidates, Rai14 (Retinoic Acid Induced Protein 14, Ankycorbin) and Palld (Palladin), are particularly noteworthy, since they are associated with retinoic acid regulation of tubulobulbar complexes (ectoplasmic specializations) in the testis.[13] Tubulobulbar complexes represent a unique junctional complex that acts as a signaling platform and organizing center for the cytoskeleton, endosomes and endoplasmic reticulum.[14,15] We have hypothesized that tight junction spikes formed by claudin-18 are a signaling platform analogous to tubulobulbar complexes and the association of Rai14/palladin with claudin-18 is consistent with this model.[16]

Proteins tagged by BirA-claudin-18 that localize to the plasma membrane and cytosol include Akr1a1, Arhgef1, Gnas, Lpp, Map2k1, and Phb and are mainly involved in signal transduction. Given the prominent role of RhoA in regulating tight junction assembly and turnover, the detection of Arhgef1 (Rho guanine nucleotide exchange factor 1) as one of these proteins helped validate this set of candidates. There were also several proteins that show nuclear localization (Aldh6a1, Elavl1, Esrp1, Impdh2, Lpp, Map2k1, Mapk3, Phb, Pkm, Ppp2r1a, Ptbp3, Rai14, Ssb). These are candidate transcriptional regulators with the potential to cycle between claudin-18 containing tight junctions and the nucleus, much the same way that the transcription factor YAP has been shown to regulate alveolar epithelial cell growth and lung morphology.[17] Surprisingly, our BioID isolation protocol only identified a single YAP PSM in the BirA-claudin-18 expressing cells, which may be due to the BirA tag interfering with the ability of

claudin-18 to bind to YAP. Nonetheless, other Hippo pathway associated proteins were labeled by claudin-18 BioID.

To identify additional candidates labeled by BirA-claudin-18, we lowered the PSM ratio threshold to 1.2 and used g:Profiler to classify hits into KEGG and WikiPathways categories (Tables 2-5). In addition to multiple tight junction-associated proteins that were BioID labeled by BirA-claudin-18, there were several adherens junction proteins that were also tagged (Table 2), consistent with both tight and adherens junctions being part of a well-organized apical junctional complex. We also found a significant number of BioID labeled candidates associated with focal adhesions, including Vcl (vinculin), Tln1 (talin-1), Flna, Flnb and Flnc (Filamin-A, -B and –C), suggesting that could represent integrin interacting proteins are part of the apical junctional complex and/or tight junction spikes in alveolar epithelial cells. Consistent with this possibility, several candidate proteins that were classified as are part of the Alpha6-Beta4 integrin signaling pathway were also identified by BioID (Table 3). Other signal transduction pathways that were tagged by BirA-claudin-18 included Estrogen, Hippo, IL-2, IL-6, Nrf2, and TNF-alpha/NF-kB signaling pathways (Table 3), in further support of claudin-18 as part of a signaling hub, pending independent validation.

We also identified several candidates in the protein processing in endoplasmic reticulum (ER) and proteosome groups labeled by claudin-18 BioID (Table 4). Given the 12 h incubation period used, these may reflect hits in the biosynthetic and turnover pathways. However, ER proteins near claudin-18 are also consistent with our model of tight junction spikes representing a structure equivalent to the tubulobulbar complex, which is a site where the ER and plasma membrane are in close contact.[18,19] We also identified several candidates involved in endocytosis and phagocytosis, which were consistent with the active secretion and internalization of claudin-18 as a part of tight junction turnover (Table 5). Again, this fits well with the tubulobulbar model of tight junction spikes, since this structure is an active site of vesicle budding and fusion.

Discussion

The findings here support the use of BioID as a method for identification of proteins proximal to claudin-18. Several known proximal proteins were confirmed by this method to be in abundance around claudin-18, such as ZO-1 and ZO-2, which validates the method. In addition, this provided a discovery-based approach to identify novel proteins that could provide insight into the mechanisms of barrier function and tight junction regulation. Furthermore, these results provide a starting point for future studies investigating tight junction spike formation and function. The experiments detailed above can serve as a guide to build upon for acquisition of proteins in future BioID experiments with BirA-claudin-18. A similar study using a biotin ligase-conjugated claudin-4 in MDCK II cells showed enrichment of several known tight junction proteins including ZO-1, ZO-2, occludin, and several claudin proteins.

We used a high stringency streptavidin Dynabead isolation protocol and, as a result, most of the proteins identified by claudin-18 BioID were cytosolic, peripheral membrane proteins or associated with the cytoskeleton (Table 1). The number of BioID identified proteins with PSM ratio above 3 included 28 proteins previously known to be associated with junctions. These could be categorized into three basic groups: 1) cytosolic scaffold proteins associated with the plasma membrane/junctions and also the cytoskeleton (Acf7/Macf1, Llgl2, Pacsin2, Palld, Parva, Pdcd6ip, Rai14, Tjp2, Vcl); 2) signal transduction proteins (Akr1a1, Arhgef1, Gnas, Lpp, Map2k1, Phb) associated with the plasma membrane and cytosol and 3) proteins that localize to the nuclear (Aldh6a1, Elavl1, Esrp1, Impdh2, Lpp, Map2k1, Mapk3, Phb, Pkm, Ppp2r1a, Ptbp3, Rai14, Ssb) which can regulate gene expression. We speculate that claudin-18 can act as part of a signaling hub where transcription factors can cycle between junction and nuclear localization, much the same way that β-catenin is well established to act as a sensor for intercellular contact that can translocate to the nucleus and regulate transcription.[20] As mentioned above, the transcription factor YAP binds to claudin-18 and regulates alveolar repair and differentiation, consistent with this model.[17]

Two proteins identified by claudin-18 BioID, Rai14 (retinoic acid induced protein 14) and palladin, have previously been shown to localize to the tubulobulbar complex and regulate their integrity in response to retinoic acid.[13,21] Retinoic acid has a key role in regulating lung development and repair and has been shown to promote lung barrier function.[22,23] Palladin is associated with the actin cytoskeleton and junctions, but precise roles for how it regulates these structures remain to be determined.[24] Interestingly, palladin interacts with filamins, which were also identified by claudin-18 BioID.[25] Other cytoskeletal associated proteins have been shown to localize to tight junctions and tight junction spikes as well as other spike-like structures.[18,26] Other proteins identified by claudin-18 BioID and also found in the spike-like tubulobulbar complex, include vinculin, components of clathrin coated pits and endoplasmic reticulum-associated proteins.[18] These data suggest that our approach identified proteins tagged by BirA-claudin-18 that are involved in forming tight junction spikes. Future validation will determine whether this is the case.

The adherens junction protein β-catenin was identified by claudin-18 BioID. β-catenin is known to localize to the apical junctional complex and our data demonstrates that it is proximal to claudin-18. We also identified several focal adhesion proteins by claudin-18 BioID, including talin-1, that play vital roles in linking integrins in focal adhesions to the actin cytoskeleton. It is not known whether these proteins interact with tight junctions though they might be regulated in a similar manner [27]. It also is possible that in squamous cells like alveolar epithelial cells, tight junctions are in closer proximity to focal adhesions, bringing talin-1 within the vicinity of BirA-claudin-18. The higher enrichment of talin-1 in BirA-claudin-18 samples compared to YFP-claudin-18 (PSM ratio 2.6) suggests that talin-1 could have a more tight junction-proximal role in addition to its role in focal adhesions, much like focal adhesion protein vinculin [28,29].

Like many discovery-based techniques, BioID is subject to some limitations and caveats. For instance, the length of time cells were exposed to biotin is likely to influence which proteins detected by BioID. Here, cells were exposed to biotin for 12 h, comparable in time to other

studies that treated cells with biotin for 15 to 17 h prior to isolation. [4,5] However, tight junction proteins turnover relatively quickly [30–32] meaning that proteins encountered throughout the lifecycle of claudin-18 will be biotinylated, and not just tight junction associated proteins.

It is possible that the BirA tag could have affected normal claudin-18 localization and interactions however, this seems unlikely, since BirA-claudin-18 did localize to tight junctions and the BirA tag was on the N-terminus, and so the C-terminus was free to interact with proteins such as ZO-1 required for tight junction localization. It is also possible that BirA-claudin-18 expression could affect normal tight junction morphology, although we did not see any major abnormalities in cell or junction morphology in BirA-claudin-18 expressing alveolar epithelial cells. In addition, the BirA tag may interfere with the ability of claudin-18 to bind to different proteins, such as YAP.

The proteins detected in samples from YFP-claudin-18 transduced cells suggests isolation of naturally biotinylated or biotin-bound proteins. Though it is rare, natural biotinylation does occur in cells and biotin is an essential cofactor for many enzymes (specifically carboxylases). It is also likely that there was nonspecific binding of proteins to streptavidin beads, such as actin, however, setting a suitable PSM ratio threshold controls for this possibility.

The isolation and washing protocols were optimized for cytosolic proteins and so we detected few transmembrane proteins. This is a caveat to this approach, although it does increase confidence that hits with a BirA-claudin-18 PSM greater than 5 and PSM ratio greater than 3 are bona fide proteins close to claudin-18 in a native setting. Decreasing the PSM ratio to less than 3 enabled more potential hits to be identified, but these results need to be interpreted with caution and are subject to validation by super resolution microscopy co-localization or through the use of the proximity ligation assay (PLA).[3] Immunoblotting was a less effective approach, and eluting proteins from streptavidin beads in order to validate samples proved difficult. Heat shocking samples at 95^{o}C eluted more biotinylated proteins than a 65 ^{o}C heat shock (Figure 5.5) but heat shocking tight junction proteins should be done with care, as tight

junction proteins have a tendency to aggregate after exposure to high temperatures. Given this issue, on-bead enzyme digestion was used to prepare peptide samples for mass spectrometry.

Despite these limitations, the BioID method provided us with several candidate claudin-18 interacting proteins that will be validated in future experiments. This approach also provides experimental support that tight junction spikes could act as a signaling hub comparable to the tubulobulbar complex in the testis.[18] In addition, our data suggests that proteins more typically associated with regulation of focal adhesions are also likely to be involved in the regulation of claudin-18 and alveolar epithelial barrier function. This model is appealing, given the recently appreciated roles for apically localized integrins in the regulation of tight junction morphology and function.[33]

Figure 5.1

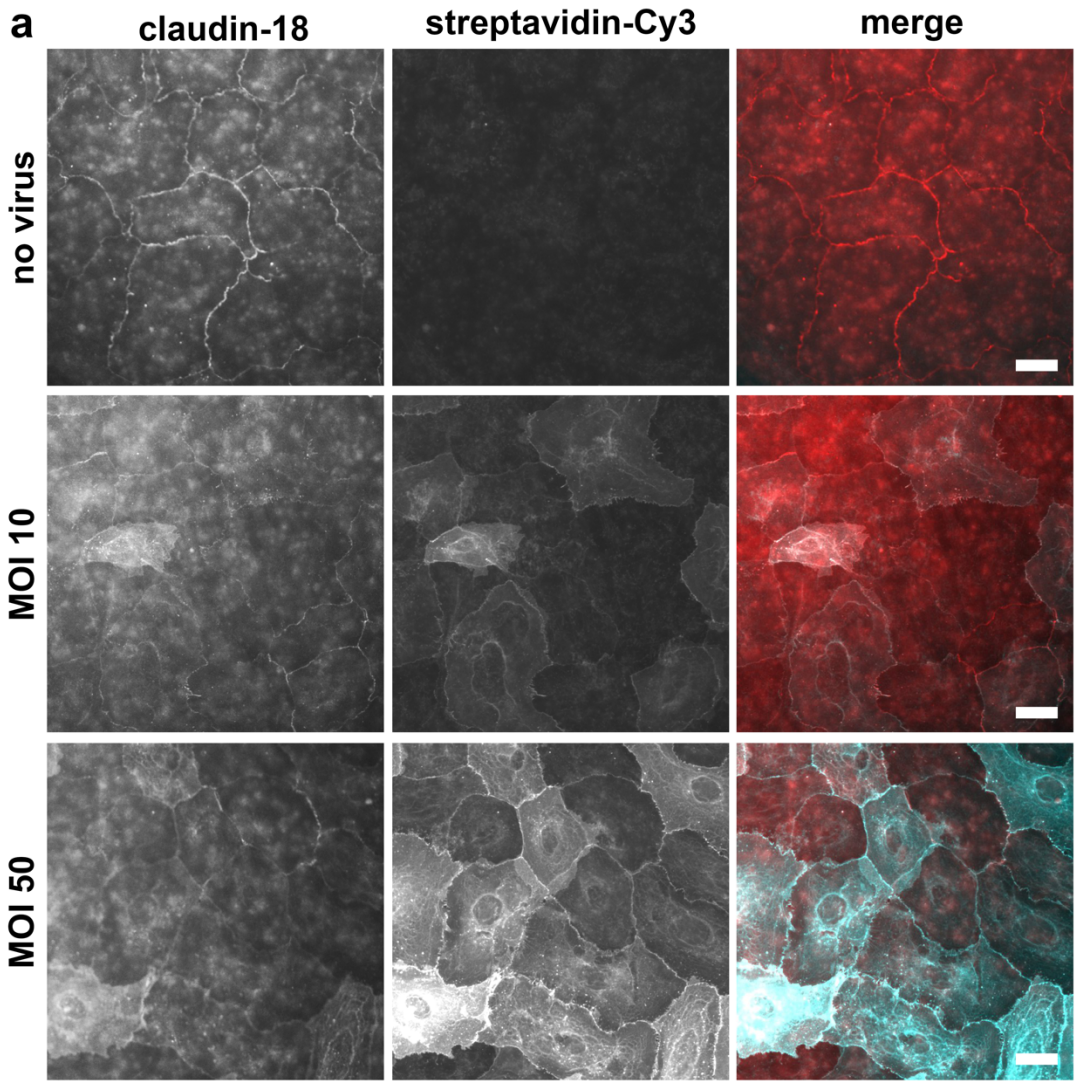

Figure 5.1: Immunofluorescence of AdBirA-claudin-18 in primary rat AECs treated with 100 uM biotin. Rat AECs were untransduced (control) or transduced with BirA-claudin-18 at MOI 10 or MOI 50 and treated with 100 uM biotin for 12 h, then fixed, permeabilized, labeled with anti-claudin-18 and steptavidin-Cy3, then imaged by immunofluorescence microscopy. Streptavidin-Cy3 staining was evident in BirA-claudin-18 transduced cells and increased staining correlated with higher MOI. Note that streptavidin-Cy3 colocalized with claudin-18 at tight junctions. Bars: 10 μm.

Figure 5.2

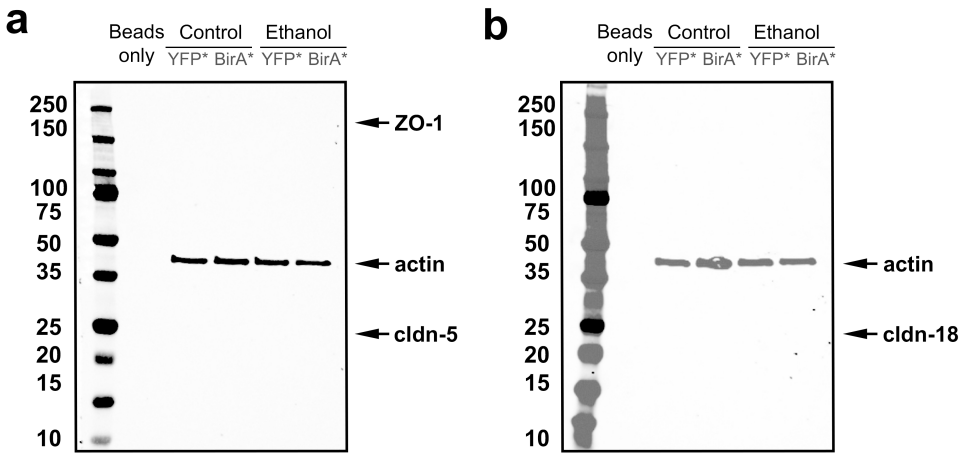

Figure 5.2: Immunoblot of samples from BioID pulldown after first protein elution attempt. Alveolar epithelial cells from control diet- or ethanol diet-fed rats were transduced with YFP-claudin-18 or BirA-claudin-18 at MOI 25. Cells were then incubated with 100 μM biotin for 12 h before cells were scraped, lysed, and sonicated. Biotinylated proteins were isolated using Streptavidin Dynabeads. 10 μL of bound beads were heated in 80 μL 1x Sample Buffer at 65°C for 10 min and 10 μL of sample was loaded per well. (a,b) β-actin was detected in all cell samples, but there was no detectable claudin-5, claudin-18, or ZO-1. Samples from YFP-claudin-18 transduced cells show non-specific binding of actin.

Figure 5.3

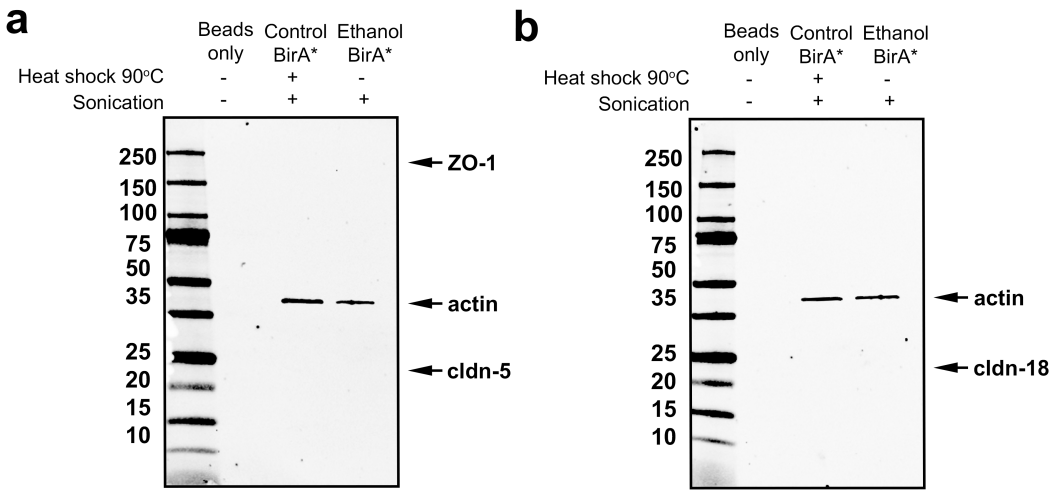

Figure 5.3: Immunoblot of samples from BioID pulldown after second protein elution attempt. Alveolar epithelial cells from control diet- or alcohol diet-fed rats were transduced with BirA-claudin-18 at MOI 25. Cells were then incubated with 100 μM biotin for 12 h before cells were scraped, lysed, and sonicated. Biotinylated proteins were isolated using Streptavidin Dynabeads. 10 μL of bound beads were heated in 80 μL 1x Sample Buffer at 65°C for 10 min. Then samples were frozen at -20°C and thawed. Control BirA-claudin-18 was heated at 90°C for 10 min. All samples were then sonicated with five 1-sec pulses and 20 μL of sample was loaded per well. (a,b) β-actin was detected in all cell samples, but there was no detectable claudin-5, claudin-18, or ZO-1.

Figure 5.4

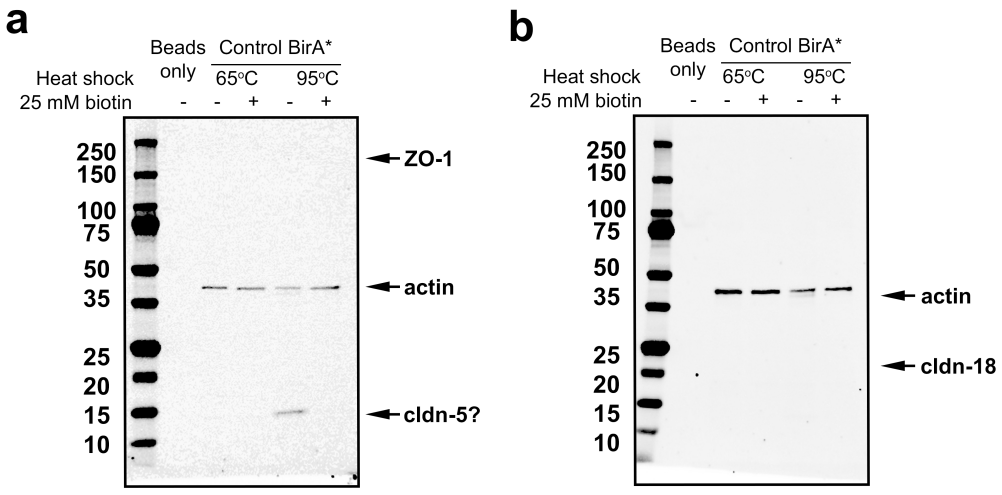

Figure 5.4: Immunoblot of samples from BioID pulldown after third protein elution attempt. Alveolar epithelial cells from control diet-fed rats were transduced with BirA-claudin-18 at MOI 25. Cells were then incubated with 100 μM biotin for 12 h before cells were scraped, lysed, and sonicated. Biotinylated proteins were isolated using Streptavidin Dynabeads. Then samples were frozen at -20°C and thawed. 20 μL of bound beads were heated in 5 μL of 6x Sample Buffer either with or without 25 mM biotin at either 65°C or 95°C for 5 min. Samples were cooled on ice and 25 uL RIPA was added to each. 10 μL of sample was loaded per well. β-actin was detected in all cell samples, but there was no detectable claudin-18 or ZO-1. (a) There appears to be a faint band that might correspond to claudin-5 in the 95°C sample without biotin-supplemented sample buffer. (b) The actin bands (green) in the claudin-18 blot appear to overlap with red bands in all cell samples, which could possibly be BirA-claudin-18 (predicted MW 63 kDa).

Figure 5.5

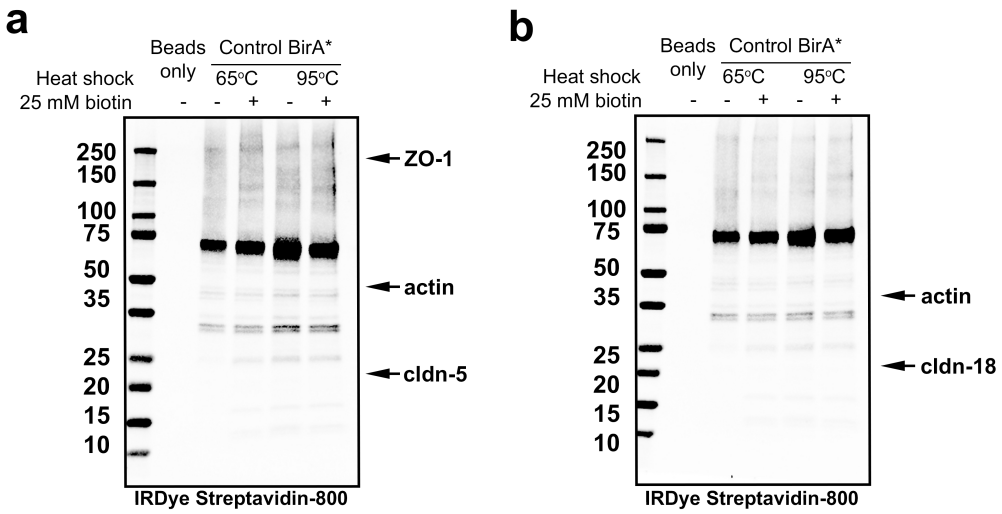

Figure 5.5: Streptavidin blot of samples from BioID pulldown after third protein elution attempt. Alveolar epithelial cells from control diet-fed rats were transduced with BirA-claudin-18 at MOI 25. Cells were then incubated with 100 μM biotin for 12 h before cells were scraped, lysed, and sonicated. Biotinylated proteins were isolated using Streptavidin Dynabeads. Then samples were frozen at -20°C and thawed. 20 μL of bound beads were heated in 5 μL of 6x Sample Buffer either with or without 25 mM biotin at either 65°C or 95°C for 5 min. Samples were cooled on ice and 25 uL RIPA was added to each. 10 μL of sample was loaded per well. When staining with Licor IRDye streptavidin-800 (1 h), a large band running at approximately 70 kDa was detected. (a,b) There are some streptavidin-stained regions where claudin-5 and ZO-1 are expected.

Table 5.1: Enriched proteins tagged by biotin ligase fused to claudin-18.

UniProt ID	Protein Name	Localization (UniProt)	Accession	BirA-claudin-18 #PSMs	PSM Ratio	Reference with tight junctions
Csde1	cold shock domain containing E1	cytosol, Stress Granule	P18395	8	>15	
RT1-CE4	RT1 class I, locus CE4	PM	D3ZQG9	8	>15	
G6pd	glucose-6-phosphate dehydrogenase	cytosol, PM, nucleus	P05370	7	>15	
Ckb	creatine kinase B	cytosol	P07335	7	>15	
Map2k1	Dual specificity MAPKK 1	cytosol, PM, nucleus	Q01986	6	>15	[34]
Nup98	nucleoporin 98	nucleus	P49793	6	>15	
Ipo5	importin 5	cytosol, nucleus	D4A781	6	>15	
Psme3	proteasome activator subunit 3	cytosol, nucleus, proteosome	Q5FVM2	6	>15	
Rai14	retinoic acid induced 14	cytoskeleton, PM, nucleus, tubulobulbar complexes, tight junctions	Q5U312	6	>15	[13,21,23]
Palld	palladin isoform X1	cytoskeleton, PM, tubulobulbar complexes, tight junctions, focal adhesions	F1M4W3	6	>15	[13,35]
Ppp2r1b	protein phosphatase 2 scaffold subunit A beta	cytosol	Q4QQT4	5	>15	
Arhgef1	Rho guanine nucleotide exchange factor 1	cytosol, PM, tight junctions	Q9Z1I6	5	>15	[36–38]
Gdi2	GDP dissociation inhibitor 2	cytosol, PM	P50399	5	>15	
Phgdh	phosphoglycerate dehydrogenase	cytosol	O08651	5	>15	
Tjp2	tight junction protein 2	PM, tight junctions	Q3ZB99	5	>15	
Mtx2	metaxin 2	mitochondria	Q5U1Z9	5	>15	
Ssb	Lupus La protein homolog	nucleus	P38656	5	>15	[39]
Aco2	aconitase 2	mitochondria	Q9ER34	5	>15	
Esrp1	epithelial splicing regulatory protein 1	nucleus	B2RYD2	5	>15	[36]

Dhx15	DEAH-box helicase 15	nucleus	D3ZD97	5	>15	
Farsb	phenylalanyl-tRNA synthetase subunit beta	cytosol	Q68FT7	5	>15	
Lpp	LIM domain containing protein in lipoma	cytosol, PM, nucleus, adherens junctions	Q5XI07	5	>15	[6,40]
Ttll12	tubulin tyrosine ligase like 12	cytosol	D4A1Q9	15	15.0	
Atic	IMP cyclohydrolase	cytosol, PM	O35567	14	14.0	
Phb	prohibitin	PM, nucleus, mitochondria	P67779	8	8.0	[41]
Pdia4	protein disulfide isomerase family A, member 4	ER	G3V6T7	14	7.0	
Dnajb11	DnaJ (Hsp40)	ER	Q6TUG0	7	7.0	
Parva	parvin, alpha	PM, cytoskeleton	G3V818	6	6.0	[42–44]
Sec24a	SEC24 homolog A, COPII coat complex component	cytosol, ER	D3ZZA8	6	6.0	
Sh3glb1	SH3 domain - containing GRB2-like endophilin B1	Golgi apparatus, mitochondria	Q6AYE2	6	6.0	[45]
Ptbp3	polypyrimidine tract binding protein 3	nucleus	Q9Z118	6	6.0	[46]
Pdcd6ip	Programmed cell death 6-interacting protein	cytosol, PM, cytoskeleton, tight junctions, secreted	Q9QZA2	22	5.5	[47,48]
Pxdn	peroxidasin homolog precursor	ER, secreted	M0R6T4	10	5.0	
Mms19	cytosolic iron-sulfur assembly component	ER	F1M0U5	5	5.0	
Nbas	NBAS subunit of NRZ tethering complex	cytoskeleton, nucleus	B5DFC3	5	5.0	
Sec23a	Sec23 homolog A, coat complex II component	cytosol, ER	D4AE96	5	5.0	
Ipo7	importin 7	cytosol	P21708-2	5	5.0	[45,49–51]
Mapk3	Mitogen-activated protein kinase 3	cytosol,nucleus	B0BMW2	5	5.0	[52,53]

Hsd17b10	hydroxysteroid (17-beta) dehydrogenase 10	caveolae, mitochondria	D3ZYS7	5	5.0	54
G3bp1	G3BP stress granule assembly factor 1	cytosol, stress granules	P70580	5	5.0	
Pgrmc1	progesterone receptor membrane component 1	ER , mitochondria	P97852	5	5.0	
Hsd17b4	hydroxysteroid (17-beta) dehydrogenase 4	peroxisome	G3V7J0	5	5.0	23,55,56
Aldh6a1	aldehyde dehydrogenase 6 family, member A1	nucleus,mitochondria	Q9QY17	5	5.0	57,58
Pacsin2	PK-C and casein kinase substrate in neurons	PM, cytoskeleton, endosome	B5DF91	5	5.0	
Elavl1	ELAV like RNA binding protein 1	cytosol, nucleus, stress granules	D3ZER6	5	5.0	59,60
Tnpo2	transportin 2	cytosol	P16617	5	5.0	
Pgk1	phosphoglycerate kinase 1	cytosol	D3ZHV2	27	4.5	
Acf7/Macf1	Microtubule-actin cross-linking factor 1	PM, cytoskeleton, Golgi apparatus	F1LS72	9	4.5	61,62
Uba2	ubiquitin-like modifier activating enzyme 2	nucleus	Q920J4	9	4.5	
Txnl1	thioredoxin-like 1	cytosol, nucleus, proteosome	Q3KRC3	9	4.5	
Srpra	SRP receptor subunit alpha	ER	D3ZD73	9	4.5	
Ddx6	DEAD-box helicase 6	cytosol, cytoskeleton, nucleus, mitochondria	Q9ER24	9	4.5	
Atxn10	ataxin 10	cytosol, PM, , Golgi Apparatus	Q5XFX0	13	4.3	

Tagln2	transgelin 2	cytosol, cytoskeleton, adherens junctions, secreted	P51635	12	4.0	55,56,63
Akr1a1	aldo-keto reductase family 1 member A1	cytosol, PM	P63095	12	4.0	64,65
Gnas	Guanine nucleotide-binding protein G(s) alpha isoform	PM	Q5XI34	12	4.0	66,67
Ppp2r1a	protein phosphatase 2 scaffold subunit A alpha	cytosol, nucleus	P54001	8	4.0	
P4ha1	prolyl 4-hydroxylase subunit alpha 1	ER	Q6PCT9	8	4.0	
Psmd6	proteasome 26S subunit, non-ATPase 6	proteasome	Q5XI78	8	4.0	
Ogdh	2-oxoglutarate dehydrogenase, mitochondrial-like	nucleus, mitochondria	Q4G061	8	4.0	
Eif3b	eukaryotic translation initiation factor 3, subunit B	cytosol	P11980-2	23	3.8	68,69
Pkm	Pyruvate kinase PKM	cytosol, nucleus	F1LNF7	19	3.8	
Idh3a	isocitrate dehydrogenase (NAD(+)) 3 catalytic subunit	mitochondria	Q9ESN0	11	3.7	
Niban1	niban apoptosis regulator 1	cytosol, PM	Q6AYT3	14	3.5	
Rtcb	RNA 2',3'-cyclic phosphate and 5'-OH ligase	cytosolnucleus	B5DFJ4	7	3.5	
Vps18	VPS18 core subunit	cytosol	D3ZQ57	7	3.5	
Plxnb2	plexin B2	PM	Q4KM73	7	3.5	
Cmpk1	UMP-CMP kinase	cytosol, nucleus	F1LRV4	7	3.5	70–72

Hspa4	heat shock protein family A (Hsp70) member 4	cytosol	E9PU28	24	3.4	[73]
Impdh2	inosine monophosphate dehydrogenase 2	cytosol, nucleus	Q5U300	10	3.3	
Uba1	ubiquitin-like modifier activating enzyme 1	cytosol, nucleus, mitochondria	D4AEH3	36	3.0	[74]
Anxa3	Annexin	cytosol, PM	G3V6B0	30	3.0	
Psmd7	proteasome 26S subunit, non-ATPase 7	nucleus, proteasome	G3V7M0	12	3.0	
Pdxdc1	pyridoxal-dependent decarboxylase domain containing	ER	P63074	9	3.0	
Cnot1	CCR4-NOT transcription complex, subunit 1	nucleus	Q5PPG2	9	3.0	[75]
Eif4e	eukaryotic translation initiation factor 4E	nucleus, stress granules	B2GV09	9	3.0	[76,77]
Lgmn	legumain	secreted, endosome	P83953	6	3.0	
Llgl2	LLGL scribble cell polarity complex component 2	PM, cytoskeleton	G3V796	6	3.0	
Kpna1	Importin subunit alpha-5	cytosol, nucleus	P85972	6	3.0	[78]
Acadm	acyl-CoA dehydrogenase medium chain	mitochondria	P41542	6	3.0	
Vcl	Vinculin	PM, cytoskeleton, adherens junctions, Focal Adhesions	D4A5G8	6	3.0	

Proteins were considered enriched if the PSM ratio was 3.0 or greater. Only proteins with 5 or more PSMs are included. PSM ratio is $PSMs_{BirA\text{-}claudin\text{-}18}/PSMs_{YFP\text{-}claudin\text{-}18}$. UniProt is the source of localization, molecular/biological function, and keywords. References were obtained by PubMed literature search.

Table 5.2: Tight junction, adherens junction, and focal adhesion proteins tagged by biotin ligase fused to claudin-18.

UniProt ID	Protein Name	Functional grouping	KEGG/WP	Accession	BirA-claudin-18 #PSMs	PSM Ratio
Arfgef1	Rho guanine nucleotide exchange factor 1	Adherens junction		Q9Z1I6	5	> 15
Rtn4	Isoform 2 of Reticulon-4	Adherens Junction		Q9JK11-2	10	2.0
Mllt4	Afadin	Adherens Junction		O35889	6	2.0
Ctnnb1	Catenin beta-1	Adherens Junction		Q9WU82	39	1.5
Yes1	YES proto-oncogene 1, Src family tyrosine kinase	Adherens junction	KEGG:04520	Q6AXQ3	6	1.5
Ptpn1	protein tyrosine phosphatase, non-receptor type 1	Adherens junction	KEGG:04520	P20417	6	2.0
Ctnna1	catenin alpha 1	Adherens junction	KEGG:04520	Q5U302	43	1.4
Ptpn6	protein tyrosine phosphatase, non-receptor type 6	Adherens junction	KEGG:04520	G3V9T9	25	1.3
Ctnnd1	catenin delta 1	Adherens junction	KEGG:04520	D3ZZZ9	64	1.3
Macf1	Microtubule-actin cross-linking factor 1	Focal adhesion	Ref 5	D3ZHV2	9	4.5
Parva	parvin, alpha	Focal adhesion	KEGG:04510 Ref 2,3	G3V818	6	6.0
Ptbp3	Polypyrimidine tract-binding protein 3	Focal adhesion		Q9Z118	6	6.0
Tln1	talin 1	Focal adhesion	KEGG:04510	G3V852	45	2.6
Flnb	filamin B	Focal adhesion	KEGG:04510	D4A8D5	123	1.6
Flna	filamin A	Focal adhesion	KEGG:04510	C0JPT7	117	1.6
Flnc	filamin C	Focal adhesion	KEGG:04510	D3ZHA0	21	1.5

Ppp1cb	protein phosphatase 1 catalytic subunit beta	Focal adhesion	KEGG:04510	P62142	14	1.4
Ppp1ca	protein phosphatase 1 catalytic subunit alpha	Focal adhesion	KEGG:04510	P62138	13	1.3
Lamb3	laminin subunit beta 3	Focal adhesion	KEGG:04510	F1LPI5	38	1.3
Ppp2r1b	protein phosphatase 2 scaffold subunit A beta	Tight junction	KEGG:04530	Q4QQT4	5	> 15
Tjp2	tight junction protein 2	Tight junction	KEGG:04530	Q3ZB99	5	> 15
Pdcd6ip	Programmed cell death 6-interacting protein	Tight junction	Ref 6	Q9QZA2	22	5.5
Ppp2r1a	protein phosphatase 2 scaffold subunit A alpha	Tight junction	KEGG:04530	Q5XI34	8	4.0
Hspa4	heat shock protein family A (Hsp70) member 4	Tight junction	KEGG:04530 Ref 22-24	F1LRV4	24	3.4
Llgl2	LLGL scribble cell polarity complex component 2	Tight junction	KEGG:04530	B2GV09	6	3.0
Vcl	Vinculin	Adherens junction, Focal adhesion	Ref 30	P85972	6	3.0
Vasp	vasodilator-stimulated phosphoprotein	Focal adhesion, Tight junction	KEGG:04510	F7EWC1	7	1.8
Tjp1	tight junction protein 1	Tight junction, Adherens junction	KEGG:04530	F1M4A0	21	1.5
Actn4	actinin alpha 4	Tight junction, Adherens junction, focal adhesion	KEGG:04530	Q9QXQ0	91	1.4
Actn1	actinin, alpha 1	Tight junction, Adherens junction, focal adhesion	KEGG:04530	Q9Z1P2	100	1.3
Actb	actin, beta	Tight junction, Adherens junction, focal adhesion	KEGG:04530	P60711	349	1.2

Only proteins with 5 or more PSMs are included. PSM ratio is $PSMs_{BirA\text{-}claudin\text{-}18}/PSMs_{YFP\text{-}claudin\text{-}18}$. UniProt, KEGG, and WikiPathways (WP) were used to obtain protein and pathway pathway information.

Table 5.3: Selected signal transduction proteins tagged by biotin ligase fused to claudin-18.

UniProt ID	Protein Name	Functional grouping	KEGG/WP	Accession	BirA-claudin-18 #PSMs	PSM Ratio
Eif4e	eukaryotic translation initiation factor 4E	Alpha6-Beta4 Integrin Signaling Pathway	WP:WP485	P63074	9	3.0
Yes1	YES proto-oncogene 1, Src family tyrosine kinase	Alpha6-Beta4 Integrin Signaling Pathway	WP:WP485	Q6AXQ3	6	1.5
Dsp	desmoplakin	Alpha6-Beta4 Integrin Signaling Pathway	WP:WP485	F1LMV6	16	1.3
Lamb3	laminin subunit beta 3	Alpha6-Beta4 Integrin Signaling Pathway	WP:WP485	F1LPI5	38	1.3
Ywhae	tyrosine 3-monooxygenase/tryptophan 5-monooxygenase activation protein, epsilon	Alpha6-Beta4 Integrin Signaling Pathway	WP:WP485	P62260	6	1.2
Ppp2r1b	protein phosphatase 2 scaffold subunit A beta	Estrogen signaling pathway	KEGG:04915	Q4QQT4	5	> 15
Tjp2	tight junction protein 2	Estrogen signaling pathway	KEGG:04915	Q3ZB99	5	> 15
Ppp2r1a	protein phosphatase 2 scaffold subunit A alpha	Estrogen signaling pathway	KEGG:04915	Q5XI34	8	4.0
Hspa4	heat shock protein family A (Hsp70) member 4	Estrogen signaling pathway	KEGG:04915	F1LRV4	24	3.4
Llgl2	LLGL scribble cell polarity complex component 2	Estrogen signaling pathway	KEGG:04915	B2GV09	6	3.0
Vasp	vasodilator-stimulated phosphoprotein	Estrogen signaling pathway	KEGG:04915	F7EWC1	7	1.8
Tjp1	tight junction protein 1	Estrogen signaling pathway	KEGG:04915	F1M4A0	21	1.5
Actn4	actinin alpha 4	Estrogen signaling pathway	KEGG:04915	Q9QXQ0	91	1.4
Actn1	actinin, alpha 1	Estrogen signaling pathway	KEGG:04915	Q9Z1P2	100	1.3
Actb	actin, beta	Estrogen signaling pathway	KEGG:04915	P60711	349	1.2

Ppp2r1b	protein phosphatase 2 scaffold subunit A beta	Hippo signaling pathway	KEGG:04390	Q4QQT4	5	20.0
Ppp2r1a	protein phosphatase 2 scaffold subunit A alpha	Hippo signaling pathway	KEGG:04390 Ref 18,19	Q5XI34	8	4.0
Llgl2	LLGL scribble cell polarity complex component 2	Hippo signaling pathway	KEGG:04390	B2GV09	6	3.0
Ctnna1	catenin alpha 1	Hippo signaling pathway	KEGG:04390	Q5U302	43	1.4
Ppp1cb	protein phosphatase 1 catalytic subunit beta	Hippo signaling pathway	KEGG:04390	P62142	14	1.4
Ppp1ca	protein phosphatase 1 catalytic subunit alpha	Hippo signaling pathway	KEGG:04390	P62138	13	1.3
Actb	actin, beta	Hippo signaling pathway	KEGG:04390	P60711	349	1.2
Ywhae	tyrosine 3-monooxygenase/tryptophan 5-monooxygenase activation protein, epsilon	Hippo signaling pathway	KEGG:04390	P62260	6	1.2
Eif3b	eukaryotic translation initiation factor 3, subunit B	IL-2 Signaling Pathway	WP:WP569	Q4G061	23	3.8
Eif4e	eukaryotic translation initiation factor 4E	IL-2 Signaling Pathway	WP:WP569	P63074	9	3.0
Lyn	LYN proto-oncogene, Src family tyrosine kinase	IL-2 Signaling Pathway	WP:WP569	Q07014	7	1.8
Stat3	signal transducer and activator of transcription 3	IL-2 Signaling Pathway	WP:WP569	P52631	12	1.7
Ptpn6	protein tyrosine phosphatase, non-receptor type 6	IL-2 Signaling Pathway	WP:WP569	G3V9T9	25	1.3
Ppp2r1b	protein phosphatase 2 scaffold subunit A beta	IL-6 Signaling Pathway	WP:WP135	Q4QQT4	5	20.0
Ppp2r1a	protein phosphatase 2 scaffold subunit A alpha	IL-6 Signaling Pathway	WP:WP135	Q5XI34	8	4.0
Eif4e	eukaryotic translation initiation factor 4E	IL-6 Signaling Pathway	WP:WP135	P63074	9	3.0
Lyn	LYN proto-oncogene, Src family tyrosine kinase	IL-6 Signaling Pathway	WP:WP135	Q07014	7	1.8

Stat3	signal transducer and activator of transcription 3	IL-6 Signaling Pathway	WP:WP135	P52631	12	1.7
Cdk5	cyclin-dependent kinase 5	IL-6 Signaling Pathway	WP:WP135	Q03114	5	1.7
Hdac1	histone deacetylase 1	IL-6 Signaling Pathway	WP:WP135	Q4QQW4	6	1.5
G6pd	glucose-6-phosphate dehydrogenase	Nrf2 Signaling	WP:WP2376	P05370	7	20.0
Akr1a1	aldo-keto reductase family 1 member A1	Nrf2 Signaling	WP:WP2376	P51635	12	4.0
Xpo1	exportin 1	Nrf2 Signaling	WP:WP2376	Q80U96	21	2.3
Psmc3	proteasome 26S subunit, ATPase 3	Nrf2 Signaling	WP:WP2376	Q6P6U2	12	2.0
Hmox1	heme oxygenase 1	Nrf2 Signaling	WP:WP2376	P06762	8	2.0
Psmc6	proteasome 26S subunit, ATPase 6	Nrf2 Signaling	WP:WP2376	G3V6W6	13	1.9
Psmc1	proteasome 26S subunit, ATPase 1	Nrf2 Signaling	WP:WP2376	P62193	14	1.8
Psmc2	proteasome 26S subunit, ATPase 2	Nrf2 Signaling	WP:WP2376	G3V7L6	10	1.7
Ran	RAN, member RAS oncogene family	Nrf2 Signaling	WP:WP2376	P62828	5	1.7
Ugdh	UDP-glucose 6-dehydrogenase	Nrf2 Signaling	WP:WP2376	G3V6C4	7	1.4
Psmc4	proteasome 26S subunit, ATPase 4	Nrf2 Signaling	WP:WP2376	Q63570	18	1.4
Hsp90ab1	heat shock protein 90 alpha family class B member 1	Nrf2 Signaling	WP:WP2376	P34058	97	1.4
Psmc5	proteasome 26S subunit, ATPase 5	Nrf2 Signaling	WP:WP2376	P62198	19	1.4
Phb	Prohibitin	TNF-alpha NF-kB Signaling Pathway	Ref 1	P67779	8	8.0
Psmd6	proteasome 26S subunit, non-ATPase 6	TNF-alpha NF-kB Signaling Pathway	WP:WP457	Q6PCT9	8	4.0
Psmd7	proteasome 26S subunit, non-ATPase 7	TNF-alpha NF-kB Signaling Pathway	WP:WP457	D4AEH3	12	3.0
Kpna6	karyopherin subunit alpha 6	TNF-alpha NF-kB Signaling Pathway	WP:WP457	F1LT58	5	2.5
Psmc3	proteasome 26S subunit, ATPase 3	TNF-alpha NF-kB Signaling Pathway	WP:WP457	Q6P6U2	12	2.0

G3bp2	G3BP stress granule assembly factor 2	TNF-alpha NF-kB Signaling Pathway	WP:WP457	Q6AY21	6	2.0
Psmd12	proteasome 26S subunit, non-ATPase 12	TNF-alpha NF-kB Signaling Pathway	WP:WP457	Q5XIC6	15	1.9
Psmc1	proteasome 26S subunit, ATPase 1	TNF-alpha NF-kB Signaling Pathway	WP:WP457	P62193	14	1.8
Psmc2	proteasome 26S subunit, ATPase 2	TNF-alpha NF-kB Signaling Pathway	WP:WP457	G3V7L6	10	1.7
Flna	filamin A	TNF-alpha NF-kB Signaling Pathway	WP:WP457	C0JPT7	117	1.6
Psmd13	proteasome 26S subunit, non-ATPase 13	TNF-alpha NF-kB Signaling Pathway	WP:WP457	B0BN93	18	1.5
Hdac1	histone deacetylase 1	TNF-alpha NF-kB Signaling Pathway	WP:WP457	Q4QQW4	6	1.5
Hsp90ab1	heat shock protein 90 alpha family class B member 1	TNF-alpha NF-kB Signaling Pathway	WP:WP457	P34058	97	1.4
Actb	actin, beta	TNF-alpha NF-kB Signaling Pathway	WP:WP457	P60711	349	1.2
Ywhae	tyrosine 3-monooxygenase/tryptophan 5-monooxygenase activation protein, epsilon	TNF-alpha NF-kB Signaling Pathway	WP:WP457	P62260	6	1.2
Lrpprc	leucine-rich pentatricopeptide repeat containing	TNF-alpha NF-kB Signaling Pathway	WP:WP457	F1LM33	51	1.2
Psmd1	proteasome 26S subunit, non-ATPase 1	TNF-alpha NF-kB Signaling Pathway	WP:WP457	G3V8B6	14	1.2

Only proteins with 5 or more PSMs are included. PSM ratio is $PSMs_{BirA\text{-}claudin\text{-}18}/PSMs_{YFP\text{-}claudin\text{-}18}$. UniProt, KEGG, and WikiPathways (WP) were used to obtain protein and pathway pathway information.

Table 5.4: Proteosome and protein processing in endoplasmic reticulum proteins tagged by biotin ligase fused to claudin-18.

UniProt ID	Protein Name	Functional grouping	KEGG/WP	Accession	BirA-claudin-18 #PSMs	PSM Ratio
Psme3	proteasome activator subunit 3	Proteosome	KEGG:03050	Q5FVM2	6	20.0
Psmd6	proteasome 26S subunit, non-ATPase 6	Proteosome	KEGG:03050	Q6PCT9	8	4.0
Psmd7	proteasome 26S subunit, non-ATPase 7	Proteosome	KEGG:03050	D4AEH3	12	3.0
Psmd14	proteasome 26S subunit, non-ATPase 14	Proteosome	KEGG:03050	Q4V8E2	5	2.5
Psmc3	proteasome 26S subunit, ATPase 3	Proteosome	KEGG:03050	Q6P6U2	12	2.0
Psmd12	proteasome 26S subunit, non-ATPase 12	Proteosome	KEGG:03050	Q5XIC6	15	1.9
Psmc6	proteasome 26S subunit, ATPase 6	Proteosome	KEGG:03050	G3V6W6	13	1.9
Psmd2	proteasome 26S subunit, non-ATPase 2	Proteosome	KEGG:03050	Q4FZT9	25	1.8
Psmc1	proteasome 26S subunit, ATPase 1	Proteosome	KEGG:03050	P62193	14	1.8
Psmc2	proteasome 26S subunit, ATPase 2	Proteosome	KEGG:03050	G3V7L6	10	1.7
Psmd13	proteasome 26S subunit, non-ATPase 13	Proteosome	KEGG:03050	B0BN93	18	1.5
Psmc4	proteasome 26S subunit, ATPase 4	Proteosome	KEGG:03050	Q63570	18	1.4
Psmc5	proteasome 26S subunit, ATPase 5	Proteosome	KEGG:03050	P62198	19	1.4
Psmd1	proteasome 26S subunit, non-ATPase 1	Proteosome	KEGG:03050	G3V8B6	14	1.2
Pdia4	protein disulfide isomerase family A, member 4	Protein processing in endoplasmic reticulum	KEGG:04141	G3V6T7	14	7.0
Dnajb11	DnaJ heat shock protein family (Hsp40) member B11	Protein processing in endoplasmic reticulum	KEGG:04141	Q6TUG0	7	7.0

Sec24a	SEC24 homolog A, COPII coat complex component	Protein processing in endoplasmic reticulum	KEGG:04141	D3ZZA8	6	6.0
Sec23a	Sec23 homolog A, coat complex II component	Protein processing in endoplasmic reticulum	KEGG:04141	B5DFC3	5	5.0
Ppa1	inorganic pyrophosphatase 1	Protein processing in endoplasmic reticulum	KEGG:04141	Q6AY18	10	2.5
Canx	calnexin	Protein processing in endoplasmic reticulum	KEGG:04141	P35565	32	2.1
Sec31a	SEC31 homolog A, COPII coat complex component	Protein processing in endoplasmic reticulum	KEGG:04141	G3V699	14	2.0
Calr	calreticulin	Protein processing in endoplasmic reticulum	KEGG:04141	P18418	63	1.9
Hspa5	heat shock protein family A (Hsp70) member 5	Protein processing in endoplasmic reticulum	KEGG:04141	P06761	17	1.7
Sec23b	Sec23 homolog B, coat complex II component	Protein processing in endoplasmic reticulum	KEGG:04141	D3ZCT7	8	1.6
Ssr4	signal sequence receptor subunit 4	Protein processing in endoplasmic reticulum	KEGG:04141	Q07984	8	1.6
Rpn2	ribophorin II, Dolichyl-diphosphooligosaccharide--protein glycosyltransferase subunit 2	Protein processing in endoplasmic reticulum	KEGG:04141	P25235	19	1.6
Hsp90ab1	heat shock protein 90 alpha family class B member 1	Protein processing in endoplasmic reticulum	KEGG:04141	P34058	97	1.4
Rpn1	ribophorin I, Dolichyl-diphosphooligosaccharide--protein glycosyltransferase subunit 1	Protein processing in endoplasmic reticulum	KEGG:04141	Q6P7A7	32	1.3
Hsp90b1	heat shock protein 90 beta family member 1	Protein processing in endoplasmic reticulum	KEGG:04141	A0A0A0MY09	44	1.2

Only proteins with 5 or more PSMs are included. PSM ratio is $PSMs_{BirA\text{-}claudin\text{-}18}/PSMs_{YFP\text{-}claudin\text{-}18}$. UniProt, KEGG, and WikiPathways (WP) were used to obtain protein and pathway pathway information.

Table 5.5: Endocytosis and phagocytosis proteins tagged by biotin ligase fused to claudin-18.

UniProt ID	Protein Name	Functional grouping	KEGG/WP	Accession	BirA-claudin-18 #PSMs	PSM Ratio
RT1-CE4	RT1 class I, locus CE4	Endocytosis	KEGG:04144	D3ZQG9	8	> 15
Sh3glb1	SH3 domain -containing GRB2-like endophilin B1	Endocytosis	KEGG:04144	Q6AYE2	6	6.0
Mapk3	Mitogen-activated protein kinase 3	Endocytosis	Ref 4,7-9	P21708-2	5	5.0
Pacsin2	Protein kinase C and casein kinase substrate in neurons 2 protein	Endocytosis		Q9QY17	5	5.0
Dnm1	Isoform 2 of Dynamin-1-like protein	Endocytosis		O35303-2	11	2.8
Opa1	Dynamin-like 120 kDa protein, mitochondrial	Endocytosis		D4A8U5	14	2.3
Vps35	VPS35 retromer complex component	Endocytosis	KEGG:04144	G3V8A5	10	2.0
Snx2	sorting nexin 2	Endocytosis	KEGG:04144	B2RYP4	6	2.0
Copb2	Coatomer subunit beta'	Endocytosis			15	1.7
Washc4	WASH complex subunit 4	Endocytosis	KEGG:04144	D4A7I6	5	1.7
Ehd1	EH-domain containing 1	Endocytosis	KEGG:04144	Q641Z6	21	1.6
Ap2a2	adaptor related protein complex 2 subunit alpha 2	Endocytosis	KEGG:04144	Q66HM2	22	1.5
Ehd4	EH-domain containing 4	Endocytosis	KEGG:04144	Q8R3Z7	24	1.4
Kif5b	kinesin family member 5B	Endocytosis	KEGG:04144	Q2PQA9	17	1.3
Ap2a1	adaptor related protein complex 2 subunit alpha 1	Endocytosis	KEGG:04144	D3ZUY8	16	1.2
Rab35	RAB35, member RAS oncogene family	Endocytosis	KEGG:04144	Q5U316	6	1.2
Vps4b	vacuolar protein sorting 4 homolog B	Endocytosis	KEGG:04144	Q4KLL7	6	1.2
Nckap1	Nck-associated protein 1	Endocytosis		P55161	7	1.2
Picalm	Phosphatidylinositol-binding clathrin assembly protein	Endocytosis		O55012	7	1.2
Cltc	clathrin heavy chain	Endocytosis	KEGG:04144	F1M779	176	1.2
RT1-CE4	RT1 class I, locus CE4	Phagosome	KEGG:04145	D3ZQG9	8	> 15
Dync1li1	dynein cytoplasmic 1 light intermediate chain 1	Phagosome	KEGG:04145	G3V7G0	7	2.3

Canx	calnexin	Phagosome	KEGG:04145	P35565	32	2.1
Calr	calreticulin	Phagosome	KEGG:04145	P18418	63	1.9
Ncf1	neutrophil cytosolic factor 1	Phagosome	KEGG:04145	F1M707	6	1.5
Tubb4a	tubulin, beta 4A class IVa	Phagosome	KEGG:04145	B4F7C2	143	1.2
Tubb4b	tubulin, beta 4B class IVb	Phagosome	KEGG:04145	G3V7C6	162	1.2
Tubb5	tubulin, beta 5 class I	Phagosome	KEGG:04145	P69897	174	1.2
Actb	actin, beta	Phagosome	KEGG:04145	P60711	349	1.2
Cybb	cytochrome b-245 beta chain	Phagosome	KEGG:04145	Q9ERL1	6	1.2
Tubb2b	tubulin, beta 2B class IIb	Phagosome	KEGG:04145	Q3KRE8	144	1.2
Tubb6	tubulin, beta 6 class V	Phagosome	KEGG:04145	Q4QQV0	108	1.2

Only proteins with 5 or more PSMs are included. PSM ratio is $PSMs_{BirA\text{-}claudin\text{-}18}/PSMs_{YFP\text{-}claudin\text{-}18}$. UniProt, KEGG, and WikiPathways (WP) were used to obtain protein and pathway pathway information.

Literature Cited

1 Itallie CM, Anderson JM. Architecture of tight junctions and principles of molecular composition. *Semin Cell Dev Biol* 2014;**36**:157–65. https://doi.org/10.1016/j.semcdb.2014.08.011.

2 Günzel D, Fromm M. Claudins and other tight junction proteins. *Comprehensive Physiology* 2012;**2**:1819–52. https://doi.org/10.1002/cphy.c110045.

3 Schlingmann B, Overgaard CE, Molina SA, Lynn KS, Mitchell LA, White SD, *et al.* Regulation of claudin/zonula occludens-1 complexes by hetero-claudin interactions. *Nat Commun* 2016;**7**:12276. https://doi.org/10.1038/ncomms12276.

4 Itallie CMV, Aponte A, Tietgens AJ, Gucek M, Fredriksson K, Anderson JM. The N and C termini of ZO-1 are surrounded by distinct proteins and functional protein networks. *J Biol Chem* 2013;**288**:13775–88. https://doi.org/10.1074/jbc.M113.466193.

5 Fredriksson K, Itallie CMV, Aponte A, Gucek M, Tietgens AJ, Anderson JM. Proteomic analysis of proteins surrounding occludin and claudin-4 reveals their proximity to signaling and trafficking networks. *PLoS One* 2015;**10**:e0117074. https://doi.org/10.1371/journal.pone.0117074.

6 Itallie CMV, Tietgens AJ, Aponte A, Fredriksson K, Fanning AS, Gucek M, *et al.* Biotin ligase tagging identifies proteins proximal to E-cadherin, including lipoma preferred partner, a regulator of epithelial cell-cell and cell-substrate adhesion. *J Cell Sci* 2014;**127**:885–95. https://doi.org/10.1242/jcs.140475.

7 Roux KJ, Kim D, Raida M, Burke B. A promiscuous biotin ligase fusion protein identifies proximal and interacting proteins in mammalian cells. *J Cell Biol* 2012;**196**:801–10. https://doi.org/10.1083/jcb.201112098.

8 Dobbs LG, Gonzalez R, Williams MC. An Improved Method for Isolating Type II Cells in High Yield and Purity1–3. *Am Rev Respir Dis* 2015;**134**:141–5. https://doi.org/10.1164/arrd.1986.134.1.141.

9 Raudvere U, Kolberg L, Kuzmin I, Arak T, Adler P, Peterson H, *et al.* g:Profiler: a web server for functional enrichment analysis and conversions of gene lists (2019 update). *Nucleic Acids Res* 2019;**47**:W191–8. https://doi.org/10.1093/nar/gkz369.

10 Martens M, Ammar A, Riutta A, Waagmeester A, Slenter DN, Hanspers K, *et al.* WikiPathways: connecting communities. *Nucleic Acids Res* 2020;**49**:gkaa1024-. https://doi.org/10.1093/nar/gkaa1024.

11 Kanehisa M, Goto S. KEGG: Kyoto Encyclopedia of Genes and Genomes. *Nucleic Acids Res* 2000;**28**:27–30. https://doi.org/10.1093/nar/28.1.27.

12 Zlatic SA, Ryder PV, Salazar G, Faundez V. Isolation of labile multi-protein complexes by in vivo controlled cellular cross-linking and immuno-magnetic affinity chromatography. *Journal of Visualized Experiments : JoVE* 2010. https://doi.org/10.3791/1855.

13 Qian X, Mruk DD, Cheng CY. Rai14 (Retinoic Acid Induced Protein 14) Is Involved in Regulating F-Actin Dynamics at the Ectoplasmic Specialization in the Rat Testis*. *Plos One* 2013;**8**:e60656. https://doi.org/10.1371/journal.pone.0060656.

14 Lyon K, Adams A, Piva M, Asghari P, Moore ED, Vogl AW. Ca2+signaling machinery is present at intercellular junctions and structures associated with junction turnover in rat Sertoli cells. *Biol Reprod* 2017;**96**:1288–302. https://doi.org/10.1093/biolre/iox042.

15 Vogl AW, Young JS, Du M. New Insights into Roles of Tubulobulbar Complexes in Sperm Release and Turnover of Blood-Testis Barrier. *Int Rev Cel Mol Bio* 2013;**303**:319–55. https://doi.org/10.1016/b978-0-12-407697-6.00008-8.

16 Lynn KS, Peterson RJ, Koval M. Ruffles and spikes: Control of tight junction morphology and permeability by claudins. *Biochim Biophys Acta Biomembr* 2020;**1862**:183339. https://doi.org/10.1016/j.bbamem.2020.183339.

17 Zhou B, Flodby P, Luo J, Castillo DR, Liu Y, Yu F-XX, *et al.* Claudin-18-mediated YAP activity regulates lung stem and progenitor cell homeostasis and tumorigenesis. *The Journal of Clinical Investigation* 2018. https://doi.org/10.1172/jci90429.

18 Vogl A, Du M, Wang XY, Young JS. Novel clathrin/actin-based endocytic machinery associated with junction turnover in the seminiferous epithelium. *Semin Cell Dev Biol* 2014. https://doi.org/10.1016/j.semcdb.2013.11.002.

19 Carrasco S, Meyer T. STIM Proteins and the Endoplasmic Reticulum-Plasma Membrane Junctions. *Biochemistry-Us* 2011;**80**:973–1000. https://doi.org/10.1146/annurev-biochem-061609-165311.

20 Taddei A, Giampietro C, Conti A, Orsenigo F, Breviario F, Pirazzoli V, *et al.* Endothelial adherens junctions control tight junctions by VE-cadherin-mediated upregulation of claudin-5. *Nature Cell Biology* 2008;**10**:923–34.

21 Qian X, Mruk DD, Cheng Y, Cheng CY. RAI14 (retinoic acid induced protein 14) is an F-actin regulator. *Spermatogenesis* 2014;**3**:e24824. https://doi.org/10.4161/spmg.24824.

22 Fernandes-Silva H, Araújo-Silva H, Correia-Pinto J, Moura RS. Retinoic Acid: A Key Regulator of Lung Development. *Biomol* 2020;**10**:152. https://doi.org/10.3390/biom10010152.

23 Lochbaum R, Schilpp C, Nonnenmacher L, Frick M, Dietl P, Wittekindt OH. Retinoic acid signalling adjusts tight junction permeability in response to air-liquid interface conditions. *Cell Signal* 2019;**65**:109421. https://doi.org/10.1016/j.cellsig.2019.109421.

24 Parast MM, Otey CA. Characterization of Palladin, a Novel Protein Localized to Stress Fibers and Cell Adhesions. *J Cell Biology* 2000;**150**:643–56. https://doi.org/10.1083/jcb.150.3.643.

25 Otey CA, Rachlin A, Moza M, Arneman D, Carpen O. The Palladin/Myotilin/Myopalladin Family of Actin-Associated Scaffolds. *Int Rev Cytol* 2005;**246**:31–58. https://doi.org/10.1016/s0074-7696(05)46002-7.

26 Ward C, Schlingmann B, Stecenko AA, Guidot DM, Koval M. NF-κB inhibitors impair lung epithelial tight junctions in the absence of inflammation. *Tissue Barriers* 2015;**3**:e982424. https://doi.org/10.4161/21688370.2014.982424.

27 Hensley PJ, Desiniotis A, Wang C, Stromberg A, Chen C-S, Kyprianou N. Novel Pharmacologic Targeting of Tight Junctions and Focal Adhesions in Prostate Cancer Cells. *Plos One* 2014;**9**:e86238. https://doi.org/10.1371/journal.pone.0086238.

28 Tornavaca O, Chia M, Dufton N, Almagro LO, Conway DE, Randi AM, *et al.* ZO-1 controls endothelial adherens junctions, cell-cell tension, angiogenesis, and barrier formation. *J Cell Biol* 2015;**208**:821–38. https://doi.org/10.1083/jcb.201404140.

29 Nita-Lazar M, Rebustini I, Walker J, Kukuruzinska MA. Hypoglycosylated E-cadherin promotes the assembly of tight junctions through the recruitment of PP2A to adherens junctions. *Exp Cell Res* 2010;**316**:1871–84. https://doi.org/10.1016/j.yexcr.2010.02.008.

30 Yamazaki Y, Tokumasu R, Kimura H, Tsukita S. Role of claudin species-specific dynamics in reconstitution and remodeling of the zonula occludens. *Mol Biol Cell* 2011;**22**:1495–504. https://doi.org/10.1091/mbc.e10-12-1003.

31 Shen L, Weber CR, Turner JR. The tight junction protein complex undergoes rapid and continuous molecular remodeling at steady state. *J Cell Biology* 2008;**181**:683–95. https://doi.org/10.1083/jcb.200711165.

32 Capaldo CT, Nusrat A. Claudin switching: Physiological plasticity of the Tight Junction. *Semin Cell Dev Biol* 2015;**42**:22–9. https://doi.org/10.1016/j.semcdb.2015.04.003.

33 Walsh L, Ryu J, Bock S, Koval M, Mauro T, Ross R, *et al.* Nanotopography facilitates in vivo transdermal delivery of high molecular weight therapeutics through an integrin-dependent mechanism. *Nano Letters* 2015;**15**:2434–41. https://doi.org/10.1021/nl504829f.

34 Elsum IA, Martin C, Humbert PO. Scribble regulates an EMT polarity pathway through modulation of MAPK-ERK signaling to mediate junction formation. *J Cell Sci* 2013;**126**:3990–9. https://doi.org/10.1242/jcs.129387.

35 Wu D, Huang C-J, Jiao X-F, Ding Z-M, Zhang J-Y, Chen F, *et al.* Olaquindox disrupts tight junction integrity and cytoskeleton architecture in mouse Sertoli cells. *Oncotarget* 2014;**5**:88630–44. https://doi.org/10.18632/oncotarget.20289.

36 Lee S, Cieply B, Yang Y, Peart N, Glaser C, Chan P, *et al.* Esrp1-Regulated Splicing of Arhgef11 Isoforms Is Required for Epithelial Tight Junction Integrity. *Cell Reports* 2018;**25**:2417-2430.e5. https://doi.org/10.1016/j.celrep.2018.10.097.

37 Elbediwy A, Zhang Y, Cobbaut M, Riou P, Tan RS, Roberts SK, *et al.* The Rho-family GEF FARP2 is activated by aPKCι to control polarity and tight junction formation. *J Cell Sci* 2019;**132**:jcs.223743. https://doi.org/10.1242/jcs.223743.

38 Dan Q, Shi Y, Rabani R, Venugopal S, Xiao J, Anwer S, *et al.* Claudin-2 suppresses GEF-H1, RHOA, and MRTF, thereby impacting proliferation and profibrotic phenotype of tubular cells. *J Biol Chem* 2019;**294**:15446–65. https://doi.org/10.1074/jbc.RA118.006484.

39 Yin H, Kosa P, Liu X, Swaim WD, Lai Z, Cabrera-Perez J, *et al.* Matriptase Deletion Initiates a Sjögren's Syndrome-Like Disease in Mice. *Plos One* 2014;**9**:e82852. https://doi.org/10.1371/journal.pone.0082852.

40 Fournane S, Charbonnier S, Chapelle A, Kieffer B, Orfanoudakis G, Travé G, *et al.* Surface plasmon resonance analysis of the binding of high-risk mucosal HPV E6 oncoproteins to the PDZ1 domain of the tight junction protein MAGI-1. *J Mol Recognit* 2011;**24**:511–23. https://doi.org/10.1002/jmr.1056.

41 Chiu C-F, Ho M-Y, Peng J-M, Hung S-W, Lee W-H, Liang C-M, *et al.* Raf activation by Ras and promotion of cellular metastasis require phosphorylation of prohibitin in the raft domain of the plasma membrane. *Oncogene* 2013;**32**:777–87. https://doi.org/10.1038/onc.2012.86.

42 Pitter B, Werner A-C, Montanez E. Parvins Are Required for Endothelial Cell–Cell Junctions and Cell Polarity During Embryonic Blood Vessel Formation. *Arteriosclerosis Thrombosis Vasc Biology* 2018;**38**:1147–58. https://doi.org/10.1161/atvbaha.118.310840.

43 Olski TM, Noegel AA, Korenbaum E. Parvin, a 42 kDa focal adhesion protein, related to the alpha-actinin superfamily. *J Cell Sci* 2001;**114**:525–38.

44 Werner A-C, Weckbach LT, Salvermoser M, Pitter B, Cao J, Maier-Begandt D, *et al.* Coronin 1B Controls Endothelial Actin Dynamics at Cell–Cell Junctions and Is Required for

Endothelial Network Assembly. *Frontiers Cell Dev Biology* 2020;**8**:708. https://doi.org/10.3389/fcell.2020.00708.

45 Liu W, Wang P, Shang C, Chen L, Cai H, Ma J, *et al.* Endophilin-1 regulates blood–brain barrier permeability by controlling ZO-1 and occludin expression via the EGFR–ERK1/2 pathway. *Brain Res* 2014;**1573**:17–26. https://doi.org/10.1016/j.brainres.2014.05.022.

46 Reardon HT, Park WJ, Zhang J, Lawrence P, Kothapalli KSD, Brenna JT. The polypyrimidine tract binding protein regulates desaturase alternative splicing and PUFA composition. *J Lipid Res* 2011;**52**:2279–86. https://doi.org/10.1194/jlr.m019653.

47 Stewart JJ, White JT, Yan X, Collins S, Drescher CW, Urban ND, *et al.* Proteins Associated with Cisplatin Resistance in Ovarian Cancer Cells Identified by Quantitative Proteomic Technology and Integrated with mRNA Expression Levels. *Mol Cell Proteomics* 2006;**5**:433–43. https://doi.org/10.1074/mcp.m500140-mcp200.

48 Campos Y, Qiu X, Gomero E, Wakefield R, Horner L, Brutkowski W, *et al.* Alix-mediated assembly of the actomyosin–tight junction polarity complex preserves epithelial polarity and epithelial barrier. *Nat Commun* 2016;**7**:11876. https://doi.org/10.1038/ncomms11876.

49 Takasawa K, Takasawa A, Osanai M, Aoyama T, Ono Y, Kono T, *et al.* Claudin-18 coupled with EGFR/ERK signaling contributes to the malignant potentials of bile duct cancer. *Cancer Lett* 2017;**403**:66–73. https://doi.org/10.1016/j.canlet.2017.05.033.

50 Rentzsch I, Santos CL, Huhle R, Ferreira JMC, Koch T, Schnabel C, *et al.* Variable stretch reduces the pro-inflammatory response of alveolar epithelial cells. *Plos One* 2017;**12**:e0182369. https://doi.org/10.1371/journal.pone.0182369.

51 Wang Y, Zheng J, Han Y, Zhang Y, Su L, Hu D, *et al.* JAM-A knockdown accelerates the proliferation and migration of human keratinocytes, and improves wound healing in rats via FAK/Erk signaling. *Cell Death Dis* 2018;**9**:848. https://doi.org/10.1038/s41419-018-0941-y.

52 Wu Q, Li G, Wen C, Zeng T, Fan Y, Liu C, *et al.* Monoubiquitination of p120-catenin is essential for TGFβ-induced epithelial-mesenchymal transition and tumor metastasis. *Sci Adv* 2020;**6**:eaay9819. https://doi.org/10.1126/sciadv.aay9819.

53 Cong X, Zhang Y, Li J, Mei M, Ding C, Xiang R-LL, *et al.* Claudin-4 is required for modulation of paracellular permeability by muscarinic acetylcholine receptor in epithelial cells. *J Cell Sci* 2015;**128**:2271–86. https://doi.org/10.1242/jcs.165878.

54 Zhang Y, Cui G, Wang Y, Gong Y, Wang Y. SIRT1 activation alleviates brain microvascular endothelial dysfunction in peroxisomal disorders. *Int J Mol Med* 2019;**44**:995–1005. https://doi.org/10.3892/ijmm.2019.4250.

55 Chaudhry KK, Samak G, Shukla PK, Mir H, Gangwar R, Manda B, *et al.* ALDH2 Deficiency Promotes Ethanol-Induced Gut Barrier Dysfunction and Fatty Liver in Mice. *Alcohol Clin Exp Res* 2015;**39**:1465–75. https://doi.org/10.1111/acer.12777.

56 Samak G, Gangwar R, Meena AS, Rao RG, Shukla PK, Manda B, *et al.* Calcium Channels and Oxidative Stress Mediate a Synergistic Disruption of Tight Junctions by Ethanol and Acetaldehyde in Caco-2 Cell Monolayers. *Sci Rep-Uk* 2016;**6**:38899. https://doi.org/10.1038/srep38899.

57 Postema MM, Grega-Larson NE, Meenderink LM, Tyska MJ. PACSIN2-dependent apical endocytosis regulates the morphology of epithelial microvilli. *Mol Biol Cell* 2019;**30**:2515–26. https://doi.org/10.1091/mbc.e19-06-0352.

58 Dorland YL, Malinova TS, Stalborch A-MDM van, Grieve AG, Geemen D van, Jansen NS, *et al.* The F-BAR protein pacsin2 inhibits asymmetric VE-cadherin internalization from tensile adherens junctions. *Nat Commun* 2016;**7**:12210. https://doi.org/10.1038/ncomms12210.

59 Xiao L, Rao JN, Cao S, Liu L, Chung HK, Zhang Y, *et al.* Long noncoding RNA SPRY4-IT1 regulates intestinal epithelial barrier function by modulating the expression levels of tight junction proteins. *Mol Biol Cell* 2016;**27**:617–26. https://doi.org/10.1091/mbc.e15-10-0703.

60 Zou T, Jaladanki SK, Liu L, Xiao L, Chung HK, Wang J-Y, *et al.* H19 Long Noncoding RNA Regulates Intestinal Epithelial Barrier Function via MicroRNA 675 by Interacting with RNA-Binding Protein HuR. *Mol Cell Biol* 2016;**36**:1332–41. https://doi.org/10.1128/mcb.01030-15.

61 Ma Y, Yue J, Zhang Y, Shi C, Odenwald M, Liang WG, *et al.* ACF7 regulates inflammatory colitis and intestinal wound response by orchestrating tight junction dynamics. *Nat Commun* 2017;**8**:15375. https://doi.org/10.1038/ncomms15375.

62 Hu L, Su P, Li R, Yin C, Zhang Y, Shang P, *et al.* Isoforms, structures, and functions of versatile spectraplakin MACF1. *Bmb Rep* 2016;**49**:37–44. https://doi.org/10.5483/bmbrep.2016.49.1.185.

63 Kim W-G, Kim HI, Kwon EK, Han MJ, Kim D-H. Lactobacillus plantarum LC27 and Bifidobacterium longum LC67 mitigate alcoholic steatosis in mice by inhibiting LPS-mediated NF-κB activation through restoration of the disturbed gut microbiota. *Food Funct* 2018;**9**:4255–65. https://doi.org/10.1039/c8fo00252e.

64 Chishiki K, Kamakura S, Hayase J, Sumimoto H. Ric-8A, an activator protein of Gαi, controls mammalian epithelial cell polarity for tight junction assembly and cystogenesis. *Genes Cells* 2017;**22**:293–309. https://doi.org/10.1111/gtc.12477.

65 González-Mariscal L, Raya-Sandino A, González-González L, Hernández-Guzmán C. Relationship between G proteins coupled receptors and tight junctions. *Tissue Barriers* 2017;**6**:00–00. https://doi.org/10.1080/21688370.2017.1414015.

66 Dunagan M, Chaudhry K, Samak G, Rao RK. Acetaldehyde disrupts tight junctions in Caco-2 cell monolayers by a protein phosphatase 2A-dependent mechanism. *Am J Physiol-Gastr L* 2012;**303**:G1356–64. https://doi.org/10.1152/ajpgi.00526.2011.

67 Eum SY, Jaraki D, András IE, Toborek M. Lipid rafts regulate PCB153-induced disruption of occludin and brain endothelial barrier function through protein phosphatase 2A and matrix

metalloproteinase-2. *Toxicol Appl Pharm* 2015;**287**:258–66. https://doi.org/10.1016/j.taap.2015.06.011.

68 Sun X, Yao L, Liang H, Wang D, He Y, Wei Y, *et al.* Intestinal epithelial PKM2 serves as a safeguard against experimental colitis via activating β-catenin signaling. *Mucosal Immunol* 2019;**12**:1280–90. https://doi.org/10.1038/s41385-019-0197-6.

69 Kim B, Jang C, Dharaneeswaran H, Li J, Bhide M, Yang S, *et al.* Endothelial pyruvate kinase M2 maintains vascular integrity. *J Clin Invest* 2018;**128**:4543–56. https://doi.org/10.1172/jci120912.

70 Lu T-S, Chen H-W, Huang M-H, Wang S-J, Yang R-C. Heat shock treatment protects osmotic stressinduced dysfunction of the blood-brain barrier through preservation of tight junction proteins. *Cell Stress Chaperon* 2004;**9**:369–77. https://doi.org/10.1379/csc-45r1.1.

71 Noda S, Tanabe S, Suzuki T. Naringenin enhances intestinal barrier function through the expression and cytoskeletal association of tight junction proteins in Caco-2 cells. *Mol Nutr Food Res* 2013;**57**:2019–28. https://doi.org/10.1002/mnfr.201300045.

72 Varasteh S, Braber S, Akbari P, Garssen J, Fink-Gremmels J. Differences in Susceptibility to Heat Stress along the Chicken Intestine and the Protective Effects of Galacto-Oligosaccharides. *Plos One* 2015;**10**:e0138975. https://doi.org/10.1371/journal.pone.0138975.

73 Campbell M, Nguyen ATH, Kiang A-S, Tam LCS, Gobbo OL, Kerskens C, *et al.* An experimental platform for systemic drug delivery to the retina. *Proc National Acad Sci* 2009;**106**:17817–22. https://doi.org/10.1073/pnas.0908561106.

74 Zhang X-D, Baladandayuthapani V, Lin H, Mulligan G, Li B, Esseltine D-LW, *et al.* Tight Junction Protein 1 Modulates Proteasome Capacity and Proteasome Inhibitor Sensitivity in Multiple Myeloma via EGFR/JAK1/STAT3 Signaling. *Cancer Cell* 2016;**29**:639–52. https://doi.org/10.1016/j.ccell.2016.03.026.

75 Kang L, Shen L, Lu L, Wang D, Zhao Y, Chen C, *et al.* Asparaginyl endopeptidase induces endothelial permeability and tumor metastasis via downregulating zonula occludens protein ZO-1. *Biochimica Et Biophysica Acta Bba - Mol Basis Dis* 2019;**1865**:2267–75. https://doi.org/10.1016/j.bbadis.2019.05.003.

76 Awadia S, Huq F, Arnold TR, Goicoechea SM, Sun YJ, Hou T, *et al.* SGEF forms a complex with Scribble and Dlg1 and regulates epithelial junctions and contractilityScribble/SGEF/Dlg1 in epithelial junctions. *J Cell Biology* 2019;**218**:2699–725. https://doi.org/10.1083/jcb.201811114.

77 Tan B, Yatim SMJM, Peng S, Gunaratne J, Hunziker W, Ludwig A. The Mammalian Crumbs Complex Defines a Distinct Polarity Domain Apical of Epithelial Tight Junctions. *Curr Biol* 2020;**30**:2791-2804.e6. https://doi.org/10.1016/j.cub.2020.05.032.

78 Konishi S, Yano T, Tanaka H, Mizuno T, Kanoh H, Tsukita K, *et al.* Vinculin is critical for the robustness of the epithelial cell sheet paracellular barrier for ions. *Life Sci Alliance* 2019;**2**:e201900414. https://doi.org/10.26508/lsa.201900414.

CHAPTER 6: DISCUSSION – CONCLUSION AND FUTURE DIRECTIONS

Since the discovery of the first tight junction proteins nearly thirty years ago,[1–3] the tight junction biology field has made significant advances in our understanding in how these vital protein complexes assemble and function.[4] The cell and tissue specific barrier properties conferred by specific tight junction protein combinations reveals the complexity of these proteins. Specific membrane lipids, mechanical force and scaffolding proteins can drive assembly and function.[5–7] Based on our work and the work of others, we now know that tight junctions not only form paracellular barriers, but they can also act as signaling hubs through specific claudin-scaffold protein interactions, respond to mechanical force, and play a role in cell polarization and differentiation.[8–13]

Accumulating evidence shows that tight junctions can play a pivotal role in facilitating disease progression and prevention.[14–16] Though our understanding of tight junctions has grown exponentially since their discovery, a deeper knowledge of the components that regulate tight junction assembly and function is necessary in order to therapeutically tune tight junctions.[17] The work presented in this dissertation characterized a specific tight junction morphology (tight junction spikes) observed with chronic alcohol consumption and associated with a decrease in epithelial barrier function. Using a chronic alcohol exposure model system, we profiled tight junction proteins for differences in expression and found that claudin-5 was upregulated. Claudin-5 overexpression was necessary and sufficient to decrease barrier function, interfering with claudin-18/ZO-1 interactions. Claudin-5 overexpression was associated with an increase in tight junction spikes, which appeared to be sites of vesicle budding and fusion. Treatment with the endocytosis inhibitor Dynasore resulted in a decrease in tight junction spikes and large molecular flux, as well as cytoskeletal rearrangement. A difference in the claudin-18/ZO-1 ratio in spikes from control-diet and alcohol-diet cells further suggests that alcohol-induced changes

in protein interactions at tight junctions can drive morphological and functional changes. We also found that BioID is a valuable method for investigating these differences in the tight junction proteome by identifying proteins within the claudin-18 interactome. Overall, this work extends our understanding of tight junction protein interactions and the relationship between tight junction morphology and barrier function in normal and pathological conditions. In this chapter, I discuss the implications of this research and several hypotheses and future directions prompted by this work.

Alcohol-induced changes in tight junction protein interactions

The discovery of claudins as the crucial components conferring tight junction barrier function has led to a flood of research characterizing the properties of individual claudins and specific combinations of claudins. We now know that claudins can have tissue-specific barrier properties which appear to be in part due to different combinations of claudins present.[18–20] Mutational studies as well as recently solved claudin crystal structures have provided insight into tight junction assembly and how claudins interact with each other.[21–24] However, the network of protein interactions at tight junctions that can influence barrier function goes beyond claudin-claudin interactions, including significant interactions with scaffold proteins and signaling molecules.[25,26] In Chapter 3, we demonstrate that claudin-5/claudin-18 interactions can disrupt interactions between claudin-18and the scaffold protein ZO-1. Previous examples of claudin heterocomplexes have been shown, but this is the first example of a claudin heterocomplex affecting claudin/scaffold interactions.[27,28] An increase in claudin-5 expression observed in our chronic alcohol model was necessary and sufficient for decreasing barrier function. This suggests that *cis* interactions between claudin-18 and claudin-5 could be part of the mechanism to disrupt barrier function in alcoholic lung syndrome.

In Chapter 4, we observed an increase in the claudin-18/ZO-1 ratio along spike length that suggests local changes in the distribution of claudin-18 and ZO-1. In spikes in AECs from

control-fed rats, the increase in the claudin-18/ZO-1 ratio suggests that more claudin-18 or less ZO-1 is present at the end of the spike projection compared to the beginning of the spike close to the intercellular tight junction. By contrast, the similar ratio between either end of tight junction spikes in AECs from alcohol-fed rats suggests an even proportion of claudin-18 to ZO-1. No significant difference in overall claudin-18 or ZO-1 expression in cells from control-fed and alcohol-fed samples was found, supporting a model where changes in the claudin-18/ZO-1 ratio within spikes are reflective of localized changes. [29] Coupled with previous observations of decreased claudin-18/ZO-1 colocalization at junctions in cells from alcohol-fed rats and an increase of Triton X-100-soluble claudin-18 in claudin-5 transfected cells, we hypothesize that claudin-18 is less integrated or tethered in tight junctions along tight junction spikes in alcohol-fed samples, resulting in a higher turnover and redistribution of claudin-18, and subsequently a deficiency in barrier function. This hints at a change in tight junction stability and turnover associated with alcohol. Whether directly triggered as a result of an increase in spikes, a disassociation of claudin-18 from ZO-1, or more indirect means is not known.

Scaffold proteins have long been thought of as the nucleators of tight junction formation, tethering passive claudin components to the actin cytoskeleton.[30–32] Exchange of claudin components interacting with the assembled scaffold can thereby tune barrier function while avoiding a drastic deconstruction of the tight junction. Recent evidence demonstrating that ZO-1 and ZO-2 phase separate to form membrane-bound compartments sheds light on how scaffold protein interactions can influence tight junction component recruitment and assembly. Conformational changes to ZO proteins that affect the ability to form intramolecular interactions determine phase separation, and thereby tight junction assembly.[33,34] Our work demonstrating disruption of claudin/scaffold protein interactions fits with this model but suggests that claudins could play an active role in regulating protein interactions at the tight junction. Claudins bind to the PDZ domains of ZO proteins via a C-terminus PDZ-binding motif, while claudin-claudin *cis* interactions occur through transmembrane and extracellular loop

regions.[21,22,35] We hypothesize that claudin-5 overexpression disrupts claudin-18/ZO-1 interactions through higher affinity interactions with claudin-18 that force claudin-18 dissociation from ZO-1, possibly promoting recruitment of other proteins to the C-terminal tail of claudin-18.[10] In this model, we hypothesize that altering claudin-18 interactions could shift the local tight junction proteome that affects the function of the tight junction complex. Whether alcohol signals tight junction changes directly or as a result of other alcohol-mediated effects such as inflammation is not fully known.[36–40]

Tight junction spikes as separate sites of activity

Interestingly, alcohol-induced changes in tight junction protein expression were associated with an increase in tight junction spikes. Furthermore, claudin-5 overexpression was sufficient to induce this morphological change. Chapter 3 and Chapter 4 describe my work to characterize tight junction spikes, with particular emphasis on identifying proteins involved in tight junction spike formation and function. Live-cell imaging allowed us to observe vesicles budding and fusing with tight junction spikes, suggesting that spikes could be nucleators of signaling activity or areas of active tight junction remodeling. Several signaling proteins are known to localize to tight junctions, including polarity complex proteins and Rho GTPases.[41–46] Additionally, our BioID experiment identified several proteins involved in vesicle trafficking enriched with BirA-claudin-18, similar to observations made with BioID of claudin-4 and occludin, though a connection to tight junction spikes cannot be drawn without additional experiments.[47]

Turnover at tight junctions can occur rapidly and via multiple endocytic routes, and recent evidence of claudins in cuboidal cells being added to the basolateral side of tight junctions suggests that addition of new proteins to existing tight junctions could occur at particular regions of the junction complex.[48–51] Spike structures in *Pemphigus vulgaris* antisera keratinocytes show similar evidence of endocytic activity, suggesting the possibility that the orientation of junctions in a squamous cell monolayer provide a more accessible view of

endocytic activity.[52] We hypothesize that the lateral membrane surface in squamous alveolar epithelial cells is formed between overlapping cells rather than an end-to-end model based on cuboidal cells. Because of this orientation, the tips of tight junction spikes could act as the basolateral side of tight junction strands within the overlapping lateral junctions where new tight junction proteins can more readily be added.

Our observation of differences in claudin-18 and ZO-1 protein composition along tight junction spikes further suggests some partitioning of tight junction proteins at spikes. One possibility of how this could occur is through enrichment of particular membrane lipids along tight junction spikes that promote localization of particular tight junction components. Depletion of cholesterol in α-catenin-deficient EpH4 cells resulted in an inability to form tight junctions.[53] Rescue with cholesterol supplementation led to tight junction formation and cholesterol-rich tight junction spikes. Membrane lipids are known to play an important role in tight junction assembly, facilitating protein recruitment and stabilization of tight junctions.[54–57] Several lipid-binding and lipid metabolism proteins were enriched in BirA-claudin-18 samples in our BioID experiments (Chapter 5). Whether tight junction spikes have a membrane lipid composition differing from linear tight junctions is important in understanding how tight junction spike form and whether there are distinct regions at the tight junction.

Dynamin-2-actin bundling and tight junction spike formation

Evidence of endocytosis at tight junction spikes initially led us to investigate a role for endocytosis machinery in tight junction spike formation and function. By treating cells with the dynamin inhibitor Dynasore, we noted a significant decrease in tight junction spikes. We then profiled the dynamin expression and determined dynamin-2 as the dominant isoform. Initially, we hypothesized that dynamin-2 could be playing a role in tight junction spike formation through localization along tight junction spikes similar to the spike structures in tubulobulbar complexes.[58] Our initial investigation shows tight junction localization of dynamin-2 but was

unable to resolve spike-localization of dynamin-2. Interestingly, we observed cytoskeletal rearrangement with Dynasore treatment, namely a recovery of cortical actin associated with the loss of tight junction spikes. There is a growing body of research suggesting dynamin-2 has an alternative function as an actin filament-bundling protein, facilitating formation of spike-like invadosome and filopodia structures.[59,60] This evidence informed our current model of spike formation where we propose that dynamin-2 acts in its role as an actin bundling protein, reorienting cortical actin into actin filaments that tight junction spikes project along. Further analysis through dynamin-2 knockdown studies is necessary to determine whether this is part of the mechanism of tight junction spike formation. Actin filament bundles are not restricted to areas with spikes nor does every spike appear to colocalize with an actin filament bundle. The necessity of actin bundling by dynamin-2 and whether it is an essential step in tight junction spike formation, as well as the presence of other actin binding proteins at spikes, are important points to address in understanding the role of the cytoskeleton in tight junction spikes.

Asymmetrical formation of tight junction spikes and β-catenin

We found that tight junction spikes typically protrude in one direction along a linear junction on the opposite side of asymmetrically localized β-catenin staining. Interestingly, tight junction spikes tend to orient along actin filaments that terminate in asymmetric β-catenin regions. It is possible that actomyosin contraction could drive tight junction spike formation, similar to force-induced focal adherens junctions.[61] There is accumulating evidence on how mechanical force plays a role in tight junction assembly, namely through ZO-1, which can confer mechanosensitive properties to tight junctions through its association with the actin cytoskeleton.[7,42] This is a tenuous balance, as too much tension can impair tight junction barrier function, which could explain the decrease in barrier function associated with tight junction spikes. [62] Additionally, ZO-1 phase separation has been shown to be dependent on mechanical force in part due to changes in ZO-1 conformations.[33,34,63] Interestingly, the link between ZO-1

and actin was recently found to be a weak association.[5] Increasing the strength of ZO-1 association with actin decreased barrier function, further emphasizing the delicate balance between tight junctions and the cytoskeleton that regulates barrier function. It is possible that changes in claudin-18/ZO-1 binding with chronic alcohol or claudin-5 overexpression could affect ZO-1 conformation, thereby affecting the strength of ZO-1's interaction with actin and result in barrier impairment.

There are two predominant roles for β-catenin, depending on whether it is junction-associated or cytosolic. In adherens junctions, β-catenin serves as a link between transmembrane cadherin proteins and the actin cytoskeleton through interactions with actin-binding proteins. By contrast, cytosolic β-catenin binds to the Tcf/Lef transcription factor, mediating transcription of genes involved in Wnt-activated cell proliferation and can regulate lung development[64–67]. The unique staining pattern of β-catenin we observed at junctions suggests two possible explanations: that non-junction associated β-catenin could be present at one side of the junction interface, or the adjacent cells are overlapping, allowing visualization of lateral adherens junctions. Cytosolic β-catenin is normally either targeted to the nucleus or rapidly degraded via the proteasome, making a large pool of cytosolic β-catenin near junctions unlikely[64,68]. In addition, β-catenin associates with the actin cytoskeleton through actin-binding proteins such as α-catenin, fascin, and Ras GTPase-activating-like protein (IQGAP)[64]. Adherens junctions in the apical junctional complex are associated with cortical F-actin bundles that form a circumferential ring around polarized cells, while less polarized epithelial and endothelial cells have adherens junctions associated with more tangential actin filaments[69]. Dynamic changes in actin can exert different intracellular forces or transmit extracellular forces through intercellular junctions.

Tight junction spikes and localized permeability

In Chapter 4, we investigated whether tight junction spikes were sites of increased barrier permeability through the use of a localized permeability assay (XPerT).[70] Though tight junction spikes were not leakier than linear tight junctions, cells overexpressing claudin-5 did have more leak overall, though it appeared as hotspots of leak as opposed to universal leak. This suggests that tight junction spikes could cause or be the result of more widespread changes to barrier function. For instance, tight junction spikes could be areas of increased tension, causing a decrease in barrier function at other junctions within the monolayer. The fact that tight junction spikes are not uniformly distributed within cell monolayers strengthens the idea that changes in barrier function are the result of a spectrum in tight junction morphologies and properties. Interestingly, Dynasore treatment only partly rescued barrier function, decreasing larger molecular leak (Texas Red-dextran, 10 kDa) but increasing small molecule (calcein) and ion permeability. This could be due to an overcompensation in the strength of cortical actin arrangement, shifting the balance to a higher tension state that is still permeable to small molecules and ions.[5,71,72] Alternatively, if tight junction spikes sequester particular tight junction proteins, the redistribution of spike-associated tight junction proteins into the linear tight junction could alter the barrier properties.

New technologies for tight junction research

The ability to analyze local areas of leak is an invaluable tool for investigating the ways in which different tight junction morphologies affect barrier function. Several assays for observing localized leak exist but are not widely used. One drawback to the XPerT assay used in Chapter 4 is its reliance on large molecule (avidin) flux in order to visualize permeability. This is easily achieved in endothelial cells, which are leakier by nature. However, in tighter model systems, this assay may only be useful if there is aberrant leak and might not be sensitive enough to visualize finer differences in permeability. The ZnUMBA assay is a similar localized leak assay

that utilizes flux of the small molecule $ZnCl_2$ to visualize leak. The use of these assays in assessing tight junction permeability is necessary to answer questions about barrier properties with heterogenous junction morphologies.

Traditional microscopy has a limited resolution at 200 nm, making it difficult to visualize strand breaks (20 to 200 nm) within tight junctions that can facilitate increased paracellular leak, but super-resolution techniques can provide an alternative for indirectly assessing areas of localized permeability.[73,74] In Chapters 3 and 4, we used stochastic optical reconstruction microscopy (STORM) and stimulated emission depletion (STED) microscopy to visualize differences in tight junction proteins within tight junction structures. However, super-resolution microscopy techniques are limited to their ability to visualize only a few known tight junction protein components at a time. This restricts our ability to understand how the larger tight junction protein network with novel protein components localize and interact at tight junction complexes. Use of the BioID technique shows promise in addressing this technology gap by using a biotinylation enzyme (BirA) conjugated to a tight junction protein to investigate the local tight junction proteome.[75] Observations utilizing this technique have revealed varying proteomes at the N-terminus and C-terminus of ZO-1, highlighting its potential for dissecting tight junction interactions.[47,76,77] In Chapter 5, we demonstrate use of this technique to explore the claudin-18 local proteome, with future applications focusing on addressing changes in the claudin-18 proteome with chronic alcohol and claudin-5 overexpression. Taken together, advances in super-resolution microscopy along with proteomic techniques will help facilitate novel observations of tight junction nanoarchitecture.

Therapeutic outlook

The ability to tune barrier permeability through targeting of tight junction protein interactions is vastly important for drug development and drug targeting. In Chapter 3, we use a claudin-5 peptide to rescue barrier function, which was coupled with a decrease in claudin-5

expression and a decrease in the number of tight junction spikes. This not only emphasizes the relationship between tight junction morphology and barrier function but shows that disrupting claudin interactions at the tight junction has potential as a therapeutic target.[78] Additionally, claudin-5 is an important component of the blood-brain barrier and is therefore an important target to consider in facilitating drug permeability across barriers.[79–82] Because monolayers with claudin-5 overexpression experienced hotspots of leak instead of uniform leak, tissue barriers could experience a range of permeabilities with different levels of tuning needed. This is an important consideration for drug development, both in considering how to target injured areas of a barrier and how to restrict barrier-breaching drugs to a specific region of tissue when a tissue-wide barrier breach is not desirable.

Summary

The evolution of our knowledge of tight junctions has grown exponentially since the discovery of the first tight junction proteins. Yet, how tight junction proteins, both individually and in complex, confer tunable barrier properties in various tissue and conditions remains an open question. The work presented in this dissertation helps to define how specific tight junction proteins in lung alveolar epithelial cells can drastically affect tight junction function. We build upon growing knowledge in the field on tight junction protein interactions while emphasizing that claudin-induced changes to these interactions can have long reaching effects on tight junction structure and barrier properties. Overexpression of claudin-5 not only affected local claudin-18/ZO-1 interactions at the tight junction but shifted linear tight junction morphology to have more tight junction spikes and produced hotspots of leak across cell monolayers. This highlights the necessity to consider how changes in the tight junction interactome can globally affect barrier permeability and whether changes in permeability are equally distributed across monolayers. This could provide insight into how barriers experience breaches or injury, and whether localized adjustments to tight junctions are sufficient to repair

barriers. Advancements in super-resolution microscopy and localized permeability assays will help future work investigating protein interactions at the tight junction and how these interactions affect the larger tight junction network within cell monolayers. Coupled with proteomic analysis of the tight junction interactome, these approaches will help address remaining gaps in our knowledge concerning the details of the local tight junction proteome, as well as how changes in the proteome affect barrier properties on a tissue-wide scale.

Literature Cited

1 Furuse M, Hirase T, Itoh M, Nagafuchi A, Yonemura S, Tsukita S, *et al.* Occludin: a novel integral membrane protein localizing at tight junctions. *J Cell Biology* 1993;**123**:1777–88. https://doi.org/10.1083/jcb.123.6.1777.

2 Furuse M, Fujita K, Hiiragi T, Fujimoto K, Tsukita S. Claudin-1 and -2: Novel Integral Membrane Proteins Localizing at Tight Junctions with No Sequence Similarity to Occludin. *J Cell Biology* 1998;**141**:1539–50. https://doi.org/10.1083/jcb.141.7.1539.

3 Stevenson BR, Siliciano JD, Mooseker MS, Goodenough DA. Identification of ZO-1: a high molecular weight polypeptide associated with the tight junction (zonula occludens) in a variety of epithelia. *J Cell Biology* 1986;**103**:755–66. https://doi.org/10.1083/jcb.103.3.755.

4 Otani T, Furuse M. Tight Junction Structure and Function Revisited. *Trends Cell Biol* 2020;**30**:805–17. https://doi.org/10.1016/j.tcb.2020.08.004.

5 Belardi B, Hamkins-Indik T, Harris AR, Kim J, Xu K, Fletcher DA. A Weak Link with Actin Organizes Tight Junctions to Control Epithelial Permeability. *Dev Cell* 2020;**54**:792-804.e7. https://doi.org/10.1016/j.devcel.2020.07.022.

6 Itallie CMV, Tietgens AJ, Anderson JM. Visualizing the dynamic coupling of claudin strands to the actin cytoskeleton through ZO-1. *Molecular Biology of the Cell* 2017;**28**:524–34. https://doi.org/10.1091/mbc.e16-10-0698.

7 Ito S, Okuda S, Abe M, Fujimoto M, Onuki T, Nishimura T, *et al.* Induced cortical tension restores functional junctions in adhesion-defective carcinoma cells. *Nat Commun* 2017;**8**:1834. https://doi.org/10.1038/s41467-017-01945-y.

8 Bhat AA, Syed N, Therachiyil L, Nisar S, Hashem S, Macha MA, *et al.* Claudin-1, A Double-Edged Sword in Cancer. *Int J Mol Sci* 2020;**21**:569. https://doi.org/10.3390/ijms21020569.

9 Angulo-Urarte A, Wal T van der, Huveneers S. Cell-cell junctions as sensors and transducers of mechanical forces. *Biochim Biophys Acta Biomembr* 2020;**1862**:183316. https://doi.org/10.1016/j.bbamem.2020.183316.

10 Zhou B, Flodby P, Luo J, Castillo DR, Liu Y, Yu F-XX, *et al*. Claudin-18-mediated YAP activity regulates lung stem and progenitor cell homeostasis and tumorigenesis. *The Journal of Clinical Investigation* 2018. https://doi.org/10.1172/jci90429.

11 Zihni C, Mills C, Matter K, Balda MS. Tight junctions: from simple barriers to multifunctional molecular gates. *Nature Reviews Molecular Cell Biology* 2016;**17**:564–80. https://doi.org/10.1038/nrm.2016.80.

12 Shen L, Weber CR, Raleigh DR, Yu D, Turner JR. Tight junction pore and leak pathways: a dynamic duo. *Annu Rev Physiol* 2011;**73**:283–309. https://doi.org/10.1146/annurev-physiol-012110-142150.

13 Cereijido M, Ponce A, Gonzalez-Mariscal L. Tight junctions and apical/basolateral polarity. *J Membr Biology* 1989;**110**:1–9. https://doi.org/10.1007/bf01870987.

14 Marchiando AM, Graham W, Turner JR. Epithelial barriers in homeostasis and disease. *Annual Review of Pathology* 2010;**5**:119–44. https://doi.org/10.1146/annurev.pathol.4.110807.092135.

15 Soini Y. Tight junctions in lung cancer and lung metastasis: a review. *International Journal of Clinical and Experimental Pathology* 2012;**5**:126–36.

16 Koval M, Sidhaye VK. Lung Epithelial Biology in the Pathogenesis of Pulmonary Disease. *Undefined* 2017:xiii–xviii. https://doi.org/10.1016/b978-0-12-803809-3.00023-3.

17 Matsuhisa K, Kondoh M, Takahashi A, Yagi K. Tight junction modulator and drug delivery. *Expert Opin Drug Del* 2009;**6**:509–15. https://doi.org/10.1517/17425240902902315.

18 Itallie CMV, Fanning AS, Anderson JM. Reversal of charge selectivity in cation or anion-selective epithelial lines by expression of different claudins. *American Journal of Physiology Renal Physiology* 2003;**285**:F1078-84. https://doi.org/10.1152/ajprenal.00116.2003.

19 Itallie CV, Rahner C, Anderson JM. Regulated expression of claudin-4 decreases paracellular conductance through a selective decrease in sodium permeability. *J Clin Invest* 2001;**107**:1319–27. https://doi.org/10.1172/jci12464.

20 Capaldo CT, Nusrat A. Claudin switching: Physiological plasticity of the Tight Junction. *Semin Cell Dev Biol* 2015;**42**:22–9. https://doi.org/10.1016/j.semcdb.2015.04.003.

21 Suzuki H, Nishizawa T, Tani K, Yamazaki Y. Crystal structure of a claudin provides insight into the architecture of tight junctions. *Null* 2014. https://doi.org/10.1126/science.1248571.

22 Suzuki H, Tani K, Tamura A, Tsukita S, Fujiyoshi Y. Model for the architecture of claudin-based paracellular ion channels through tight junctions. *J Mol Biol* 2014;**427**:291–7. https://doi.org/10.1016/j.jmb.2014.10.020.

23 Rossa J, Protze J, Kern C, Piontek A, Günzel D, Krause G, *et al.* Molecular and structural transmembrane determinants critical for embedding claudin-5 into tight junctions reveal a distinct four-helix bundle arrangement. *Biochem J* 2014;**464**:49–60. https://doi.org/10.1042/bj20140431.

24 Saitoh Y, Suzuki H, Tani K, Nishikawa K, Irie K, Ogura Y, *et al.* Structural insight into tight junction disassembly by Clostridium perfringens enterotoxin. *Science* 2015;**347**:775–8. https://doi.org/10.1126/science.1261833.

25 Otani T, Ichii T, Aono S, Takeichi M. Cdc42 GEF Tuba regulates the junctional configuration of simple epithelial cells. *J Cell Biology* 2006;**175**:135–46. https://doi.org/10.1083/jcb.200605012.

26 Matter K, Balda. Signalling to and from tight junctions. *Null* 2003.

27 Rossa J, Ploeger C, Vorreiter F, Saleh T, Protze J, Günzel D, *et al.* Claudin-3 and Claudin-5 Protein Folding and Assembly into the Tight Junction Are Controlled by Non-conserved Residues in the Transmembrane 3 (TM3) and Extracellular Loop 2 (ECL2) Segments. *J Biol Chem* 2014;**289**:7641–53. https://doi.org/10.1074/jbc.m113.531012.

28 Hou J, Renigunta A, Gomes AS, Hou M, Paul DL, Waldegger S, *et al.* Claudin-16 and claudin-19 interaction is required for their assembly into tight junctions and for renal reabsorption of magnesium. *Proc National Acad Sci* 2009;**106**:15350–5. https://doi.org/10.1073/pnas.0907724106.

29 Schlingmann B, Overgaard CE, Molina SA, Lynn KS, Mitchell LA, White SD, *et al.* Regulation of claudin/zonula occludens-1 complexes by hetero-claudin interactions. *Nat Commun* 2016;**7**:12276. https://doi.org/10.1038/ncomms12276.

30 Shen L, Weber CR, Turner JR. The tight junction protein complex undergoes rapid and continuous molecular remodeling at steady state. *J Cell Biology* 2008;**181**:683–95. https://doi.org/10.1083/jcb.200711165.

31 Fanning AS, Itallie CM, Anderson JM. Zonula occludens-1 and -2 regulate apical cell structure and the zonula adherens cytoskeleton in polarized epithelia. *Molecular Biology of the Cell* 2012;**23**:577–90. https://doi.org/10.1091/mbc.e11-09-0791.

32 Umeda K, Ikenouchi J, Katahira-Tayama S, Furuse K, Sasaki H, Nakayama M, *et al.* ZO-1 and ZO-2 independently determine where claudins are polymerized in tight-junction strand formation. *Cell* 2006;**126**:741–54. https://doi.org/10.1016/j.cell.2006.06.043.

33 Schwayer C, Shamipour S, Pranjic-Ferscha K, Schauer A, Balda M, Tada M, *et al.* Mechanosensation of Tight Junctions Depends on ZO-1 Phase Separation and Flow. *Cell* 2019;**179**:937-952.e18. https://doi.org/10.1016/j.cell.2019.10.006.

34 Beutel O, Maraspini R, Pombo-García K, Martin-Lemaitre C, Honigmann A. Phase Separation of Zonula Occludens Proteins Drives Formation of Tight Junctions. *Cell* 2019;**179**:923-936.e11. https://doi.org/10.1016/j.cell.2019.10.011.

35 Itallie CMV, Mitic LL, Anderson JM. Claudin-2 forms homodimers and is a component of a high molecular weight protein complex. *J Biol Chem* 2011;**286**:3442–50. https://doi.org/10.1074/jbc.m110.195578.

36 Laksitorini MD, Yathindranath V, Xiong W, Parkinson FE, Thliveris JA, Miller DW. Impact of Wnt/β-catenin signaling on ethanol-induced changes in brain endothelial cell permeability. *J Neurochem* 2020. https://doi.org/10.1111/jnc.15203.

37 Rubio-Araiz A, Porcu F, Pérez-Hernández M, García-Gutiérrez MS, Aracil-Fernández MA, Gutierrez-López MD, *et al.* Disruption of blood–brain barrier integrity in postmortem

alcoholic brain: preclinical evidence of TLR4 involvement from a binge-like drinking model. *Addict Biol* 2017;**22**:1103–16. https://doi.org/10.1111/adb.12376.

38 Guidot DM, Modelska K, Lois M, Jain L, Moss IM, Pittet J-F, *et al.* Ethanol ingestion via glutathione depletion impairs alveolar epithelial barrier function in rats. *Am J Physiol Lung Cell Mol Physiol* 2000;**279**:L127–35. https://doi.org/10.1152/ajplung.2000.279.1.l127.

39 Joshi PC, Applewhite L, Mitchell PO, Fernainy K, Roman J, Eaton DC, *et al.* GM-CSF receptor expression and signaling is decreased in lungs of ethanol-fed rats. *Am J Physiol-Lung C* 2006;**291**:L1150–8. https://doi.org/10.1152/ajplung.00150.2006.

40 Downs CA, Trac DQ, Kreiner LH, Eaton AF, Johnson NM, Brown LA, *et al.* Ethanol Alters Alveolar Fluid Balance via Nadph Oxidase (NOX) Signaling to Epithelial Sodium Channels (ENaC) in the Lung. *Plos One* 2013;**8**:e54750. https://doi.org/10.1371/journal.pone.0054750.

41 Arnold TR, Stephenson RE, Miller AL. Rho GTPases and actomyosin: Partners in regulating epithelial cell-cell junction structure and function. *Exp Cell Res* 2017;**358**:20–30. https://doi.org/10.1016/j.yexcr.2017.03.053.

42 Itoh M, Tsukita S, Yamazaki Y, Sugimoto H. Rho GTP exchange factor ARHGEF11 regulates the integrity of epithelial junctions by connecting ZO-1 and RhoA-Myosin II signaling. *Proc National Acad Sci* 2012;**109**:9905–10. https://doi.org/10.1073/pnas.1115063109.

43 Lemmers C, Médina E, Delgrossi M-H, Michel D, Arsanto J-P, Bivic AL. hINADl/PATJ, a Homolog of Discs Lost, Interacts with Crumbs and Localizes to Tight Junctions in Human Epithelial Cells. *J Biol Chem* 2002;**277**:25408–15. https://doi.org/10.1074/jbc.m202196200.

44 Michel D, Arsanto J-P, Massey-Harroche D, Béclin C, Wijnholds J, Bivic AL. PATJ connects and stabilizes apical and lateral components of tight junctions in human intestinal cells. *J Cell Sci* 2005;**118**:4049–57. https://doi.org/10.1242/jcs.02528.

45 Hurd TW, Gao L, Roh MH, Macara IG, Margolis B. Direct interaction of two polarity complexes implicated in epithelial tight junction assembly. *Nat Cell Biol* 2003;**5**:137–42. https://doi.org/10.1038/ncb923.

46 Izumi Y, Hirose T, Tamai Y, Hirai S, Nagashima Y, Fujimoto T, *et al.* An Atypical PKC Directly Associates and Colocalizes at the Epithelial Tight Junction with ASIP, a Mammalian Homologue of Caenorhabditis elegans Polarity Protein PAR-3. *J Cell Biology* 1998;**143**:95–106. https://doi.org/10.1083/jcb.143.1.95.

47 Fredriksson K, Itallie CMV, Aponte A, Gucek M, Tietgens AJ, Anderson JM. Proteomic analysis of proteins surrounding occludin and claudin-4 reveals their proximity to signaling and trafficking networks. *PLoS One* 2015;**10**:e0117074. https://doi.org/10.1371/journal.pone.0117074.

48 Matsuda M, Kubo A, Furuse M, Tsukita S. A peculiar internalization of claudins, tight junction-specific adhesion molecules, during the intercellular movement of epithelial cells. *J Cell Sci* 2004;**117**:1247–57. https://doi.org/10.1242/jcs.00972.

49 Zwanziger D, Staat C, Andjelkovic AV, Blasig IE. Claudin-derived peptides are internalized via specific endocytosis pathways. *Annals of the New York Academy of Sciences* 2012;**1257**:29–37. https://doi.org/10.1111/j.1749-6632.2012.06567.x.

50 Daugherty BL, Mateescu M, Patel AS, Wade K, Kimura S, Gonzales LW, *et al.* Developmental regulation of claudin localization by fetal alveolar epithelial cells. *Am J Physiol Lung Cell Mol Physiol* 2004;**287**:L1266-73. https://doi.org/10.1152/ajplung.00423.2003.

51 Itallie CM, Lidman K, Tietgens A, Anderson J. Newly synthesized claudins but not occludin are added to the basal side of the tight junction. *Molecular Biology of the Cell* 2019;**30**:1406–24. https://doi.org/10.1091/mbc.e19-01-0008.

52 Stahley SN, Saito M, Faundez V, Koval M, Mattheyses AL, Kowalczyk AP. Desmosome assembly and disassembly are membrane raft-dependent. *PLoS One* 2014;**9**:e87809. https://doi.org/10.1371/journal.pone.0087809.

53 Shigetomi K, Ono Y, Inai T, Ikenouchi J. Adherens junctions influence tight junction formation via changes in membrane lipid composition. *J Cell Biol* 2018. https://doi.org/10.1083/jcb.201711042.

54 Lynch RD, Francis SA, McCarthy KM, Casas E, Thiele C, Schneeberger EE. Cholesterol depletion alters detergent-specific solubility profiles of selected tight junction proteins and the phosphorylation of occludin. *Exp Cell Res* 2007;**313**:2597–610. https://doi.org/10.1016/j.yexcr.2007.05.009.

55 Kusumi A, Fujiwara TK, Tsunoyama TA, Kasai RS, Liu A, Hirosawa KM, *et al.* Defining raft domains in the plasma membrane. *Traffic* 2020;**21**:106–37. https://doi.org/10.1111/tra.12718.

56 Itallie CMV, Gambling TM, Carson JL, Anderson JM. Palmitoylation of claudins is required for efficient tight-junction localization. *J Cell Sci* 2005;**118**:1427–36. https://doi.org/10.1242/jcs.01735.

57 Nusrat A, Parkos CA, Verkade P, Foley CS, Liang TW, Innis-Whitehouse W, *et al.* Tight junctions are membrane microdomains. *J Cell Sci* 2000;**113 (Pt 10)**:1771–81.

58 Vogl A, Du M, Wang XY, Young JS. Novel clathrin/actin-based endocytic machinery associated with junction turnover in the seminiferous epithelium. *Semin Cell Dev Biol* 2014. https://doi.org/10.1016/j.semcdb.2013.11.002.

59 Zhang R, Lee DM, Jimah JR, Gerassimov N, Yang C, Kim S, *et al.* Dynamin regulates the dynamics and mechanical strength of the actin cytoskeleton as a multifilament actin-bundling protein. *Nat Cell Biol* 2020;**22**:674–88. https://doi.org/10.1038/s41556-020-0519-7.

60 Abe T, La TM, Miyagaki Y, Oya E, Wei F-Y, Sumida K, *et al.* Phosphorylation of cortactin by cyclin-dependent kinase 5 modulates actin bundling by the dynamin 1-cortactin ring-like complex and formation of filopodia and lamellipodia in NG108-15 glioma-derived cells. *Int J Oncol* 2018;**54**:550–8. https://doi.org/10.3892/ijo.2018.4663.

61 Dorland YL, Malinova TS, Stalborch A-MDM van, Grieve AG, Geemen D van, Jansen NS, *et al.* The F-BAR protein pacsin2 inhibits asymmetric VE-cadherin internalization from tensile adherens junctions. *Nat Commun* 2016;**7**:12210. https://doi.org/10.1038/ncomms12210.

62 Zolotarevsky Y, Hecht G, Koutsouris A, Gonzalez DE, Quan C, Tom J, *et al.* A membrane-permeant peptide that inhibits MLC kinase restores barrier function in in vitro models of intestinal disease. *Gastroenterology* 2002;**123**:163–72. https://doi.org/10.1053/gast.2002.34235.

63 Spadaro D, Le S, Laroche T, Mean I, Jond L, Yan J, *et al.* Tension-Dependent Stretching Activates ZO-1 to Control the Junctional Localization of Its Interactors. *Current Biology : CB* 2017. https://doi.org/10.1016/j.cub.2017.11.014.

64 Hartsock A, Nelson WJ. Adherens and tight junctions: Structure, function and connections to the actin cytoskeleton. *Biochim Biophys Acta Biomembr* 2008;**1778**:660–9. https://doi.org/10.1016/j.bbamem.2007.07.012.

65 Sucre JMS, Deutsch GH, Jetter CS, Ambalavanan N, Benjamin JT, Gleaves LA, *et al.* A Shared Pattern of β-Catenin Activation in Bronchopulmonary Dysplasia and Idiopathic Pulmonary Fibrosis. *Am J Pathol* 2018;**188**:853–62. https://doi.org/10.1016/j.ajpath.2017.12.004.

66 Sucre JMS, Vickers KC, Benjamin JT, Plosa EJ, Jetter CS, Cutrone A, *et al.* Hyperoxia Injury in the Developing Lung is Mediated by Mesenchymal Expression of Wnt5A. *Am J Respir Crit Care Med* 2019;**0**:1249–62. https://doi.org/10.1164/rccm.201908-1513oc.

67 Sucre JMS, Vijayaraj P, Aros CJ, Wilkinson D, Paul M, Dunn B, *et al.* Posttranslational modification of β-catenin is associated with pathogenic fibroblastic changes in bronchopulmonary dysplasia. *Am J Physiol Lung Cell Mol Physiol* 2017;**312**:L186–95. https://doi.org/10.1152/ajplung.00477.2016.

68 Aberle H, Bauer A, Stappert J, Kispert A, Kemler R. β-catenin is a target for the ubiquitin–proteasome pathway. *EMBO J* 1997;**16**:3797–804. https://doi.org/10.1093/emboj/16.13.3797.

69 Ladoux B, Nelson WJ, Yan J, Mège RM. The mechanotransduction machinery at work at adherens junctions. *Integr Biol (Camb)* 2015;**7**:1109–19. https://doi.org/10.1039/c5ib00070j.

70 Dubrovskyi O, Birukova AA, Birukov KG. Measurement of local permeability at subcellular level in cell models of agonist- and ventilator-induced lung injury. *Lab Invest* 2013;**93**:254–63. https://doi.org/10.1038/labinvest.2012.159.

71 Ivanov AI, Parkos CA, Nusrat A. Cytoskeletal Regulation of Epithelial Barrier Function During Inflammation. *Am J Pathol* 2010;**177**:512–24. https://doi.org/10.2353/ajpath.2010.100168.

72 Madara JL, Moore R, Carlson S. Alteration of intestinal tight junction structure and permeability by cytoskeletal contraction. *Am J Physiol Cell Physiol* 1987;**253**:C854–61. https://doi.org/10.1152/ajpcell.1987.253.6.c854.

73 Milatz S, Krug SM, Rosenthal R, Günzel D, Müller D, Schulzke J-DD, *et al.* Claudin-3 acts as a sealing component of the tight junction for ions of either charge and uncharged solutes. *Biochimica et Biophysica Acta* 2010;**1798**:2048–57. https://doi.org/10.1016/j.bbamem.2010.07.014.

74 Zeissig S, Bürgel N, Günzel D, Richter J, Mankertz J, Wahnschaffe U, *et al.* Changes in expression and distribution of claudin 2, 5 and 8 lead to discontinuous tight junctions and barrier dysfunction in active Crohn's disease. *Gut* 2007;**56**:61. https://doi.org/10.1136/gut.2006.094375.

75 Roux KJ, Kim D, Raida M, Burke B. A promiscuous biotin ligase fusion protein identifies proximal and interacting proteins in mammalian cells. *J Cell Biol* 2012;**196**:801–10. https://doi.org/10.1083/jcb.201112098.

76 Itallie CMV, Aponte A, Tietgens AJ, Gucek M, Fredriksson K, Anderson JM. The N and C termini of ZO-1 are surrounded by distinct proteins and functional protein networks. *J Biol Chem* 2013;**288**:13775–88. https://doi.org/10.1074/jbc.M113.466193.

77 Itallie CMV, Tietgens AJ, Aponte A, Fredriksson K, Fanning AS, Gucek M, *et al.* Biotin ligase tagging identifies proteins proximal to E-cadherin, including lipoma preferred partner, a regulator of epithelial cell-cell and cell-substrate adhesion. *J Cell Sci* 2014;**127**:885–95. https://doi.org/10.1242/jcs.140475.

78 Baumgartner HK, Beeman N, Hodges RS, Neville MC. A d-Peptide Analog of the Second Extracellular Loop of Claudin-3 and -4 Leads to MisLocalized Claudin and Cellular Apoptosis in Mammary Epithelial Cells. *Chem Biol Drug Des* 2011;**77**:124–36. https://doi.org/10.1111/j.1747-0285.2010.01061.x.

79 Hashimoto Y, Tachibana K, Krug SM, Kunisawa J, Fromm M, Kondoh M. Potential for Tight Junction Protein–Directed Drug Development Using Claudin Binders and Angubindin-1. *Int J Mol Sci* 2019;**20**:4016. https://doi.org/10.3390/ijms20164016.

80 Neuhaus W, Piontek A, Protze J, Eichner M, Mahringer A, Subileau E-AA, *et al.* Reversible opening of the blood-brain barrier by claudin-5-binding variants of Clostridium perfringens enterotoxin's claudin-binding domain. *Biomaterials* 2018;**161**:129–43. https://doi.org/10.1016/j.biomaterials.2018.01.028.

81 Nitta T, Hata M, Gotoh S, Seo Y, Sasaki H, Hashimoto N, *et al.* Size-selective loosening of the blood-brain barrier in claudin-5-deficient mice. *J Cell Biol* 2003;**161**:653–60. https://doi.org/10.1083/jcb.200302070.

82 Dithmer S, Staat C, Müller C, Ku M-CC, Pohlmann A, Niendorf T, *et al.* Claudin peptidomimetics modulate tissue barriers for enhanced drug delivery. *Annals of the New York Academy of Sciences* 2017;**1397**:169–84. https://doi.org/10.1111/nyas.13359.